AN ABSTRACT OF THE THESIS OF

Russell J. Sanderson for the degree Doctor of Philosophy in Biochemistry and Biophysics presented on September 23, 1998. Title: Uracil-DNA Glycosylase Inhibitor Protein: Role of Carboxylic Acid Residues and Use for Measuring the Fidelity of Uracil-Excision DNA Repair Synthesis in Human Cell Extracts.

ABSTRACT APPROVED:

Redacted for privacy

Dale W. Mosbaugh

Chemical modification of the *Bacillus subtilis* bacteriophage PBS2 uracil-DNA glycosylase inhibitor (Ugi) protein with carbodiimide and glycine ethyl ester resulted in the selective adduction of amino acid residues Glu-28 and Glu-31 in the α2-helix. Increased modification at these sites correlated with a decreased ability to inactivate *Escherichia coli* uracil-DNA glycosylase (Ung) and to compete with unmodified Ugi for complex formation with Ung. Competition experiments utilizing unmodified Ugi and poly(U) revealed that modified Ugi was defective in achieving an irreversible association with Ung since modified Ugi was displaced from preformed Ung•Ugi complexes.

The fidelity of DNA repair synthesis associated with highly efficient uracil-initiated base excision repair (BER) events in human U251 and LoVo whole cell extracts was measured by using an M13mp2 *lacZα* reversion assay. Production of Form I DNA reaction products insensitive to cleavage by *E. coli* uracil-DNA glycosylase and endonuclease IV indicated that complete BER had occurred. The majority of repair involved a Ugi-insensitive uracil-DNA

glycosylase while a secondary BER reaction occurred that was insensitive to Ugi. Both BER reactions involved a DNA polymerase that was insensitive to aphidicolin. The size of the BER repair patch extended from one to eight nucleotides in length and the predominant patch involved the incorporation of one nucleotide. The fidelity of DNA repair synthesis in U251 and LoVo cell extracts at a site-specific uracil residue was determined to be about one misincorporated nucleotide per 1900 and 1850 repaired uracil residues, respectively. For the Ugi-insensitive BER repair pathway, the fidelity of DNA repair synthesis decreased to one misincorporated nucleotide per 350 and 850 repaired uracil residues for U251 and LoVo cell extracts, respectively. In all cases, the most frequent base substitution propogated transversion mutations and involved T to G and T to A changes in the template.

The activity responsible for the Ugi-insensitive BER pathway observed in U251 cell extracts was further examined *in vitro* by utilizing U251 cells transduced with a *ugi* expression construct. This Ugi-insensitive activity removed uracil residues from U•G mispairs more efficiently (~3.5-fold) than from U•A base pairs but was refractory to uracil in single-stranded DNA.

Uracil-DNA Glycosylase Inhibitor Protein: Role of Carboxylic Acid Residues and Use for Measuring the Fidelity of Uracil-Excision DNA Repair Synthesis in Human Cell Extracts.

by

Russell J. Sanderson

A THESIS
submitted to
Oregon State University

in partial fulfillment of
the requirements for the
degree of

Doctor of Philosophy

Presented September 23, 1998
Commencement June 1999

Doctor of Philosophy thesis of Russell J. Sanderson presented on September 23, 1998

APPROVED:

Redacted for privacy

Major Professor, representing Biochemistry and Biophysics

Redacted for privacy

Chair of Department of Biochemistry and Biophysics

Redacted for privacy

Dean of Graduate School

I understand that my thesis will become part of the permanent collection of Oregon State University libraries. My signature below authorizes release of my thesis to any reader upon request.

Redacted for privacy

Russell J. Sanderson, Author

ACKNOWLEDGMENTS

I would like to thank my research advisor, Dr. Dale Mosbaugh, for his support and expert guidance in my scientific training. I am deeply grateful for having had the opportunity to work with such a dedicated, careful, and thorough scientist. I would also like to thank my parents, John and Norma Sanderson, for their love and encouragement over the course of all of my studies. And finally, I am eternally grateful to my best friend, Kyoung Hee Kim, for her companionship, patience, and optimism. Thank you.

TABLE OF CONTENTS

TABLE OF CONTENTS (Continued)

TABLE OF CONTENTS (Continued)

TABLE OF CONTENTS (Continued)

LIST OF FIGURES

LIST OF FIGURES (Continued)

LIST OF FIGURES (Continued)

LIST OF FIGURES (Continued)

LIST OF TABLES

LIST OF TABLES (Continued)

Uracil-DNA Glycosylase Inhibitor Protein: Role of Carboxylic Acid Residues and Use for Measuring the Fidelity of Uracil-Excision DNA Repair Synthesis in Human Cell Extracts.

1. INTRODUCTION

1.1 Uracil Residues in DNA

1.1.1 Incorporation of dUMP During DNA Synthesis

Low levels of deoxyuridine triphosphate (dUMP) are normally incorporated into the genomic DNA of a variety of organisms, including *Escherichia coli* (279, 281), *Bacillus subtilis* (154, 262), and mammalian cells (22, 86). Incorporation occurs because deoxyuridine triphosphate (dUTP) can be efficiently utilized as a precursor for DNA replication in place of deoxythymidine triphosphate (dTTP) by both prokaryotic and eukaryotic DNA polymerases (59, 195, 281). Incorporation of dUMP in place of dTMP culminates in the formation of a U•A base pair (195). The ability of DNA polymerases to incorporate dUMP into newly synthesized DNA suggests that dUTP and dTTP are not readily discriminated within the nucleotide binding pocket of the enzyme. *In vitro* experiments have demonstrated that *E. coli* DNA polymerases I, II, and III are all capable of substituting dUTP in place of dTTP during DNA synthesis (19, 82, 307). The K_m values for incorporation of dTTP and dUTP by DNA polymerase I were observed to be 4.1 and 5.4 μM, respectively (279). DNA polymerase III exhibited similar K_m values of 2.4 and 2.6 μM for incorporation of dTTP and dUTP (279). Mammalian DNA polymerase α (pol α) and DNA polymerase β (pol β) also efficiently employed dUTP as a nucleotide precursor in place of dTTP and yielded K_m values of 18 and 10 μM for dTTP and 20 and 8 μM for dUTP, respectively (59, 68, 316). Conversely, porcine liver DNA polymerase γ (pol γ) preferentially

incorporated dTMP over dUMP by a factor of ~3-fold (170). Since DNA polymerases do not discriminate efficiently between dUTP and dTTP during DNA replication, it is of the utmost importance for the cell to minimize the size of the intracellular dUTP pool available for DNA synthesis if the uracil content of DNA is to remain at low levels.

The frequency of dUMP incorporation by DNA polymerases is principally dictated by the relative pool sizes of dTTP versus dUTP (279) . Based on the estimate that intracellular levels of dUTP and dTTP in *E. coli* are 0.5 μM and 150 μM, respectively, approximately 1 uracil residue would be incorporated into DNA for every 300 thymine nucleotides polymerized (245). In *E. coli*, intracellular dUTP accumulates following phosphorylation of dUDP to yield dUTP or by the conversion of dCTP to dUTP by deoxycytidine triphosphate (dCTP) deaminase (194). In bacteria, uracil incorporation into DNA is minimized by the enzymatic activities of deoxyuridine 5'-triphosphate nucleotidohydrolase (dUTPase) and uracil-DNA glycosylase (Ung). The enzyme dUTPase hydrolyzes dUTP to dUMP and pyrophosphate (PP_i), and provides a source of dUMP for *de novo* dTTP biosynthesis (245). The small amount of dUTP remaining may be incorporated into DNA by DNA polymerases but it is rapidly eliminated by the uracil-initiated base excision repair (BER) pathway (245, 279, 280). *E. coli* mutants defective in Ung incorporated approximately 1 dUMP residue per 2,000 to 3,000 nucleotides polymerized (279). Mutants defective in dUTPase exhibited approximately 5 % replacement of thymine by uracil in DNA, displayed reduced growth rates, and were eventually inviable, presumably due to double-strand breaks which occur when both strands of the DNA are repaired (297). Double mutants defective in both Ung and dUTPase incorporated uracil into DNA at a frequency of 1 per 100 nucleotides polymerized (279). These mutants also exhibited a reduced growth rate after replacing ~20 % of thymine residues in DNA with uracil (297). Thus, dUTPase plays a significant role in lowering the level of uracil incorporation into DNA in *E. coli*.

Steady-state levels of dUTP in mammalian cells are significantly lower than those of *E. coli*. The absence of a mammalian counterpart to the *E. coli* dCTP deaminase or the presence of an abundant dUTPase could account for the difference in the molar ratio of dUTP to dTTP between mammalian and bacterial cells (37, 188). Human lymphoid cells maintain a dUTP concentration of less than 0.3 fmol/10^6 cells whereas the dTTP concentration is sustained at approximately 40 fmol/10^6 cells (85, 86). The ratio of dUTP to dTTP in mammalian cells indicates that less than 1 dUMP is incorporated into DNA for every 10^5 dTMP polymerized (85, 86). As a result, a lower frequency of uracil residues would be expected to accumulate in human genomic DNA as compared to *E. coli*.

Although eukaryotic mutants lacking uracil-DNA glycosylase or dUTPase are unavailable at present, drugs that inhibit thymidylate synthetase have been used to increase intracellular levels of dUTP in order to study the toxic effects of increased uracil incorporation into DNA (85, 86). Thymidylate synthase catalyzes the reductive methylation of dUMP to dTMP with concomitant conversion of 5,10-methylenetetrahydrofolate to 7,8-dihydrofolate following transfer of its methyl group to dUMP (233). Regeneration of 5,10-methylenetetrahydrofolate by dihydrofolate reductase is inhibited by methotrexate, which reduces the utilization of dUMP by thymidylate synthase, ultimately decreasing the dTTP pool and increasing the dUTP pool (233). Methotrexate reduced the level of dTTP from ~40 pmol/10^6 cells to ~1 pmol/10^6 cells and increased the ratio of dUTP/dTTP from $\leq 10^{-5}$ to 0.2 (85). As expected, the level of dUMP in genomic DNA increased from <1 fmol/μmol of DNA (nucleotides) to 0.8 pmol/μmol of DNA in human lymphoid cells (86). An increased level of intracellular dUTP was accompanied by DNA fragmentation due to excessive degradation of the DNA (31, 202, 277). Thus, the toxic effects observed for cells treated with agents that depress thymidylate synthase activity and increase uracil

incorporation appear to be associated with removal of dUMP from DNA by the uracil-initiated BER pathway.

1.1.2 Cytosine Deamination

1.1.2.1 Spontaneous/Hydrolytic Cytosine Deamination

The spontaneous deamination of cytosine is the second route for the introduction of uracil into DNA and results in the formation of G•U mispairs from pre-existing G•C base pairs (241). There are two proposed chemical mechanisms for the deamination of cytosine in solution (241). (1) The direct mechanism involves alkali-catalyzed hydrolysis at the C4-position of the pyrimidine ring by a water molecule or a hydroxyl ion to release ammonia and requires protonation of the base at the N3-position. (2) The addition-elimination mechanism involves addition of a water molecule across the 5,6 double bond of protonated cytosine to form 5,6-dihydrocytosine. Addition of a second water molecule results in the loss of the ammonia group (deamination) to yield dihydrouracil which is followed by the elimination of water to produce uracil. By using the cytosine analogue N^3 -methyl-2'-deooxycytidine, Sowers *et al.* (254) experimentally determined that the deamination rate was proportional to the concentration of hydroxide ion concentration and the protonated state of cytosine. Previously, the spontaneous rate of cytosine deamination had been determined at extremes of temperature or pH (147, 242). By using a sensitive genetic assay under physiological conditions (37°C, pH 7.4), the deamination rate constants for cytosine in single- and double-stranded DNA were calculated to be 1×10^{-10} and 7×10^{-13} sec^{-1}, respectively (71). The calculated half-life for cytosine in single- and double-stranded DNA obtained by using these deamination rate constants translates to ~200 years and ~30,000 years, respectively, under conditions of temperature and ionic strength that approximate those *in vivo*.

The latter figure translates into ~100 cytosine deamination events per human duplex DNA genome per day (286).

Several studies have suggested that cytosine deamination events in genomic DNA contribute to the overall spontaneous mutation frequency of the cell (61, 63, 165). A pre-mutagenic G•U mispair will produce a G•C→A•T transition mutation if repair does not occur prior to replication (61). For example, *E. coli ung* mutant strains exhibited a 30-fold stimulation of G•C→A•T transition mutations relative to that of wild-type *E. coli* (63). Thus, uracil-DNA glycosylase helps reduce the spontaneous mutation rate caused by cytosine deamination. In a related study, analysis of spontaneous mutations observed in the *E. coli lacI* gene revealed that ~75 % of the mutations resulted in G•C→A•T transitions that were potential sites for cytosine deamination (47, 164). By utilizing an identical target for mammalian cells, base substitution mutations induced in transfected plasmid vector DNA containing the *lacI* gene uniquely occurred at G•C base pairs and involved G•C→A•T transitions (165). Presumably, these mutational events involved deamination of both cytosine and 5-methylcytosine, (66). Deamination of 5-methylcytosine in a G•m^{5}C base pair generates a T•G mispair which produces G•C→A•T transition mutations following DNA replication (66).

As the rate of cytosine deamination in single-stranded DNA is more than two orders of magnitude greater than that of double-stranded DNA, it is likely that the accessibility of the N3 and C4 positions of cytosine to protons, hydroxyl ions, and water leads to the enhancement of deamination events (71). Thus, double-stranded DNA would sterically interfere with compounds that protonate the N3 position or hydrolyze the C4 position of cytosine to induce deamination. Watson-Crick-type pairing involves a hydrogen bond between the N1 of guanine and the N3 of cytosine, thus making protonation of cytosine more difficult. Aberrant base-pair formation or base modification of cytosine or its cross-strand pairing partner, however, has been shown to

result in accelerated protonation and deamination of cytosine within double-stranded DNA (66, 72, 255). For example, 5-methylcytosine exhibits a spontaneous deamination rate that is 4-5-fold higher than that observed for cytosine under identical conditions (66). In addition, cytosine residues within a C•C or C•T mispair were found to deaminate at 10-100 times the rate of cytosine within a normal C•G base pair, closely approaching the rate of cytosine deamination in single-stranded DNA (72). These results support the notion that stabilization/protection of cytosine by Watson-Crick base-pairing apparently accounted for the ~100-fold difference in the rate of deamination between single- and double-stranded DNA (71, 72). On the other hand, stable base pairing between O^6-methylguanine and cytosine required protonation of cytosine at the N3 position and promoted cross-strand deamination of cytosine to produce uracil (255). Thus, improper Watson-Crick base pairing interactions and accessibility of cytosine to protonation are detrimental factors in maintaining the genetic integrity of DNA and indicate that the secondary structure dramatically influences the rate of deamination.

The deamination of cytosine in double-stranded DNA is thought to occur via a single-stranded intermediate (21). This suggests that processes such as transcription, replication, or "breathing" transiently transforms double-stranded DNA into regions of single-stranded character that are more susceptible to deamination (21, 147). In support of this idea, the rate of spontaneous deamination in *S. cerevisiae* was observed to be 40-fold greater than that in *E. coli*, possibly due to the slower rate of eukaryotic transcription, which maintains DNA in a single-stranded format for longer periods of time (110).

1.1.2.2 Chemical Modification of Cytosine

Deamination of cytosine can also be enhanced by certain intercalating agents (175) or by chemical modification with nitrous acid (161, 239) or sodium bisulfite (42, 43, 100). Incubation of double-stranded M13mp2 DNA

with the *bis*-intercalating antitumor drug, echinomycin, resulted in a 3-fold greater increase in G•C→A•T transition mutations than in untreated DNA (175). Previous observations indicated that echinomycin bound at CpG sites and unwound the DNA helix by ~48° (79). These results suggested that an open (single-stranded) DNA structure induced by intercalation of echinomycin into DNA increased the cytosine deamination rate at nearby sites (175). Nitric oxide treatment of gapped M13mp2 DNA has been shown to increase levels of cytosine deamination as compared to untreated DNA and almost exclusively (~98 %) produced C→T transition mutations (161). Unlike sodium bisulfite, nitrous oxide also reacted nonspecifically and induced deamination of adenine and guanine residues (142). Selective deamination of cytosine can be achieved using high concentrations of sodium bisulfite (~2 M) under acidic conditions (pH ~5) (100). The reaction proceeds by an acid-catalyzed addition-elimination mechanism, beginning with the addition of bisulfite across the 5,6 double bond of cytosine to form the reaction intermediate, 5,6-dihydrocytosine-6-sulfonate (100). This unstable intermediate undergoes hydrolytic deamination of the C4 amino group to produce 5,6-dihydrouracil-6-sulfonate. Elimination of bisulfite from the C6 position of 5,6-dihydrouracil-6-sulfonate ultimately generates uracil. At physiological pH and temperature, the sodium bisulfite-induced deamination rate for cytosine in single-stranded DNA was calculated to be 3.5×10^{-10} sec^{-1} as compared to 0.6×10^{-10} sec^{-1} for untreated DNA (42). When low levels of sodium bisulfite (10 mM) were used under physiologically relevant conditions, C→T transition mutations were detected (42). Under identical reaction conditions, the rate of cytosine deamination within a four-base target in a double-stranded DNA substrate ranged between 0.06×10^{-10} and 0.36×10^{-10} sec^{-1} and also showed a sequence context effect (43). Sequencing of revertants showed that all mutations were C→T point mutations and CC→TT tandem double mutations (43). The presence of tandem double mutations suggested that bisulfite-induced deamination can occur by a concerted mechanism

promoting deamination events between two neighboring cytosine residues, an event previously attributed to UV-damage (43). These events were found to be time and bisulfite concentration-dependent (43).

1.1.2.3 UV-induced Deamination of Cytosine

Ultraviolet (UV) irradiation (<300 nm) of DNA produces multiple cytosine photoproducts, including monomeric species such as cytosine hydrate (6-hydroxy-5,6-dihydrocytosine) and cytosine glycol (90, 199) and dimeric species such as cyclobutyl pyrimidine-pyrimidine dimers (C<>T, T<>C, C<>C) and the pyrimidine-pyrimidone 6-4 photoadducts (199). Although the quantum yield of cytosine photohydrates is lower (~1-2 %) than that of dimeric cytosine photoproducts, both lesions are potentially mutagenic when formed in DNA (166).

Cytosine hydrate is potentially mutagenic because it forms a base pair with thymine or cytosine rather than the complementary guanine during DNA replication (136). Cytosine hydrates are removed from *E. coli* and mammalian genomic DNA by the pyrimidine hydrate-DNA glycosylase activities of *E. coli* endonuclease III and the related mammalian homologue (4, 23). If left unrepaired, the intrinsic instability of this cytosine derivative for deamination can produce a uracil hydrate that forms a base pair with adenine during DNA replication (136). Elimination of a water molecule from uracil hydrates ultimately generates uracil (23). UV-induced cytosine hydrates were shown to persist in irradiated poly(dG-dC) for extended periods of time, resulting in the formation of uracil hydrate and uracil at neutral pH (24). A later study demonstrated that formation of uracil hydrate was greatest at acidic pH (pH 3.1>5.4>7.4) at 37°C and dehydration of uracil hydrate to uracil was a rare event (193). This result suggested that the mutagenic properties associated with UV-induced cytosine hydration is a consequence of its mispairing properties and its propensity to deaminate to the uracil hydrate.

The mode of UV-induced mutagenesis associated with cyclobutyl pyrimidine-pyrimidine dimers (CPDs) is a controversial issue and several models have been proposed. One model involves a misincorporation/bypass DNA synthesis reaction, involving replication across a UV lesion by DNA polymerase (28). In this model, an incorrect nucleotide is incorporated opposite the damage (usually adenine) and bypass replication fixes the mutation, precipitating C→T transitions (28). A sensitive bioassay system using the λ *cro* reporter gene in *E. coli* indicated that cytosine deamination in CPDs following UV-irradiation follows first order kinetics with a rate constant of 3.9×10^{-5} sec^{-1}, or a half-life of ~5 hours, and ~93 % of the mutations were C→T transitions (8). This half-life was increased to ~12 hours under physiological salt conditions (8). These results suggested that at least in *E. coli*, the rate of deamination of cytosine-containing dimers was too slow to contribute to UV-induced mutagenesis and suggested mutation fixation by a replication bypass mechanism (8).

The second model suggests that the high rate of cytosine deamination to uracil within CPDs results in a high degree of G•C→A•T transition mutations (201, 227, 240). Early studies demonstrated that cytosine residues in cyclobutyl pyrimidine-pyrimidine dimers could rapidly deaminate to form uracil (240). Irradiated poly dI:dC containing cytosine dimers was shown to deaminate to uracil with a half-life of ~2 hours at 37°C (240). By using a natural DNA substrate, the rate constant for cytosine deamination in a C<>C cyclobutane pyrimidine dimer was 1.5×10^{-6} sec^{-1}, corresponding to a half life of ~5 days (201). In a separate study, the deamination rate constants for cytosine in a C<>T dimer at two different sites were 5×10^{-6} and 11×10^{-6} sec^{-1} and corresponded to half-lives of 38 and 17 hours, respectively (67). Following deamination and subsequent photoreactivation of the uracil-containing dimer, accurate replication past the uracil could fix the C→T transition mutation by incorporation of an adenine opposite the uracil. This

model was later amended because the delayed appearance of C→T transition mutations in *E. coli* suggested that the DNA polymerase is blocked at cytosine-containing dimers (267, 268). Tessman and co-workers suggested that following deamination, however, the replication machinery was able to correctly replicate past the uracil-containing dimers (267, 268). Another study by Jiang and Taylor showed that UV-induced C→T mutations at pyrimidine dimer sites could be introduced by replicative bypass of cyclobutane dimers or their deaminated products (113).

1.2 Uracil-DNA Glycosylases

Uracil-DNA glycosylase is ubiquitously distributed in nature and provides the first catalytic step of the uracil-DNA BER pathway (38, 121, 135, 146). The catalytic mechanism of the enzyme involves hydrolysis of the *N*-glycosylic bond linking the uracil base to the deoxyribose phosphate backbone of DNA (146). The substrate specificity of uracil-DNA glycosylase includes removal of uracil residues that arise in DNA by dUMP incorporation or cytosine deamination in both prokaryotes and eukaryotes. The biological importance of this enzyme is underscored by its high degree of evolutionary conservation, as indicated by the ~56 % amino acid sequence homology between proteins isolated from *E. coli* and humans (196). These similarities suggest a degree of conservation that interrelates the structural and functional elements of this enzyme.

1.2.1 *Escherichia coli* Uracil-DNA Glycosylase

Uracil-DNA glycosylase (Ung) was the first DNA glycosylase to be discovered and was purified to apparent homogeneity from *E. coli* (146). As determined by hydrodynamic properties and sodium dodecyl sulfate polyacrylamide gel electrophoresis, the active monomeric enzyme was calculated to have a molecular weight of ~24,500 daltons (146). Subsequently,

the uracil-DNA glycosylase gene (*ung*) was cloned and overexpressed in *E. coli* to more than 100-fold above the levels in a wild-type cell (60). The open reading frame of the *ung* gene encoded a protein of 229 amino acids with a molecular weight of 25,664 daltons (284). N-terminal sequence analysis indicated that the N-terminal methionine residue was post-translationally removed, a phenomenon common to many prokaryotic proteins (284). Cloning and overexpression of large quantities of *E. coli* Ung have helped to enable a more complete characterization of its biochemical properties.

Uracil-DNA glycosylase does not require divalent metal ions or other cofactors for activity and catalyzes the hydrolytic removal of uracil from single-stranded DNA or double-stranded DNA containing U•A base pairs and U•G mispairs (16, 146). The reaction products following hydrolysis are free uracil and an apyrimidinic site in the DNA (146). Unlike dUMP in long stretches of DNA, free uracil is not hydrolyzed from RNA, dUMP, or deoxyuridine (146). *E. coli* Ung also catalyzes the removal of 5-fluorouracil from DNA (159) and the cytosine-derived oxidative DNA damage products, 5-hydroxyuracil and 5,6-dihydroxyuracil (95, 317). The modifying groups at the C5 or C6 position of these uracil base analogues apparently do not exclude binding in the uracil-binding pocket of the enzyme. However, larger modifying groups at the C5 position of uracil, such as those present on thymine, 5-methylcytosine, or 5-bromouracil, sterically hinder binding in the uracil-binding pocket and thus cannot be positioned for enzyme-catalyzed hydrolysis (143, 168).

Uracil-DNA glycosylase utilizes single-stranded DNA substrates ~2-fold more efficiently than double-stranded substrates (16, 146). On the subject of double-stranded DNA substrates, the enzyme preferentially excises uracil residues mispaired opposite guanine (U•G) ~2-fold more efficiently than uracil residues base paired opposite adenine (U•A) (16, 124, 286). The sequence context surrounding the uracil was found to be another important determinant for the rate of uracil removal from U•A base pairs or U•G

mispairs (192). For example, uracil removal from the consensus sequence 5'-(A/T)UA(A/T)-3' was ~17-fold greater than removal from the consensus sequence 5'-(G/C)U(T/G/C)-3' in an analysis that involved 70 different nucleotide sequences (192). In general, sequences that were GC-rich or contained a T located to the 3' side of U were poorly repaired although a few exceptions deviated from this rule (192). Good consensus sequences notably were AT-rich (192). Although Ung prefers single-stranded DNA substrates, excision of uracil from loop regions of hairpins was shown to be inefficient, probably because the conformation of the sugar-phosphate backbone is not conducive for efficient binding by the enzyme (124). This phenomenon might provide an explanation as to why some dUMP residues in single-stranded M13 DNA are poorly cleaved and result in areas of higher mutation frequency (51). In the presence of single-stranded DNA binding protein, the hairpin structures are melted and Ung can efficiently remove the uracil residue (125). Together, both sequence context and DNA structure potentially influence the efficiency of uracil excision which can directly impact the mutation frequency at specific sites in genomic DNA.

The K_m value for dUMP residues in DNA has been reported to be 40 nM and the turnover number of uracil-DNA glycosylase is ~800 uracil residues released per minute (146). Ung was shown to be noncompetitively inhibited by free uracil for single-stranded (K_i = 2 mM) and double-stranded (K_i = 0.12 mM) DNA substrates. A limited number of uracil derivatives, such as 6-aminouracil, 5-azauracil, and 5-fluorouracil but not deoxyuridine, dUMP, thymine, 5-bromouracil, 5-aminouracil, 2-thiouracil, and orotic acid, also inhibited the enzyme activity when tested at concentrations of 4 mM (146). Ung is competitively inhibited by its other reaction product, the AP site, at concentrations approximately 2-3 orders of magnitude lower than that of uracil (58).

Several studies have investigated the minimum substrate size required for DNA binding and catalysis by uracil-DNA glycosylase. Ung was shown to remove a 5'-terminal uracil residue from synthetic oligonucleotides only if

the 5'-end was phosphorylated (285). This suggested that amino acid residues near the active site pocket of the enzyme might specifically interact with the 5'-phosphate group of uracil in DNA during hydrolysis of the N-glycosyl bond. Oligonucleotides containing uracil at the 3'-terminus or at the second position from the 3'-OH end were not excised (285). However, a uracil residue in the second position from the 3'-terminus could be hydrolyzed if a 3'-PO_4 group was present, suggesting another important protein-DNA contact point required for efficient uracil removal (285). These results suggested that an oligonucleotide trimer with uracil located at the phosphorylated 5'-terminus provides the minimum substrate requirement for uracil excision by uracil-DNA glycosylase. A recent study demonstrated that the phosphodiester bond 3' to a deoxyuridine residue was crucial for substrate binding by uracil-DNA glycosylase (217). Together, these studies have provided initial information concerning potential contact points on a uracil-containing substrate involved in Ung binding or catalysis.

Several conflicting reports have addressed the mechanism by which uracil-DNA glycosylase locates and hydrolyzes the N-glycosylic bond at uracil target sites (16, 101, 216). A distributive mechanism for locating the next uracil residue following catalysis requires dissociation from the DNA and random three-dimensional diffusion whereas a processive mechanism is established when the enzyme remains bound to the DNA and locates sequential uracil residues by facilitated diffusion (18). Thus, a processive mechanism substantially increases the likelihood of locating the next uracil target due to decreased dimensionality in the search.

Higley and Lloyd (101) concluded that uracil-DNA glycosylase acted with partial processivity at ≤50 mM NaCl on a covalently-closed circular duplex uracil-containing DNA substrate when treated simultaneously with *E. coli* Ung and T4 endonuclease V. In these experiments, processivity was determined by measuring the conversion of Form I DNA to linear Form III DNA. Form III DNA was produced only following removal of closely spaced

uracil residues on opposite DNA strands followed by AP-site cleavage by T4 endonuclease V to produce two single-strand breaks. Significant accumulation of Form III DNA accompanied by unreacted Form I DNA was observed, which was indicative of a processive "search" mechanism. The processivity of Ung was also shown to decrease with increasing salt concentrations, a phenomenon observed for other processive DNA metabolizing enzymes (91, 266). However, the interpretation of these results was complicated due to the simultaneous use of T4 endonuclease V during Ung treatment of the substrate. As demonstrated previously, T4 endonuclease V is a processive enzyme (149)

Contrary to these observations, Purmal and co-workers proposed a distributive mode of action for uracil-DNA glycosylase (216). This study utilized a linear double-stranded concatemeric polynucleotide with deoxyuridine located at every 20th nucleotide along both DNA strands. Following incubation with Ung, apyrimidinic sites were thermally cleaved which eliminated the need for the T4 endonuclease V. A rapid accumulation of larger fragments (>20-mers) was taken to be indicative of a distributive mechanism. Their interpretation, however, was somewhat compounded since the uracil residues were closely spaced on both sides of the double-stranded concatemeric polynucleotide, the uracil targets were located in a poor consensus sequence (5'-CUT-3') for efficient catalysis, and the analysis was performed after significant levels of uracil (>95 %) had been hydrolyzed from the substrate as argued by Bennett *et al.* (16, 216).

Utilizing a concatemeric polynucleotide substrate with uracil residues located at intervals of 25 nucleotides on one DNA strand, Bennett, Sanderson, and Mosbaugh (16) demonstrated that both *E. coli* and rat liver mitochondrial uracil-DNA glycosylases located successive uracil residues by a processive mechanism in the absence of NaCl. These results were identical for both of the U•A- and U•G-containing DNA substrates and indicated that the nature of the uracil target site did not influence the search mechanism. At low ionic

strength, a rapid accumulation of 25-mers and reduced levels of larger fragments was observed, which suggested uracil-DNA glycosylase located sequential uracil residues by a processive "search" mechanism. The addition of NaCl (≥50 mM) reduced the processivity of the enzyme on both U•A- and U•G-containing substrates (16). These results were consistent with those previously reported by Higley and Lloyd (101).

1.2.2 Mammalian

1.2.2.1 Nuclear and Mitochondrial Uracil-DNA Glycosylase

In mammalian cells, active uracil-DNA glycosylase (UDG) has been isolated as a monomeric protein from both the mitochondria and the nucleus (3, 57, 92, 121, 305). Nuclear UDG has been purified from rat liver (57, 58), calf thymus (65, 260, 261), and human cells (121) and the mitochondrial form of the enzyme has been extensively purified from rat liver (57, 58). The biochemical properties of mammalian nuclear and mitochondrial UDGs are similar to those observed for prokaryotes. Both enzymes hydrolyze uracil from single-stranded DNA approximately 2-fold more efficiently than from double-stranded DNA (38, 57, 121, 135), with an approximate 2-fold preference for U•G mispairs over U•A base pairs (16, 286). Substrate specificity analysis has indicated that free uracil was not released from deoxyuridine and dUMP (57, 261). As demonstrated for *E. coli* Ung, both the nuclear and mitochondrial UDG were noncompetitively inhibited by uracil (38, 58, 135) and were competitively inhibited by apyrimidinic sites (58, 260). AP sites inhibited mitochondrial UDG at a concentration approximately 3 orders of magnitude lower than that of free uracil (1.2 μM versus 600 μM) (58).

Initial reports suggested that the nucleotide sequence surrounding dUMP residues in DNA were important for mammalian uracil-DNA glycosylase binding and/or recognition of dUMP as a substrate (58). It was later demonstrated that an approximate 10-fold difference in the rate of uracil

excision existed between different DNA sequence contexts utilizing calf thymus uracil-DNA glycosylase (65). Analysis of 40 different consensus sequences showed that efficient repair occurred within the DNA sequence 5'-(A/T)UA(A/T)-3' whereas inefficient repair was observed for the DNA sequences 5'-(G/C)UT-3' and 5'-(G/C)U(G/C)-3' (65). These good and poor consensus sequences were identical to those observed for *E. coli* Ung (65, 192). Since this DNA sequence phenomenon was not observed in single-stranded DNA, these results suggested that the stability provided by double-stranded DNA surrounding the dUMP residues influenced the rate of uracil release (65).

Mitochondrial and nuclear uracil-DNA glycosylase activities have been jointly isolated from few biological systems and characterization has been generally limited to partially purified preparations of each enzyme (92, 305). An extensive comparison of homogeneous preparations of nuclear and mitochondrial uracil-DNA glycosylase from rat liver indicated distinct differences in molecular weight and catalytic properties (57, 58). The nuclear and mitochondrial species of rat liver uracil-DNA glycosylase have apparent molecular weights of ~35,000 and ~24,000, respectively (57). These results are similar to those of other reports that suggested a high molecular weight (~30,000 to ~37,000) for the nuclear enzyme and a lower molecular weight (~18,000 to ~20,000) for the mitochondrial species (38, 92, 135, 305). For the rat liver nuclear uracil-DNA glycosylase, the apparent K_m for uracil in DNA was reported to be 0.5 μM with a turnover rate of ~10 uracil residues per minute (58). In contrast, the rat liver mitochondrial uracil-DNA glycosylase was shown to have an apparent K_m for uracil in DNA of 1.1 μM with a turnover number of ~1000 uracil residues hydrolyzed per minute (58). Despite these differences, the relatedness of the mitochondrial and nuclear enzymes was demonstrated by antibody cross-reactivity which suggested that the two enzymes shared similar polypeptide domains (181, 249, 250). Immunofluorescence studies also demonstrated a similar relationship in which the *UNG* gene product was shown to be translocated to both the

nuclear and mitochondrial compartments (181, 250). Mitochondrial translocation was dependent on the N-terminal 77-amino acid UNG presequence (250). These observations were explicated after it was discovered that both nuclear and mitochondrial enzymes were encoded by the same *UNG* gene (96, 191).

The full length human uracil-DNA glycosylase gene (*UNG*) has been isolated and cloned (191, 196). The gene consists of seven exons that encode a nuclear (UNG2) and a mitochondrial (UNG1) form of uracil-DNA glycosylase (191). The gene spans a region of approximately 13.5 kb and is located on chromosome 12q23-q24.1 as determined by radiation hybrid mapping (97). The mRNAs for both forms are generated from the *UNG* gene by alternative transcription start points and alternative splicing (191). Promoter P_A is utilized to produce an mRNA transcript encoding UNG2 and requires splicing of exon 1A into a consensus splice site located after codon 35 of exon 1B (191). Promoter P_B initiates transcription of the UNG1 mRNA beginning at codon 1 of exon 1B and does not require alternative splicing (191). Thus, UNG2 (313 amino acids) differs from UNG1 (304 amino acids) in the first 44 amino acids of the N-terminus which are required for nuclear and mitochondrial import, respectively (191). The remaining 269 amino acids are identical between both species and constitute the catalytic domain of the enzyme (191). This structural organization suggests that signals exist in the divergent N-terminal regions of UNG1 and UNG2 in order to direct each protein to its respective subcellular location.

A recent study has corroborated the presence of multiple forms of uracil-DNA glycosylase (UNG1 and UNG2) in HeLa cells that are either translocated to the mitochondria (UNG1) or the nucleus (UNG2) (178). To investigate the signals involved in sub-cellular targeting, the N-terminal regions of UNG1 (77 amino acids) and UNG2 (86 amino acids) were used to create fusion proteins with a variant of green fluorescent protein (GFP) and were shown to localize to the mitochondria and nucleus, respectively (178). Deletion mutation analysis studies indicated that the first 20 amino acids of

UNG2 contain the nuclear localization signal necessary for nuclear targeting (178). Interestingly, purified UNG2 migrated as a group of at least three proteins in the 35,000 to 37,000 molecular weight range when analyzed by SDS-polyacrylamide gel electrophoresis (178). Transfection of the UNG1/GFP and UNG2/GFP constructs (containing the N-terminal regions of UNG1 and UNG2, respectively) into NIH 3T3 cells in the presence of [^{32}P]orthophosphate demonstrated that UNG2 is differentially phosphorylated on serine and threonine residues whereas UNG1 is unphosphorylated (178). The significance of *in vivo* phophorylation of UNG2 is unknown at present but such phosphorylation might modulate enzymatic activity or protein-protein interactions.

Early studies of cultured human cells demonstrated that the expression of uracil-DNA glycosylase was regulated during the cell cycle (93, 252, 311). This regulation was shown to occur at the transcriptional level (252). In synchronized human fibroblasts, transcription of the *UNG* gene was upregulated 8-12-fold in the late G1-phase and led to a 2-3-fold increase in total uracil-DNA glycosylase activity in the early S-phase (252). A corroborating study demonstrated that uracil-DNA glycosylase activity in the G2-phase was ~2.8-fold greater than that detected in early G1-phase (181). Analysis of the P_B promoter region of the *UNG* gene demonstrated the presence of an E2F element, which is known to be involved in cell cycle regulation of several genes induced in late G1-phase (98, 189). Additional cell-cycle regulation elements, such as c-Myc and Yi, are also located in the P_A and P_B promoter regions of the human *UNG* gene (98). Levels of both UNG2 and UNG1 mRNA transcripts have been shown to be increased in late G1-phase/early S-phase and were accompanied by an approximate 4-5-fold increase in uracil-DNA glycosylase activity (96). Thus, the coordinated expression of the uracil-DNA glycosylase gene and translation of the gene product relative to the S-phase implicates its importance in maintaining the genetic integrity of the genome prior to DNA replication.

Crystal structure and mutational analysis of human (117, 167, 168, 251) and herpes simplex virus type-I (197, 235) uracil-DNA glycosylases have helped elucidate the DNA binding properties and catalytic mechanism for the enzyme. The structure of human uracil-DNA glycosylase is closely related to that of the herpes simplex virus type-I enzyme and consists of a single α/β catalytic domain composed of a central four-stranded parallel and twisted β-sheet surrounded by eight α-helices (168). Sequence-conserved amino acids within and around the UDG α/β fold create an active-site groove, with an area of positive electrostatic potential, approximately equal to the diameter of a DNA double helix (168, 251). The location of the uracil-binding pocket, deep in the active-site groove, necessitates that the enzyme recognizes uracil that is extrahelical or "flipped out" from the double-stranded DNA helix (168). Structural data of the enzyme complexed with the free uracil analog base, 6-aminouracil, has indicated that the C2, N3, and C4 positions of uracil interact through hydrogen bonds with conserved active-site residues (Asn-204, Tyr-147, and Phe-158) that form part of the uracil-binding pocket (168). These hydrogen-bonding requirements are not achieved with cytosine so hydrolysis of the N-glycosidic bond of cytosine does not occur (117, 168). The side chain of Tyr-147 also helps to create a rigid pocket which discriminates against bases substituted at the C5 position, such as thymine (168). Mutations at either Asn-204 (Asn204Asp) or Tyr-147 (Tyr147Ala, Tyr147Cys, and Tyr147Ser) perturbed ordered interactions within the uracil-binding pocket that normally provide specific contacts for uracil-recognition and have resulted in mutant enzymes that hydrolyze cytosine or thymine from DNA, respectively (117). These studies have helped elucidate the structural mechanism by which uracil-DNA glycosylase recognizes uracil in preference to the normal pyrimidines in DNA.

Mutational studies of the uracil-binding pocket of human mitochondrial UNG1 (lacking the 84 N-terminal amino acids) have been conducted in order to understand the biochemistry of uracil release (168).

Four amino acid residues (Asn-204, Gln-144, Asp-145, and His-268) are absolutely required for catalysis (168). His-268 has been implicated in catalysis and uracil recognition (168, 251). Two different mechanisms for uracil hydrolysis by human uracil-DNA glycosylase have been proposed (168). His-268 potentially could act as the active-site nucleophile (general base) for cleavage of the N-C1' glycosylic bond and form a transient covalent enzyme-DNA intermediate between the imidazole group of His-268 and the C1' of the deoxyribose. Displacement of the uracil followed by hydrolysis of the transient covalent intermediate would produce free uracil and an AP site in the DNA (168). Alternatively, hydrolysis of the N-C1' bond could be achieved by activation of a water molecule through His-268 acting as a general base (168). Site directed mutagenesis of Ser-270 suggested an important role for an interaction with the 3' DNA sugar-phosphate backbone, necessary for stabilizing the imidazole group of His-268 to achieve catalysis (168).

DNA-binding and kinetic analysis of wild-type and mutant uracil-DNA glycosylases indicated that the Leu-272 residue plays an active role in uracil recognition and base flipping (168, 251). Structural analysis of human uracil-DNA glycosylase complexed with uracil-containing double-stranded DNA has identified five components for uracil recognition and catalysis which has been described as a "push and pull" mechanism (251). (1) Shape and electrostatic charge complementarity properly orients DNA into the active-site groove of the enzyme. (2) Upon encountering a uracil residue, insertion of the side chain of Leu-272 into the DNA minor groove facilitates flipping ("pushing") of the uracil base out of the major groove. This is accompanied by conformational changes in the Leu-272 loop that promote the formation of a stable protein-DNA complex. (3) Specific contacts with the DNA sugar-phosphate backbone compresses the DNA to help stabilize the extrahelical uracil residue. (4) The substrate specificity pocket of the enzyme establishes required uracil-recognition contacts with the uracil base, the deoxyribose sugar, and phosphate groups ("pulling") and aligns the residue for final productive binding. (5) Polarization of the uracil-deoxyribose N-C1' bond by

active-site residues promotes hydrolysis of the N-glycosyl bond. Thus, nucleotide flipping is the established mechanism by which uracil-DNA glycosylase recognizes uracil residues within duplex DNA.

1.2.2.2 Cyclin-like Uracil-DNA Glycosylase

A human cDNA encoding a uracil-DNA glycosylase of ~36,000 molecular weight has been isolated and cloned (176). The amino acid sequence of the cloned DNA showed limited homology with other uracil-DNA glycosylases, including those isolated from *E. coli* (284) and both of the mitochondrial and nuclear species isolated from human cells (191, 196). However, significant similarity was shown to exist with the cyclin A protein family (25-30 % identity and 51 % similarity) (177). Thus, the enzyme has been called cyclin-like uracil-DNA glycosylase. Transcription and translation of this cDNA *in vitro* apparently generated uracil-DNA glycosylase activity (176). Unfortunately, the biochemical characterization and substrate specificities of this enzyme at present are relatively incomplete. Uracil-DNA glycosylase activity is routinely assayed by using U•A base pair-containing native PBS2 [^{3}H]DNA (176) or [^{3}H]uracil-containing calf-thymus DNA (179) as substrates.

The gene encoding the cyclin-like uracil-DNA glycosylase spans 4.2-kb and is composed of 2 exons (177). Sequence analysis of the genomic DNA indicated a 1.4-kb upstream promoter region that lacks TATA and CAAT boxes but contains an AP2 consensus sequence, which mediates transcriptional activation in response to phorbol esters and cAMP. In addition, two inverted SP1 consensus sites have been identified that might be involved in mediating basal constitutive expression (177). Furthermore, a consensus CCB element and an inverted CCB element are present within the promoter region and could potentially be recognized as a "half-site" by the transcriptional regulator, E2F (177). Deletion of an SP1-like binding site and an inverted CCB element within the promoter region (nucleotides -812 to -

603) suggested this region was responsible for inhibition or repression of transcription (177). Analysis of the cyclin-like uracil-DNA glycosylase gene expression as a function of the cell cycle indicated that mRNA levels increased 3- to 4-fold during G_1 phase and was accompanied by elevated levels of uracil-DNA glycosylase protein as determined by an immunoprecipitation assay (177). Complete turnover of the enzyme was observed during the course of one cell cycle (177).

Affinity-purified uracil-DNA glycosylase from HeLa cell extracts initially suggested that the cyclin-like uracil DNA glycosylase (termed UDG2 in this study) was the major uracil-DNA glycosylase activity associated with the nucleus (36). Immunostaining with antibodies for the highly conserved uracil-DNA glycosylase (termed UDG1 in this study) indicated it was not associated with the uracil-DNA glycosylase activity detected in nuclear extracts and thus was likely associated with the mitochondria (36). However, earlier work by Slupphaug and co-workers suggested that both the mitochondrial and nuclear forms of the enzyme were encoded by the same gene (*UNG*) and post-translationally processed for subcellular targeting (249, 250). In fact, antibodies raised against the human recombinant uracil-DNA glycosylase eliminated >98 % of the total uracil-DNA glycosylase activity in HeLa cell extracts, indicating that the *UNG* gene encoded both the mitochondrial and nuclear forms of the enzyme (249). A recent study has demonstrated that nuclear uracil-DNA glycosylase obtained from HeLa cell nuclear extracts has a unique 44-amino acid N-terminus and a C-terminal region that is identical to the catalytic domain of uracil-DNA glycosylase encoded by the *UNG* gene (178). Since the protein sequence analysis did not confirm the identity of the cyclin-like uracil-DNA glycosylase, it appears that the major nuclear uracil-DNA glycosylase is encoded by the *UNG* gene as originally reported by Nilsen and co-workers (191).

1.3 Other Enzymes with UDG Activity

1.3.1 Thymine-DNA Glycosylase

Correction of G•T mispairs to G•C base pairs in DNA following the deamination of 5-methylcytosine involves excision of the thymine residue by thymine-DNA glycosylase (TDG) (29, 301). This activity was originally identified in simian cell extracts and later confirmed as a glycosylase activity in human cell extracts. Purification of the mismatch-specific TDG activity from HeLa cell extracts identified a 55,000 molecular weight protein capable of hydrolyzing the N-glycosyl bond between the sugar-phosphate backbone and a mispaired thymine opposite guanine, cytosine, and thymine in the order G•T>>C•T>T•T (185, 298). No detectable endonucleolytic/lyase activity toward apyrimidinic sites or 5'-terminal deoxyribophosphate moieties was observed (185). Interestingly, TDG was also shown to excise uracil from a G•U mispair but not from an A•U base pair or uracil-containing single-stranded DNA (186). Band-shift experiments demonstrated that thymine-DNA glycosylase had a higher affinity for double-stranded oligonucleotides containing a G•U mispair than for those containing G•T mispairs (186). Activity assays demonstrated that uracil was removed from G•U mispairs more efficiently than thymine was removed from G•T mispairs (186). Thus, aside from counteracting the mutagenic potential of 5-methylcytosine deamination events within CpG dinucleotide repeats, the uracil-DNA glycosylase activity of TDG might also function to remove uracil residues that accumulate as a result of cytosine deamination (186). Since uracil residues within a sequence context area rich in guanine and cytosine nucleotides are poor substrates for mammalian uracil-DNA glycosylase (65), it has been suggested that thymine-DNA glycosylase could perform this duty more efficiently and in place of uracil-DNA glycosylase (186).

The human cDNA for thymine-DNA glycosylase has been cloned and contains an open reading frame encoding a 410-amino acid polypeptide (184). Expression of the cDNA in rabbit reticulocyte lysates and in *E. coli* yielded a polypeptide with an apparent molecular weight of 60,000 that possessed the same enzymatic activities and substrate specificities as thymine-DNA glycosylase purified from HeLa cells (184, 186). Amino acid sequence analysis did not reveal any regions of sequence homology between the recombinant TDG and other characterized human DNA glycosylases (184). However, the core region is homologous (30 % sequence identity) to a mismatch-specific uracil-DNA glycosylase identified in *Escherichia coli* (80).

With respect to sequence context specificities, recombinant TDG was shown to preferentially hydrolyze thymine from G•T mispairs within a CpG dinucleotide but also processed thymine residues mispaired opposite O^6-methylguanine (m6G) (184) or S^6-methylthioguanine (298). A detailed analysis of the substrate specificity of the recombinant thymine-DNA glycosylase confirmed that G•T mispairs in a CpG context were incised at an efficiency that was 3- to 12-fold greater than that observed for TpG, GpG, and ApG sequence contexts (246). The rate of incision was greatest for G•T mispairs (0.7 fmol/min) followed by m^6G•T mispairs (0.38 fmol/min) and then 2-amino-6-(methylamino)purine•T mispairs (0.15 fmol/min) (246). This was consistent with the proposal that the primary role of the enzyme involves repairing G•T mismatches that arise through the deamination of 5-methylcytosine. Recent evidence indicated that the highly mutagenic adduct, 3,N^4-ethenocytosine, was also processed by the enzyme (234).

A recent study has measured the kinetics of the action of TDG on G•T and G•U mispairs (298). In this report, the 5' flanking base pair next to the G•T mispair influenced the rate of thymine removal with k_{cat} values of 0.91, 0.023, 0.0046, and 0.0010 min^{-1} for the consensus sequences CpG, TpG, GpG,

and ApG, respectively (298). In addition to removing uracil from G•U mispairs, thymine-DNA glycosylase was shown to hydrolyze uracil from other uracil-containing mispairs in the order G•U>C•U> T•U>> A•U although the k_{cat} values for uracil hydrolysis from these substrates were not measured (298). The rate of uracil hydrolysis from an A•U base pair was observed to be extremely slow. The k_{cat} value for uracil hydrolysis from double-stranded DNA by the mismatch-specific uracil-DNA glycosylase, a homologue of thymine-DNA glycosylase, was measured at 0.4 min^{-1} (9). The k_{cat} value for the removal of uracil in double-stranded DNA by human uracil-DNA glycosylase was measured at 2500 min^{-1} (117). Interestingly, the enzyme was found to bind tightly to apyrimidinic sites following thymine hydrolysis and limited each thymine DNA glycosylase molecule to one hydrolysis event (298). Sibghat-Ullah and co-workers previously observed a limited level of TDG activity and attributed this phenomenon to enzyme inactivation (246). Although the physiological significance of this AP-site inhibition is unknown at present, it is possible that *in vivo*, the bound glycosylase could nucleate other enzymes involved in the base excision repair process to facilitate efficient repair (298). Alternatively, the bound glycosylase might act to block replication past a potentially mutagenic AP site, a model that was previously proposed for AP-site inhibition of uracil-DNA glycosylase (58).

Transition state destabilization studies using nonhydrolyzable uracil analogs that preserve TDG binding to the substrate but prevent excision have been conducted (238). The results of these experiments suggested that the enzyme contacts a guanine base on the 3' side of the mismatched residue in the 5'-CpG-3'/3'-GpU-5' sequence context (238). Methylation interference analysis suggested that the G residue mismatched opposite U was not contacted at the N7 position (238). Thymine mispaired opposite O^6-methylguanine or 2-amino-6-methylaminopurine are efficiently hydrolyzed, suggesting that the 6- and perhaps the 1-position of guanine are also not contacted by the enzyme (246). Since the 6- and 7-positions of guanine are

located in the major groove, it has been suggested that the enzyme recognizes mismatched guanine residues through interactions in the minor groove (238). At present, there is no published structural information for human thymine-DNA glycosylase, although some comparisons have been made with the structure of the mismatch-specific uracil-DNA glycosylase purified from *E. coli* (9).

1.3.2 Mismatch-Specific Uracil-DNA Glycosylase

A class of uracil-DNA glycosylases that specifically recognize uracil residues in double-stranded DNA has been identified in *E. coli* (80). The *E. coli* enzyme has strong amino acid sequence homology to the core region of human thymine-DNA glycosylase enzyme (80). To distinguish this enzyme from the ubiquitous class of uracil-DNA glycosylase, it has been named mismatch-specific uracil-DNA glycosylase (MUG) (9). The bacterial cDNA has been cloned and contains an open reading frame encoding a 169-amino acid polypeptide. Expression of the cDNA in *E. coli* or rabbit reticulocyte lysates produced a polypeptide that could hydrolyze uracil from G•U mispairs but not thymine from G•T mispairs (80). *E. coli* MUG was also found to be inactive on uracil in U•A base pairs and in single-stranded DNA (80). In an attempt to co-crystallize purified recombinant MUG with a G•T mispair-containing DNA substrate, very high concentrations of the enzyme were observed to hydrolyze the mismatched thymine residue. This suggested that MUG was a dual uracil/thymine-DNA glycosylase (9).

The crystal structures of *E. coli* MUG alone and in complex with AP site-containing duplex DNA have recently been determined (9). Interestingly, *E. coli* MUG shares several structural elements with HSV-1 and human UDGs, even though significant regions of amino acid sequence homology do not exist between these two classes of glycosylases (9, 168, 235). The core of the enzyme consists of a central five-stranded β-sheet surrounded by α-helices

and a distinct DNA-binding groove with an area of high positive electrostatic potential (9). This groove is connected to a pocket that penetrates into the core of the enzyme (similar to that observed in human and HSV-1 UDGs), suggesting that MUG might employ a nucleotide-flipping mechanism for uracil removal when bound to DNA (9). The MUG uracil-binding pocket appears similar to those of both human and HSV-1 UDG and defines the substrate specificity of the enzyme. On one face of the binding pocket, the side chain of Phe-30 (corresponding to human UDG Phe-158 and HSV-1 UDG Phe-191 (283)) has been proposed to provide π-π stacking interactions with uracil, as previously observed in UDG-base complexes (168, 235). On the opposite face and along one edge of the pocket, the MUG sequence GINPG (residues 16-20) displays significant homology to the human UDG sequence GQDPY (residues 143-147) and the HSV-1 UDG sequence GQDPY (residues 176-180) (9, 168, 235, 283). For both human and HSV-1 UDG, base selection against thymine is provided by the tyrosine side chain side in the GQDPY sequence (Tyr-147 from human UDG and Tyr-180 from HSV-1 UDG) and is proposed to involve steric exclusion of the methyl group at the C5 position of thymine (168, 235, 283). The corresponding side chain (Gly-20) of *E. coli* MUG does not allow for this selection (9). Thus, MUG is able to hydrolyze this base but only at extremely high concentrations of enzyme (9). Both classes of glycosylase do provide a mechanism for the prevention of cytosine hydrolysis on the basis of specific hydrogen bonding interactions within the catalytic pocket (9, 168, 235). Thus, the mechanism of substrate recognition by *E. coli* MUG depends on the structural features of the uracil-binding pocket in a manner similar to that proposed for uracil-DNA glycosylase.

The proposed catalytic mechanism of MUG involves nucleophilic attack of the N-glycosidic bond by a water molecule poised between a main chain carbonyl group and the amide side chain of Asn-18 (9). However, abstraction of a proton to activate the water molecule to a hydroxyl ion by a general-base mechanism cannot be provided by the amide side chain of Asn-

18 (9). This results in a weakly nucleophilic water molecule. Additionally, the catalytic histidine present in UDG (His-210 in HSV-1 UDG and His-268 in human UDG), which protonates the O2 of the bound deoxyuridine to promote hydrolysis, is replaced by an arginine in *E. coli* MUG and a methionine in human TDG (9). Neither one of these residues can act as a general acid. Thus, the MUG/TDG enzymes cannot initiate general base or general acid-catalyzed hydrolysis and instead most likely relies on weak nucleophilic attack by a coordinated water molecule (9). This may explain the several order of magnitude slower rate of uracil excision by *E. coli* MUG as compared to human UDG (9).

Unlike uracil-DNA glycosylase, MUG has an absolute requirement for double-stranded DNA since substrate recognition relies on interactions with the complementary strand (9). In the MUG•DNA co-crystal, hydrogen bonds are maintained between the enzyme and five phosphate groups of the uracil-containing DNA strand, including the phosphate groups immediately 3' and 5' to the "flipped-out" uracil residue (9). The gap in the double-stranded helix left by the extrahelical uracil residue appears to be occupied by a "wedge" formed by Gly-143, Leu-144, and Arg-146 of the enzyme (9). This structure provides a similar function to that observed for the conserved leucine "loop" of UDGs (251). In both cases, this "wedge" enters the DNA base stack via the minor groove (9). The MUG enzyme makes three absolutely specific hydrogen bonds with the guanine residue after the uracil is "flipped-out" into the active-site binding pocket (9). These specific interactions would purportedly provide the enzyme with a strand discriminatory mechanism (9). It has also been proposed that although thymine from a T•A base pair or uracil from a U•A base pair can fit into the active-site binding pocket, the unpaired adenine residue does not provide the three required hydrogen bonds that stabilize the extrahelical base for hydrolysis (9). These interpretations provide an attractive model for the structural and mechanistic basis of G•U/G•T mismatch specificity.

1.3.3 Glyceraldehyde-3-phosphate Dehydrogenase

A human uracil-DNA glycosylase cDNA isolated from human placenta was reported to direct the synthesis of a fusion protein that exhibited uracil-DNA glycosylase activity (162). The gene product was a protein of 335 amino acids and did not exhibit amino acid sequence homology with either *E. coli* Ung or human UNG1 or UNG2 (162). However, nucleotide sequence analysis revealed complete homology with the 36,050-kDa subunit of human glyceraldehyde-3-phosphate dehydrogenase (GAPDH) (162). Human erythrocyte GAPDH reportedly contains uracil-DNA glycosylase activity but only after subunit dissociation of the tetrameric form (162). This required purifying monomeric GAPDH by SDS-polyacrylamide gel electrophoresis followed by electroelution from the gel slice and renaturation. Some caution must be noted since human nuclear uracil-DNA glycosylase (UNG2) also migrates at a molecular weight of about 36,000 and potentially could have been a contaminant in the GAPDH preparation. Characterization of the biochemical properties and substrate requirements of the glyceraldehyde-3-phosphate dehydrogenase (GAPDH)/uracil-DNA glycosylase (UDG) gene product are relatively incomplete. Uracil-DNA glycosylase activity is routinely assayed by using a poly (dA•[^{3}H]dU) substrate (162). In order to determine the relative efficiency of uracil removal by GADPH, purified GAPDH protein (1.5 μg) was assayed by using poly (dA•[^{3}H]dU) as a substrate and was shown to exhibit 0.565 units of uracil-DNA glycosylase activity (10). Based on these results, the specific activity of GAPDH was calculated to be ~377 units/mg of GAPDH. However, the unit definition used in this study to define the specific activity of GAPDH was 1000-fold lower than that normally used to define that of *E. coli* Ung. In order to make the direct comparison, the specific activity of GAPDH was corrected according to the *E. coli* unit definition. The specific activity of GAPDH was re-calculated as 0.377 units/mg and compared to the specific activity of 2×10^6 units/mg defined for

E. coli Ung. Thus, the specific activity of GAPDH is ~5.3 x 10^6-fold lower than that of *E. coli* uracil-DNA glycosylase. Several investigators have reported an inability to detect uracil-DNA glycosylase activity associated with GAPDH purified from human erythrocytes (36, 190, 232, 249). These results suggest that either GAPDH is a highly inefficient enzyme or the purified GAPDH preparation examined by Sirover and co-workers (159) may have been contaminated with uracil-DNA glycosylase.

1.4 Bacteriophage PBS2 Uracil-DNA Glycosylase Inhibitor Protein

1.4.1 Bacteriophage PBS2

Bacillus subtilis bacteriophages PBS1 and PBS2 are unique because their double-stranded genomic DNA naturally contains uracil in place of thymine residues (259). Nucleotide analysis of PBS1 and PBS2 DNA have indicated that the guanine plus cytosine (G+C) content represent ~28 % of the genome whereas the adenine plus uracil (A+U) content constitute the remaining ~72 % (108, 259). Following bacteriophage infection, the expression of several early gene products facilitates the incorporation of uracil into the replicating phage DNA by a phage-induced DNA polymerase (212). Induction of dUMP kinase (115), dTMP phophohydrolase (213), and dCTP deaminase (273) activities in addition to inactivation of the host dUTPase activity (214) act collectively to increase the intracellular dUTP pool while decreasing the dTTP pool. Preservation of the bacteriophage uracil-DNA genome is facilitated by a phage-encoded inhibitor of the host uracil-DNA glycosylase (74).

1.4.2 PBS2 Uracil-DNA Glycosylase Inhibitor

The PBS2 phage-encoded uracil-DNA glycosylase inhibitor (Ugi) protein was originally purified from crude extracts of PBS2-infected *B. subtilis* and characterized as a heat-stable, acidic protein of ~18,500 molecular weight, as determined by gel-filtration chromatography (46). Ugi was demonstrated to

specifically inhibit uracil-DNA glycosylases isolated from a diverse spectrum of biological species, including *Escherichia coli, Micrococcus luteus, Saccharomyces cerevisiae,* herpes simplex virus types 1 and 2, rat liver (nuclear and mitochondrial), human placenta, and human KB cells, but was inactive against DNA glycosylases specific for 3-methyladenine, 2,6-diamino-4-hydroxy-5-(*N*-methylformamido)pyrimidine, or hypoxanthine (116, 292, 304). In retrospect, this would be expected since the amino acid sequence of uracil-DNA glycosylase has conservatively evolved (~40-56 % identical residues) between phylogenetically diverse species (196, 283) and shows no homology with other classes of DNA glycosylases (284). To specifically address uracil-DNA glycosylase activities in human cells, it has been demonstrated that Ugi inhibits the nuclear (167), mitochondrial (292), and cyclin-like (36) uracil-DNA glycosylase enzymes. In contrast, human erythrocyte glyceraldehyde-3-phosphate dehydrogenase has not been found to bind Ugi, and neither HeLa nor recombinant thymine-DNA glycosylase have been shown to be inhibited by Ugi (80, 186).

The PBS2 *ugi* gene has been cloned and expressed in *E. coli* (291). Expression of the *ugi* gene was found to reduce *E. coli* uracil-DNA glycosylase activity by ≥14,000-fold but did not alter growth rate. *E. coli* that produced Ugi also had a 10-fold-higher spontaneous mutation rate, and supported productive infection of uracil-containing M13mp19 phage (291). These physiological properties are consistent with those observed for *E. coli ung* mutants (62). The complete nucleotide sequence of the *ugi* gene has been determined and encodes a highly acidic polypeptide (pI=4.2) of 9,477 daltons (84 amino acids) (15, 292). Previous studies had determined that the inhibitor had a molecular weight of 18,500 daltons, suggesting that Ugi might exist as a homodimer in solution (46, 291). However, mass spectrometry and sedimentation equilibrium centrifugation studies demonstrated that Ugi exists as a monomeric protein of ~9,475 daltons, which was in excellent agreement with the deduced amino acid sequence of the cloned *ugi* gene (15).

Finally, Ugi was observed to migrate anomalously as an ~3,500 molecular weight protein during 20 % SDS-polyacrylamide gel electrophoresis (288). Inconsistent molecular weight determinations among various analytical techniques may have resulted from the extreme acidic nature, heat stability, and/or unusual structural configuration of the inhibitor protein (15).

The secondary and tertiary structures of Ugi were determined by solution state multidimensional nuclear magnetic resonance (7, 12). Secondary structural features include two α-helices and five β-strands arranged contiguously as α1-β1-α2-β2-β3-β4-β5 to form an antiparallel β-sheet. The inhibitor protein contains 12 glutamic acid and 6 aspartic acid residues. Seven acidic amino acid residues (Glu-38, Asp-40, Glu-49, Asp-52, Asp-61, Glu-64, Glu-78), not directly involved in secondary structural elements, appear in small loop or turn regions that sequentially connect the β-strands. In addition, four of the β-strands contain terminal acidic residues (Glu-20, Asp-48, Glu-53, Asp-74). The remaining seven negatively charged residues are located in either the α1-helix (Asp-6, Glu-9, Glu-11) or the α2-helix (Glu-27, Glu-28, Glu-30, Glu-31). The α2-helix is partitioned into a hydrophobic face and a charged face where the four glutamic acid residues project (12).

Several unique features of Ugi suggest that the negatively charged amino acids of the Ugi protein play an important role in mediating the Ung/Ugi interaction. First, the overall electronegative potential of the Ugi protein, engendered by its high (21 %) Glu and Asp content, is quite unusual (15, 292). Second, the NMR structure shows that 11 of the 18 Glu and Asp residues terminate the β-strands or are located in the more flexible loops in a nonrandom distribution (7). Third, the tertiary structure brings together seven of these residues (Glu-20, Asp-48, Glu-49, Asp-52, Glu-53, Asp-74, and Glu-78) into close proximity on one surface of the Ugi protein, forming a unique structural element (12). The negative electrostatic potential of this

region is >6.6 kcal, similar to that generated by the phosphate backbone of DNA (12). Fourth, both the α1 and α2 helices contain regions with similar high electronegative potential (12). Involvement of these negatively charged amino acids in Ung•Ugi complex formation have been specifically addressed by selective chemical modification techniques and site-directed mutagenesis studies (152, 231).

The *ugi* gene from bacteriophage PBS1 has been cloned and reported to have an identical nucleotide sequence to that previously documented for the *ugi* gene cloned from bacteriophage PBS2 (236). By inference, this indicated that the PBS1 and PBS2 Ugi primary amino acid sequences should also be identical. However, several discrepancies existed between the deduced amino acid sequence reported for PBS1 Ugi (237) and that reported for PBS2 Ugi (292). Savva and Pearl (237) have stated that the X-ray crystal structure of PBS1 Ugi, observed in the Ung•Ugi complex with HSV-1 uracil-DNA glycosylase, consisted of 83 amino acid residues as would be expected if the N-terminal Met was removed from an 84 amino acid polypeptide. However, the reported amino acid sequence of PBS1 Ugi contained only 82 amino acids, including three amino acid substitutions (237). These amino acid substitutions in PBS1 Ugi relative to PBS2 Ugi included Glu-30→Ala-30, Glu-38→Gly-38, and Lys-66→Gly-66. The smaller size of the PBS1 Ugi was explained by an amino acid deletion of Asn-35. Contrary to the published amino acid sequence of PBS1 Ugi (237), the amino acid spatial coordinates of PBS1 Ugi obtained from the "UDI Protein Data Bank Full Table Release" database indicated complete amino acid sequence homology between PBS1 and PBS2 Ugi. Thus, the discrepancies in the literature for PBS1 must be incorrectly reported and PBS1 and PBS2 Ugi are identical proteins.

1.4.3 Mechanism of Uracil-DNA Glycosylase Inhibitor Action

Ugi physically associates with *E. coli* uracil-DNA glycosylase (25,664 daltons) to form a complex of ~35,400 molecular weight that was shown to be essentially irreversible under physiological conditions (15, 292). Free Ugi was unable to exchange with Ugi bound in a preformed Ung•Ugi complex, emphasizing the stability of this interaction (17). The Ung•Ugi complex exhibited a 1:1 stoichiometry of enzyme to inhibitor protein (15). Recovery of Ung and Ugi from a dissociated complex following urea treatment/SDS-polyacrylamide gel electrophoresis revealed that the mechanism of inhibitor action involved protein binding only and did not involve covalent protein modification as a mode of inhibition (15). The association of Ugi with Ung prevented enzyme binding to DNA and also dissociated an Ung•DNA complex, suggesting that Ugi binds at or near the DNA binding site of the enzyme (15, 17). Several other observations have supported this interpretation: (i) photochemical cross-linking of Ung to single-stranded oligonucleotide dT_{20} prevented Ugi binding to Ung (14); (ii) inclusion of Ugi in UV-induced cross-linking reactions prevented formation of the Ung x dT_{20} cross-link (14); and (iii) X-ray crystallographic studies of Ugi complexed to the human (167, 168) and herpes simplex virus type-I (237) uracil-DNA glycosylases revealed that Ugi binds within the DNA binding domain of the enzyme and mimics the structure of DNA.

Stopped-flow kinetic analysis have indicated that the association of Ugi with Ung involves a two-step kinetic mechanism (17). The first step is initiated by a reversible Ung/Ugi interaction to form a precomplex, distinguished by a dissociation constant (K_d) of 1.3 μM. The second step results in the formation of the final irreversible Ung•Ugi complex characterized by the rate constant k=195 sec^{-1}. Thus, complex formation involves a preliminary "docking" step followed by a "locking" reaction through which the two proteins achieve optimal alignment and become very

tightly bound. The slower transition to the locked configuration suggests that one or both proteins experience a conformational change in structure (17). Inhibition of Ung occurs, since the Ung•Ugi complex fails to recognize the DNA substrate (15, 17).

1.4.4 Structure of UDG-Ugi Complex

The X-ray crystal structures of Ugi complexed with human placental (167) and HSV-1 (237) UDGs have been determined. The structures of human (251) and HSV-1 (235) UDG in complex with Ugi exhibit minor structural changes when compared to the X-ray crystal structure of the respective free enzymes. At this point in time, an X-ray crystal structure of uncomplexed Ugi has not been published. The structure of PBS1 Ugi in complex with the HSV-1 UDG is essentially identical to that observed for PBS2 Ugi in complex with the human enzyme (237).

A comparison of the free and complexed tertiary solution structures of Ugi, as determined by nuclear magnetic resonance, indicate that Ugi undergoes a conformational change upon binding to *E. coli* Ung (12, 152). All of the secondary structural elements and the tertiary structure of the β2-β3-β4-β5 portion of the antiparallel β-sheet remain relatively unchanged. However, the polypeptide segments containing the α1- and α2-helix undergo structural rearrangement. Other conformational changes include twisting of the β1-strand and a reorientation of the loop between the β3- and β4-strands. The occurrence of these structural transitions potentially mediate the "locking" reaction involved in the kinetics of Ung•Ugi complex formation.

1.5 Uracil-Initiated Base Excision Repair in *Escherichia coli*

Initial evidence for delineating enzyme components of the uracil-initiated BER pathway was obtained from studies utilizing various *E. coli*

mutants, particularly *dut* mutants which are defective in dUTPase (105). Studies of *dut ung* double mutants indicated a requirement for uracil-DNA glycosylase whereas *dut xth, dut polA,* and *dut lig* double mutants were conditionally lethal under circumstances where any of the single mutations were not (265, 280, 297). These results suggested that uracil-DNA glycosylase, exonuclease III, DNA polymerase I, and DNA ligase, respectively, were essential components of the base excision repair pathway for uracil-containing DNA in *E. coli.*

The initial step of the uracil-initiated base excision repair pathway requires hydrolysis of the N-glycosyl bond linking the uracil base to the DNA deoxyribose phosphate backbone. This is catalyzed by uracil-DNA glycosylase, which acts to release free uracil and generate an apyrimidinic site (146). Subsequently, a class II AP endonuclease incises the phosphodiester backbone on the 5'-side of the AP site (172). There are several endonucleases in *E. coli* that could participate in the incision of AP site-containing DNA. *In vitro* studies have demonstrated that exonuclease III represents 80-85 % of the AP endonuclease activity in crude extracts (300), whereas endonuclease IV constitutes approximately 10 % of this activity (148). Both exonuclease III and endonuclease IV are class II endonucleases. Other potential participants involved in processing AP sites are endonuclease III, which cleaves to the 3'-side of the AP site, (296) and endonuclease V, which cleaves uracil-containing DNA (81). Following AP-site incision by a class II AP endonuclease, the BER substrate intermediate is a nick containing a 3'-OH terminus and a 5'-terminal deoxyribose phosphate (dRp) moiety. The 3'-OH group provides an appropriate primer-terminus for DNA polymerase I (173). However, the 5'-dRp residue must be removed in order to complete the BER pathway.

Excision of the 5'-dRp moiety must be conducted in connection with gap filling DNA synthesis. *In vitro* studies with *E. coli* DNA polymerase I demonstrated that 5'-terminal dRp residues located at strand breaks are subject to strand displacement synthesis rather than DNA polymerase-catalyzed nick translation synthesis (173). This suggested that another

enzyme was responsible for removing the dRp residue. In principle, the dRp residue could be enzymatically excised in its free form or as part of a small oligonucleotide. While the previous observation suggested that DNA polymerase I may not efficiently remove the terminal dRp residue prior to conducting DNA synthesis, other studies have indicated that the 5'→3' exonuclease activity of DNA polymerase I may liberate dRp as part of a small oligonucleotide (5). The AP lyase activity of endonuclease III was also considered as a candidate for the removal of dRp (70, 138). However, this enzyme was found not to be capable of cleaving on the 3'-side of a dRp residue following hydrolytic incision on the 5'-side by a class II endonuclease (70, 138). Further studies have suggested that the most likely candidate is a DNA deoxyribophosphodiesterase activity that acts on dRp-containing termini formed from endonucleolytically incised AP sites (70). The product of this reaction is free dRp. This protein, termed dRpase, has a molecular weight of ~50,000 and has no detectable intrinsic exonuclease, AP endonuclease, or DNA phosphatase activity (70). The relationship between purified dRpase and the *recJ* gene product was recognized following biochemical characterization of these two proteins (55). The *recJ* gene encodes an enzyme with a 5'→3' single-strand specific exonuclease activity that has previously been implicated in recombinational DNA repair (151). Similarly, purified dRpase was found to contain a 5'→3' single-strand specific exonuclease activity with identical properties to that of the purified *recJ* gene product (56). Furthermore, the Rec J protein was shown to possess dRpase activity (55). From this study, it was concluded that the *recJ* gene encoded the dRpase enzyme. The BER substrate intermediate produced by the combined action of uracil-DNA glycosylase, AP endonuclease, and dRpase/Rec J is a one-nucleotide gap with 3'-OH and 5'-PO_4 termini. This substrate intermediate will support DNA repair synthesis and ligation by DNA polymerase I and DNA ligase, respectively.

The role of *E. coli* DNA polymerase I in excision repair was first recognized in genetic analysis of *E. coli* mutants (52, 280, 281). It was observed that the introduction of DNA polymerase I or DNA ligase mutations into *E. coli dut* mutants reduced the rate of the joining of short Okazaki DNA fragments (280). These results implied a role for DNA polymerase I and DNA ligase in the excision repair of uracil-containing DNA.

The entire BER reaction has been reproduced by using cell extracts derived from *E. coli* and the prevalent repair reaction products were found to contain repair patches of one nucleotide (54). This indicated that the 5'→3' exonuclease or strand displacement activities of DNA polymerase I did not significantly participate in the removal of the 5'-terminal dRp moiety (54). Specifically, more than 70 % of the repair patches involved the incorporation of a single nucleotide (54). This suggested that the BER pathway was largely conducted as a concerted series of reactions.

Reconstitution of the uracil-initiated BER pathway was achieved using five purified enzymes from *E. coli* (uracil-DNA glycosylase, AP endonuclease IV, Rec J, DNA polymerase I, and DNA ligase) (53). As observed for BER in cell extracts, *in vitro* DNA repair synthesis primarily involved the incorporation of a single nucleotide and was dependent on the Rec J protein (54). Thus, it appeared that the 5'-terminal deoxyribose phosphate was released as a free dRp residue to generate a one-nucleotide gap for subsequently acted upon by DNA polymerase I and DNA ligase (53). An alternative pathway was proposed to explain the ~30 % of the repair patches that involved the incorporation of two or more nucleotides. This pathway involved excision of the dRp residue as part of a small oligonucleotide by the structure-specific 5' nuclease activity of DNA Pol I and generated larger repair patches due to strand displacement DNA synthesis (53). The results were similar to those observed with *E. coli* crude cell extracts, suggesting that no additional proteins or cofactors are required for BER (54).

1.6 Eukaryotic DNA Polymerases

Six different polymerases have been identified in eukaryotic cells and are designated DNA polymerase α, β, δ, ε, γ, and ζ (289). Three essential replicative DNA polymerases, α, δ, and ε, and two non-replicative polymerases, β and ζ, are located in the nucleus whereas DNA polymerase γ is localized to the mitochondria. DNA polymerase γ is responsible for replication of the mitochondrial genome and presumably mitochondrial DNA repair processes as well. DNA polymerases δ and ε appear to be linked to BER in eukaryotic cells and DNA polymerase β has been strongly implicated in mammalian BER. The evidence for the involvement of these three DNA polymerases in BER will be described in a succeeding section of the "Introduction". As eukaryotic cells display a complex mixture of DNA polymerases, general overview of each is described below.

The DNA polymerase α/primase complex is composed of a 165-180-kDa "core" catalytic subunit (pol α), a 70-kDa subunit with no detectable enzymatic activity, and two smaller subunits of 49- and 58-kDa that are associated with the primase activity (289). The 70-kDa subunit appears to act as a molecular tether between T antigen and the catalytic subunit of pol α and it has been suggested that this interaction promotes DNA chain initiation at the origin of replication and/or promotes DNA priming and synthesis on the lagging strand template (45). All subunits have been purified to apparent homogeneity and cDNAs have been cloned and characterized from a wide range of phylogenetic species (78, 289). The main function of the pol α/primase complex is to synthesize short RNA primers and elongate them into DNA primers (Okazaki fragments) for both leading and lagging strand DNA synthesis during replication (287, 288). Pol α is the only DNA polymerase with an associated primase activity and lacks associated

endonuclease, 5'→3' exonuclease, and 3'→5' proofreading exonuclease activities (289). It is moderately processive and has surprisingly high fidelity, even without an intrinsic 3'→5' exonuclease activity. Pol α is especially sensitive to aphidicolin and butylphenyl dGTP but not dideoxynucleoside triphosphates (ddNTPs).

DNA polymerase β (pol β) is the smallest naturally occurring eukaryotic DNA polymerase and has been purified as a single polypeptide of 39- to 45-kDa from a variety of vertebrate sources (41, 257, 264, 290, 310). Purified human pol β does not catalyze detectable levels of dNTP turnover, pyrophosphate exchange, or pyrophosphorolysis and lacks intrinsic endonuclease, 3'→5' exonuclease, and 5'→3' exonuclease activities. Recently, it was demonstrated that rat pol β contained an intrinsic deoxyribophosphodiestersase (dRpase) and AP lyase activity, both associated with the N-terminal 8-kDa domain (157, 208). Pol β from human, rat, and *Xenopus laevis* have been cloned and overexpressed in *E. coli* in order to accurately examine biophysical properties and structure-function relationships of the purified recombinant enzymes (1, 49, 220). Recombinant pol β, in all cases, was virtually indistinguishable from the natural source of pol β in terms of size, template-primer specificity, antigenicity, and lack of associated exo- and endonuclease activities. The recombinant enzymes were found to be fully active as compared to purified enzymes from the original source. Pol β is not inhibited by aphidicolin, is inhibited weakly by butylphenyl dGTP, and is strongly inhibited by ddNTPs.

DNA polymerase δ (pol δ) is a heterodimer with subunits of approximately 125-kDa and 48-kDa (103). Both subunits have been purified to apparent homogeneity and cDNAs have been cloned from mammalian cells for characterization (44, 48, 102, 312, 318). In addition to the polymerase activity, the 125-kDa catalytic subunit contains an intrinsic 3'→5' proofreading

exonuclease activity which readily distinguishes it from Pol-α and Pol-β (308, 319). This activity hydrolyzes mismatched termini with significantly greater efficiency than base-paired termini. As of yet, the function of the small subunit is still unknown. The low processivity of pol δ was stimulated in the presence of PCNA on long stretches of single-stranded DNA templates (263). Pol δ has been implicated as the leading strand DNA polymerase during DNA replication as well as completion of lagging strand DNA synthesis of each Okazaki fragment (278, 288). Pol δ also occupies important roles in nucleotide excision repair, base excision repair, and VDJ recombination (103, 289).

The catalytic properties of pol δ must be considered in the context of two auxiliary proteins, called proliferating cell nuclear antigen (PCNA) and replication factor C (RF-C). Non-specifically bound RF-C loads PCNA directly onto double-stranded DNA in an ATP-dependent fashion to form a protein complex clamp that tracks along the DNA until a 3'-OH primer-template junction is encountered, where the complex is transformed into a competent clamp (206). Subsequently, pol δ stably associates with the PCNA/RF-C complex in a replication competent fashion (207) (34). PCNA stimulates the activity and processivity of the heterodimer but has no effect on the isolated catalytic subunit, indicating that the ~50 kDa subunit appears to be necessary for the stimulation of processivity by PCNA (87).

DNA polymerase ε (pol ε) purified from human cells consists of a catalytic 255-kDa subunit and smaller 55-kDa subunit. Like pol δ, pol ε also has an intrinsic 3'→5' proofreading exonuclease activity associated with the 255-kDa subunit (258). Pol ε can be biochemically distinguished from pol δ by its moderate processivity in the absence of PCNA and an apparent low stimulation of processivity in its presence (258). A role for pol ε in DNA replication is presently unclear but several lines of evidence have indicated that this polymerase has a role in DNA repair, including nucleotide excision

repair, base excision repair, and DNA double-strand break repair (289). Both pol δ and pol ε are sensitive to aphidicolin but are resistant to ddNTPs.

DNA polymerase γ (pol γ) isolated from humans is a heterodimer composed of a 140-kDa subunit and a 54-kDa subunit (89). Both subunits have been purified and the cDNAs for the large subunit have been cloned from a variety of organisms, including *Drosophila melanogaster* (139), *Xenopus laevis* (314), and humans (226). Biochemical characterization of the large subunit demonstrated the presence of both DNA polymerase activity and 3'→5' exonuclease activity in the absence of any accessory factors (88, 139). The small subunit has been proposed to enhance the interaction between the catalytic subunit and the DNA and to increase processivity (88). Several studies have documented repair of some types of damage in mitochondrial DNA, including damage by purine base alkylating agents (180) and bleomycin (243), and suggest a possible role for a BER mechanism in mitochondria. Recently, a combination of a mitochondrial class II AP endonuclease, pol γ, and mitochondrial DNA ligase purified from *X. laevis* mitochondria were found to be capable of conducting complete repair of AP site-containing DNA (204). Thus, in addition to a role in mitochondrial DNA replication, pol γ apparently participates in DNA repair synthesis. Pol γ is inhibited by ddNTPs but is resistant to the inhibitory effects of aphidicolin.

DNA polymerase ζ (pol ζ) was originally identified in *S. cerevisiae* as a heterodimer composed of the *REV3* and *REV7* gene products (187). The *S. cerevisiae REV3* and *REV7* cDNAs have been cloned and encoded polypeptides with predicted masses of ~173-kDa and ~29-kDa, respectively (169, 276). Pol ζ is thought to conduct error-prone translesion DNA synthesis across damaged DNA templates in yeast and was demonstrated to replicate past a thymine-thymine dimer, a lesion that inhibits DNA synthesis, with an efficiency of ~10 % (187). It has also been implicated in mutagenesis associated with double-strand break DNA repair (106). The polymerase activity associated with the

REV3 subunit is nonprocessive and appears to lack 3'→5' proofreading exonuclease activity (187). Recently, the human homologue of the *REV3* gene has been cloned and found to encode a polypeptide with a predicted mass of ~353-kDa (84). Further characterization of this gene product should promote a better understanding of translesion DNA repair synthesis in human cells. Pol ζ is insensitive to aphidicolin and ddNTPs but moderately sensitive to butylphenyl dGTP (187).

1.7 Uracil-Initiated Base Excision Repair in Eukaryotes

The general strategy of the BER pathway in eukaryotic cells is similar to that of *E. coli* and entails a multienzyme repair process involving base release, phosphodiester bond incision, deoxyribose phosphate removal, DNA synthesis, and DNA ligation (122, 171). Uracil-DNA BER is initiated by a uracil-DNA glycosylase that releases the free uracil base to generate an apyrimidinic (AP) site (171). The AP-site produced during uracil-initiated BER is also a common intermediate in the repair of several other types of DNA damage involving N-glycosylic bond hydrolysis or spontaneous depurination/depyrimidation events (142, 144). The second step of the pathway requires hydrolysis of the phosphodiester bond on the 5'-side of the AP site by a class II AP endonuclease (172). This generates a 5'-terminal deoxyribose-phosphate group that is subsequently removed by a deoxyribophosphodiesterase (dRpase) activity. Thus, the initial reaction steps of the uracil-DNA BER pathway generate a one-nucleotide gap with 3'-OH and 5'-PO_4 termini in a process that is highly conserved from microorganisms to man. In eukaryotes, recent studies have demonstrated a functional redundancy at the DNA synthesis and DNA ligation steps (53, 77, 183). This leads to one of two alternative pathways for DNA repair synthesis and ligation. As a result, repair patches are heterogeneous in size. The major pathway in higher eukaryotes appears to be dependent on pol β and results in

the synthesis of a one-nucleotide repair patch (123, 183, 247). The minor pathway is PCNA-dependent, implying a role for pol δ and/or ε in the DNA synthesis step, and results in the incorporation of up to 7 nucleotides (77, 158, 183). Unlike short-patch repair, long-patch BER most likely depends on strand displacement and/or exonuclease activity to carry out additional DNA synthesis. Five distinct DNA ligases (I, II, III, IV, and V) have been identified in proliferating human cells (145, 224, 275, 299) but their definitive role in BER remains to be elucidated (35, 215, 299).

The entire BER reaction has been detected by using cell extracts derived from *S. cerevisiae* (294, 295), *X. laevis* (155, 156, 158), hamster (76), bovine (247), and human cells (54, 183). Experimental approaches involving genetic analysis, DNA polymerase inhibitors, neutralizing antibodies, and reconstitution systems have provided valuable insights into delineating the enzymatic components of short- and long-patch eukaryotic BER.

Short-patch BER appears to be dependent on the dRpase activity associated with the 8-kDa N-terminal domain of Pol-β (157). This observation suggested that pol β conducts two consecutive steps (dRp removal and DNA repair synthesis) of the BER pathway. Alternatively, another enzyme has also been partially purified from human cells that catalyzes the release of 5'-terminal deoxyribose phosphate residues from abasic sites when previously incised with AP endonuclease (211). If this activity were to function in short-patch BER, it would require access to the AP site prior to cleavage by the dRpase activity of pol β. Removal of the 5'-terminal dRp group during long-patch BER most likely depends on strand displacement synthesis by DNA polymerases followed by a structure-specific endonuclease activity. In this case, the release of the 5'-terminal dRp moiety could occur as part of a short oligonucleotide. Experimental evidence for all of these mechanisms is described in more detail below.

The exclusive participation of pol β in eukaryotic BER was initially observed in studies utilizing DNA polymerase inhibitors and neutralizing

antibodies in order to inhibit DNA synthesis associated with BER. Experiments with HeLa cell nuclear extracts supplemented with ddCTP demonstrated that mismatch-specific thymine-DNA glycosylase and pol β exclusively mediated the repair of G•T mismatches by the short-patch BER pathway (302). In a separate study, a pol β neutralizing polyclonal antibody and ddCTP were shown to completely inhibit uracil-initiated BER of a synthetic 51-bp uracil-containing duplex DNA substrate (247). These observations indicated that pol β was exclusively responsible for gap-filling synthesis in HeLa cell and bovine testis nuclear extracts, respectively. No significant effect on DNA repair synthesis in bovine testis nuclear extracts was observed with aphidicolin, suggesting that pol α, δ, and ε were not involved in the DNA synthesis step (247). By using a genetic approach, extracts derived from an embryonic fibroblast cell line homozygous for a deletion mutation in the gene encoding pol β were unable to perform BER of a uracil-containing synthetic oligonucleotide and the cells exhibited increased sensitivity to monofunctional DNA-alkylating agents (253). Stable transfection with a minigene encoding pol β restored the deficiency in BER and eliminated the hypersensitivity to DNA-alkylating agents, demonstrating that pol β specifically functions in BER *in vivo* (253). However, recent studies have indicated that circular DNA substrates may be required for the interaction of pol δ and ε with auxiliary proteins involved in polymerase loading and DNA synthesis (20, 205, 206). Linearization of circular substrates DNA substrates was shown to abolish DNA synthesis by pol δ and prevent the interaction of pol ε with the auxiliary proteins, replication factor C (RF-C) and proliferating cell nuclear antigen (PCNA) (205). Thus, the use of linear DNA in the aforementioned studies (248, 253, 302) may have inadvertently biased the results against recognizing the participation of a PCNA-dependent DNA polymerase(s) in uracil-initiated BER.

These studies concluded that the DNA synthesis step was exclusively conducted by pol β but have since been critically reevaluated. Experiments utilizing human lymphoblastoid nuclear extracts demonstrated that ~70-80 % of the newly synthesized repair patches following uracil-DNA BER contained only one nucleotide, providing strong evidence that short-patch BER is the dominant repair pathway and suggesting that the associated DNA repair synthesis was conducted by pol β (54). However, the completed BER reaction was found to be only partly inhibited (67 %) by 100 μM ddTTP, an inhibitor of pol β, and limited inhibition (~23 %) of DNA repair synthesis was observed following inclusion of 50 μg/ml aphidicolin (54). In a similar study, Nealon and co-workers (183) were able to reduce uracil-initiated base excision repair synthesis in HeLa crude extracts by ~50 % and ~20 % using ddNTPs and aphidicolin, respectively. Neutralizing antibodies specific to pol β only inhibited DNA repair synthesis by ~70 % (183). These results suggested that pol β was the major DNA polymerase associated with DNA repair synthesis during uracil-initiated BER in mammalian cells due to the sensitivity of the repair process to ddNTPs and neutralizing antibodies. However, an inability to completely repress DNA synthesis following neutralization of pol β implicated a role for other DNA polymerases, particularly pol δ and/or ε, in this repair mechanism.

Fractionation of crude cell extracts that supported repair of uracil residues and AP sites provided another approach to identifying DNA polymerase requirements for short- and long-patch BER (158, 183). The addition of purified pol β to a pol β-depleted HeLa cell extract completely restored DNA repair synthesis while purified pol δ and pol ε only supported repair synthesis to a limited extent (183). It was estimated that pol β catalyzed ~75 % of base excision DNA repair synthesis in this system while other DNA polymerase(s) (notably pol δ) contributed the remaining ~25 % of the activity.

In a separate study, a PCNA-dependent long-patch BER pathway was reconstituted by using a fractionated *X. laevis* ovarian extract (158). Three of these fractions were demonstrated to individually contain AP endonuclease, pol δ, and PCNA and were able to repair natural AP sites and tetrahyrdofuran residues in BER reactions involving the incorporation of no more than four nucleotides. This indicated that a distinct PCNA-dependent repair pathway that excluded pol β was responsible for conducting long-patch DNA repair synthesis (158). In a PCNA-independent BER reaction, pol β was able to replace pol δ for the repair of the DNA substrate containing the natural AP site but not the tetrahydrofuran residue (158). Since tetrahydrofuran residues are resistant to cleavage by β-elimination (6), the associated dRpase activity of pol β, which operates by a β-elimination mechanism, most likely eliminated the ability of pol β to repair synthetic tetrahydrofuran AP sites in this system (157, 158, 203). This is another piece of evidence linking pol β to two consecutive steps of the BER pathway (dRpase activity and DNA synthesis). These observations using fractionated eukaryotic cell extracts demonstrated that uracil residues and AP sites can be repaired by two distinct pathways separately involving pol β or pol δ.

Similar to that observed for BER conducted by pol δ in *X. laevis*, studies utilizing *S. cerevisiae* extracts have implicated pol ε in both the short- and long-patch BER pathways (294, 295). DNA repair synthesis associated with BER was found to be conducted exclusively by pol ε in a PCNA-dependent fashion (294). There seems to be no apparent role for pol β in yeast BER since this enzyme is rarely expressed in vegetative cells and pol β deletion mutants are not sensitive to DNA damaging agents (32, 210, 244). Approximately 50 % of the DNA repair synthesis events during BER of uracil-containing DNA in yeast resulted in a one-nucleotide repair patch whereas repair patches of 2, 3,

and 5 nucleotides accounted for ~25 %, 13 %, and 5 % of the repair events, respectively (295).

Genetic studies have also demonstrated a role for pol δ and/or ε in both short- and long-patch BER using the identical embryonic fibroblast cell line homozygous for a deletion mutation in the gene encoding pol β previously described (69, 253). The difference between this study and the previous study was the use of a circular substrate versus a linear substrate. *In vitro* repair of circular duplex plasmid DNA containing a uracil residue or a single abasic site by the pol β-deficient cell extracts showed that both short- and long-patch BER could be performed by DNA polymerases other than pol β (69). Short-patch BER was performed in the absence of PCNA, but the repair kinetics were significantly slower than pol β-proficient extracts (69). This result suggested that pol β was the predominant DNA polymerase involved in one-nucleotide gap-filling but other DNA polymerases could act as back-up polymerases when pol β was defective. The repair kinetics of long-patch BER were unaffected by the absence of pol β. Furthermore, the BER reaction was PCNA-dependent, providing the additional evidence that pol δ and/or ε are specifically involved in long-patch BER (69).

Reconstitution of the BER pathway with purified human proteins has provided important information detailing the biochemistry of short- and long-patch BER in mammalian cells and has demonstrated that the core BER reaction may be modulated by accessory factors. Short-patch BER was reconstituted by using purified uracil-DNA glycosylase (UDG), AP endonuclease (HAP1), pol β, and either DNA ligase III (123) or DNA ligase I (190). Pol β primarily produced one-nucleotide repair patches but patches of two or three nucleotides in length were also observed, suggesting strand displacement activity by pol β (123). These longer repair patches were shown to undergo ligation but only after the addition of purified human DNase

IV/FEN1, which specifically removes overhang structures at DNA strand breaks (94, 225). Replacement of DNA ligase III with DNA ligase I also facilitated ligation of repair patches, suggesting a potential role for DNA ligase I in BER (123). Addition of XRCC1, a protein with no known catalytic function, to the reconstituted BER reaction expedited repair synthesis with little or no strand displacement, suggesting that XRCC1 might coordinate repair events so as to prevent the accumulation of repair intermediates (123). Uracil-initiated BER in cell extracts procured from an XRCC1 mutant CHO cell line resulted in pronounced strand displacement activity and excessive gap filling (123). These observations suggest that XRCC1 may support short-patch DNA repair synthesis by suppressing unnecessary strand displacement *in vivo*. Alternatively, DNase IV/FEN1 may act in conjunction with pol β to promote long-patch DNA repair synthesis during strand displacement DNA synthesis. Together, these studies suggest that pol β, in cooperation with specific accessory proteins, can participate in the short- and long-patch BER pathways.

Reduced AP site- and natural AP site-containing DNA substrates were used to probe the complexities of long-patch BER as it involved pol β (118). The pathway was reconstituted using purified AP endonuclease (HAP1), pol β, and DNA ligase I (118). The use of the reduced AP site-containing DNA substrate provided a strategy for selecting against the dRpase activity of pol β, since the dRpase activity operates by a β-elimination mechanism. Reduced AP sites are not subject to β-elimination. This provided a means for examining the ability of pol β to perform strand displacement associated with long-patch BER. By using this system, natural AP sites were found to be efficiently repaired by a short-patch BER mechanism whereas reduced AP sites were incompletely repaired (119). The incomplete repair products were generated by unligated repair intermediates containing repair patches of up to six nucleotides, which presumably formed as a result of strand displacement

DNA synthesis (118). Addition of purified DNase IV/FEN1 to the reconstituted repair reaction released the 5'-terminal deoxyribose phosphate group as part of a small oligonucleotide and generated a repair intermediate that was acted upon by DNA ligase I. Under these conditions, repair patches of 2-6 nucleotides in length were produced (118). These results demonstrated a coordination of activities between pol β, DNase IV, and PCNA to complete long-patch BER *in vitro*. DNA ligase III was also able to substitute for DNA ligase I in this reconstituted system, indicating an apparent lack of specificity for a defined ligase (118). The ability of PCNA to stimulate DNase IV in this study and in others (140, 309) provided an alternative interpretation for the PCNA-dependent long-patch BER pathway reportedly involving pol δ and/or ε.

1.8 Physical Interactions Detected Between BER Enzymes

Several studies have detected physical interactions between mammalian BER proteins, suggesting that protein-protein contacts are important for the coordinated regulation of individual reactions involved in the multistep BER pathway. In this way, the accumulation of DNA repair intermediates during the reaction may be reduced and the overall efficiency of the pathway enhanced. Since both the nucleotide excision repair (230, 306) and DNA mismatch repair (75) pathways act in a coordinated fashion, it has been of great interest to probe for protein-protein interactions between BER enzymes that might provide evidence for an orchestrated BER pathway.

Evidence for a direct physical interaction *in vivo* between pol β and human AP endonuclease has been demonstrated using the yeast two-hybrid assay system (13). Electrophoretic mobility-shift assays have provided evidence for an *in vitro* interaction between pol β, AP endonuclease, and uncleaved double-stranded AP-site-containing oligonucleotides (in the absence of Mg^{2+}), indicating that this complex can be achieved in association

with a BER substrate intermediate (13). In this complex, AP endonuclease appears to act as a loading factor for pol β onto AP sites in DNA (303). After addition of Mg^{2+} and incision by AP endonuclease, only pol β was stably associated with the nicked AP site (13). Additionally, the intrinsic dRpase activity of pol β was observed to be stimulated up to 4.3-fold by AP endonuclease (13). This interaction provides an efficient mechanism for one-nucleotide gap-filling by pol β and implies coordination between AP site incision, dRp removal, and DNA repair synthesis.

A physical interaction between pol β and XRCC1 was detected *in vitro* by using an affinity precipitation assay and *in vivo* by using the yeast two-hybrid system (123). Affinity precipitation experiments using full length XRCC1 and internal/C-terminal deletion mutants of XRCC1 demonstrated that pol β binds to the N-terminal region of XRCC1, between amino acids 84 and 183 (123). Gel retardation assays also demonstrated that complex formation occurred between pol β and XRCC1 at incised AP sites, indicating that pol β and XRCC1 can physically interact in association with a BER substrate intermediate (123). XRCC1 was also shown to bind to DNA ligase III under similar conditions (35, 299). Deletion mutant analysis demonstrated that DNA ligase III binds to the C-terminal 96 amino acids of XRCC1 (182). The physical interaction between XRCC1 and DNA ligase III, coupled with genetic evidence for a role of XRCC1 in the BER pathway (271), provides an argument for the participation of DNA ligase III in eukaryotic BER. Together, these studies suggest that pol β interacts with DNA ligase III via the XRCC1 protein.

A multiprotein complex (~180 kDa) from bovine testis nuclear extracts that was capable of performing complete *in vitro* uracil-initiated BER was purified by affinity chromatography using pol β or pol β antibody as the immobilized ligand (209). By inference, this complex contained uracil-DNA glycosylase and AP endonuclease activities and the presence of pol β and

DNA ligase I was definitively determined by using more direct biochemical and immunological techniques (209). This is the only study that provides evidence for the physical association of uracil-DNA glycosylase with other enzyme components of the BER pathway. The ~180-kDa complex appeared to contain equal stoichiometric levels of pol β (39-kDa), UDG (32-kDa), and AP endonuclease (34-kDa) in addition to DNA ligase I, which has an estimated molecular weight of ~98-kDa, as previously determined by sedimentation velocity and gel filtration (274). An antibody specific for pol β was able to supershift the complex to a larger molecular weight in sucrose density gradients, and the presence of pol β and DNA ligase I in the complex were confirmed by immunoblotting using antibodies specific for both enzymes (209). Co-immunoprecipitation of pol β and DNA ligase I from the testis nuclear extract was also achieved using anti-pol β IgG (209). This interaction has recently been characterized by affinity chromatography, analytical ultracentrifugation, and domain mapping techniques (56). The physical association was mediated by an interaction between the non-catalytic N-terminal domain of DNA ligase I and the N-terminal 8-kDa domain of pol β and binding stoichiometry is influenced by temperature (56). At temperatures below 18°C, a 1:1 stoichiometry was observed whereas above 18°C, a pol β :DNA ligase I protein ratio of 3:3 was detected (57). Domain mapping results imply that a temperature-mediated conformational change occurred in the 31-kDa domain of pol β (56). Since a physical interaction between pol β and DNA ligase I has been shown to exist *in vitro*, it is likely that these enzymes also associate within the naturally occurring BER complex *in vivo*. The influence of a pol β:DNA ligase I heterodimer (1:1) or heterohexamer (3:3) on the BER pathway remains to be determined.

1.9 Fidelity of Repair DNA Synthesis

1.9.1 Error Discrimination Steps During Polymerization

During DNA synthesis, base substitution fidelity is dictated by base selectivity and exonucleolytic proofreading of DNA polymerases. These two error discrimination steps occur upon incorporation of a nucleotide during a single cycle of polymerization (223). These proofreading mechanisms begin with the formation of the ternary complex formed between the DNA polymerase, the template-primer DNA, and the incoming deoxyribonucleoside triphosphate. Following complex formation, a conformational change occurs to correctly position the incoming dNTP for phosphodiester bond formation. After proper alignment is achieved, the chemical reaction step to form the bond is executed, a second conformational change releases the pyrophosphate (PP_i) end-product, and the polymerase translocates in the 5'→3' direction to the next nucleotide position for the next cycle of polymerization. If the 3'-terminal base of the primer DNA strand is not properly base paired with the template strand, a 3'→5' exonuclease activity, if intrinsic to the DNA polymerase, will perform exonucleolytic proofreading. As DNA polymerases play an important role in most DNA repair processes, it is important that gaps in the DNA are filled accurately to ensure the success of the DNA repair process.

Base selectivity begins with dNTP binding in the polymerase triphosphate binding site of the DNA polymerase/template-primer DNA complex in the "open" conformation. Dissociation of an incorrect dNTP at this stage is influenced by hydrogen bonding potentials between the incoming dNTP and the template base and localized base stacking interactions (64). However, the free energy of binding for a base pair versus a mispair is not sufficient to account for the high fidelity observed for the enzyme-catalyzed polymerization step (114). Because some incorrect base pairs (for example, G•T *versus* A•T) do not exhibit large structural or energetic differences from

those of a correct Watson-Crick base pair (198), a second level of discrimination occurs when the DNA polymerase/dNTP/template-primer DNA complex transforms to the "closed" conformation to perform catalysis (64). This conformational change appears to be inhibited by mismatches between the dNTP and the template or in any of the three terminal base pairs of the primer/template (114). The rate of misincorporation and polymerization for incorrect nucleotide mispairs can be 2000- to 4000-fold slower than that of a Watson-Crick base pair (114). Thus, the replication fidelity associated with base selectivity ultimately depends on the level of discrimination in the active site pocket of the DNA polymerase in question, the composition of the mispair, and the surrounding DNA sequence context (64).

Exonucleolytic proofreading is provided by DNA polymerases containing an intrinsic 3'→5' exonuclease activity and is influenced by the rate of nucleotide extension from each of the 12 possible mispairs and by enzyme- and sequence-specific factors (30). The rate of primer extension from a terminal mispair is much slower than onto a properly base paired terminus. As a result, the selectivity of the DNA polymerase toward hydrolysis of a 3'-terminal mismatch is favored when the enzyme stalls and is unable to achieve the critical catalytic configuration for catalyzing phosphodiester bond formation (114). This requires movement of the 3' terminus from the polymerase active site to the exonucleolytic site with or without enzyme dissociation from the primer-template DNA (223). Of the six characterized eukaryotic DNA polymerases, pol δ, ε, and γ contain intrinsic 3'→5' exonuclease activities while pol α, β, and ζ do not. This is an important concept when weighing the contribution of specific DNA polymerases implicated in DNA repair synthesis during BER, namely pol β, δ, and ε.

Pol β is the least accurate of the eukaryotic DNA polymerases, in part, due to its lack of an intrinsic 3'→5' exonuclease activity. The fidelity of

distributive long gap DNA synthesis by DNA pol β has been examined on M13mp2 partial duplex DNA with a 390-nucleotide single-stranded gap containing a 250-base mutational target (127, 129, 133). Using an *in vitro* M13mp2 *lacZα* DNA-based forward mutation assay, Kunkel and co-workers (127) (129) (132) demonstrated that purified pol β from rat Novikoff hepatoma and chick embryos conducted error-prone DNA synthesis that resulted in a high frequency of frameshift, base substitution, and deletion errors at a frequency of 4-6 % per single round of gap-filling DNA synthesis (127, 129). The average base substitution error frequency of pol β was calculated to be approximately one error per 1500 bases polymerized and involved nucleotide misincorporation events propagated by direct miscoding and transient misalignment of the primer-template (129, 133). Distinct site preferences were apparent for single-base substitution errors by pol β and averaged error frequencies for individual mispairs ranged from 0.45×10^{-4} (A•dCMP) to 10×10^{-4} (A•dAMP) (129). Transition mutations produced by C•dAMP, A•dCMP, T•dGMP, and G•dTMP mispair insertions accounted for ~78 % of the base substitution mutation spectra where dAMP was the most frequently misinserted nucleotide (127). Since the fidelity of pol β is not influenced by exonucleolytic proofreading, these results can be interpreted on the basis of base selectivity alone.

The fidelity of pol β on a M13mp2 DNA substrate containing a 5-nucleotide gap was also examined (11). This type of substrate more likely resembles that encountered by pol β during base excision repair. By using an *in vitro* M13mp2 *lacZα* DNA-based reversion assay, short gap-filling DNA synthesis by human pol β resulted in frequent T•dGTP and A•dGTP misincorporation events opposite an opal (TGA) codon and yielded a reversion frequency of 27×10^{-4} (1 revertant per 370 filled gaps) (11). DNA sequence analysis of these revertants often detected two consecutive

misincorporations and suggested that a difference in fidelity might exist between processive short-gap filling and distributive long-gap filling by pol β (11). Consecutive misincorporations were not previously observed using the large-gapped M13mp2 DNA template (127, 133). Under pre-steady-state kinetic assay conditions, the formation of T•dCMP and T•dGMP mispairs were recently reported to be the most kinetically favorable misinsertions out of all 12 possible mispairs for purified rat pol β (2). Transition mutations were favored over transversion mutations as previously reported (129). In a separate study, the nucleotide insertion fidelity of pol β was demonstrated to be 10- to 100-fold higher on a 5'-phosphorylated single-nucleotide gapped DNA substrate as compared to non-phosphorylated one nucleotide gaps, 5'-phosphorylated and non-phosphorylated gaps of 6 nucleotides, and recessed 3'-termini (40). Specifically, misinsertion of dGTP, dTTP, and dATP opposite a template G occurred at frequencies of 2×10^{-6}, 1×10^{-5}, and 6×10^{-5}, respectively (40). These results establish the fidelity of pol β DNA synthesis *in vitro* on gapped DNA substrates of various size.

The base substitution fidelity of DNA pol δ and ε are considerably less error prone than polymerases lacking exonuclease activity. By using an M13mp2 *lacZα* DNA-based forward mutation assay on a 390-base single-stranded gap, the fidelities of gap-filling synthesis by purified pol δ and ε were compared (270). Pol δ was unable to fill gaps to completion unless its accessory protein, PCNA, was included in the reaction. Base substitution error rates for pol δ were dependent on the type of mispair and were $< 0.1 \times 10^{-4}$ for 7 out of 12 types of base substitution errors. The error rates for the remaining 5 types of base substitution errors ranged between 0.11×10^{-4} (C•dTTP) and 0.29×10^{-4} (G•dATP) (266). Several studies have shown that misinsertion of dGTP opposite a template T is one of the most common mistakes made by exonuclease-deficient eukaryotic DNA polymerases (error

frequency > 1.0 x 10^{-4}) but the error frequency for pol δ was measured at ~0.04 x 10^{-4} for T•dGTP errors (2, 129, 270). The fidelity of pol ε in this study was even greater than that of pol δ, did not require PCNA, and produced an error frequency that was equal to the background mutation frequency of uncopied DNA (≤ 0.0067 x 10^{-4}) (270). In fact, base substitution errors were detected only when dGMP, a reported inhibitor of exonucleolytic proofreading, was included in the reaction (270). This high level of misinsertion fidelity is consistent with a 3'→5' exonucleolytic proofreading activity as suggested in a previous study using pol ε (131). By using an M13mp2 *lacZα* DNA-based reversion assay, an average of less than 1 base substitution error per 10^6 nucleotides polymerized was detected for this polymerase (131). The fidelity of pol ε isolated from calf thymus was 500-fold more accurate than pol β, in part, due to its intrinsic proofreading exonuclease activity (131).

1.9.2 Base Substitution Errors Involving Template-Primer Misalignment

In addition to direct nucleotide misinsertion during replication, an alternative means of producing base substitution errors occurs by transient misalignment of the primer-template and has been termed dislocation mutagenesis (129). These types of errors are sequence- and polymerase-dependent. Misalignment of the primer-template followed by incorporation of the next correct nucleotide as dictated by the template provides a DNA intermediate containing a "looped out" nucleotide in the template strand. If the "looped out" nucleotide resumes its normal position in the DNA before continued nucleotide incorporation, a terminal mispair is created (128). Of the DNA polymerases involved in BER, pol β appears to frequently misincorporate nucleotides by a dislocation event within specific DNA sequence contexts.

Previously, two base-substitution mutational hot spot locations for T→G transversions by pol β were detected by using an M13mp2 *lacZα* DNA-based forward mutation assay (127). Both errors occurred within the sequence contexts 5'-C-G-T-T-T-T-A-C-3' and 5'-C-G-T-T-A-C-3' where the mutation occurred at the site of the underlined T nucleotide. As the error specificity for pol β appeared to be related to the DNA sequence, the dislocation mutagenesis model was proposed for pol β errors at these two sites. These same sites were not mutational hot spots for base substitution errors by purified pol δ and ε and suggested a greatly decreased propensity for these DNA polymerases to conduct dislocation mutagenesis within the aforementioned sequence contexts (270). To test the premise that the next nucleotide position in the template encoded these pol β-catalyzed mutations, the G preceding the T on the 5' side was changed to an A (133). This template change resulted in the disappearance of T→G transversion mutations at this site and exclusively generated T→A transversion mutations by >300-fold (133). In a kinetic study, the misinsertion rate by dislocation for pol β was calculated to be between 10- and 110-fold greater than by direct miscoding (25). Thus, base-substitution errors by pol β can be initiated by primer-template misalignments and at least within these sequence contexts, pol δ and ε do not appear to introduce errors by this mechanism.

1.10 Research Objectives

The bacteriophage PBS2 uracil-DNA glycosylase inhibitor (Ugi) protein inactivates uracil-DNA glycosylase (Ung) by forming a stable protein-protein complex in which Ugi mimics electronegative and structural features of DNA (12, 167). Two primary features of Ugi suggest that the negatively charged amino acid residues are involved in mediating the Ung/Ugi interaction.

First, the overall electronegative potential of the inhibitor is engendered by its unusually high (21 %) glutamic acid and aspartic acid content (15, 293). Second, analysis of the tertiary NMR structure of the free inhibitor indicate that these residues are distributed in a nonrandom fashion, primarily in the loop and turn regions that terminate the β-strands and in the both the α1 and α2 helices (7, 12). As a first step in elucidating the functional role of these negatively charged amino acids in the formation of the irreversible Ung•Ugi complex, experiments were conducted to selectively modify specific carboxylic acid residues of the Ugi protein. Modification of important Glu and Asp residues was expected to disrupt essential protein/protein interactions and interfere with the preliminary "docking" step or destabilize the final "locked" complex. This approach was anticipated to provide important insights that relate biochemical, structural, and kinetic elements of Ugi in its association with Ung.

Studies were also undertaken which utilized the Ugi protein to assess the fidelity and error specificity of DNA repair synthesis associated with the uracil-initiated base excision repair (BER) pathway. In this regard, the Ugi protein was also used as a tool to probe the biological importance of Ugi-insensitive uracil-DNA repair systems in human cell extracts. To investigate the fidelity of DNA synthesis associated with uracil-initiated BER, to determine the mutational spectrum, and to quantitate the distribution of short-patch and long-patch BER, an M13mp2 *lacZα* DNA-based reversion assay was designed, developed, and successfully implimented. The results provided in this dissertation offer the first report of DNA synthesis fidelity measurements associated with the complete BER process.

2. MATERIALS AND EXPERIMENTAL PROCEDURES

2.1 Materials

2.1.1 Chemicals

Trizma (Tris-base), HEPES, EDTA, ampicillin, streptomycin sulfate, bovine serum albumin, 2-mercaptoethanol, 1-ethyl-3-(3-dimethylamino-propyl(carbodiimide)) (EDC), glycine ethyl ester, transfer ribonucleic acid (type X-SA), β-nicotinamide adenine dinucleotide (NAD), phosphocreatine di-Tris salt, phenylmethylsulfonyl fluoride (PMSF), leupeptin, pepstatin A, aprotinin, and chymostatin were obtained from Sigma. Isopropyl-β-δ-thiogalactopyranoside (IPTG), dithiothreitol (DTT), 1-kb DNA ladder, L-glutamine, penicillin-streptomycin, geneticin (G418), RPM I medium 1640, F-12 nutrient mixture (Ham's), and ultra-pure cesium chloride, urea, sodium dodecyl sulfate, glycine, sucrose, ammonium sulfate, and agarose were purchased form Life Technologies. 2'-deoxyribonucleoside triphosphates and poly(U) were obtained from Pharmacia Biotech and 2'-deoxyribonucleoside α-thiotriphosphates were from Amersham Life Science. 5-bromo-4-chloro-3-indolyl β-D-galactopyranoside (X-Gal) came from United States Biological and dextrose, boric acid, sulfuric acid, monobasic and dibasic potassium phosphate, 1-butanol, iso-amyl alcohol, glycerol, dimethylformamide, and dimethyl sulfoxide were obtained from J.T. Baker. Fisher was the source of methanol, toluene, acetic acid, hydrochloric acid, ammonium hydroxide (50%), trichloroacetic acid, and phenol. Chloroform was obtained from Mallinckrodt, and Boehringer Mannheim was the source for aphidicolin. Acrylamide (>99% pure), bis N,N'-methylene-bis-acrylamide, ammonium persulfate, TEMED, and protein assay (Bradford reaction) dye reagent concentrate was from Bio-Rad. Cyanogen bromide came from Aldrich.

Fluoroscein-5-isothiocyanate (Isomer I) was purchased from Molecular Probes. HyClone Laboratories Inc. was the source of defined fetal bovine serum.

2.1.2 Radioisotopes

[^{35}S]methionine, [α-^{32}P]dATP, [γ-^{32}P]ATP, and [^{3}H]dTTP were purchased from DuPont-New England Nuclear. [^{3}H]dUTP was obtained from Amersham Corp.

2.1.3 Bacterial Media

M9 medium contained 1.28 % $Na_2HPO_4 \bullet 7H_2O$, 0.3 % KH_2PO_4, 0.05% NaCl, and 0.1 % NH_4Cl. Following sterilization, M9 medium was adjusted to 2 mM $MgSO_4$, 0.1 mM $CaCl_2$, 0.4 % glucose, and 10 µg/ml thiamine from individual sterile stocks. TYN medium was composed of 1 % yeast extract (Difco), 1 % tryptone (Difco), and 0.5 % NaCl. YT medium was composed of 0.5 % yeast extract, 0.8 % tryptone, and 0.5 % NaCl. LB medium was composed of 0.5 % yeast extract, 1 % tryptone, and 1 % NaCl. VAT medium contained 1 % tryptone, 0.4 % yeast extract, 1 % K_2HPO_4, and 0.1 % KH_2PO_4. SOC medium contained 0.5 % yeast extract, 2 % tryptone, 0.05 % NaCl, 2.5 mM KCl, 10 mM $MgCl_2$, and 20 mM glucose and the pH was adjusted to pH 7.0 with 5 N NaOH. SM medium was composed of 50 mM Tris-HCl (pH 7.5) 0.58 % NaCl, 0.2 % $MgSO_4 \bullet 7H_2O$, and 1 % gelatin. Solid plates and topagar were prepared by the addition of 1.5 % and 0.7 % (w/v) bacto-agar (Difco), respectively, to the appropriate liquid media. Where appropriate, liquid media or media plates were supplemented with 100 µg/ml ampicillin from a sterilized stock (100 mg/ml) as needed to enforce maintenance of recombinant plasmids. In order to detect α-complementation of *lacZ*α, M9 topagar was adjusted to 0.4 mM IPTG and 1 mg/ml X-Gal.

2.1.4 Bacterial Strains

The strains of *E. coli* used for this research and their representative genotypes are listed in Table 1. Strain JM105 was provided by W. Ream (Oregon State University) and strains CJ236, MC1061, NR9162, and CSH50 were provided by T.A. Kunkel (NIEHS, Research Triangle Park, NC). Strain RR1 was provided by W.H. Konigsberg (Yale University). JM109 was obtained from New England Biolabs.

2.1.5 Plasmids and Bacteriophage

Plasmid pSB1051, an overexpression vector for Ung, was constructed by S. Bennett (NIEHS, Research Triangle Park, NC) as described (17). The Ugi overexpression plasmid, pZWtac1, was constructed by Z. Wang (University of Kentucky) as described (293). Plasmid pTL43W, an overexpression vector for producing T4 DNA polymerase, was provided by W.H. Konigsberg (Yale University) and constructed as described (141). Bacteriophage M13mp2 was obtained from T.A. Kunkel (NIEHS, Research Triangle Park, NC) and M13mp2op14 was constructed as described in this thesis. The eukaryotic replication-defective MLV retroviral vector pvBiPNeo1001 containing the *ugi* gene was provided by E.H. Radany (University of Michigan) and constructed as described (219).

2.1.6 Tissue Culture Media

For growth of human glioblastoma U251 cells, RPMI 1640 medium was supplemented with 2 mg/ml $NaHCO_3$, 0.3 mg/ml L-glutamine, 50 units/ml penicillin, and 50 µg/ml streptomycin. The medium was adjusted to pH 7.2 with 1 N HCl and sterilized by passage through a 0.2 µm membrane filter unit (Nalgene). RPMI 1640 medium was supplemented with 10% (v/v) fetal bovine serum. For the selection of U251 cells transfected with the pvBiPNeo1001 construct, RPMI 1640 medium was adjusted to 400 µg/ml G418

Table 1

E. coli Strains and Genotypes

E. coli Strain	Genotype	Reference
CJ236	*dut ung⁻ thi-1 relA spoT1 mcrA/* F'*cat* (pCJ105; $M13^{S}Cm^{r}$)	(105)
CSH50	*ara⁻ thi⁻ Δ(pro-lac)/* F' *traD36 proAB lacI^q ZΔM15*	(126)
JM105	*thi rpsl* (Str^{r}) *endA sbcB15 sbcC hsdR4* (r_k^- m_k^+) *Δ(lac-proAB)*/F' *traD36 lacI^q Δ(lacZ)M15 proA⁺B⁺*	(313)
JM109	*recA1* e14⁻(McrA⁻) *Δ(lac-proAB) thi gyrA96* (Nal^{r}) *endA1 hsdR17* (r_k^- m_k^+) *relA1 supE44/* F' *traD36 lacI^q Δ(lacZ)M15 proA⁺B⁺*	(313)
MC1061	*hsdR⁻ hsdM⁺ araD Δ(ara,leu) Δlac1POZY galU galK strA*	(132)
NR9162	*hsdR⁻ hsdM⁺ araD Δ(ara,leu) Δlac1POZY*	(222)
RR1	F⁻ *hsdS20* (r_B^- ,m_B^-) *ara-14 proA2 lacY1 galK2 rpsL20* (Sm^{r}) *xyl-5 mtl-1 supE44* λ^-	(141)

from a sterile stock (100 mg/ml). For growth of human colon adenocarcinoma LoVo cells, Ham's F-12 medium was supplemented with 1.2 mg/ml $NaHCO_3$ and the pH was adjusted to pH 7.2 with 1 N HCl. Ham's F-12 medium was supplemented with 20 % (v/v) fetal bovine serum. All supplemented medium was sterilized by passage through a second 0.2 μm membrane filter unit prior to use.

2.1.7 Human Cell Lines

The human glioblastoma U251 cell line and daughter cell lines transfected with and stably expressing the pvBiPNeo1001 or pvBiPNeo1001-*mugi* constructs were kindly provided by E.H. Radany (University of Michigan). The human colon adenocarcinoma LoVo cell line was procured from the American Type Culture Collection. All cell cultures were grown at 37°C, 5 % CO_2, and 90 % humidity.

2.1.8 Chromatographic Resins

DE52 anion exchange resin and P-11 cation exchange resin were obtained from Whatman. Sephadex G-25, G-50, and G-75 were purchased from Pharmacia Biotech. Bio-Gel P-4 (130 ± 40 μm), hydroxyapatite Bio-Gel HTP, and AG 501-X8(D) (20-50 mesh) and AG 1-X8 (100-200 mesh) ion exchange resins were purchased from Bio-Rad.

2.1.9 Oligonucleotides

Oligonucleotides used for this research are listed below. Oligonucleotides A-41-mer, C-41-mer, and PMR PLUS were synthesized on an Applied Biosystems 380B DNA synthesizer by the Center for Gene Research and Biotechnology (Oregon State University). Oligonucleotides U-34-mer, T-34-mer, A-34-mer, and G-34-mer were synthesized by Midland Certified Reagent Company. Oligonucleotides U-23-mer and A-23-mer were synthesized and

gel purified by Oligos Etc. The nucleotide sequence and use of each synthetic oligonucleotide are indicated below:

1. Oligonucleotides for site-directed mutagenesis of M13mp2op14 and M13mp2R14G

   A-41-mer: 5'-GGG TAA CGC CCG GGT TTT CCC AGT CAC GTC ATT GTA AAA CG-3'

   C-41-mer: 5'-GGG TAA CGC CCG GGT TTT CCC AGT CAC GTC CTT GTA AAA CG-3'

2. Base excision DNA repair substrate oligonucleotides

   U-23-mer: 5'-CCC AGT CAC GTC UTT GTA AAA CG-3'

   A-23-mer: 5'-CCC AGT CAC GTC ATT GTA AAA CG-3'

3. Uracil- and thymine-DNA glycosylase substrate oligonucleotides

   U-34-mer: 5'-AGC TTG GCT GCA GGT UGA CGG ATC CCC GGG AAT T-3'

   T-34-mer: 5'-AGC TTG GCT GCA GGT TGA CGG ATC CCC GGG AAT T-3'

   A-34-mer: 5'-AAT TCC CGG GGA TCC GTC AAC CTG CAG CCA AGC T-3'

   G-34-mer: 5'-AAT TCC CGG GGA TCC GTC GAC CTG CAG CCA AGC T-3'

4. DNA sequencing primer

   PMR-PLUS: 5'-GCA CTC CAG CCA GCT TTC CGG-3'

2.1.10 Enzymes

Proteinase K and creatine phosphokinase (type I, rabbit) were from Sigma. T4 DNA polymerase, T4 DNA ligase, T4 polynucleotide kinase, *E. coli* exonuclease III, and restriction endonucleases *Eco*RI, *Hin*fI, and *Sma*I were obtained from New England Biolabs. Worthington Biochemicals was the

source of ribonuclease A and endoproteinase Asp-N was from Boehringer Mannheim. Trypsin-EDTA was supplied by Life Technologies. *E. coli* endonuclease IV (fraction V) was kindly provided by B. Demple (Harvard University).

2.2 Experimental Procedures

2.2.1 Preparation of Chromatographic Resins

2.2.1.1 Preparation of DE52, P-11, Sephadex G-25, G-50, and G-75, Bio-Gel P-4, and Hydroxyapatite Bio-Gel HTP

Pre-swollen DE52 diethylaminoethyl cellulose was used to prepare DEAE-cellulose resin. The resin was defined at a 1:5 ratio (w/v) and equilibrated in TED buffer (50 mM Tris-HCl (pH 8.0), 1 mM EDTA, 1 mM DTT) for the purification of Ugi protein, buffer A (50 mM Tris-HCl (pH 7.0), 1 mM EDTA, 1 mM DTT) containing 50 mM NaCl for the purification of EDC/GEE-modified Ugi, or DAB buffer (30 mM Tris-HCl (pH 7.4), 1 mM EDTA, 1 mM DTT, 5 % (w/v) glycerol) containing 50 mM NaCl for the isolation of the Ung•Ugi complex. Fibrous P-11 cellulose phosphate resin was defined and equilibrated in buffer P (50 mM Tris-HCl (pH 7.5), 10 mM KCl, 5 mM 2-mercaptoethanol, 0.1 mM EDTA, 25 % (w/v) glycerol). Both resins were stored at 4°C.

Bio-Gel P-4 and Sephadex G-25, G-50, and G-75 resins were hydrated under various buffer conditions at room temperature and defined, equilibrated, and stored as described above. Bio-Gel P-4 was equilibrated in TE buffer (10 mM Tris-HCl (pH 8.0), 1 mM EDTA) or 50 mM potassium phosphate (pH 6.0) buffer depending on the application and stored as a 50 % slurry. Sephadex G-25 was equilibrated and stored in KEG buffer (50 mM potassium phosphate (pH 9.5), 1 mM EDTA, 5 % (w/v) glycerol). Sephadex G-50 was equilibrated and stored in TEAB buffer (10 mM triethylamine-

bicarbonate (pH 7.0)). Sephadex G-75 was equilibrated and stored in Ugi equilibration buffer (Ugi EB) (50 mM Tris-HCl (pH 8.0), 1 mM EDTA, 1 mM DTT, 100 mM NaCl, 10 % (w/v) glycerol) or Ung equilibration buffer (Ung EB) (10 mM Hepes-KOH (pH 7.4), 1 mM EDTA, 10 mM 2-mercaptoethanol, 1 M NaCl, 5 % (w/v) glycerol) for the purification of Ugi and Ung, respectively.

Hydroxyapatite Bio-Gel HTP was defined and equilibrated in HA buffer (10 mM potassium phosphate (pH 7.4), 1 mM DTT, 200 mM KCl).

2.2.1.2 *Preparation of Single-Stranded DNA-Agarose*

Calf thymus DNA (Type I, Sigma) was solubilized at 15 mg/ml in 300 ml of 20 mM NaOH and slowly stirred overnight at room temperature. After thorough mixing, the DNA solution was divided into 100-ml aliquots and incubated for 15 min at 95°C. An aliquot of the denatured DNA mixture equilibrated at 95°C was added to an equal volume of molten 4 % agarose solution equilibrated at 70°C, mixed thoroughly, and poured into an ice cold glass dish (Pyrex, 196 mm x 100 mm) held on ice and allowed to solidify. The solidified DNA-agarose mixture was pressed twice through a stainless steel sieve (60 mesh) and suspended in 300 ml of resuspension buffer (10 mM Tris-HCl (pH 7.5), 1 mM EDTA, 100 mM NaCl) per 200 ml of the sieved DNA-agarose. Each resuspended gel mixture was placed in a Buchner funnel (17 cm diameter) and washed with 9000 ml of resuspension buffer at room temperature until the A_{260} of the wash dropped below 0.02. The single-stranded DNA-agarose was stored at 4 °C as a 50 % slurry in buffer containing 10 mM Tris-HCl (pH 7.5), 1 mM EDTA, and 1 M NaCl.

2.2.1.3 *Preparation of Dowex 1-X8 Ion Exchange Resin*

Dowex AG 1-X8 (100-200 mesh, chloride form) was converted to the intermediate hydroxyl counterion form prior to conversion to the final formate counterion form for use in the uracil-DNA glycosylase and uracil-

DNA glycosylase inhibitor assays. Dowex AG 1-X8 was added to 400 ml of 1 M NaOH until the volume was equal to 500 ml. After mixing, the resin was allowed to settle for 20 min and the 1 M NaOH was decanted by aspiration. This step was repeated until 2000 ml of 1 M NaOH had been used. The resin was transferred to three 150-ml glass filter funnels (60-C) and the remaining 1 M NaOH was filtered from the resin by gravity. The contents of each funnel was washed with 100 ml of 1 M ammonium formate buffer (pH 4.2) followed by three ~333-ml washes of 10 mM ammonium formate buffer (pH 4.2). The resin was allowed to fully drain between each addition. Dowex AG 1-X8 was stored at 4°C in 10 mM ammonium formate buffer (pH 4.2).

2.2.2 Miscellaneous Methods

2.2.2.1 Preparation of Dialysis Tubing

Dialysis tubing (SpectraPor) was cut into lengths of 20 to 30 inches and soaked in 1 % acetic acid solution for 1 h. The soaking solution was decanted and tubing was rinsed with distilled H_2O prior to boiling in 1 L of 1 % $NaHCO_3$ and 0.1 % EDTA with intermittent stirring. The $NaHCO_3$/EDTA solution was exchanged after it became cloudy and/or yellow. This step was repeated three times. The tubing was rinsed and boiled in distilled H_2O, rinsed again, and stored at 4°C in 10 mM EDTA (pH 8.0).

2.2.2.2 Protein Concentration Measurements

The protein concentrations of *E. coli* Ung and Ugi were determined by absorbance spectroscopy by using the molar extinction coefficients $\varepsilon_{280\ nm} = 4.2 \times 10^4$ liters/mol•cm (Ung) and $\varepsilon_{280\ nm} = 1.2 \times 10^4$ liters/mol•cm (Ugi). The concentration of *E. coli* Ung•[^{35}S]Ugi complex was determined from [^{35}S]Ugi radioactivity since the complex exhibits 1:1 stoichiometry (15). The concentration of human UDG was determined by absorbance spectroscopy by

using the molar extinction coefficient $\varepsilon_{280\ nm} = 5.04 \times 10^4$ and the concentration of the human UDG•Ugi complex by using the molar extinction coefficient $\varepsilon_{280\ nm} = 6.3 \times 10^4$ which was calculated from the sum of the extinction coefficients from UDG and Ugi, respectively. The concentration of human whole cell extract protein was measured by the Bradford reaction using the Bio-Rad protein assay and was capable of accurately determining concentrations of 5.0 - 15.0 µg/ml extract protein. Bovine serum albumin (Standard II) was used as the protein standard for the microassay. The concentration of the protein standard was determined by using the molar extinction coefficient $\varepsilon_{280\ nm} = 0.67$ ml/mg•cm. Standards were diluted from 0-20 µg/ml in 2.5-µg/ml increments to generate a standard curve.

2.2.2.3 *Rapid Protein Staining of Nondenaturing Polyacrylamide Gels*

Proteins resolved by nondenaturing polyacrylamide gel electrophoresis were visualized by staining with Coomassie Brilliant Blue G-250 in 3.5 % $HClO_4$ as described by Reisner (221). The rapid stain solution was prepared by diluting 100 ml of 70 % $HClO_4$ into 1900 ml of distilled H_2O followed by the addition of 0.8 g of Coomassie Brilliant Blue G-250. The mixture was stirred at room temperature for 1 h and filtered through Whatman No. 1 paper. Nondenaturing polyacrylamide gels were submerged in ~ 500 ml of rapid stain solution and most protein bands were typically visualized after 10 min of incubation with gentle agitation at room temperature. In some cases, gels were also stained overnight. The background color of the gel turned a light amber color while protein bands stained a darker amber hue. After staining, the gels were placed in 5 % (v/v) acetic acid (~500 ml) which helped increase the sensitivity of detection by about three-fold. Under these conditions, the background color of the gel turned a light blue while protein bands stained a dark blue. Several changes of the 5 % acetic acid wash greatly reduced the light blue background color.

2.2.2.4 *Isolation of M13mp2 Single-Stranded DNA*

M13mp2 or M13mp2op14 bacteriophage stocks of unknown concentration were titered against mid-log *E. coli* JM109 or CJ236 cells to determine the number of plaque forming units per ml of stock (pfu/ml). *E. coli* JM109 or CJ236 cells were streaked on M9 plates and incubated at 37°C until isolated colonies were visible. An isolated colony was picked and placed into 25 ml of YT medium and incubated overnight at 37°C with shaking. The overnight culture was diluted 10-fold into a fresh volume (25 ml) of YT medium and incubated with vigorous shaking at 37°C for 1 h. The M13mp2 or M13mp2op14 bacteriophage stocks were serially diluted into SM medium and 100 µl aliquots of each dilution point were placed into sterile 13 x 100 mm glass test tubes. Bacteriophage dilutions were supplemented with 500 µl of mid-log bacterial culture and gently agitated to mix the bacterial cells and bacteriophage. Prewarmed YT topagar containing 0.4 mM IPTG and 1 mg/ml X-Gal equilibrated at ~45°C (2.5 ml) was added to each tube, mixed, and quickly poured onto YT plates prewarmed at 37°C. Topagar was allowed to solidify for 5-10 min at room temperature and plates were incubated overnight at 37°C. The concentration of viable bacteriophage was calculated from the discernible number of plaques scored at appropriate dilutions.

Single-stranded M13mp2 or M13mp2op14 DNA was isolated from bacteriophage grown in *E. coli* JM109 cells. Overnight cultures of *E. coli* JM109 cells grown in YT medium were used to inoculate a 2.5-L culture in 2X YT medium. Bacterial growth was monitored by absorbance spectroscopy (1 $OD_{595\ nm}$ = 8 x 10^8 cells/ml) until the cells reached early mid-log phase (~3.2 x 10^8 cells/ml). The total number of cells in the culture medium was calculated and bacteriophage were added to an MOI (multiplicity of infection - ratio of infectious particles to host) of 0.5. The bacteriophage infection mixture was incubated for an additional 9 h with extremely vigorous shaking (250 rpm) at

37°C. After placing the culture on ice for 10 min, bacterial cells were pelleted by centrifugation (GSA rotor, 7,000 rpm, 15 min, 4°C) and the supernatant containing the bacteriophage particles was saved and the volume measured. Approximately 5 ml of the supernatant was stored at 4°C for future infections. To the remaining supernatant, 5X PEG/NaCl (15 % PEG_{8000}, 2.5 M NaCl) was added to a final 1X concentration (equal to 25 % of the supernatant volume) and the mixture incubated on ice for 1 h with gentle mixing. Precipitated bacteriophage were isolated by centrifugation (GSA rotor, 7,000 rpm, 15 min, 4°C) and pellets were thoroughly drained for 15 min at room temperature. The pellet in each centrifuge bottle was resuspended in 2.5 ml of buffer PEB (100 mM Tris-HCl (pH 8.0), 300 mM NaCl, and 1 mM EDTA) and incubated on ice for 1 h with intermittent shaking. Resuspended bacteriophage were pooled, centrifuged (SA600 rotor, 6,000 rpm, 15 min, 4°C), and the supernatant was adjusted to 0.1% SDS using a 20 % SDS stock. The phage suspensions (5-ml aliquots) were extracted twice with an equal volume of phenol equilibrated in PEB buffer and twice with an equal volume of chloroform:isoamyl alcohol (24:1). All extractions involved rocking by hand for 3 min and phases were separated in a clinical centrifuge (IEC, setting #6 for 2 min). The recovered aqueous phase containing the single-stranded M13mp2 or M13mp2op14 DNA was concentrated in a Centriprep 30 concentrator (Amicon) by centrifugation (GSA rotor, 4,500 rpm, 4°C) and buffer exchanged against TE buffer. The concentration of DNA was measured by absorbance spectroscopy (1 $OD_{260\,nm}$ = 36 μg/ml) and the purity was determined by the $OD_{280\,nm}/OD_{260\,nm}$ ratio (~0.500).

Uracil-containing single-stranded M13mp2 DNA was similarly isolated from M13mp2 bacteriophage infections of *E. coli* CJ236 except that YT medium was supplemented with 34 μg/ml chloramphenicol and 0.25 μg/ml uridine was added to the 1.5-L cell culture medium 10 min prior to infection.

2.2.2.5 *Preparation of Oligonucleotides*

Preparations of synthetic oligonucleotides were deblocked and supplied as a lyophilized powder by the Center for Gene Research and Biotechnology (Oregon State University) and by the Midland Certified Reagent Company. Synthetic oligonucleotides prepared by Oligos Etc. were deblocked, gel purified, and supplied as a lyophilized powder.

Lyophilized oligonucleotides A-41-mer, C-41-mer, and PMR-PLUS were resuspended in 1 ml of TEAB buffer (10 mM triethylamine-bicarbonate (pH 7.0)). The pH of the TEAB buffer was adjusted by "bubbling" CO_2 gas produced by sublimation of dry ice into the buffer solution. Each sample was applied to a separate Sephadex G-50 column (1.8 cm^2 x 3.1 cm) equilibrated in TEAB buffer (pH 7.0) at room temperature and eluted with equilibration buffer. Fractions (1 ml) were collected at a flow rate of ~15 ml/h and oligonucleotide-containing fractions were detected by absorbance spectroscopy at 260 nm. Peak fractions (~4 ml) containing the oligonucleotides were evaporated to dryness in a Speed-Vac Concentrator (Savant) and each oligonucleotide preparation was resuspended in a total of 300-500 µl of distilled H_2O. The concentration of resuspended oligonucleotide was determined by absorbance spectroscopy (1 A_{260} = 20 µg/ml) and the purity was determined by the $OD_{280\ nm}/OD_{260\ nm}$ ratio (~0.500).

Oligonucleotides A-41-mer, C-41-mer, U-34-mer, T-34-mer, A-34-mer, and G-34-mer were subjected to further purification by polyacrylamide gel electrophoresis. Samples (300-500 µl containing ~100-200 nmol oligonucleotide) were combined with native sample buffer to a final concentration of 50 mM Tris-HCl (pH 6.8), 10 % (w/v) glycerol, and 0.1 % bromophenol blue and loaded onto separate nondenaturing 12 % polyacrylamide gels (30 x 40 x 0.16 cm) buffered with 1X TBE (90 mM Tris, 90 mM boric acid, 2 mM EDTA). Electrophoresis was conducted using TBE buffer at 1000 V until the tracking dye had migrated ~25 cm. After electrophoresis, the polyacrylamide gel was placed on top of a sealed TLC plate

(Polygram Cel 300 PEI/UV254) and the oligonucleotide bands were visualized by UV-shadowing. Oligonucleotide bands were excised from the gel by using a clean razor blade and the gel slice was placed into SpectraPor dialysis tubing (6,000-8,000 MWCO; 25.5 mm diameter) containing ~5 ml of a 0.1X concentration of TBE buffer. Oligonucleotides were electroeluted in 0.1X TBE buffer at 95 V for 2.5 h in a horizontal agarose gel chamber (35 x 21 cm). The dialysis tubing was positioned parallel to the electrodes and held in place by a glass plate. Following electroelution, the current was reversed for ~30 sec and the DNA solution was transferred into fresh dialysis tubing and dialyzed overnight in distilled H_2O at 4°C. The concentration of oligonucleotide was determined by absorbance spectroscopy (1 $OD_{260\,nm}$ = 20 μg/ml) and oligonucleotides were aliquoted into 5-nmol quantities, evaporated to dryness, and stored at -80°C.

2.2.2.6 5'-End Phosphorylation of Oligonucleotides

Oligonucleotides (4 nmol) were 5'-end phosphorylated in reaction mixtures (137.5 μl) containing 50 mM Tris-HCl (pH 7.6), 10 mM $MgCl_2$, 5 mM DTT, 0.1 mM EDTA, 250 μCi [γ-^{32}P]ATP (6,000 Ci/mmol), and 50 units of T4 polynucleotide kinase. Samples were incubated for 15 min at 37°C and adjusted to 200 μM ATP by using a 5 mM ATP stock. The reaction was incubated an additional 45 min at 37°C and terminated by adjustment to 10.7 mM EDTA and heated for 10 min at 70°C. The terminated reaction volume was adjusted to 250 μl with TE buffer and unreacted [γ-^{32}P]ATP was removed from the mixture by passage through two consecutive P-4 (Bio-Rad) spun columns containing 1.4 ml of resin and equilibrated in TE buffer. P-4 spun columns were centrifuged in a clinical centrifuge (IEC, setting #4 for 2.5 min).

Oligonucleotides were also 5'-end phosphorylated under similar reaction conditions except the 250 μCi [γ-^{32}P]ATP addition was omitted. Instead, these reaction mixtures were initially adjusted to 0.3 μM ATP by

using a 1.67 μM ATP stock in 10 mM tricine (pH 8.0). These conditions are identical to those of the reaction mixture containing [γ-^{32}P]ATP since the [γ-^{32}P]ATP stock was supplied at a concentration of 1.67 μM in 10 mM tricine (pH 8.0).

2.2.2.7 *Annealing Reaction of U/A-, U/G- and T/G-34-mer Duplex DNA*

Hybridization of 750 pmol of [^{32}P]U-34-mer or [^{32}P]T-34-mer to 1,500 pmol of A-34-mer or G-34-mer to construct duplex [^{32}P]U/A-, [^{32}P]U/G-, and [^{32}P]T/G-34-mer DNA substrates was conducted in annealing reaction mixtures (186 μl) containing 20 mM Tris-HCl (pH 7.4), 2 mM $MgCl_2$, and 50 mM NaCl. Reaction mixtures were placed in a 500-ml beaker containing 70°C distilled H_2O and allowed to cool to room temperature (~4 h). Duplex DNA was stored at -80°C.

2.2.2.8 *Transfection of Competent E. coli Cells by Electroporation*

In order to prepare competent *E. coli* JM109, NR9162, or MC1061 cells for electroporation of M13mp2 DNA, overnight cultures of bacterial cells were used to inoculate 500 ml of LB medium at a 1:100 ratio and growth continued with vigorous shaking at 37°C. The cell density was monitored by absorbance spectroscopy (1 $OD_{595\ nm}$ = 8 x 10^8 cells/ml). After the cells reached the early mid-log phase ($OD_{595\ nm}$ = 0.300-0.400) of growth, the culture was placed on ice for 10 min. Cells were placed into 250-ml centrifuge bottles and harvested by centrifugation (GSA rotor, 5,000 rpm, 10 min, 4°C). Each cell pellet was resuspended in 250 ml of cold, sterile distilled H_2O. Centrifugation was repeated as described above and each cell pellet was resuspended in 125 ml of cold, sterile distilled H_2O. Centrifugation was again conducted as described above and each pellet was resuspended in 5 ml of cold, sterile 10 % (w/v) glycerol, transferred to a 30 ml Corex tube, and centrifugation (SS34

rotor, 5,700 rpm, 10 min, 4°C) was again repeated. The final cell pellet was resuspended in a volume of ~3 ml of ice cold, sterile 10 % (w/v) glycerol to a final cell density of ~0.5-1.0 x 10^{11} cells/ml. The resuspended cell mixture was aliquoted (70 µl) into Eppendorf tubes, frozen in liquid nitrogen, and stored at -80°C until ready for use.

Electroporation was conducted using a Gene Pulser electroporation system (BioRad) and 0.2-cm gapped electroporation cuvettes. To a prechilled 1.5-ml Eppendorf tube, competent *E. coli* cells (40-50 µl) were mixed with 0.5-2.5 µl of transfection DNA and held on ice for 1-2 min. The DNA/cell mixture was transferred to a cold electroporation cuvette and placed into the chamber with tapping to eliminate any air bubbles. A single pulse set at 25 µF capacitance, 2.5 kV, and 200-400 Ω was applied. The time constant of the pulse was ~9.3 ms. Transfected cells were serially diluted into YT medium ($1/10^2$ to $1/10^7$) and a sample (100 µl) of each dilution point was placed into a sterile 13 x 100 mm test tube and 500 µl of mid-log *E. coli* JM109 or CSH50 cells was added. Prewarmed YT topagar containing 1 mg/ml X-Gal and 2.5 mM IPTG was equilibrated at ~45°C and 2.5 ml was added to each tube, mixed, and the mixture quickly poured onto YT plates prewarmed at 37°C. Plates were incubated overnight at 37°C.

2.2.2.9 Detection of ^{35}S-labeled Protein

[^{35}S]Ugi or Ung•[^{35}S]Ugi complex was resolved by nondenaturing polyacrylamide tube gel electrophoresis or nondenaturing polyacrylamide slab gel electrophoresis. Polyacrylamide tube gels were removed from cylindrical glass casting tubes (12.5 cm length x 0.5 cm internal diameter) by injecting distilled H_2O between the tube gel and the wall of the glass cylinder with a 30-ml syringe and a 22G1½ hypodermic needle and simultaneously pushing the gel outward with a cotton swab applicator, wrapped in a strip of cheese cloth to form a tight seal. The tube gel was horizontally sliced into 3.1

mm discs using a tube gel slicing device (Hoeffer). Gel discs were placed into separate scintillation vials (Wheaton, 7 ml) and dried overnight at room temperature. A 500-µl volume of 30 % hydrogen peroxide was added to each vial, and vials were tightly capped and incubated at 55°C for 24-48 hours to solubilize the polyacrylamide gel. After cooling to room temperature, each vial was supplemented with 5 ml of scintillation fluor (Formula 989, DuPont NEN), mixed by inversion, and analyzed for ^{35}S radioactivity in a Beckman LS 6800 liquid scintillation counter. Polyacrylamide slab gels were dried under vacuum, and autoradiography was performed with X-OMAT AR5 film (Kodak). Bands containing ^{35}S radioactivity were excised from the dried gels and processed as described above.

2.2.2.10 *Transfer of DNA to Nitrocellulose*

[^{32}P]DNA bands resolved by 0.8% agarose gel electrophoresis were transferred onto Gene Screen Plus (NEN) membranes using a downward alkaline blotting technique (119). Following electrophoresis, agarose gels were incubated for 15 min in 0.25 N HCl until the bromophenol blue tracking dye turned yellow and then soaked in 0.4 M NaOH for ~5 min. The transfer apparatus was prepared by placing a stack of paper towels in a Pyrex baking dish. On top of the paper towels, three gel-sized Whatman No. 1 filters (Whatman, Clifton, NJ) were positioned and the top filter was soaked in the 0.4 M NaOH transfer solution. Next, a gel-sized sheet of Gene Screen Plus soaked in 0.4 M NaOH was placed, followed by the agarose gel. On top of the gel, two additional gel-sized Whatman No. 1 filters soaked in 0.4 M NaOH were placed followed by two long, wet blotting strips of Whatman No. 1 filter paper used to wick the transfer solution from two 0.4 M NaOH reservoirs positioned on either side of the transfer apparatus. A glass plate (19 x 20 cm) was positioned on top to secure the gel and promote even distribution of the transfer solution. Air bubbles were carefully removed from each layer of the transfer apparatus during construction. Additionally, a strip of plastic wrap

was tucked under both edges of the gel between the paper towels and the wick to prevent a short circuit of transfer solution directly to the paper towels. Transfer of DNA was allowed to proceed overnight and the filter was hung to dry at room temperature prior to autoradiography.

2.2.3 Purification of Uracil-DNA Glycosylase

E. coli JM105 cells transformed with pSB1051 were grown at 37°C in 9 liters of TYN-ampicillin medium (1 % tryptone, 1 % yeast extract, 0.5 % NaCl, 0.01 % ampicillin) with vigorous shaking. When the cells reached a density of 6.4×10^8 cells/ml, *ung* gene expression was induced by adjusting the medium to 1 mM IPTG and incubation was continued for an additional 3 h. Cells were harvested by centrifugation (GSA rotor, 6,000 rpm, 15 min, 4°C), pellets were thoroughly drained, and frozen overnight at -80°C. All subsequent purification steps were conducted at 4°C. Cell pellets were thawed, resuspended in a total of 360 ml of TED buffer (50 mM Tris-HCl (pH 8.0), 1 mM EDTA, 0.1 mM DTT), Dounce homogenized to break up cell aggregates, and lysed in 40-ml aliquots in a French pressure cell at 15,000 psi. The cell lysate was collected, pooled, and centrifuged (SS34 rotor, 13,000 rpm, 20 min) to remove the cellular debris. The volume of the supernatant was measured and an equal volume of 1.6 % streptomycin sulfate in TED buffer was slowly added by burette with stirring over a period of 30 min. After equilibration for an additional 30 min, precipitated material was removed by centrifugation (SS34 rotor, 13,000 rpm, 20 min) and powdered ammonium sulfate was slowly added to the recovered supernatant to 35 % saturation and equilibrated for 10 min. The precipitate was removed by centrifugation (SS34 rotor, 13,000 rpm, 15 min) and powdered ammonium sulfate was slowly added to the collected supernatant to 70 % saturation and equilibrated for 10 min. The precipitate was recovered by centrifugation (SS34 rotor, 13,000 rpm, 15 min) and resuspended in ~20 ml of Ung EB (10 mM Hepes-KOH (pH 7.4), 1

mM EDTA, 10 mM 2-mercaptoethanol, 1.0 M NaCl, 5 % (w/v) glycerol) and dialyzed overnight against Ung EB. The dialyzed sample was loaded onto a Sephadex G-75 column (6 cm^2 x 88 cm) equilibrated in Ung EB and fractions (5.0 ml) were eluted with equilibration buffer at a flow rate of ~20 ml/h and assayed for uracil-DNA glycosylase activity. Active fractions were pooled (~120 ml) and dialyzed against HA buffer (10 mM potassium phosphate (pH 7.4), 1 mM DTT, 200 mM KCl) overnight. The dialyzed sample was loaded onto a hydroxyapatite column (19.6 cm^2 x 3.6 cm) equilibrated in HA buffer, fractions (7.5 ml) were eluted with equilibration buffer at a flow rate of ~30-40 ml/h and assayed for uracil-DNA glycosylase activity. Active fractions were detected in the flow through, pooled (~120 ml), and dialyzed against DA buffer (30 mM Tris-HCl (pH 7.4), 1 mM EDTA, 1 mM DTT, 5 % (w/v) glycerol) overnight. The dialyzed sample was applied to a single-stranded DNA-agarose column (19.6 cm^2 x 44 cm) equilibrated in DA buffer, washed with ~1,720 ml of equilibration buffer, and step eluted with 1,600 ml of DA buffer containing 150 mM NaCl at a flow rate of 40 ml/h. Fractions containing uracil-DNA glycosylase activity were analyzed by 12.5% SDS-polyacrylamide gel electrophoresis and fractions (~680 ml) were pooled and concentrated (6.8-fold) under N_2 gas (55 psi) in a 200-ml Amicon stirred cell (62 mm YM10 membrane) attached to a 4-liter Amicon reservoir. Following the concentration step, diafiltration was performed using 700 ml of DA buffer lacking NaCl and the resulting sample was designated uracil-DNA glycosylase (fraction V).

2.2.4 Purification of Uracil-DNA Glycosylase Inhibitor Protein

2.2.4.1 Large Scale Purification of Ugi

E. coli JM105 cells transformed with pZWtac1 were grown at 37°C in 9 liters of TYN-ampicillin medium (1 % tryptone, 1 % yeast extract, 0.5 % NaCl, 0.01 % ampicillin) supplemented with 10 µg/ml thiamine. When the cells reached a density of 6.4 x 10^8 cells/ml, *ugi* gene expression was induced by

adjusting the medium to 1 mM IPTG and incubation was continued for an additional 3 h. Cells were harvested by centrifugation (GSA rotor, 6,000 rpm, 15 min, 4°C), pellets were thoroughly drained, and frozen overnight at -80°C. Frozen cell pellets were thawed, resuspended in 360 ml of TED buffer (50 mM Tris-HCl (pH 8.0), 1 mM EDTA, 1 mM DTT), and Dounce homogenized to break up cell aggregates. The resuspended cells were lysed in 40-ml aliquots using a French pressure cell at 15,000 psi. The cell lysate was collected on ice and centrifuged (SS34 rotor, 13,000 rpm, 20 min, 4°C) to pellet the cellular debris. The supernatant was transferred into 30-ml Corex tubes, heated at 100° for 10 min, and allowed to cool to room temperature. The extract was centrifuged (SS34 rotor, 13,000 rpm, 15 min, 4°C) to remove precipitated material and the supernatant was dialyzed overnight against TED buffer. The dialyzed sample was loaded onto a DEAE-cellulose (Whatman DE52) column (19.6 cm^2 x 10.2 cm) equilibrated in buffer TED, washed with 600 ml of equilibration buffer, and Ugi was eluted by using a 1,100-ml linear gradient from 0 to 650 mM NaCl in TED buffer. Fractions (8 ml) were collected at a flow rate of 40 ml/h and assayed for uracil-DNA glycosylase inhibitor activity. Fractions containing peak inhibitor activity and an $OD_{280\ nm}$:$OD_{260\ nm}$ ratio of >0.5 were pooled (~230 ml) and concentrated (2.3-fold) under N_2 gas (55 psi) in a 200-ml Amicon stirred cell (62 mm YM10 membrane) attached to a 4.0-liter Amicon reservoir. After the concentration step, diafiltration was performed using 700 ml of Ugi EB (50 mM Tris-HCl (pH 8.0), 1 mM EDTA, 1 mM DTT, 100 mM NaCl, 10 % (w/v) glycerol) until the volume was ~25 ml. The diafiltered sample was applied to a Sephadex G-75 column (5.3 cm^2 x 60 cm) equilibrated in Ugi EB and protein was eluted with equilibration buffer at a flow rate of 20 ml/h. Fractions (4.2 ml) containing inhibitor activity were analyzed for purity by 20 % SDS-polyacrylamide gel electrophoresis and fractions (~65 ml) were pooled.

2.2.4.2 *Purification of [Methionine-^{35}S]Ugi*

E. coli JM105 transformed with pZWtac1 was grown in 2.5 liters of M9 medium supplemented with 10 μg/ml thiamine and 0.01 % ampicillin at 37°C. Upon reaching a cell density of 6.5 x 10^8 cells/ml, 9.4 nmol of [^{35}S]methionine (specific activity, 1,175 Ci/mmol) was added, and 35 min later, 25 ml of 100 mM IPTG was added to induce *ugi* gene expression. Cells were grown for an additional 3 h, harvested by centrifugation (GSA rotor, 6,000 rpm, 15 min, 4°C), pellets were thoroughly drained, and stored frozen at -80°C. Cells were thawed and resuspended in a total volume of 50 ml TED buffer. Resuspended cells were aliquoted (5 ml) and sonicated on ice in 1-min bursts separated by 1-min breaks for a total of eight cycles. The remaining steps of the purification were performed similarly to that of unlabeled Ugi with the following modifications: (i) DEAE-cellulose chromatography (fraction II) was performed using a 4.9 cm^2 x 10.2 cm column, and the inhibitor was eluted with a 300 ml linear gradient from 0 to 650 mM NaCl in TED buffer; and (ii) following Sephadex G-75 chromatography, fractions containing inhibitor activity (fraction IV) were pooled (~80 ml) and concentrated (4-fold) in an Amicon stirred cell as described above. [^{35}S]Ugi was then extensively dialyzed into 50 mM potassium phosphate (pH 6.0) buffer.

2.2.5 Purification of T4 DNA Polymerase

E. coli RR1 cells transformed with pTL43W were grown in 1.5 liters of VAT medium (1 % tryptone, 0.4 % yeast extract, 1 % K_2HPO_4, 0.1 % KH_2PO_4) supplemented with 1 % glucose and 0.01 % ampicillin at 30°C. Bacterial growth was monitored by absorbance spectroscopy until the cells reached a density of 6.4 x 10^8 cells/ml and *gp43* gene expression was induced by the addition of 1.5 liters of supplemented VAT medium equilibrated at 50°C.

Incubation was continued at 40°C for 2 h, cells were harvested by centrifugation (GSA rotor, 6,000 rpm, 15 min, 4°C), pellets were thoroughly drained, and stored overnight at -80°C. Cell pellets were weighed (16.7 g) and resuspended at 70 g/L in TEDM buffer (50 mM Tris-HCl (pH 8.0), 2 mM EDTA, 0.1 mM DTT, 1 mM 2-mercaptoethanol) supplemented with 20 mg/L of lysozyme. Following resuspension, the cell mixture was adjusted to 1 mM PMSF and stirred vigorously for 30 min at room temperature. Sodium deoxycholate was then added to a concentration of 0.05 % (w/v) and PMSF was added to a final concentration of 1.5 mM. The cell suspension was then transferred to ice and stirred for an additional 20 min. Cells were aliquoted (20 ml) and sonicated on ice in 1 min bursts separated by 1 min breaks for a total of five cycles. Centrifugation was performed (SA600 rotor, 8,500 rpm, 20 min, 4°C) to pellet cellular debris. Twelve aliquots (200 µl) of the recovered supernatant were removed and polyethyleneimine (PEI) was added to each to achieve final concentrations of PEI ranging from 0.05 % to 0.60 % in 0.05 % increments by using a 5 % (v/v) PEI stock. Mixtures were placed on ice for 30 min with intermittent mixing, precipitated material was removed by microcentrifugation (12,000 x g, 5 min, 4°C), and aliquots of the supernatant (10 µl) were analyzed by 10 % SDS-polyacrylamide gel electrophoresis for their T4 DNA polymerase content and silver stained. T4 DNA polymerase was detected and migrated as an ~94 kDa polypeptide. Based on this analysis, the most quantitative precipitation of T4 DNA polymerase occurred at a PEI concentration of 0.20 %. Using the 5 % (v/v) PEI stock, the supernatant from the cell lysate was adjusted to 0.20 % PEI over a 15-min period on ice with gentle mixing. After an additional 20 min, the precipitated material was collected by centrifugation (SA600 rotor, 8,500 rpm, 20 min, 4°C) and pellets were resuspended in buffer X (50 mM Tris-HCl (pH 7.5), 2 mM EDTA, 10 mM 2-mercaptoethanol) supplemented with 50 mM NaCl using a volume equal to 1/20th of the volume of the cell lysate supernatant prior to PEI

precipitation. Pellets were Dounce homogenized (20 strokes) and the suspension was diluted with an equal volume of buffer X lacking NaCl. After mixing on ice for 30 min, centrifugation (SA600 rotor, 8,500 rpm, 20 min, 4°C) was conducted and the supernatants were saved. The resultant pellets were re-extracted with 10 ml of buffer X containing 50 mM NaCl, diluted, mixed, and centrifuged as described above. Supernatant fractions from both extractions were combined and powdered ammonium sulfate was added to 35 % (saturation) over a 15 min period followed by a 20 min equilibration period. Centrifugation (SA600 rotor, 14,500 rpm, 20 min, 4°C) was performed, the supernatant fraction was saved, and powdered ammonium sulfate was added to 55 % (saturation) as described above. Precipitated material was recovered by centrifugation (SA600 rotor, 14,500 rpm, 20 min, 4°C) and resuspended in a volume of buffer X containing 200 mM NaCl equal to 1/5th of the cell lysate supernatant volume prior to the ammonium sulfate precipitation step. The resuspended pellet was dialyzed extensively against buffer D (50 mM Tris-HCl (pH 7.5), 50 mM KCl, 5 mM 2-mercaptoethanol, 0.1 mM EDTA, 25 % (w/v) glycerol) and applied to a single-stranded DNA agarose column (19.6 cm^2 x 40 cm) equilibrated in buffer D at 20 ml/h and fractions (8 ml) were collected at a flow rate of 40 ml/h. After washing the column with equilibration buffer (~1,800 ml), T4 DNA polymerase was step eluted with 1,600 ml of buffer D containing 200 mM KCl. Fractions containing peak T4 DNA polymerase activity were analyzed by 10 % SDS-polyacrylamide gel electrophoresis, fractions were pooled (~560 ml) and concentrated (14-fold) under N_2 gas (55 psi) in an Amicon stirred cell (62 mm YM10 membrane) attached to a 4-liter Amicon reservoir. The concentrated sample was dialyzed extensively against buffer P (50 mM Tris-HCl (pH 7.5), 10 mM KCl, 5 mM 2-mercaptoethanol, 0.1 mM EDTA, 25 % (w/v) glycerol) and loaded onto a P-11 phosphocellulose column (19.6 cm^2 x 7 cm) equilibrated in buffer P at 20 ml/h. After washing the column with equilibration buffer (~ 600 ml), T4 DNA polymerase was eluted by using a 1,100-ml linear gradient

from 10 to 400 mM KCl in buffer P. Fractions (5 ml) containing polymerase activity were analyzed by 10 % SDS-polyacrylamide gel electrophoresis, fractions were pooled, concentrated (~7.5-fold) as described above. The pooled fractions were dialyzed extensively against buffer S (20 mM Tris-HCl (pH 8.1), 50 mM NaCl, 2 mM DTT) containing 10 % (w/v) glycerol followed by extensive dialysis against buffer S containing 50 % (w/v) glycerol. T4 DNA polymerase was stored at -80°C.

2.2.6 Resolution of Ung•Ugi Complexes by DEAE-Cellulose Chromatography

Ung•[^{35}S]Ugi complexes were formed by mixing 26.4 nmol of *E. coli* Ung with 5.3 nmol of either unmodified or EDC/GEE-modified [^{35}S]Ugi forms I-V and were incubated at 25°C for 10 min and then at 4°C for 20 min. Following complex formation, each Ung•[^{35}S]Ugi sample was loaded onto a DEAE-cellulose (Whatman DE52) column (0.8 cm^2 x 1.9 cm) to resolve the complex from its component proteins. The column was equilibrated in DAB buffer containing 50 mM NaCl. After sample application, the column was shut off for 5 min and then washed with 30 ml of equilibration buffer at a flow rate of 20 ml/h. Proteins were eluted with a two-step gradient consisting of 25 ml and 10 ml of DAB buffer containing 150 and 250 mM NaCl, respectively. Fractions were collected, and samples were analyzed for Ung activity and ^{35}S radioactivity. Fractions containing Ung•[^{35}S]Ugi complex were pooled and concentrated by using a Centriplus-10 (Amicon) concentrator.

The UDG•Ugi complex was formed by combining 0.5 µmol of human placental UDG with 1.0 µmol of Ugi and incubated under standard complex formation conditions described above. UDG•Ugi complex was purified from excess Ugi by a DEAE-cellulose column (1.8 cm^2 x 5.7 cm) equilibrated in buffer DAB containing 50 mM NaCl. The complex was loaded at a flow rate

of 20 ml/h, washed with equilibration buffer (~40 ml), and eluted by the addition of 120 ml of equilibration buffer containing 125 mM NaCl. Fractions (4 ml) were collected at a flow rate of 40 ml/h and aliquots (25 µl) were analyzed by both 18 % nondenaturing and 20 % SDS-polyacrylamide gel electrophoresis to verify that complex was resolved from free UDG and Ugi. Peak fractions containing UDG•Ugi complex were pooled, concentrated (32-fold) to ~ 1 ml, and diafiltered into equilibration buffer without NaCl by using an Amicon stirred cell (25 mm YM10 membrane). Following the concentration step, the UDG•Ugi complex (A_{280} = 10.8) was determined to contain 170 µM protein by absorbance spectroscopy.

2.2.7 Enzyme Assays

2.2.7.1 Uracil-DNA Glycosylase

Standard uracil-DNA glycosylase assay mixtures (100 µl) contained 70 mM Hepes-KOH (pH 8.0), 1 mM EDTA, 1 mM DTT, and 8.2 nmol of activated calf-thymus [*uracil*-^{3}H]DNA (181-195 cpm/pmol of uracil). Exogenous *E. coli* Ung, human UDG, or human whole cell extract protein were introduced as samples (25 µl) and were typically diluted in Ung dilution buffer (50 mM Hepes-KOH (pH 7.4), 1 mM EDTA, 1 mM DTT, 100 µg/ml bovine serum albumin) as needed. Reaction mixtures were incubated at 37°C for 30 min and terminated on ice with 250 µl of 10 mM ammonium formate (pH 4.2). Free [^{3}H]uracil was resolved from unhydrolyzed [*uracil*-^{3}H]DNA by applying 300 µl of the terminated reaction mixture to a Dowex 1-X8 ion exchange column (0.2 cm^2 x 2.0 cm) equilibrated in 10 mM ammonium formate (pH 4.2). Columns were washed with 1.7 ml of equilibration buffer and two 1-ml fractions were collected. Fractions were combined with 5 ml of Formula 989 Fluor, mixed by inversion, and ^{3}H radioactivity was measured. One unit of uracil-DNA glycosylase is defined as the amount that releases 1 nmol of uracil/h under standard conditions.

Uracil-DNA glycosylase activity in human crude cell extracts was also measured on single-stranded [^{32}P]U-34-mer, and double-stranded [^{32}P]U/A-34-mer and [^{32}P]U/G-34-mer DNA substrates. Reaction mixtures (100 µl) contained 25 mM Hepes-KOH (pH 7.8), 0.5 mM EDTA, 0.5 mM DTT, 4 pmol of uracil-containing [^{32}P]34-mer oligonucleotide and various amounts of crude cell extract (0.16-160 µg) diluted with HE buffer (25 mM Hepes-KOH (pH 7.8), 1 mM EDTA, 1 mM DTT, 10 % (w/v) glycerol). Crude cell extract dilutions were introduced as 20-µl samples. Samples containing uracil-DNA glycosylase inhibitor protein were prepared by mixing 1000 units of Ugi (fraction IV) with the crude cell extract prior to the addition of DNA substrates. Reaction mixtures were incubated at 30°C for 30 min and terminated with an equal volume of a stop solution containing 2 % SDS and 50 mM EDTA. Samples were adjusted to a final concentration of 0.3 mg/ml yeast tRNA and 2 M ammonium acetate, extracted twice with an equal volume of phenol/chloroform (50:50), ethanol-precipitated, and resuspended in 20 µl of distilled H_2O. Apyrimidinic sites (AP-sites) generated by uracil removal from DNA substrates were hydrolyzed by the addition of 0.55 µl of 3 M K_2HPO_4 (pH 13.7) to 5 µl of resuspended DNA and incubated for 3 h at 55°C. Samples were then neutralized with 1.2 µl of 1.5 M KH_2PO_4 and combined with an equal volume of denaturing sample buffer (95 % deionized formamide, 10 mM EDTA, 0.1 % bromophenol blue, 0.1 % xylene cyanol). After heat treatment at 95°C for 3 min, samples were analyzed by denaturing 12 % polyacrylamide/8.3 M urea gel electrophoresis. Electrophoresis was performed using TBE buffer (90 mM Tris, 90 mM boric acid, 2 mM EDTA) at 1,200 V until the bromophenol blue tracking dye migrated ~20 cm. Gels were dried under vacuum and autoradiography was performed by using X-OMAT AR5 film (Kodak). Bands containing ^{32}P radioactivity were excised from the dried gel, placed in scintillation vials (7 ml) containing 0.5 ml of 30 % H_2O_2, and incubated at 55°C for 24 h. Once solubilized, 5 ml of Formula 989 Fluor

was added and ^{32}P radioactivity was measured by using a Beckman LS 6800 liquid scintillation counter.

Thymine-DNA glycosylase and double-stranded uracil-DNA glycosylase activities in human crude cell extracts were assayed similarly to that described above. Reaction mixtures (100 µl) contained 25 mM Hepes-KOH (pH 7.9), 50 mM KCl, 1 mM DTT, 0.5 mM EDTA, 0.01 mM $ZnCl_2$, 0.1 mg/ml acetylated bovine serum albumin (BSA), 4 pmol of either [^{32}P]T/G-34-mer, [^{32}P]U/A-34-mer, or [^{32}P]U/G-34-mer, and various amounts of crude cell extract (0.16-160 µg) diluted with HE buffer. Samples containing uracil-DNA glycosylase inhibitor protein were prepared by mixing 1000 units of Ugi (fraction IV) with the crude cell extract prior to the addition of DNA substrates. Enzymatic activity was determined following incubation at 30°C for 30 min. [^{32}P]oligonucleotide reaction products were processed and analyzed by denaturing polyacrylamide gel electrophoresis as described above.

2.2.7.2 *Uracil-DNA Glycosylase Inhibitor Protein*

Uracil-DNA glycosylase inhibitor activity was measured in reaction mixtures containing 70 mM Hepes-KOH (pH 8.0), 1 mM EDTA, 1 mM DTT, 8.2 nmol of [*uracil*-^{3}H]DNA, 0.05-0.15 units of *E. coli* uracil-DNA glycosylase (fraction V) and various amounts of uracil-DNA glycosylase inhibitor protein diluted in Ugi dilution buffer (50 mM Tris-HCl (pH 8.0), 1 mM EDTA, 1 mM DTT, 100 mM NaCl) or heat-treated human crude cell extract protein. Ugi and heat-treated cell extract were introduced as 25 µl samples. Reactions were conducted for 30 min at 37°C. The amount of [^{3}H]uracil released was measured by using a Dowex 1X-8 column as described for uracil-DNA glycosylase. One unit of uracil-DNA glycosylase inhibitor is defined as the amount that inactivates 1 unit of uracil-DNA glycosylase under standard reaction conditions.

2.2.7.3 *DNA Polymerase*

T4 DNA polymerase activity was measured in reaction mixtures (100 µl) containing 67 mM Tris-HCl (pH 8.8), 6.7 mM $MgCl_2$, 16.7 mM $(NH_4)_2SO_4$, 6.7 µM EDTA, 10 mM 2-mercaptoethanol, 200 µg/ml acetylated BSA, 10 µg activated calf thymus DNA, 33 µM each of dATP, dTTP, dCTP, and dGTP, and [^{3}H]dTTP (1700 cpm/pmol). Exogenous T4 DNA polymerase was introduced as samples (25 µl) and diluted in T4 DNA polymerase buffer S. Reaction mixtures were incubated at 37°C for 30 min and terminated on ice by the addition of 200 µl of 1 mg/ml BSA in 0.1 M sodium pyrophosphate. DNA was precipitated with 1 ml of 10 % (saturated) trichloroacetic acid (0.30 g/ml) and held on ice for 5 min. Acid-insoluble DNA was collected on #30 glass fiber filters (Schleicher and Schuell) pre-soaked in 0.1 M sodium pyrophosphate, washed with 18 ml (six x 3 ml applications) of 0.1 M sodium pyrophosphate in 1 N HCl, and dried with 95 % ethanol. Glass filters were dried under a heating lamp for 10 min, placed into glass vials containing 10 ml of 0.4 % 2,5-bis-2-(5-tertbutylbenzoxazolyl)-thiophene (BBOT) in toluene, and [^{3}H]dTMP incorporation into DNA was measured by using a Beckman LS6800 liquid scintillation spectrometer. One unit of T4 DNA polymerase activity catalyzes the incorporation of 10 nmol of total dNMP into activated calf thymus DNA in 30 min at 37°C.

DNA polymerase activity in human whole cell extracts was measured in reaction mixtures (100 µl) containing 100 mM Tris-HCl (pH 7.5), 5 mM $MgCl_2$, 1 mM DTT, 0.1 mM EDTA, 2 mM ATP, 0.5 mM β-NAD, 20 µM each of dATP, dTTP, dCTP, and dGTP, 5 mM phosphocreatine di-Tris salt, 40 units of creatine phosphokinase, 10 µg activated calf thymus DNA, and [^{3}H]dTTP (1700 cpm/pmol). Human whole cell extract protein was introduced as samples (40 µl) diluted in whole cell extract dialysis buffer (25 mM Hepes-KOH (pH 7.9), 100 mM KCl, 12 mM $MgCl_2$, 1 mM EDTA, 2 mM DTT, 17 % (w/v) glycerol). Samples supplemented with various amounts of aphidicolin in DMSO

(constituting 1 % of the total reaction volume) were mixed with the crude cell extract protein prior to the addition of the DNA substrate. Reaction mixtures containing human U251 cell extract protein were incubated for 60 min and reaction mixtures containing human LoVo cell extract protein were incubated for 45 min at 30°C. Samples were terminated and the amount of [^{3}H]dTMP incorporated into activated calf thymus DNA was determined as described above.

2.2.8 Electrophoresis

2.2.8.1 Sodium Dodecyl Sulfate Polyacrylamide Slab Gel Electrophoresis

Sodium dodecyl sulfate polyacrylamide slab gel electrophoresis was performed similarly to that described by Laemmli (134). Slab gels contained a resolving gel (13 cm) composed of various concentrations of acrylamide and N,N'-methylenebis(acrylamide) (typically 20 %:0.53 %, 12.5 %:0.33 %, or 10 %:0.27 %) from a stock solution of 30 % acrylamide:0.8 % N,N'-methylenebis(acrylamide) (37:1 ratio), 0.1 % SDS, and 375 mM Tris-HCl (pH 8.8). The resolving gel was polymerized by adjustment to 0.03 % (w/v) ammonium persulfate and 0.075 % (v/v) TEMED. The stacking gel (1 cm) contained 3 % acrylamide, 0.08 % N,N'-methylenebis(acrylamide), 0.1 % SDS, and 125 mM Tris-HCl (pH 6.8). The stacking gel was polymerized by adjustment to 0.10 % (w/v) ammonium persulfate and 0.10 % (v/v) TEMED. Protein samples were mixed with an equal volume of cracking dye buffer (50 mM Tris-HCl (pH 6.8), 1 % SDS, 143 mM 2-mercaptoethanol, 10 % (w/v) glycerol, 0.04 % bromophenol blue) and heated at 100°C for 10 min before being loaded onto the gel. Electrophoresis was conducted at room temperature at 100 V until the tracking dye reached the resolving gel and then the voltage was increased to 200 V until the tracking dye was ~2 cm from the bottom of the gel. The running buffer contained 25 mM Trizma base, 192 mM glycine, and 0.1 % SDS. Gels were fixed in a solution containing 10 %

acetic acid and 50 % methanol and protein bands were visualized by staining in a solution of 10 % acetic acid, 50 % methanol, and 0.05 % Coomassie brilliant blue G-250. Gels were destained in 7 % acetic acid and 5 % methanol.

2.2.8.2 *Nondenaturing Polyacrylamide Slab Gel Electrophoresis*

Nondenaturing polyacrylamide slab gel electrophoresis was performed by a modification of that described by Laemmili (134). Slab gels contained a resolving gel (13 cm) composed of 18 % acrylamide, 0.36 % N,N'-methylenebis(acrylamide), and 375 mM Tris-HCl (pH 8.8) and a stacking gel (1 cm) containing 3 % acrylamide, 0.08 % N,N'-methylenebis(acrylamide), and 125 mM Tris-HCl (pH 6.8). Both the resolving and stacking gels were polymerized as described above. Protein samples (30-60 µl) were adjusted to final concentrations of 50 mM Tris-HCl (pH 6.8), 10 % (w/v) glycerol, and 0.01 % bromophenol blue prior to being loaded on the gel. Electrophoresis was performed at 4°C and 100 V until the tracking dye migrated through the stacking gel, at which point the electrical potential was increased to 200 V. Electrophoresis continued until the tracking dye migrated within ~2 cm from the bottom of the gel. The native running buffer contained 25 mM Trizma base and 192 mM glycine. Protein bands were detected by a rapid protein staining method originally described by Reisner (221) with modifications as described above.

2.2.8.3 *Nondenaturing Polyacrylamide Tube Gel Electrophoresis*

Nondenaturing polyacrylamide tube gel electrophoresis was performed as described by Davis (50) with some modifications. Tube gels (0.6 cm diameter) contained a resolving gel (9 cm) composed of 18 % acrylamide, 0.36 % N,N'-methylenebis(acrylamide), and 375 mM Tris-HCl (pH 8.8) and a stacking gel (1 cm) containing 3 % acrylamide, 0.08 % N,N'-methylenebis(acrylamide), and 125 mM Tris-HCl (pH 6.8). Both the resolving

and stacking gels were polymerized as described above but at 4°C. Protein samples were adjusted to final concentrations of 50 mM Tris-HCl (pH 6.8), 10 % (w/v) glycerol, and 0.01 % bromophenol blue and electrophoresis was performed at 4°C as described above. After electrophoresis, gels were either stained by rapid protein staining (221) or solubilized for radioactivity as described previously.

2.2.8.4 Urea-Polyacrylamide Sequencing Gel Electrophoresis

Analysis of uracil-DNA glycosylase or whole cell extract base excision repair reaction products was performed using denaturing polyacrylamide gels (30 x 40 x 0.08 cm) composed of 12 % acrylamide, 0.40 % N,N'-methylenebis(acrylamide), 8.3 M urea, and TBE buffer (90 mM Tris, 90 mM boric acid, 2 mM EDTA). Polymerization was catalyzed by adjustment to 0.067 % (w/v) ammonium persulfate and 0.012 % (v/v) TEMED. Samples were mixed with an equal volume of denaturing formamide dye buffer (95 % deionized formamide, 10 mM EDTA, 0.1 % bromophenol blue, 0.1 % xylene cyanol) and heated at 95°C for 3 min. Samples (5-15 µl) were loaded and electrophoresis was performed at 1000-1200 V in TBE buffer until the bromophenol blue tracking dye had migrated ~20-25 cm. The gels were soaked in tepid water for ~2-3 min to diffuse urea out of the gel and gels were dried under vacuum and autoradiography was performed with X-OMAT AR5 film (Kodak). Bands containing ^{32}P radioactivity were either excised from the gel for solubilization and measurement of ^{32}P radioactivity by liquid scintillation or the intact gel was quantitated by using a PhosphorImager.

Nondenaturing 5 % polyacrylamide sequencing gels were similarly prepared but without urea. Samples (~5-10 µl) were adjusted to 50 mM Tris-HCl (pH 6.8), 10 % (w/v) glycerol, and 0.01 % bromophenol blue and electrophoresis was performed at 750 V as described above. Gels were dried under vacuum, autoradiography was performed, and ^{32}P radioactivity was quantitated by using a PhosphorImager.

2.2.8.5 *Agarose Gel Electrophoresis*

Agarose slab gels (0.8 %) were prepared by heating electrophoresis grade agarose powder in a volume of TAE buffer (40 mM Tris-acetate and 1 mM EDTA (pH 8.0)) in a microwave oven for ~1-2 min. After cooling to ~50-60°C, ethidium bromide (500 µg/ml) was added to 0.1 µg/ml, the mixture was poured into 12 x 13 cm or 7 x 8 cm casting trays (Owl Scientific) containing a 20-well or 10-well teflon comb, respectively, and allowed to polymerize for ~1 h. To physically separate Form I from Form II DNA or to measure M13mp2 DNA recoveries or primer extension reaction products, samples were combined with agarose dye buffer to a final concentration of 10 mM EDTA (pH 8.0), 0.1% SDS, 5% (w/v) glycerol, and 0.01% bromophenol blue, loaded onto 0.8% agarose gels, and electrophoresis was performed at 100 V (12 x 13 cm gel) or 70 V (7 x 8 cm gel) in TAE buffer containing 0.1 µg/ml ethidium bromide until the tracking dye had migrated ~75% of the distance of the gel. DNA was visualized by UV-light transillumination (~302 nm).

2.2.9 EDC/GEE Modification of [^{35}S]Ugi

An EDC/GEE modification reaction mixture (16.9 ml) containing 1,050 nmol of [^{35}S]Ugi (fraction IV), 228 µmol of glycine ethyl ester (GEE), and 45.6 µmol of 1-ethyl-3-(3-dimethylaminopropyl)carbodiimide (EDC) in 50 mM potassium phosphate buffer (pH 6.0) was incubated at 25°C for 30 min. GEE was introduced into the reaction mixture with [^{35}S]Ugi prior to the addition of EDC. The reaction was terminated by addition of 16.9 ml of 2 M sodium acetate (pH 4.75). Excess EDC and GEE were removed from the EDC/GEE-modified [^{35}S]Ugi by processing 250-µl aliquots through spun columns containing 1.4 ml of Bio-Gel P-4 resin (Bio-Rad) equilibrated in 50 mM potassium phosphate buffer (pH 6.0). P-4 spun columns were centrifuged in a clinical centrifuge (IEC, setting #4 for 2.5 min). After processing, all aliquots

were pooled and extensively dialyzed against buffer A (50 mM Tris-HCl (pH 7.0), 1 mM EDTA, 1 mM DTT) containing 50 mM NaCl.

2.2.10 Purification of EDC/GEE-Modified [^{35}S]Ugi Forms I-V

In order to isolate individual forms of EDC/GEE-modified [^{35}S]Ugi protein, a sample containing 486 nmol of the EDC/GEE-modified [^{35}S]Ugi mixture was applied to a DEAE-cellulose (Whatman DE52) column (0.6 cm^2 x 7.9 cm) equilibrated at 4°C in buffer A containing 50 mM NaCl. The column was washed with 15 ml of equilibration buffer , and [^{35}S]Ugi was eluted with a 100 ml linear gradient of 50-300 mM NaCl in buffer A at a flow rate of 10 ml/h. Fractions (1 ml) were collected in Eppendorf tubes, samples (10 µl) were mixed with 5 ml of Formula 989 Fluor, and ^{35}S radioactivity was measured in a Beckman LS 6800 liquid scintillation counter. Fractions containing EDC/GEE-modified [^{35}S]Ugi forms I-V were analyzed by 18 % nondenaturing polyacrylamide gel electrophoresis. Each form was separately pooled and evaporated to dryness in a Speed-Vac Concentrator (Savant), resuspended with 1 ml of buffer A, and then dialyzed extensively against Ugi EB.

2.2.11 Fluorescein 5-Isothiocyanate Labeling of Ung

Four preparations of Ung (fraction V) were extensively dialyzed against buffer KEG containing 50 mM potassium phosphate (pH 8.5, 9.0, 9.5, or 10.0), 1 mM EDTA, and 5 % (w/v) glycerol at 4°C. Fluorescein 5-isothiocyanate stock (810 µM) was freshly prepared in dimethylformamide, and 1.5 ml was added to 14 ml of Ung (2.9 mg) with thorough mixing. After 2.5 h in the dark, the mixture was placed on ice and then loaded onto four separate Sephadex G-25 columns (4.9 cm^2 x 13.5 cm) equilibrated in buffer KEG (pH 8.5, 9.0, 9.5, or 10.0). The columns were washed with equilibration buffer at a flow rate of 20 ml/h and fractions (2 ml) were monitored at 260, 280, and 496 nm for

absorbance. After the FITC-Ung (F-Ung) containing fractions were pooled, the concentration of F-Ung was determined based on absorbance at 280 and 496 nm. The concentration of FITC in the dye-protein conjugate was determined by the absorbance, where $\varepsilon_{496\ nm} = 7.8 \times 10^4$ liter/mol•cm. It was experimentally determined that 1 μM FITC contributed 0.025 A_{280}. Thus, the concentration of F-Ung was determined by subtracting the A_{280} contributed by FITC from the overall A_{280} of the dye-protein conjugate and dividing by the molar extinction coefficient of Ung.

2.2.12 Steady-State Fluorescence Measurements

Steady-state fluorescence measurements were conducted at 25°C using an LS50 luminescence spectrometer (Perkin-Elmer) equipped with a xenon flash tube and a thermostatted minicell (4 mm). Excitation and emission wavelengths were 496 and 520 nm, respectively; both slit widths were set at 5 mm.

2.2.13 Isolation of Cyanogen Bromide-Generated Peptide Fragments from EDC/GEE-Modified [^{35}S]Ugi Forms I-V

Cyanogen bromide cleavage reaction mixtures (200-650 μl) contained 20 mM CNBr, 0.1 N HCl, and 25 μM of [^{35}S]Ugi or EDC/GEE-modified [^{35}S]Ugi forms I-V. After incubation at 25°C for 24 h, samples were evaporated to dryness, resuspended in 65 μl of distilled H_2O, and analyzed by using MALDI mass spectrometric methods. Samples utilized for peptide C3 purification were resuspended in 600 μl of buffer A and applied to individual DEAE-cellulose (Whatman DE52) columns (0.79 cm^2 x 1.3 cm) equilibrated in buffer A at 4°C. After sample loading, the flow was stopped for 5 min, and then the column was washed with 2.5 ml of buffer A. Peptide fragments were eluted at a flow rate of 10 ml/h with a 50-ml linear gradient of 0-250 mM NaCl in buffer A. Fractions (500 μl) were collected in Eppendorf tubes, and samples were analyzed for CNBr-cleaved peptide fragments by MALDI mass

spectrometry. Fractions containing peptide C3 were pooled and concentrated to ~300 µl by using a Centricon-3 (Amicon) concentrator, buffer was exchanged with distilled H_2O, and fractions were submitted for amino acid sequence analysis.

2.2.14 Asp-N Endoproteinase Digestion of Ugi Protein

Proteolysis reaction mixtures contained Asp-N (0.04 mg/ml in 10 mM Tris-HCl (pH 7.5)) and unmodified [^{35}S]Ugi or EDC/GEE modified [^{35}S]Ugi forms II-III (10 mM Tris-HCl (pH 7.5)) in a 1:100 (w/w) ratio. Incubation was carried out for 3 h at 25°C, and the extent of proteolysis was monitored by MALDI mass spectrometry.

2.2.15 Amino Acid Sequence Analysis

Samples (30 µl in distilled H_2O) containing purified peptide C3 from unmodified [^{35}S]Ugi or EDC/GEE-modified [^{35}S]Ugi forms I-IV were applied to a cartridge filter precycled with Biobrene (Applied Biosystems). Amino acid sequencing was conducted using an Applied Biosystems model 475A gas protein sequencer by the Center for Gene Research and Biotechnology (Oregon State University).

2.2.16 MALDI Mass Spectrometric Analysis

MALDI mass spectrometry was performed by the Mass Spectrometry Facilities and Service Core Unit (Environmental Health Science Center, Oregon State University) using a custom-built time of flight instrument (112). Two different matrices were used in the sample preparation: (i) 10 mg/ml of sinapinic acid dissolved in 33 % acetonitrile and 67 % trifluoroacetic acid (0.1 % solution) was mixed (3:1) with samples (0.5 µl) containing 10 µM EDC/GEE-modified or unmodified Ugi protein; and (ii) a saturated solution of α-cyano-4-hydroxycinnamic acid in 33 % acetonitrile and 67 % trifluoroacetic acid (0.1

% solution) was mixed (10:1) with samples (0.5 µl) containing CNBr-treated Ugi, purified peptide C3, and Asp-N-digested Ugi protein. Each matrix solution was applied to a mass spectrometric probe and allowed to dry on the probe by slow evaporation. A mass spectrum was generated from 30 individual laser pulses (+24 kV), and the summed signals were calibrated by using standard ion signals from the matrix.

2.2.17 Site-Directed Mutagenesis of the M13mp2 *lacZα* Gene

M13mp2 DNA was isolated from *E. coli* CJ236 cells and purified as described by Kunkel (130). Site-specific mutations in the *lacZα* gene were introduced by annealing 5'-end phosphorylated A-41-mer to M13mp2 DNA. Oligonucleotide A-41-mer (192 pmol) was hybridized to uracil-containing M13mp2 DNA (64 pmol) in a reaction mixture (440 µl) containing 150 mM NaCl and 15 mM sodium citrate (pH 7.0). Hybridization was facilitated by heating to 70°C and cooling slowly to room temperature (~4 h). Oligonucleotide A-41-mer shared sequence complementarity with *lacZα* from nucleotide positions 68-108 except for discrepancies at positions 78-80 and 98. These two sites introduced an opal codon (TGA) in place of an arginine codon (CGT) coding for amino acid residue 14 of the *lacZα* gene product and a silent mutation generating a unique *Sma*I restriction site, respectively. Primer extension reaction mixtures (300 µl) contained 20 mM Hepes-KOH (pH 7.4), 2 mM DTT, 13 mM $MgCl_2$, 1 mM ATP, 500 µM each of dATP, dTTP, dGTP, and dCTP, 50 µg/ml acetylated bovine serum albumin, 27 units of T4 DNA polymerase, 1,200 units of T4 DNA ligase, and 8.8 pmol of heteroduplex A-41-mer/M13mp2 DNA. After incubation for 5 min on ice, 5 min at 25°C, and 4 h at 37°C, the reaction was terminated with the addition of 53 µl of 0.1 M EDTA. Competent *E. coli* JM109 cells (~1.4×10^{11} cells/ml) in 10 % (w/v) glycerol (40 µl) were mixed with the primer-extended DNA (0.5 µl) and electroporation was carried out using a Gene Pulser system (Bio-Rad) with a single pulse set at

2.5 kV, 25 μF capacitance, and 200 Ω. Transfected cells were diluted into SOC medium, serially diluted, and aliquots (100 μl) were mixed with prewarmed M9 topagar (2.5 ml) containing 0.4 mM IPTG and 1 mg/ml X-Gal and grown on M9 plates. An isolated clear plaque was placed into sterile 0.9 % NaCl solution (200 μl) in an Eppendorf, heated to 60°C for 5 min, vortexed vigorously for 30 sec, centrifuged (12,000 x g, 3 min, 25°C), and retitered using mid-log *E. coli* JM109 cells on M9 plates with M9 topagar containing IPTG and X-Gal. An isolated clear plaque from the secondary screening was placed into sterile 0.9 % NaCl (1 ml) and phage were propagated in *E. coli* JM109 and M13mp2op14 DNA was purified as described previously. DNA sequence analysis was conducted using an Applied Biosystems 373 DNA sequencer by the Center for Gene Research and Biotechnology (Oregon State University) and verified that M13mp2op14 DNA contained the desired *lacZα* opal codon and a unique *Sma*I restriction site.

2.2.18 Preparation of Base Excision DNA Substrates

M13mp2op14 DNA was isolated from *E. coli* JM109 cells as described by Kunkel (130). Oligonucleotides U-23-mer and A-23-mer were 5'-end phosphorylated as described previously and annealed to M13mp2op14 DNA in separate hybridization reaction mixtures (1515 μl) containing 1,500 pmol of U-23-mer or A-23-mer, 500 pmol of M13mp2op14 DNA, 20 mM Tris-HCl (pH 7.4), 2 mM $MgCl_2$, and 50 mM NaCl. The mixtures were placed in a 500-ml beaker filled with 70°C distilled H_2O and slowly cooled to room temperature (~4 h). The heteroduplex U-23-mer/M13mp2op14 substrate formed a U•T mispair at nucleotide position 78 of the *lacZα* gene whereas the homoduplex A-23-mer/M13mp2op14 substrate formed an A•T basepair. Heteroduplex [^{32}P]U-23-mer/M13mp2op14 substrate was also prepared by 5'-end ^{32}P-labeling

oligonucleotide U-23-mer followed by hybridization to M13mp2op14 DNA as described above. The duplex DNA was stored at -80°C.

Pilot primer extension reaction mixtures (50 µl) were prepared and contained 3.3 pmol of heteroduplex U-23-mer/M13mp2op14 or homoduplex A-23-mer/M13mp2op14 DNA substrate, 20 mM Hepes-KOH (pH 7.8), 2 mM DTT, 10 mM $MgCl_2$, 1 mM ATP, 500 µM each of dATP, dTTP, dCTP, and dGTP, and various amounts of T4 DNA polymerase and T4 DNA ligase as indicated in the figure legends. T4 DNA ligase was introduced into the primer extension reaction mixtures as a 100-fold unit excess over T4 DNA polymerase. Enzyme stocks were diluted in T4 DNA polymerase dilution buffer (20 mM Tris-HCl (pH 8.1), 50 mM NaCl, 2 mM DTT, 50 % (w/v) glycerol) or T4 DNA ligase dilution buffer (10 mM Tris-HCl (pH 7.4), 50 mM KCl, 1 mM DTT, 0.1 mM EDTA, 200 µg/ml acetylated bovine serum albumin, 50 % (w/v) glycerol). Individual components of the reaction mixture contributed to a specific percentage of the overall reaction volume and were strictly enforced. The DNA addition constituted 20 % of the reaction mixture volume while the T4 DNA polymerase and T4 DNA ligase additions contributed 8.6 % and 13.2 %, respectively. T4 DNA polymerase and T4 DNA ligase were the second to last and final additions, respectively. After incubation for 5 min on ice, 5 min at 25°C, and 4 h at 37°C, the reaction was terminated with 8.8 µl of 0.1 M EDTA. Aliquots (2 µl) of the primer extension reaction mixtures were adjusted to a final concentration of 10 mM EDTA (pH 8.0), 0.1% SDS, 5% (w/v) glycerol, and 0.01% bromophenol blue and analyzed by 0.8 % agarose gel electrophoresis. This process was repeated for each annealing reaction mixture preparation. Pilot primer extension reaction mixtures containing 6.6 units of T4 DNA polymerase and 660 units of T4 DNA ligase per 3.3 pmol of primed template consistently yielded the best results as was determined by the amount of Form I DNA detected by 0.8 % agarose gel electrophoresis.

Preparative primer extension reaction mixtures (3030 µl) were prepared that contained 200 pmol of U-23-mer/M13mp2op14 or A-23-mer/ M13mp2op14 substrate DNA, 20 mM Hepes-KOH (pH 7.8), 2 mM DTT, 10 mM $MgCl_2$, 1 mM ATP, 500 µM each of dATP, dTTP, dCTP, and dGTP, 400 units of T4 DNA polymerase, and 40,000 units of T4 DNA ligase. The specific percentage of individual components of the reaction mixture and order of addition are described above. After incubation for 5 min on ice, 5 min at 25°C, and 4 h at 37°C, the reaction was terminated with the addition of 535 µl of 0.1 M EDTA. An aliquot (2 µl) was saved for analysis by 0.8 % agarose gel electrophoresis.

Covalently closed circular duplex DNA reaction products (Form I DNA) from the preparative primer extension reactions described above were isolated by ethidium bromide-cesium chloride gradient centrifugation as described by Sambrook *et al.* (228). The terminated primer extension reaction was mixed with 18.12 g of optical grade CsCl (Gibco BRL) and ~10-15 ml of TE buffer at 30°C. After the CsCl had dissolved, the mixture was adjusted to a volume of 23.12 ml with TE buffer followed by the addition of 1.88 ml of ethidium bromide from a 10 mg/ml stock dissolved in distilled H_2O to achieve a final volume of 25 ml. The final concentrations of CsCl and ethidium bromide were 0.725 g/ml and 0.752 mg/ml, respectively. The sample was divided and loaded into two 12.5-ml polyallomer centrifuge tubes (Beckman) fitted for an SW41 ultracentrifuge rotor (Beckman). Centrifugation was performed at 39,000 rpm for 60 h at 20°C and the deceleration step occurred without braking. Form I DNA was collected from the centrifuge tubes by using a 22G1½ gauge hypodermic needle by inserting the needle beveled side up through the wall of the tube and underneath the Form I DNA band. The Form I DNA band (~500-600 µl) was removed, extracted four times with an equal volume of 1-butanol saturated with 5 M NaCl, concentrated by using a Centricon-30 (Amicon) concentrator, and buffer exchanged into TE buffer (10 mM Tris-HCl (pH 8.0), 1 mM EDTA).

2.2.19 Preparation of Human Whole Cell Extracts

Human glioblastoma U251 or colon adenocarcinoma LoVo cells were grown to ~85 % confluency in 75 cm^2 tissue culture flasks and were harvested by scraping into 8 ml of PBS buffer (8.1 mM Na_2HPO_4, 1.5 mM KH_2PO_4, 2.7 mM KCl, 137 mM NaCl (pH 7.2)). The approximate cell yield of a 75 cm^2 tissue culture flask at confluency was 2 x 10^7 cells (73). By extrapolation, standard whole cell extract preparations (40 flasks) at 85 % confluency yielded an approximated 6.8 x 10^8 cells. Cells were pelleted in a Dynac centrifuge (Becton Dickinson) (3 min, speed setting 65) and cell pellets were combined, washed once with ice cold PBS buffer (~10 ml), and pelleted again. The supernatant fraction was carefully removed and the packed cell volume (PCV) was estimated. Cells were resuspended in 4 PCV of hypotonic lysis buffer (10 mM Tris-HCl (pH 8.0), 1 mM EDTA, 5 mM DTT). For each 1 ml PCV measured, the cell suspension was supplemented with 5 µl of 87 mg/ml PMSF in methanol, 2 µl of 5 mg/ml leupeptin in distilled H_2O, 2 µl of 5 mg/ml pepstatin in DMSO, 2 µl of 5 mg/ml chymostatin in DMSO, and 50 µl aprotinin. The suspension was mixed, placed on ice for 20 min, transferred to a 30-ml glass homogenizer (Jencons), and cells were homogenized on ice by using a Teflon pestle (~20-30 strokes) to break the cells. The homogenate was then transferred to a glass beaker on ice and 4 PCV of sucrose-glycerol buffer (50 mM Tris-HCl (pH 8.0), 10 mM $MgCl_2$, 2 mM DTT, 25 % sucrose, 50 % (w/v) glycerol) were slowly added. After mixing was complete, 1 PCV of saturated ammonium sulfate (pH 7.0) was slowly added with stirring at a rate of ~ 1 revolution per second to avoid shearing the DNA. The homogenate was stirred on ice for an additional 30 min, poured into 5-ml polyallomer centrifuge tubes (Beckman) fitted for an SW50.1 ultracentrifuge rotor (Beckman). Centrifugation was performed at 32,000 rpm for 3 h at 4°C. The supernatant fraction was carefully removed (leaving the last 1 ml above the pellet in the tube), volume measured, and transferred to a glass beaker on ice.

While mixing, 0.33 g of powdered ammonium sulfate per ml of supernatant was slowly added followed by a 10 µl addition of 1 M NaOH per gram of ammonium sulfate to neutralize the mixture. Mixing was continued for 30 min and the precipitate was recovered by centrifugation (SS34 rotor, 13,000 rpm, 20 min, 4°C). The pellets were resuspended in ~200-300 µl of whole cell extract dialysis buffer (25 mM Hepes-KOH (pH 7.9), 100 mM KCl, 12 mM $MgCl_2$, 1 mM EDTA, 2 mM DTT, 17 % (w/v) glycerol), transferred into SpectraPor dialysis tubing (6-8,000 MWCO, 6.4 mm diameter), and dialyzed for 1-2 h against ~500 ml of whole cell extract dialysis buffer. The buffer was exchanged once and dialysis was continued for an additional 8-12 h. The dialysate was transferred to an Eppendorf tube (1.5 ml) and centrifugation conducted (12,000 rpm, 10 min, 4°C) to remove precipitated material. The supernatant was frozen in small aliquots (100 µl) and stored at -80°C. Each aliquot was used only once, without refreezing.

2.2.20 Preparation of Human Crude Cell Extracts

Human glioblastoma U251 cells were grown to ~85 % confluency in tissue culture flasks (75 cm^2) and harvested by scraping in the presence of 8 ml of PBS buffer. Following centrifugation, the cell pellet was washed with PBS and resuspended in HE buffer (25 mM Hepes-NaOH (pH 7.8), 1 mM EDTA, 1 mM DTT, 10 % (w/v) glycerol) equal to the volume of the packed cell pellet. Resuspended cells were placed on ice and disrupted by using an Ultrasonic Processor (Model W-380, Heat Systems-Ultrasonic, Inc.) equipped with a microtip probe. After five 15-second pulses (35 % output control, 45 % duty cycle), the sample was centrifuged at 15,000 x g for 10 min at 4°C to pellet cell debris and the supernatant fraction was stored in 100 µl aliquots at -80°C. The crude cell extract was assayed for uracil-DNA glycosylase or Ugi activity. Uracil-DNA glycosylase assays were performed using standard assay conditions with activated calf-thymus [*uracil*-^{3}H]DNA or in some cases with

the single-stranded [^{32}P]U-34-mer and double-stranded [^{32}P]U/A-34-mer or [^{32}P]U/G-34-mer DNA substrates as described previously. Ugi assays were performed similarly to the standard uracil-DNA glycosylase inhibitor assay except crude cell extract was heated to 95°C for 10 min and centrifuged at 13,000 x g for 10 min to remove the precipitate. The supernatant fraction containing the heat-stable Ugi protein was then measured for Ugi activity.

2.2.21 Base Excision DNA Repair Reactions

Standard base excision repair (BER) reaction mixtures contained 100 mM Tris-HCl (pH 7.5), 5 mM $MgCl_2$, 1 mM DTT, 0.1 mM EDTA, 2 mM ATP, 0.5 mM β-NAD, 20 μM each of dATP, dTTP, dCTP, and dGTP, 5 mM phosphocreatine di-Tris salt, 200 units/ml phosphocreatine kinase, 10 μg/ml of M13mp2op14 (U•T) heteroduplex DNA (Form I) or M13mp2op14 (A•T) homoduplex DNA (Form I), and 2 mg/ml human whole cell extract protein. In some cases, 200 μCi/ml of [α-^{32}P]dATP (6,000 Ci/mmol) was also included in the reaction. Standard BER reaction mixtures used to measure repair patch sizes contained 2'-deoxyribonucleoside α-thiotriphosphates in place of the standard 2'-deoxyribonucleoside triphosphates at identical concentrations. In all cases, DNA and whole cell extract protein additions constituted 20 % and 40 % of the reaction mixture volume, respectively. Incubation occurred at 30°C for various amounts of time. Reactions were terminated by the addition of 2000 units of Ugi and adjustment to 20 mM EDTA. RNase A was then added to 80 μg/ml and incubated at 37°C for 10 min. Following addition of SDS to 0.5 %, proteinase K was added to 190 μg/ml and the mixture was incubated an additional 30 min at 37°C. The samples were extracted with an equal volume of phenol:chloroform:isoamyl alcohol (25:24:1), ethanol precipitated for 1 h at -80°C, washed with 75 % ethanol, and resuspended in 30 μl of TE buffer.

2.2.22 Isolation of Repaired DNA

Samples of repaired M13mp2op14 (U•T) DNA, isolated as described above, were treated with 400 units of Ung per μg of DNA for 30 min at 37°C. After terminating the reaction with a 10-fold unit excess of Ugi, 4 units of *E. coli* endonuclease IV (Endo IV) was added per μg of DNA and incubation continued at 37°C for 30 min. This reaction was then terminated by heating for 3 min. Form I DNA that was insensitive to the Ung/Endo IV cleavage was isolated by 0.8 % agarose gel electrophoresis. DNA samples were combined with agarose dye buffer to a final concentration of 0.1 % SDS, 10 mM EDTA, 5 % (w/v) glycerol, and 0.01 % bromophenol blue. After loading the sample (~15 μl per well) onto an agarose gel (12 x 13 cm) containing TAE buffer (40 mM Tris-acetate, 1 mM EDTA (pH 8.0)) and 0.1 μg/ml ethidium bromide, electrophoresis was performed at 100 V until the tracking dye had migrated ~75 % of the distance through the gel. By restricting 95 % of the gel from UV-light transilluminescence with aluminum foil, Form I DNA was localized using an external Form I standard on the outer-most lane and excised from the gel with a clean razor blade. Form I DNA was recovered from the agarose gel slice by electroelution into TAE buffer using an Elutrap (Schleicher and Schuell) apparatus placed in a 35 x 21 cm agarose gel electrophoresis chamber filled with TAE buffer. Electroelution was conducted at 150 V (50-60 mA) for 3 h at room temperature. Following electroelution, the current was reversed for ~15 sec and the DNA solution (~1 ml) was transferred into a Centricon-30 (Amicon) concentration device, concentrated, and buffer exchanged with distilled H_2O.

2.2.23 Analysis of Base Excision Repair Reaction Products

2.2.23.1 Quantitation of Form I and II DNA

Standard BER reactions were performed except that 200 mCi/ml [α-^{32}P]dATP (6,000 cpm/mmol) was included in the reaction mixture. DNA reaction products were isolated, treated in the presence or absence of *E. coli* Ung/Endo IV, and Form I and II DNA were resolved by 0.8 % agarose gel electrophoresis as described above. Ethidium bromide-stained DNA bands were visualized by transillumination (302 nm) and the percentage of Form I and II DNA was quantitated against Form I and II standards from the same gel by using a Gel Documentation System (Model GDS7500; Ultra-Violet Products Ltd.) and Image Quant (Molecular Dynamics) software. The amount of Form I and II DNA recovered after incubation with whole cell extract protein decreased in a time dependent manner. The percentage of Form I DNA measured was calculated from the total amount of Form I and II detected in any given time point. To detect [^{32}P]DNA, the gel was blotted onto a Gene Screen Plus (NEN) membrane by using a downward alkaline transfer technique described by Koetsier *et al.* (119). Autoradiography was conducted using X-OMAT AR5 film (Kodak) and quantitation of Form I and II [^{32}P]DNA bands was performed using a PhosphorImager (Molecular Dynamics) and Image Quant software.

2.2.23.2 HinfI Restriction Analysis

In order to detect uracil-initiated base excision repair-specific DNA synthesis, standard BER reactions supplemented with 200 μCi/ml [α-^{32}P]dATP (6,000 cpm/mmol) were performed. DNA reaction products were isolated as described above and subjection to restriction analysis using *Hin*fI restriction endonuclease. Samples (2.5 μl, ~50 ng) were digested with 5 units of *Hin*fI for 1 h at 37°C and restriction fragments were resolved by 5 % nondenaturing

polyacrylamide gel electrophoresis. After drying the gel under vacuum, autoradiography was performed and the amount of each [^{32}P]DNA fragment was quantitated by using a PhosphorImager. The relative intensity of various bands was determined and the amount of [^{32}P]DNA fragments (253-, 261-, 486-, 529-bp) was compared after subtracting background values obtained from a blank lane.

2.2.23.3 *EcoRI and SmaI Restriction Analysis*

In order to analyze the strand specificity of DNA repair synthesis, standard BER reactions were performed in the presence of 200 μCi/ml of [α-^{32}P]dATP as described above. DNA reaction products were isolated and simultaneously digested with *Eco*RI and *Sma*I (10 units/μg of DNA) for 1 h at 25°C. The restriction endonuclease reactions (10 μl) were terminated by adjustment to 12.2 mM EDTA. A modification of this procedure involved the digestion of DNA reaction products with *Eco*RI for 1 h at 25°C followed by digestion with *Sma*I for 1 h at 25°C. Both individual restriction digestion reactions were terminated by heat for 20 min at 70°C. Samples were treated with or without *E. coli* Ung and Endo IV as indicated, combined with an equal volume of denaturing formamide dye buffer (95 % deionized formamide, 10 mM EDTA, 0.1 % bromophenol blue, 0.1 % xylene cyanol), heated for 3 min at 95°C, and DNA fragments were resolved by 12 % polyacrylamide/8.3 M urea gel electrophoresis as previously described.

2.2.23.4 *Determination of Repair Patch Size*

Standard BER reaction mixtures were prepared as described above except that 2'-deoxyribonucleoside α-thiotriphosphates were used in place of the standard 2'-deoxyribonucleoside triphosphates and [^{32}P]M13mp2op14 (U•T) Form I DNA was used as the BER substrate. The ^{32}P label was

introduced at the 5'-end of oligonucleotide U-23-mer prior to the primer extension reaction and isolation of Form I DNA. In the Form I DNA molecule, the radiolabel was located between the uracil target and the *Sma*I restriction site at nucleotide position 90 on the transcribed strand of the *lacZ*α gene sequence. Reaction mixtures were incubated at 30°C for 45 min (LoVo) or 60 min (U251) and DNA reaction products were isolated. Samples (8.0 µl, ~500 ng) were removed for digestion with 25 units of *Eco*RI for 1 h at 25°C. Following termination at 70°C for 20 min, samples were incubated in the absence or the presence of various amounts of *E. coli* exonuclease III (Exo III) for 30 min at 37°C as indicated. Following Exo III digestion, samples were heated at 70°C for 20 min and reaction products were then restricted with 25 units of *Sma*I for 1 h at 25°C. Samples were then combined with an equal volume of denaturing formamide dye buffer and DNA reaction products were resolved by 12% polyacrylamide/8.3 M urea gel electrophoresis. After drying the gel under vacuum, autoradiography was performed and the amount of each [^{32}P]DNA band was quantitated by using a PhosphorImager.

2.2.24 Transfection of *E. coli* and Determination of Reversion Frequencies and Mutational Spectrum

E. coli MC1061 or NR9162 cells were transfected with repaired and purified Form I DNA recovered from human whole cell extract BER reactions. Form I DNA samples (0.5-2.5 µl) were mixed with competent *E. coli* MC1061 or NR9162 cells (~1-2 x 10^{11} cells/ml) in 10 % (w/v) glycerol (50 µl) and incubated on ice for 1-2 min. Transfection was conducted using a Gene Pulser electroporation system with a single pulse set at 2.0 kV, 25 µF capacitance, and 400 Ω. Transfected cells were serially diluted into SOC media ($1/10^2$ to $1/10^7$) and 100 µl of each diluted sample was placed into a sterile 13 x 100 mm test tube, mixed with 500 µl of mid-log *E. coli* CSH50 cells and prewarmed M9 topagar (2.5 ml) containing 0.4 mM IPTG and 1 mg/ml X-Gal

was added. The cells were plated on M9 plates and incubated overnight at 37°C. One diluted sample from each transfection experiment was increased in volume (~3.0 ml) to allow for the mass plating of ~25 individual M9 plates. A separate titration series was prepared for each transfection experiment in order to quantitate the number of plaques detected for each mass plating. Typical dilutions for mass platings yielded a concentration of 1,000 to 3,000 plaque forming units per plate. After scoring plaques as either colorless or blue, the reversion frequency was calculated from the ratio of the number of blue plaques to total (colorless plus blue) plaques detected. Blue plaques were picked, placed into 200 µl of sterile 0.9 % NaCl solution, and extracted phage were diluted into SM media and titered against mid-log *E. coli* CSH50 cells on M9 plates with IPTG and X-Gal as described above. An individual blue plaque from each secondary screening was placed into 1 ml of sterile 0.9 % NaCl solution and used to isolate M13mp2op14 derived single-stranded DNA for nucleotide sequence analysis as previously described but with one modification. Aliquots (100 µl) of the extracted phage were placed into 100 ml of 2X YT medium inoculated with 5 ml of an *E. coli* CSH50 overnight culture and infection was allowed to proceed for 9 h. DNA sequence analysis was performed using the dideoxynucleotide chain termination method. The nucleotide sequence of the *lacZα* gene was determined by using an oligonucleotide DNA primer (PMR PLUS) complementary to the (+) strand at nucleotide positions 249 to 269.

3. IDENTIFICATION OF SPECIFIC CARBOXYL GROUPS ON URACIL-DNA GLYCOSYLASE INHIBITOR PROTEIN REQUIRED FOR ACTIVITY

This chapter presents the results and interpretations generated from studies involving the chemical modification of carboxylic acid residues of Ugi to determine their role in the formation of the Ung•Ugi complex. The approach involved the use of the water-soluble carbodiimide, 1-ethyl-3-(3-dimethylaminopropyl)carbodiimide (EDC), and the nucleophile, glycine ethyl ester (GEE), to chemically modify specific glutamic acid and aspartic acid residues. It was hoped that charge neutralization of highly reactive residues brought about by EDC/GEE-modification would interfere with the function of Ugi. Five differentially modified forms of Ugi were purified and each form was characterized with regards to the effect of modification on Ugi specific activity, stability of the Ung•Ugi complex, and reversibility of the Ung•Ugi complex in the presence of unmodified Ugi and nucleic acid competitors. Identification of specific sites of adduction were determined utilizing matrix-assisted laser desorption ionization (MALDI) mass spectrometry and amino acid sequencing techniques. This study established the importance of two glutamic acid residues (Glu-28 and Glu-31) involved in achieving stable Ung•Ugi complex formation.

3.1 Results

3.1.1 Modification of Carboxylic Acid Residues in Uracil-DNA Glycosylase Inhibitor Protein

To assess the importance of Glu and Asp residues in mediating the Ung/Ugi interaction, chemical modification of Ugi was conducted, and the effect on inhibitor activity was investigated. Glu and Asp residues of Ugi that are potential candidates for modification are indicated in Figure 1. The water-

Figure 1. Tertiary structure of bacteriophage PBS2 uracil-DNA glycosylase inhibitor protein. The tertiary structure of Ugi has been determined by solution state multidimensional nuclear magnetic resonance (12). Secondary structural elements include the α1-helix (Ser-5 to Lys-14), β1-strand (Glu-20 to Met-24), α2-helix (Glu-27 to Asn-35), β2-strand (Ile-41 to Asp-48), β3-strand (Glu-53 to Ser-60), β4-strand (Ala-69 to Asp-74), and β5-strand (Asn-79 to Leu-84). In the tertiary structure, the 12 Glu residues are shown in *red* and the 6 Asp residues are in *yellow*.

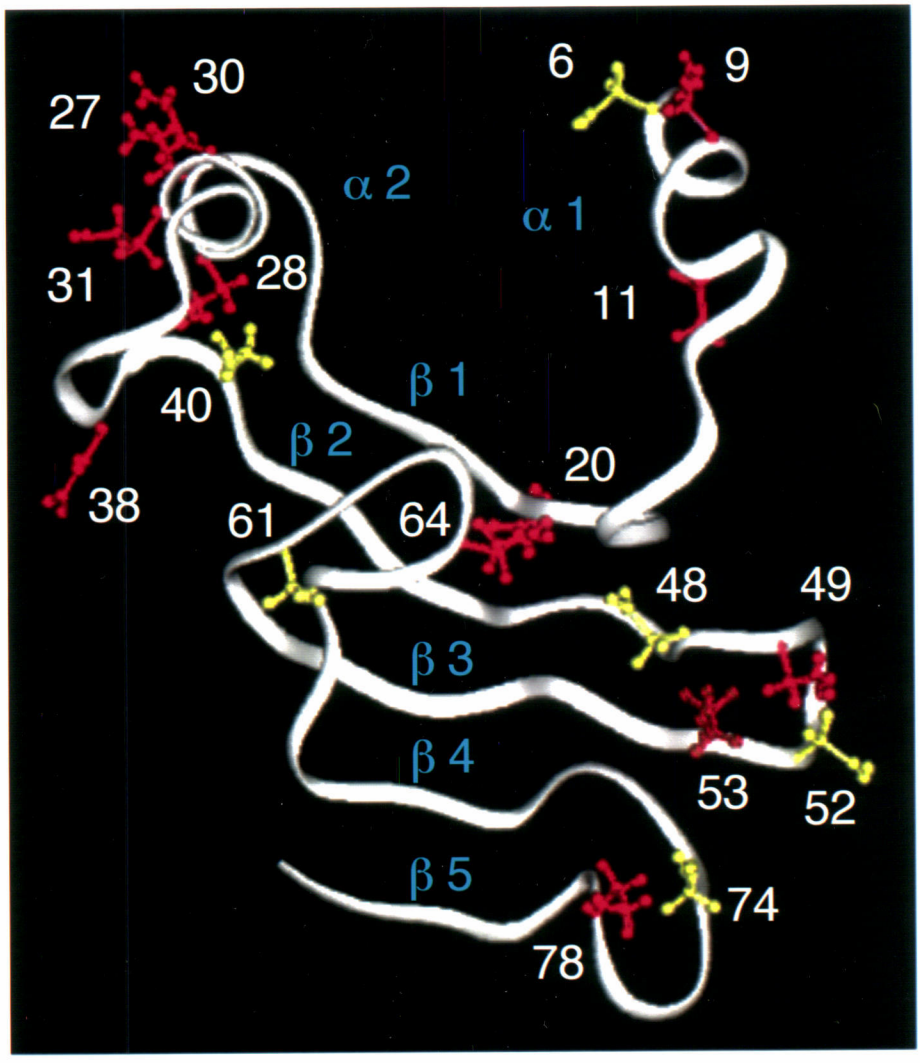

Figure 1

soluble carbodiimide, EDC, was used in a two-stage modification reaction with the nucleophile, GEE, to selectively modify carboxyl groups (39). Under mild reaction conditions, this carbodiimide preferentially forms an O-acylisourea-activated carboxyl group that subsequently undergoes nucleophilic attack by GEE to form a terminal acyl-glycine ethyl ester reaction product (39) as depicted in Figure 2. The extent of carboxyl group modification was optimized by varying the molar ratio of carbodiimide to carboxyl groups and the effect of modification on uracil-DNA glycosylase inhibitor activity was analyzed at different time points (Figure 3). Pilot reaction mixtures containing 1, 4, and 20 μmol of EDC over 1.75 μmol of potentially reactive carboxyl groups were prepared and the specific activity of Ugi was determined following each reaction. The ability of EDC/GEE-modified Ugi to inhibit uracil-DNA glycosylase activity decreased as a function of increasing EDC concentration. Within 30 minutes, the specific activity of Ugi was reduced by 63, 80, and 98 % following incubation with 1, 4, and 20 μmol of EDC when compared to that of an unmodified Ugi control. By using an EDC to carboxyl group molar ratio of 2.3:1, a limited modification reaction was conducted, and modified forms of [^{35}S]Ugi were resolved by DEAE-cellulose chromatography (Figure 4). Five distinct forms (I-V) were identified and eluted at approximately 180, 165, 150, 140, and 100 mM NaCl, respectively. The order of elution of [^{35}S]Ugi forms I-V from the DEAE-cellulose column commenced with form V, eluting at 100 mM NaCl, and terminated with form I which eluted at 180 mM NaCl. [^{35}S]Ugi forms I (fractions 118-131), II (fractions 101-106), III (fraction 89-93), IV (fractions 79-84), and V (fractions 68-74) were separately pooled after analysis by nondenaturing polyacrylamide gel electrophoresis (Figure 5). The amount of [^{35}S]Ugi forms I-V recovered was determined to be approximately 267, 493, 589, 502, and 305 μg, respectively.

Figure 2. Scheme for acyl-glycine ethyl ester adduction of Ugi by EDC/GEE modification. Uracil-DNA glycosylase inhibitor (Ugi) is an acidic protein containing 19 carboxyl groups (12 glutamic acid, 6 aspartic acid, carboxyl-terminus) which are available for activation by the water-soluble carbodiimide, 1-ethyl-3-dimethylaminopropylcarbodiimide (EDC). A protonated carboxylic acid group is activated by EDC to form an EDC-carboxyl adduct which is subsequently attacked by the nucleophile, glycine ethyl ester (GEE), to form the acyl-glycine ethyl ester adduct. Standard modification reaction conditions involved a 1:2.3:11.5 molar ratio of COOH:EDC:GEE in 50 mM potassium phosphate buffer (pH 6). Following incubation at 25°C for 30 min, the reaction was terminated by adjustment to 1 M sodium acetate (pH 4.75). The acyl-glycine ethyl ester adduct is electrically neutral in charge and adds 85 daltons to the overall molecular weight of the Ugi protein.

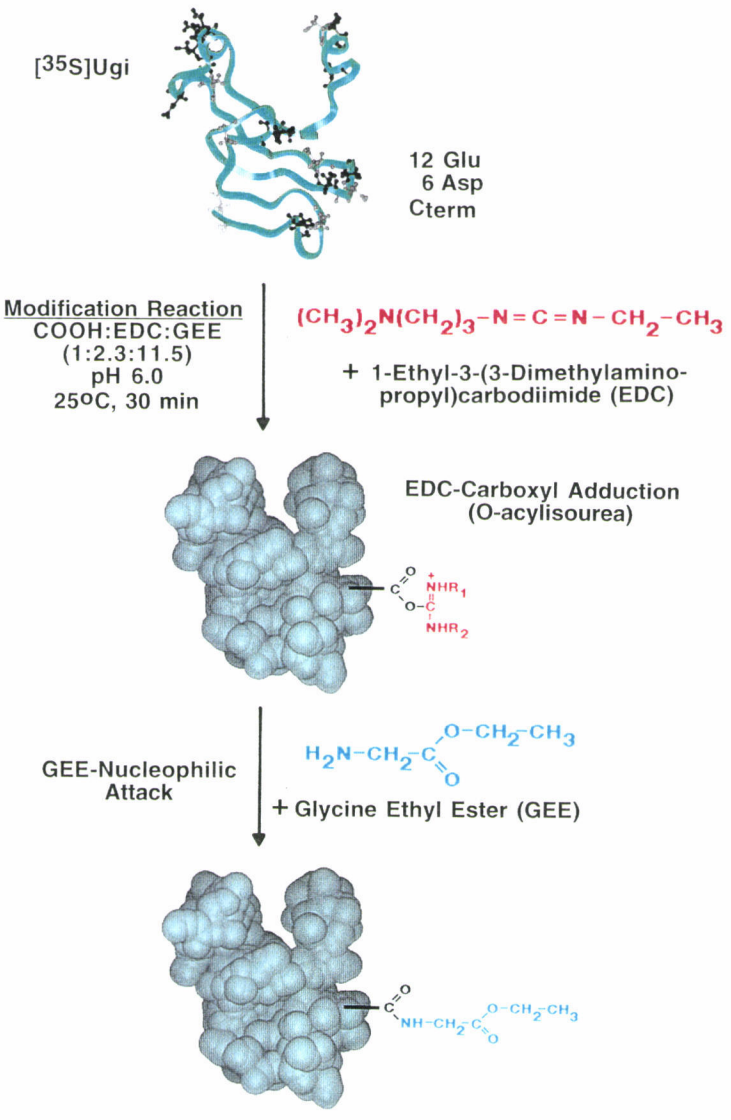
[35S]Ugi
12 Glu
6 Asp
Cterm
Modification Reaction
COOH:EDC:GEE
(1:2.3:11.5)
pH 6.0
25°C, 30 min
(CH3)2N(CH2)3–N=C=N–CH2–CH3
+ 1-Ethyl-3-(3-Dimethylamino-propyl)carbodiimide (EDC)
EDC-Carboxyl Adduction
(O-acylisourea)
GEE-Nucleophilic Attack
H2N–CH2–C(=O)–O–CH2–CH3
+ Glycine Ethyl Ester (GEE)

Figure 2

Figure 3. Effect of EDC:COOH ratio and EDC/GEE modification time on Ugi activity. Three EDC/GEE modification reaction mixtures (1000 µl) containing 92 nmol of Ugi (~1.75 µmol COOH groups) were supplemented with 1 (*closed squares*), 4 (*open circles*), or 20 (*closed circles*) µmols of EDC and a five-fold molar excess of GEE over EDC. Samples (100 µl) were removed after various amounts of time at 25°C and the modification reaction was terminated with an equal volume of 2 M sodium acetate (pH 4.75). Excess EDC and GEE were removed from the terminated reactions by P-4 spun columns equilibrated in 50 mM potassium phosphate (pH 6.0) and standard uracil-DNA glycosylase inhibitor assays were conducted for each sample as described under "Experimental Procedures". The activity of Ugi at each time point was determined and expressed as a percentage relative to the activity of mock modified Ugi.

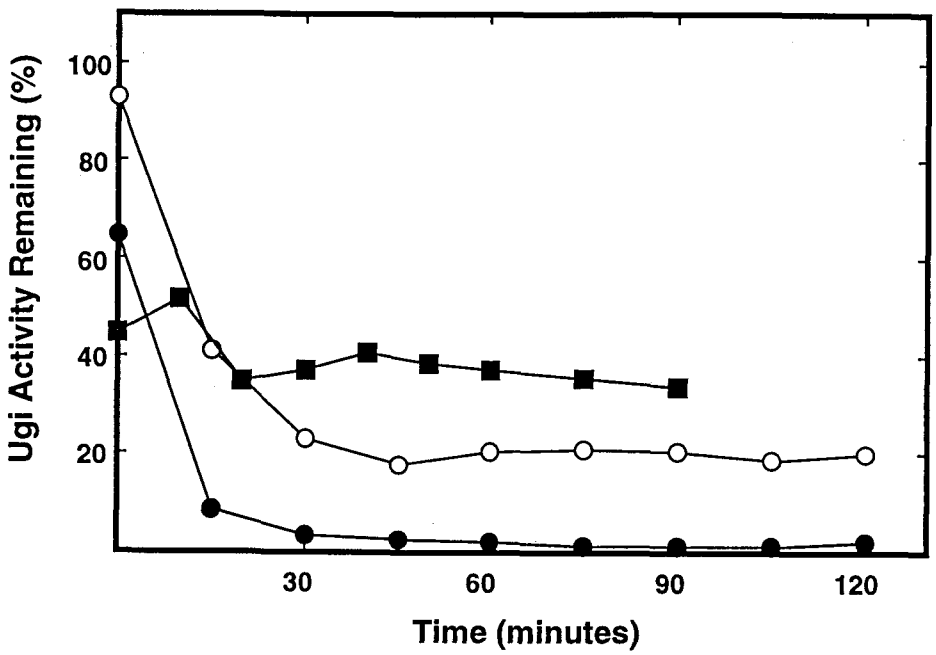
Ugi Activity Remaining (%)
100
80
60
40
20
30
60
90
120
Time (minutes)

Figure 3

Figure 4. Isolation of EDC/GEE-modified [^{35}S]Ugi forms I-V by DEAE-cellulose chromatography. Chemical modification of [^{35}S]Ugi (1,050 µl) was performed using EDC and GEE as described under "Experimental Procedures". After terminating the reaction and removing the excess EDC and GEE, the modified [^{35}S]Ugi was dialyzed against buffer A (50 mM Tris-HCl (pH 7.0), 1 mM EDTA, 1 mM DTT) containing 50 mM NaCl. A sample (32 ml) containing 486 nmol of [^{35}S]Ugi was then applied to a DE-52 cellulose column (0.6 cm^2 x 7.9 cm) equilibrated in the same buffer. The column was washed and eluted with a linear gradient of 50-300 mM NaCl in buffer A, fractions (1 ml) were collected, and samples were monitored for conductivity (*closed squares*) and ^{35}S radioactivity (*closed circles*) as described under "Experimental Procedures". Fractions were pooled corresponding to the various forms (I-V), as indicated by *brackets*, and evaporated to dryness; each pool was resuspended in buffer A (1 ml) and dialyzed against Ugi EB (50 mM Tris-HCl (pH 8.0), 1 mM EDTA, 1 mM DTT, 100 mM NaCl, 10 % (w/v) glycerol).

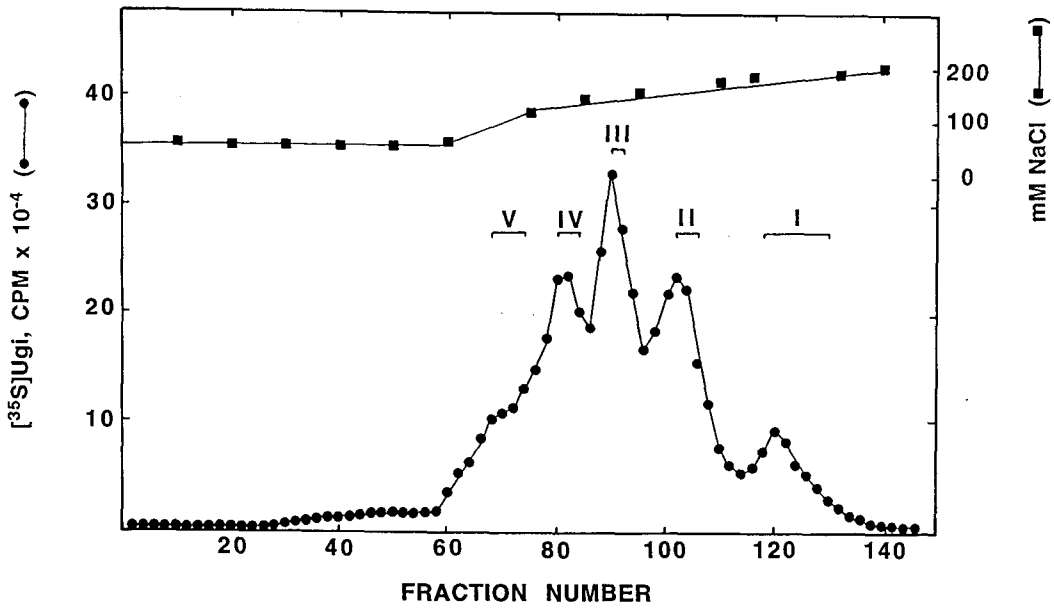
[35S]Ugi, CPM x 10-4 (●—●)
40
30
20
10
200
100
0
mM NaCl (■—■)
III
V
IV
II
I
20
40
60
80
100
120
140
FRACTION NUMBER

Figure 4

Figure 5. Nondenaturing polyacrylamide gel electrophoresis of DEAE-cellulose column fractions containing EDC/GEE-modified [^{35}S]Ugi forms I-V. Samples (15 µl) of fractions containing [^{35}S]Ugi forms I-V separated by DEAE-cellulose chromatography (Figure 4) were combined with an equal volume of native dye buffer, loaded onto 18% polyacrylamide gels (panel A, fractions 58-94; panel B, fractions 96-132), and electrophoresis was conducted at 4°C using 200V as described under "Experimental Procedures." A sample (~300 pmol) of the unfractionated EDC/GEE-modified [^{35}S]Ugi reaction mixture was included as a reference standard (lane C). Protein bands were detected by rapid protein staining with Coomassie Brilliant Blue G-250. The location of EDC/GEE-modified [^{35}S]Ugi forms I-V are located by *arrows*. Fractions of EDC/GEE-modified [^{35}S]Ugi forms I-V were separately pooled according to their purity as designated above each panel.

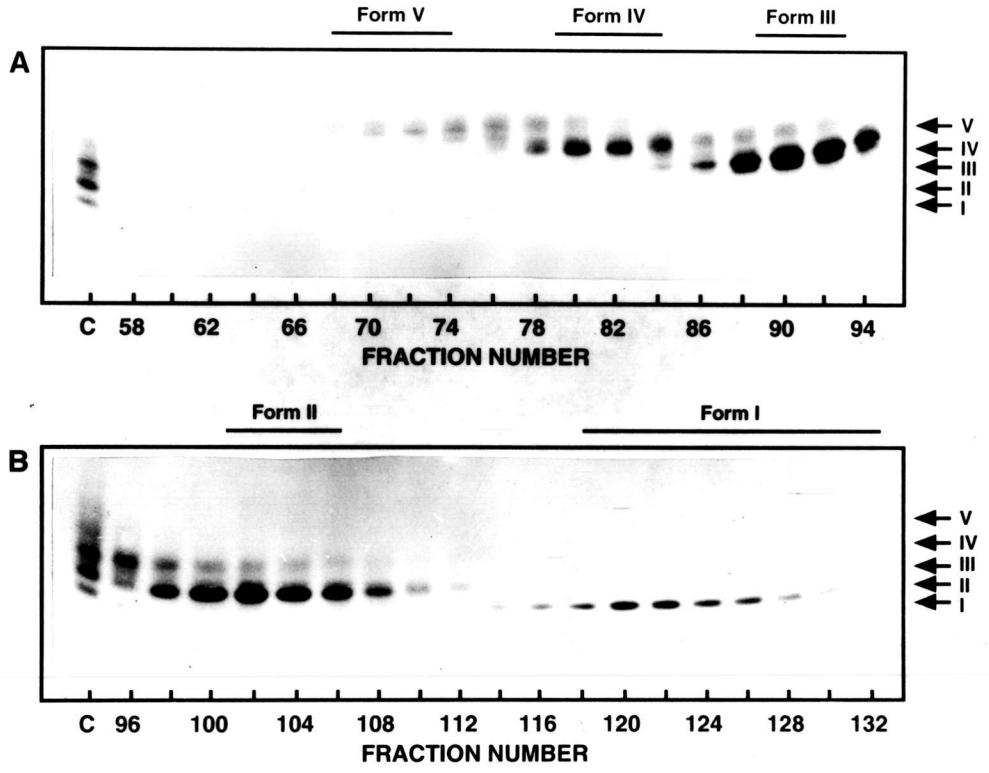
Form V
Form IV
Form III
A
V
IV
III
II
I
C 58 62 66 70 74 78 82 86 90 94
FRACTION NUMBER
Form II
Form I
B
V
IV
III
II
I
C 96 100 104 108 112 116 120 124 128 132
FRACTION NUMBER

Figure 5

3.1.2 Identification and Purity of Ugi Forms I-V

After separately pooling and concentrating the five [^{35}S]Ugi peaks, each Ugi form was again analyzed by nondenaturing polyacrylamide gel electrophoresis to assess the purity of each form (Figure 6, lanes 4-8). Samples of unmodified [^{35}S]Ugi (lane 1), [^{35}S]Ugi from the unfractionated modification reaction mixture (lane 2), and mock-modified [^{35}S]Ugi (lane 3) were analyzed for comparative purposes. The unfractionated [^{35}S]Ugi sample contained five protein bands; three were very discrete (bands I-III), and two appeared to be more diffuse (bands IV and V). Band I corresponded to unmodified Ugi (lane 1) which comigrated with the single protein band of [^{35}S]Ugi form I (lane 4). The other protein bands (II-V) observed in the reaction mixture (lane 2) were individually represented by [^{35}S]Ugi forms II-V, respectively (lanes 5-8). Forms II-V showed progressively reduced electrophoretic mobility that inversely correlated with their order of elution from the DEAE-cellulose column (Figure 4). Taken together, these results indicate that EDC/GEE-mediated modification of Ugi (forms II-V) caused negative charge neutralization of carboxyl groups.

The purity of [^{35}S]Ugi forms I-V was assessed based on the relative Coomassie Brilliant Blue staining intensities of individual fractions from across the DEAE-cellulose column (Figure 5). These results indicated that forms I-III are ≥90 % pure, whereas forms IV and V appear to contain ≥65 % of the corresponding form. From the ^{35}S radioactivity detected in gel slices of forms I-V (Figure 6, lane 2), it was determined that forms I-V constituted approximately 14, 23, 26, 18, and 10 % of the total unfractionated [^{35}S]Ugi sample, respectively.

To determine the extent of EDC/GEE-mediated modification, each Ugi form along with unmodified Ugi was analyzed by MALDI mass spectrometry (Figure 7 and Table 2). As previously observed (15), two mass peaks were obtained for the unmodified Ugi protein; peak I (9,475 daltons) closely agreed with the predicted mass of the complete amino acid sequence of Ugi, and peak

Figure 6. Purity and activity of EDC/GEE-modified [^{35}S]Ugi forms I-V. Eight samples (30 µl) containing 106 pmol of unmodified [^{35}S]Ugi (lane 1), 318 pmol of EDC/GEE-modified [^{35}S]Ugi reaction mixture (lane 2), 106 pmol of mock-modified [^{35}S]Ugi (lane 3), or 106 pmol of purified [^{35}S]Ugi forms I-V (lanes 4-8, respectively) were loaded onto an 18% nondenaturing polyacrylamide gel. Following electrophoresis, the gel was stained with Coomassie Brilliant Blue G-250. The direction of migration was from *top* to *bottom*, and the locations of unmodified Ugi and the tracking dye (TD) are indicated by *arrows*. Prior to electrophoresis, standard uracil-DNA glycosylase inhibitor assays were conducted on each sample as described under "Experimental Procedures". The specific activity of each Ugi form was determined and expressed relevant to that of unmodified [^{35}S]Ugi control. Gel slices of the EDC/GEE-modified [^{35}S]Ugi reaction mixture sample (lane 2) were analyzed for ^{35}S radioactivity in order to quantitate the distribution of [^{35}S]Ugi forms I-V.

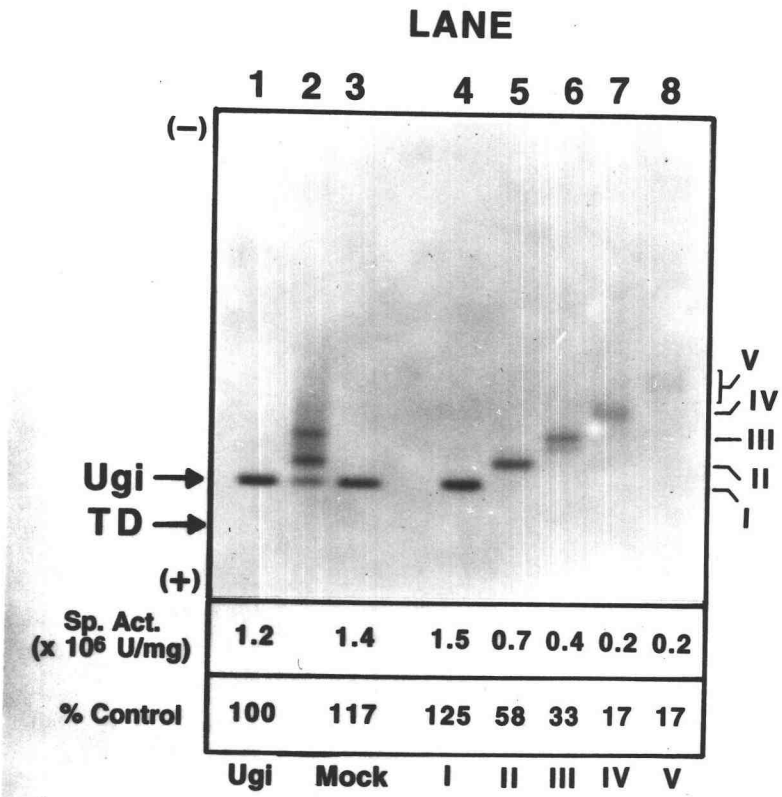
LANE
1 2 3 4 5 6 7 8
(–)
Ugi
TD
(+)
V
IV
III
II
I
Sp. Act.
(x 10⁶ U/mg)
1.2 1.4 1.5 0.7 0.4 0.2 0.2
% Control
100 117 125 58 33 17 17
Ugi Mock I II III IV V

Figure 6

Figure 7. Molecular weight determination of EDC/GEE-modified [^{35}S]Ugi forms I-V by MALDI mass spectrometry. Samples of unmodified [^{35}S]Ugi and [^{35}S]Ugi forms I-V were analyzed by MALDI mass spectrometry as described under "Experimental Procedures". The mass spectra of unmodified [^{35}S]Ugi and [^{35}S]Ugi form I showed two singly charged ion species (Peaks I and II). The mass spectra of EDC/GEE-modified [^{35}S]Ugi forms II-V also showed two primary mass peaks with relative mass increases due to EDC/GEE-modification over that of unmodified [^{35}S]Ugi, as indicated in Table 2. Samples containing [^{35}S]Ugi forms III-V included an internal standard (S).

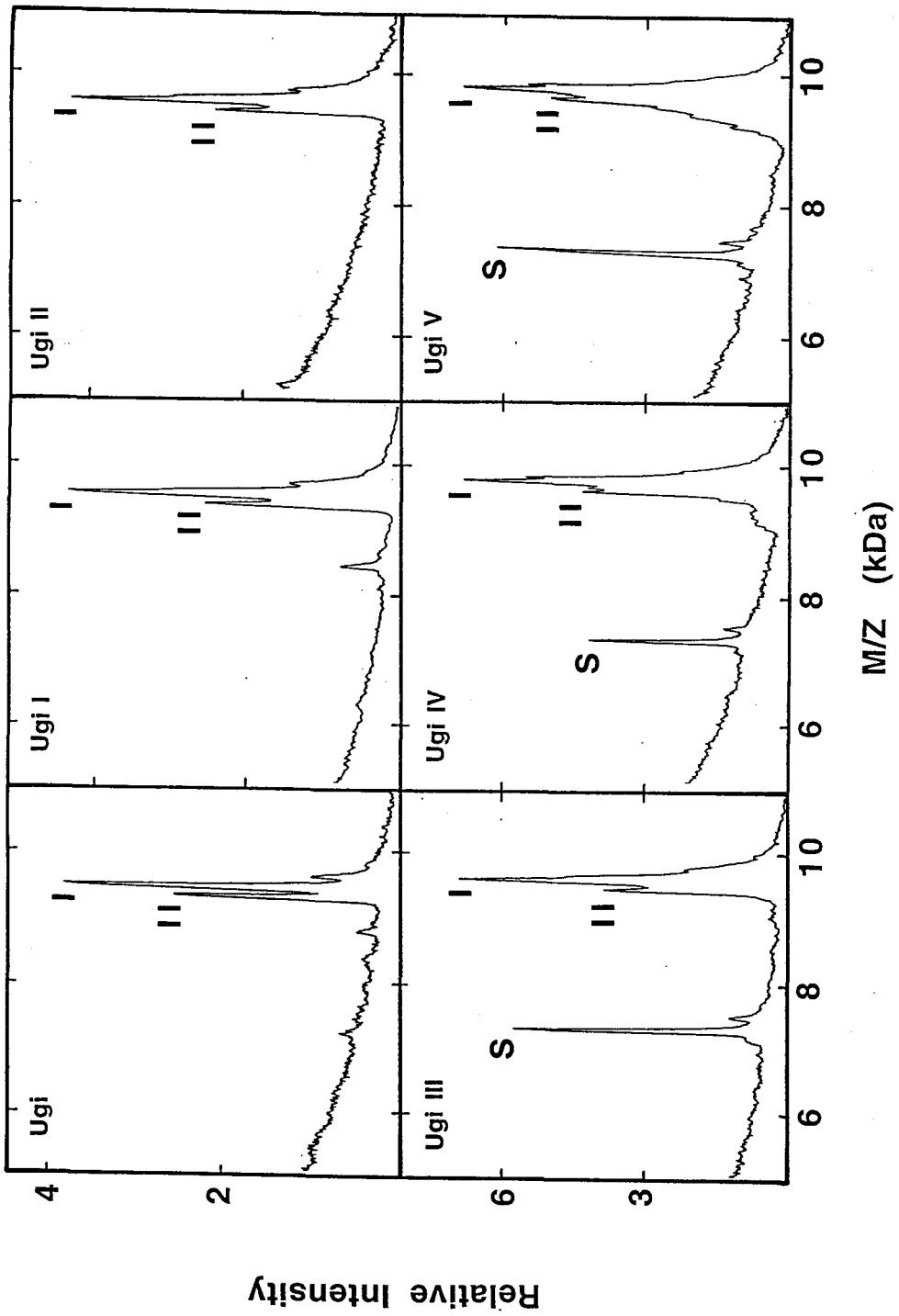
Ugi
Ugi I
Ugi II
Ugi III
Ugi IV
Ugi V
I
II
S
4
2
6
3
6
8
10
Relative Intensity
M/Z (kDa)

Figure 7

Table 2

Acyl-glycine Ethyl Ester Adducts Detected on EDC/GEE-modified Ugi Using MALDI Mass Spectrometry

Ugi	Predicted Mass[a](A)	Experimental Mass[b] (B)	Mass Increase (B-A)	Acyl-GEE Adducts/Ugi[c]
Unmodified				
Peak I[d]	9,477	9,475 ± 10.5		
Peak II[e]	9,346	9,341 ± 3.0		
Form I				
Peak I	9,477	9,478 ± 8.1	1	0
Peak II	9,346	9,346 ± 6.1	0	0
Form II				
Peak I	9,477	9,569 ± 4.7	92	1.1
Peak II	9,346	9,437 ± 0.6	91	1.1
Form III				
Peak I	9,477	9,646 ± 8.4	169	2.0
Peak II	9,346	9,507 ± 0.1	161	1.9
Form IV				
Peak I	9,477	9,727 ± 0.8	250	2.9
Peak II	9,346	9,594 ± 0.7	248	2.9
Form V				
Peak I	9,477	9,794 ± 0.5	317	3.7
Peak II	9,346	9,665 ± 5.7	319	3.8

[a] Predicted mass values were determined by the computer program MacProMass, version 1.05, by Lee and Vermuri (137).

[b] Average molecular weights and standard errors are determined from two independent measurements.

[c] One acyl-glycine ethyl ester adduct per Ugi protein would be expected to result in an 85-dalton mass increase.

[d] Peak I corresponds to the intact Ugi protein.

[e] Peak II corresponds to the Ugi protein minus 131 daltons, which correlates to the loss of the amino-terminal methionine residue (15).

II (9,341 daltons) corresponded with Ugi protein minus the N-terminal methionine. Ugi form I also contained two species with masses nearly identical to those of the unmodified Ugi control and apparently escaped modification during the EDC/GEE reaction. Ugi form II appeared to contain a single acyl-glycine ethyl ester modification, since this adduct would be expected to add 85 daltons per modified carboxyl group. By dividing the mass increase observed for each modified Ugi form by 85 daltons, it was deduced that forms II-V contained approximately 1.1, 2.0, 2.9, and 3.8 adducts, respectively per Ugi protein.

3.1.3 Effect of EDC/GEE Modification on the Specific Activity of Ugi Forms I-V

The effect of chemical modification on the inhibitor activity of purified Ugi forms I-V was determined by using *E. coli* uracil-DNA glycosylase (Figure 6). The specific activity of unmodified Ugi was essentially the same as either mock EDC/GEE-modified Ugi or Ugi form I. The slight increase in specific activity observed for the modified protein sample may have resulted from the removal of inactivated Ugi contained in the original preparation during DEAE-cellulose chromatography. In contrast, the specific activity of Ugi forms II-V displayed progressively decreased levels (58-17 %) of inhibitor activity coinciding with the increased extent of Ugi modification.

3.1.4 Ability of Ugi Forms I-V to Form a Complex with Ung

Ugi forms I-V were incubated with a 3-fold molar excess of Ung under conditions that typically promote Ung•Ugi complex formation. The complex was then resolved from its individual components by nondenaturing polyacrylamide gel electrophoresis. As controls, unmodified [^{35}S]Ugi, EDC/GEE-modified [^{35}S]Ugi reaction mixture, and Ung were individually separated by electrophoresis (Figure 8, lanes 1-3, respectively). The addition of unmodified Ugi or EDC/GEE-modified Ugi reaction mixture to excess Ung resulted in Ung•[^{35}S]Ugi complex formation of 99 and 75 % of [^{35}S]Ugi,

Figure 8. Ability of [^{35}S]Ugi forms I-V to complex with *E. coli* uracil-DNA glycosylase. Ten samples (60 µl) containing 106 pmol of unmodified [^{35}S]Ugi (lane 1), 318 pmol of EDC/GEE-modified [^{35}S]Ugi reaction mixture (lane 2), 318 pmol of Ung (lane 3), 106 pmol of unmodified [^{35}S]Ugi plus 318 pmol of Ung (lane 4), 318 pmol of EDC/GEE-modified [^{35}S]Ugi reaction mixture plus 951 pmol of Ung (lane 5), or 106 pmol each of [^{35}S]Ugi forms I-V plus 318 pmol of Ung (lanes 6-10, respectively) were incubated under standard Ung•Ugi complexing conditions as described under "Experimental Procedures". Each sample was loaded onto an 18% nondenaturing polyacrylamide gel, electrophoresis was performed, and the gel was stained with Coomassie Brilliant Blue G-250 to visualize protein. The *arrows* indicate the location of Ung, Ung•[^{35}S]Ugi, [^{35}S]Ugi, and tracking dye (TD). Proteins migrated from top (-) to bottom (+).

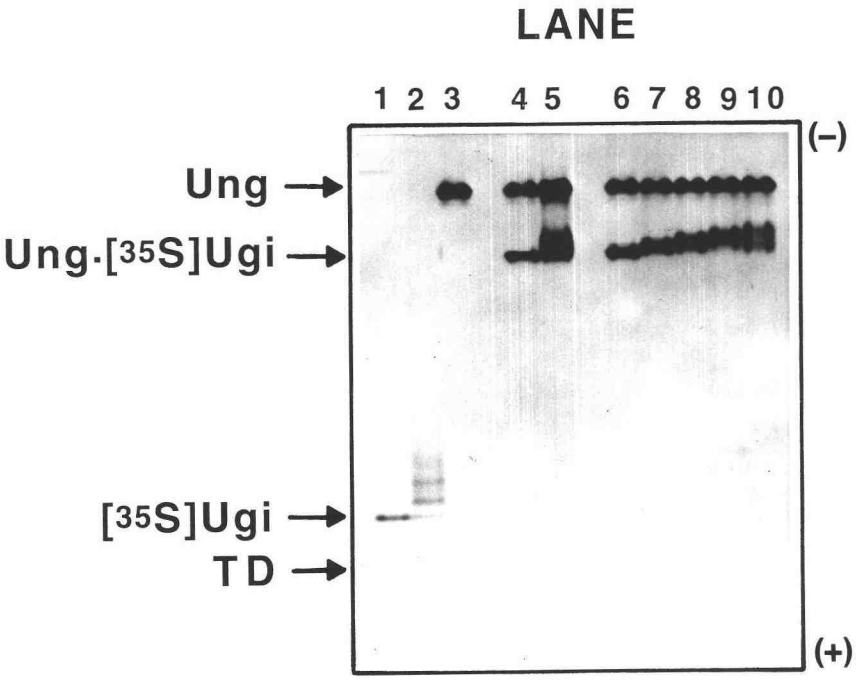

Figure 8

respectively (Figure 8, lanes 4 and 5). Interestingly, the Ung•Ugi complex formed by Ugi from the EDC/GEE reaction mixture resulted in a series of bands with decreased mobility (lane 5). When individual Ugi forms I-V were analyzed, the uncomplexed [^{35}S]Ugi bands disappeared coincident with the appearance of 97, 90, 77, 67, and 61 % of the [^{35}S]Ugi in complex with Ung (lanes 6-10). The reduced electrophoretic mobility of each complex was explained by the decreased electronegativity of individual EDC/GEE-modified Ugi forms. These findings demonstrate that modified Ugi forms remain capable of forming a Ung•Ugi complex.

3.1.5 Competitive Interaction Between Ugi and EDC/GEE-modified Ugi Forms I-V for Ung Binding

Experiments were conducted to determine the competitive ability of unmodified Ugi and EDC/GEE-modified [^{35}S]Ugi forms I-V to form a stable complex with Ung. In the first set of experiments, unlabeled unmodified Ugi was separately mixed with each of the modified [^{35}S]Ugi forms in various molar ratios (100:0, 80:20, 60:40, 40:60, and 20:80; modified:unmodified Ugi). Each Ugi mixture was combined with Ung in a 2-fold molar excess of inhibitor over enzyme to form complex, and the proteins were resolved by nondenaturing polyacrylamide gel electrophoresis and analyzed for ^{35}S radioactivity. Samples containing various ratios of unmodified Ugi competitor were mixed with unmodified [^{35}S]Ugi, as controls, and analyzed by electrophoresis (Figure 9A). Two peaks of [^{35}S]Ugi radioactivity were observed in each sample, one corresponding to unbound [^{35}S]Ugi and the other to the Ung•[^{35}S]Ugi complex. As expected, the percentage of [^{35}S]Ugi forming a complex almost exactly reflected the ratio of [^{35}S]Ugi to competitor Ugi in the unmodified reaction mixture (Figure 10, inset). Similar results were obtained when [^{35}S]Ugi form I competed with unmodified Ugi for complex formation, indicating that both preparations shared an equal ability to stably and irreversibly associate with Ung (Figure 9B and Figure 10). In contrast, [^{35}S]Ugi forms II-V showed a sequential decrease in their ability to compete with

Figure 9. Ability of unmodified Ugi to compete with modified [^{35}S]Ugi forms I-V for complex formation with Ung. (A) Competition reaction mixtures (70 µl) contained 158 pmol of Ung and 316 pmol combinations of unmodified [^{35}S]Ugi and non-radioactive competitor Ugi at [^{35}S]Ugi:Ugi ratios of 100:0 (*closed circles*), 80:20 (*open circles*), 60:40 (*closed squares*), 40:60 (*open squares*), and 20:80 (*closed triangles*). Following the Ung addition, the reaction mixtures were incubated under standard complexing conditions and then loaded onto 18% nondenaturing polyacrylamide tube gels as described under "Experimental Procedures". After electrophoresis, each gel was horizontally sliced (3.1 mm), dried overnight, solubilized in 30% H_2O_2 (500 µl), and analyzed for ^{35}S radioactivity. The direction of migration was from *left* to *right*. Competition reaction mixtures containing [^{35}S]Ugi form I (B), form II (C), form III (D), form IV (E), and form V (F) were mixed with non-radioactive competitor Ugi at [^{35}S]Ugi:Ugi ratios described above and similarly analyzed.

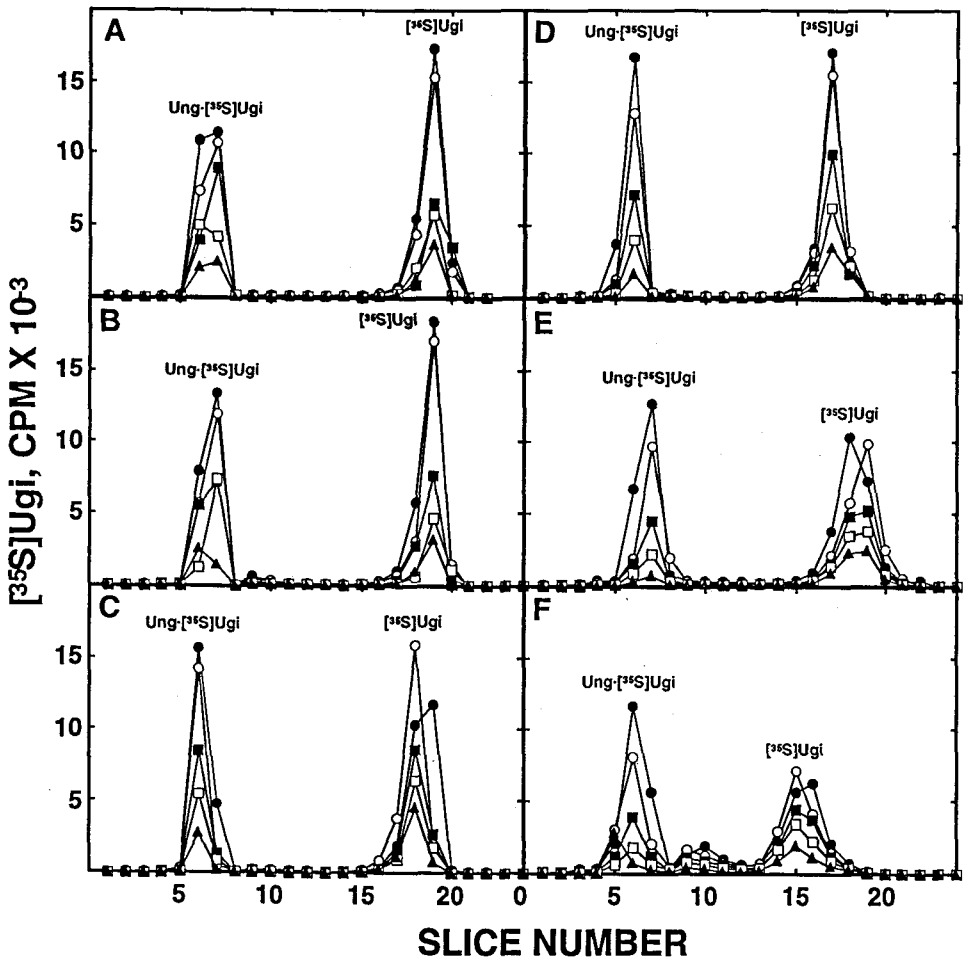
A
B
C
D
E
F
Ung-[35S]Ugi
[35S]Ugi
[35S]Ugi, CPM X 10-3
SLICE NUMBER
0
5
10
15
20

Figure 9

Figure 10. Quantitation of modified [^{35}S]Ugi forms I-V in the Ung•[^{35}S]Ugi complex after competition with unmodified Ugi. The competition reactions mixtures described in Figure 9 that contained unmodified [^{35}S]Ugi (■) and EDC/GEE-modified [^{35}S]Ugi form I (▨), form II (▩), form III (▨), form IV (▨), and form V (□) were analyzed and the amount of [^{35}S]Ugi (pmol) in complex was plotted. The amount of [^{35}S]Ugi (pmol) forming complex in the absence of competitor (100:0) is given in *parenthesis* in the *inset*. The relative percentage of unmodified or modified (forms I-V) [^{35}S]Ugi that formed a complex during the competition reactions relative to the 100:0 control was determined for each ratio of [^{35}S]Ugi to unmodified Ugi. Each reaction was conducted in duplicate, and the percentages of [^{35}S]Ugi complexed represent averaged values.

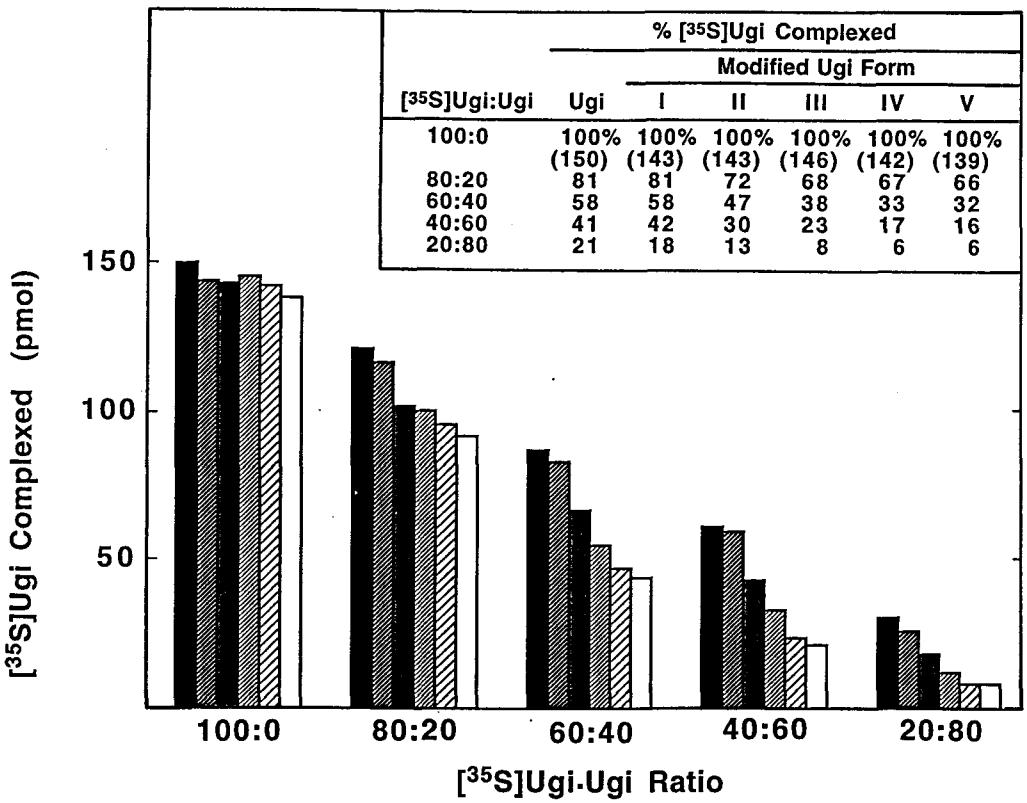
% [35S]Ugi Complexed
Modified Ugi Form
[35S]Ugi:Ugi
Ugi
I
II
III
IV
V
100:0
100% (150)
100% (143)
100% (143)
100% (146)
100% (142)
100% (139)
80:20
81
81
72
68
67
66
60:40
58
58
47
38
33
32
40:60
41
42
30
23
17
16
20:80
21
18
13
8
6
6
[35S]Ugi Complexed (pmol)
150
100
50
100:0
80:20
60:40
40:60
20:80
[35S]Ugi-Ugi Ratio

Figure 10

unmodified Ugi, since the amount of [^{35}S]Ugi detected in complex was significantly less than that reflected by the modified [^{35}S]Ugi:unmodified Ugi ratios (Figure 9C-F and Figure 10). The decreased competitive performance by the modified forms II-V of Ugi directly correlated with the extent of EDC/GEE adduction.

As a second approach in examining the ability of EDC/GEE-modified Ugi forms I-V to compete with unmodified Ugi for complex formation with Ung, each of the modified [^{35}S]Ugi forms (360 pmol) was separately mixed with increasing molar amounts of unlabeled Ugi such that the [^{35}S]Ugi component constituted 100, 95, 90, 85, 80, 75, 50, 25, or >1 % of the total [^{35}S]Ugi/Ugi mixture. Each Ugi mixture was then combined with Ung (160 pmol), and the proteins were resolved by nondenaturing polyacrylamide gel electrophoresis and analyzed for ^{35}S radioactivity. If the ability of any modified [^{35}S]Ugi form to form a complex with Ung was equal to that of the unmodified Ugi competitor, then the percentage of [^{35}S]Ugi in complex would reflect the component percentage of [^{35}S]Ugi in the [^{35}S]Ugi/Ugi mixture. As a verification, unmodified [^{35}S]Ugi was combined with increasing amounts of unmodified Ugi and analyzed by electrophoresis (Figure 11). The percentage of unmodified [^{35}S]Ugi in complex was 100, 94, 92, 86, 81, 76, 50, 25, and <1 % and almost exactly matched the expected values as exhibited by the percentage of [^{35}S]Ugi in the [^{35}S]Ugi/Ugi mixture. [^{35}S]Ugi form I also yielded similar results, indicating an equal ability to compete with unmodified Ugi in binding and stabilizing a complex with Ung. However, [^{35}S]Ugi forms II-V showed a reduced ability to effectively compete with unmodified Ugi as indicated by the reduced amounts of [^{35}S]Ugi detected in complex at each titration point (Figure 11). These results substantiate the previous observation that the decreased competitive performance by EDC/GEE-modified Ugi forms II-V is directly correlated to an increased level of EDC/GEE modification.

Figure 11. Ability of modified [^{35}S]Ugi forms I-V to compete with unmodified Ugi in forming a complex with Ung. Competition reaction mixtures (175 µl) contained 158 pmol of Ung and combinations of 318 pmol of unmodified [^{35}S]Ugi (*closed circles*) plus 0, 16, 32, 80, 107, 320, and 960 pmols of unlabeled competitor Ugi to generate [^{35}S]Ugi:[^{35}S]Ugi plus Ugi ratios of 1.0, 0.95, 0.9, 0.8, 0.75, 0.5, and 0.25. Following Ung addition, the reaction mixtures were incubated under standard complexing conditions and then loaded onto 18% nondenaturing polyacrylamide tube gels as described under "Experimental Procedures". After electrophoresis, each gel was horizontally sliced (3.1 mm), dried overnight, solubilized in 30% H_2O_2 (500 µl), and analyzed for ^{35}S radioactivity. The relative percentage of unmodified [^{35}S]Ugi that forms a complex during the competition reactions relative to the control ([^{35}S]Ugi:[^{35}S]Ugi plus Ugi ratio of 1.0) was determined for each sample. Competition reaction mixtures containing [^{35}S]Ugi form I (*open circles*), form II (*closed squares*), form III (*open squares*), form IV (*closed triangles*), and form V (*open triangles*) were mixed with unlabeled competitor Ugi at [^{35}S]Ugi:[^{35}S]Ugi plus Ugi ratios described above and were similarly analyzed. Each reaction was conducted in duplicate, and the percentages of [^{35}S]Ugi complexed represent averaged values.

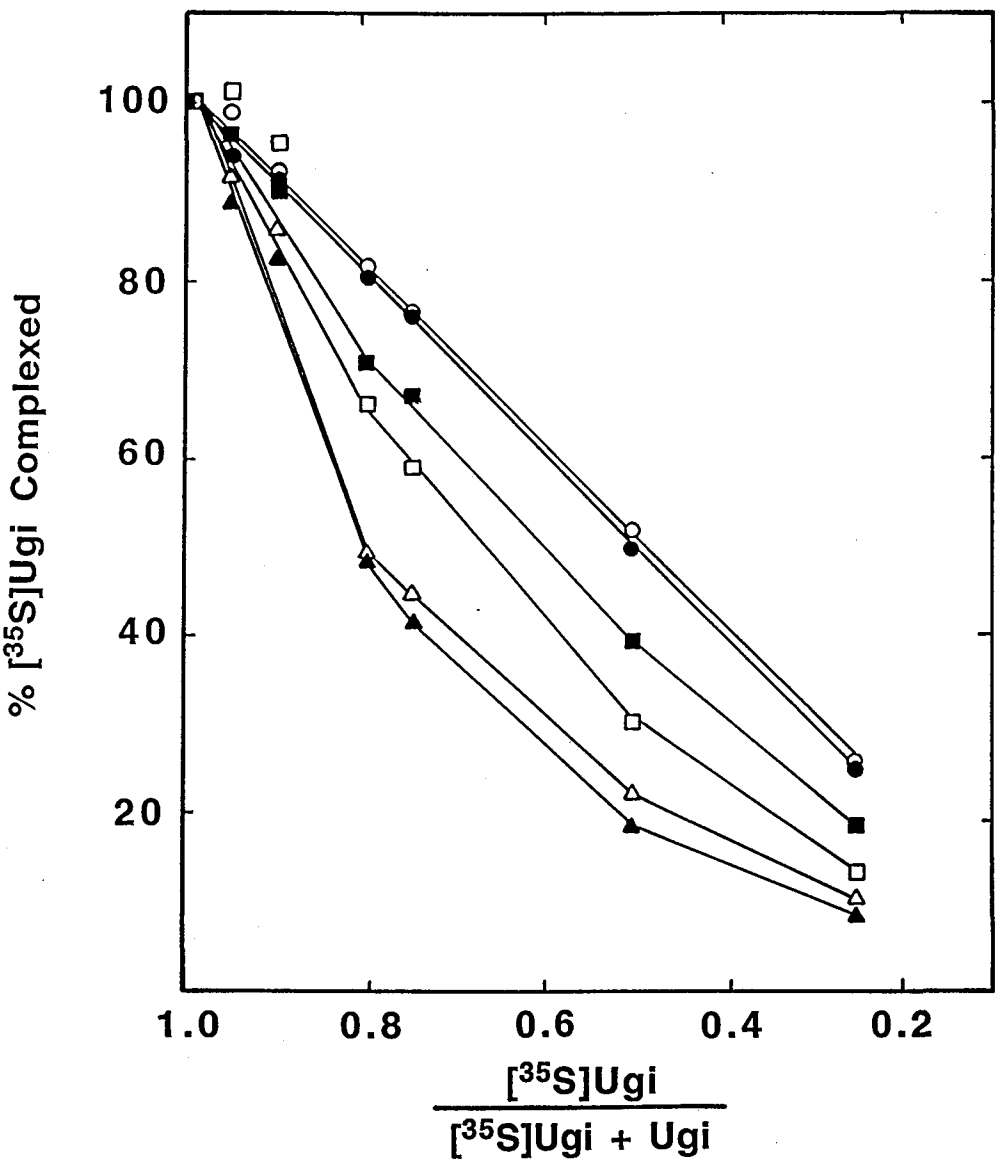
100
80
60
40
20
% [35S]Ugi Complexed
1.0
0.8
0.6
0.4
0.2
[35S]Ugi
[35S]Ugi + Ugi

Figure 11

3.1.6 Stability of the Ung•Ugi Complex Containing EDC/GEE-modified Ugi Forms I-V

To examine the complex stability of modified Ugi forms I-V, 5.3 nmol of [^{35}S]Ugi (unmodified or modified forms (I-V)) was incubated with a ~5-fold molar excess of Ung, and the Ung•[^{35}S]Ugi complex was purified from its constituent components by DEAE-cellulose chromatography (Figure 12). In each case, almost all of the [^{35}S]Ugi eluted as Ung•[^{35}S]Ugi complex following the 150 mM NaCl step as determined by ^{35}S radioactivity. No significant amount of free inhibitor protein was detected after the 250 mM NaCl elution step, and excess Ung eluted in the wash fractions. After pooling Ung•[^{35}S]Ugi-containing fractions, each Ung•[^{35}S]Ugi complex preparation was then analyzed by nondenaturing polyacrylamide gel electrophoresis to assess complex formation and stability (Figure 13). Purified Ung•[^{35}S]Ugi complexes containing unmodified and modified [^{35}S]Ugi forms I and II each contained >95 % of the total inhibitor protein in complex (Figure 14A). In contrast, free [^{35}S]Ugi was observed for Ugi forms III-V in complex with Ung, as demonstrated by 17, 34, and 30 % of the total [^{35}S]Ugi migrating as uncomplexed inhibitor protein, respectively. A diffuse band of free Ung also appeared in these samples. These results were consistent with an interpretation that more extensive levels of EDC/GEE modification of Ugi cause less stable complexes to dissociate during electrophoresis.

To determine if modified forms I-V of [^{35}S]Ugi in complex could exchange with free Ugi, each complex preparation was incubated with a 3- and 30-fold molar excess of unmodified Ugi, and gel electrophoresis was performed, as before, to resolve the constitutive components and analyzed for ^{35}S radioactivity. The analysis of unmodified and modified forms I-V of [^{35}S]Ugi in complex incubated with a 3-fold molar excess of unmodified Ugi is represented in Figure 15. As anticipated for the control Ung•[^{35}S]Ugi, no significant release of unmodified [^{35}S]Ugi (<2.5 %) was detected, indicating the irreversibility of complex formation. A nearly identical result was obtained for the Ung•[^{35}S]Ugi form I complex. In contrast, the presence of a 3-fold

Figure 12. Purification of Ung•[^{35}S]Ugi complexes containing unmodified and EDC/GEE-modified Ugi forms I-V by DEAE-cellulose chromatography. (A) A reaction mixture (1.5 ml) containing 26.4 nmol of Ung and 5.3 nmol of unmodified [^{35}S]Ugi was incubated under standard Ung•Ugi complexing conditions and then applied to a DE-52 cellulose column (0.8 cm^2 x 1.9 cm). The column was washed and step-eluted with DAB buffer (30 mM Tris-HCl (pH 7.4), 1 mM EDTA, 1 mM DTT, 5 % (w/v) glycerol) containing 150 mM and 250 mM NaCl (*arrows*) as described under "Experimental Procedures". Fractions (1 ml) were collected and analyzed for ^{35}S-radioactivity (*closed circles*) and uracil-DNA glycosylase activity (*open circles*). Fractions (numbers 33-44) containing the Ung•[^{35}S]Ugi complex were pooled and concentrated ~12-fold using a Centriplus-10 (Amicon) concentrator. Five similar reaction mixtures containing Ung and [^{35}S]Ugi form I (B), form II (C), form III (D), form IV (E), and form V (F) were prepared and purification of each corresponding Ung•[^{35}S]Ugi complex was carried out as described above.

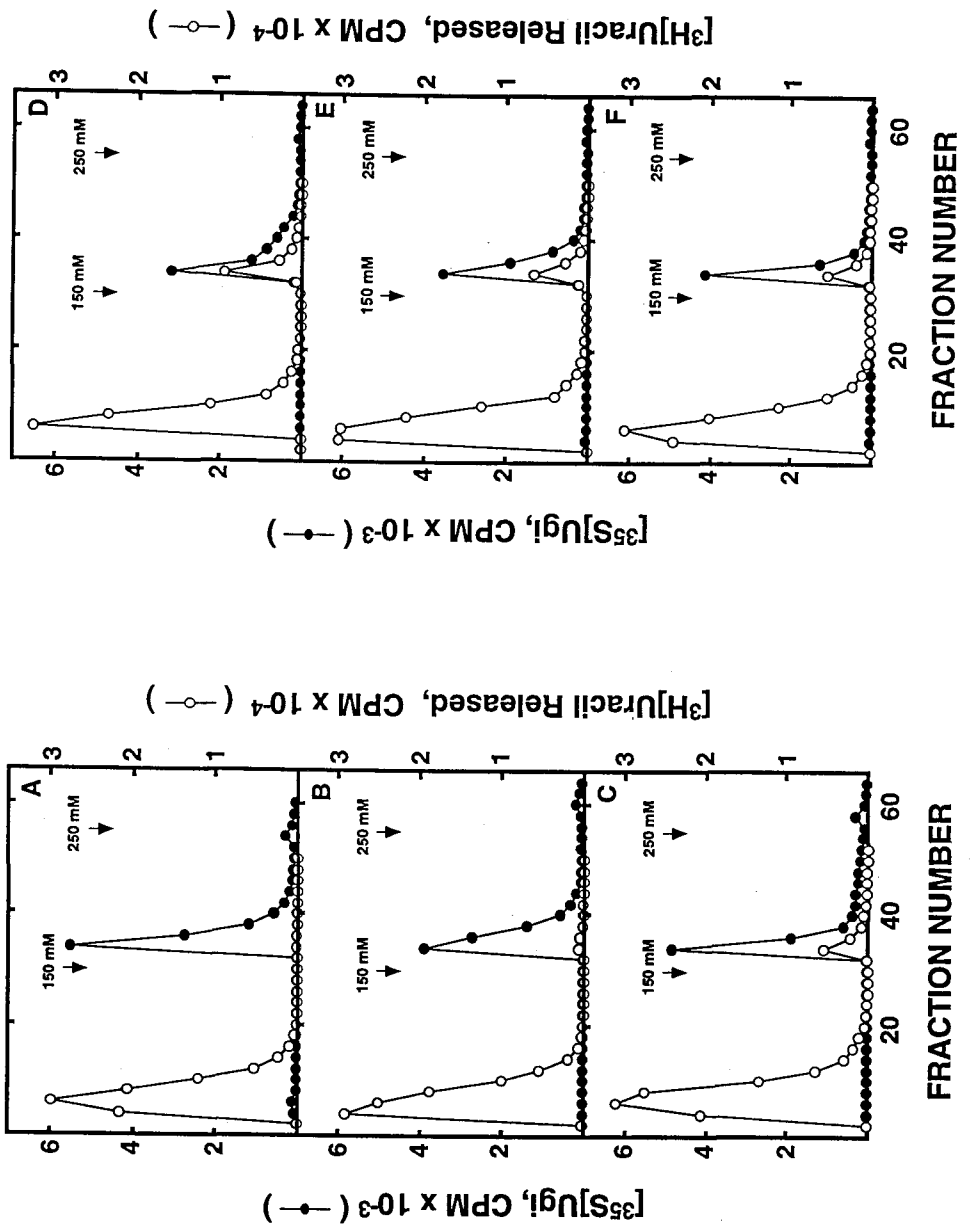
[35S]Ugi, CPM x 10-3 (—●—)
[3H]Uracil Released, CPM x 10-4 (—○—)
A
B
C
D
E
F
150 mM
250 mM
FRACTION NUMBER
20
40
60
1
2
3
4
6

Figure 12

Figure 13. Purity and stability of the various Ung•[^{35}S]Ugi complexes. Six samples (50 µl) containing 85 pmol of purified complex formed with unmodified [^{35}S]Ugi (lane 1) and EDC/GEE-modified [^{35}S]Ugi forms I-V (lanes 2-6, respectively) were analyzed by 18% nondenaturing polyacrylamide gel electrophoresis. Protein was visualized after staining with Coomassie Brilliant Blue G-250. The *arrows* indicated the location of Ung and the *bracket* denotes the location of the Ung•[^{35}S]Ugi complex. Prior to electrophoresis, standard uracil-DNA glycosylase assays were conducted on each sample as described under "Experimental Procedures". The percentage of Ung activity detected for each complex was determined by dividing the specific activity of Ung measured in each Ung•[^{35}S]Ugi complex (U/mg) by the specific activity of an equal amount of uncomplexed Ung (2×10^6 U/mg).

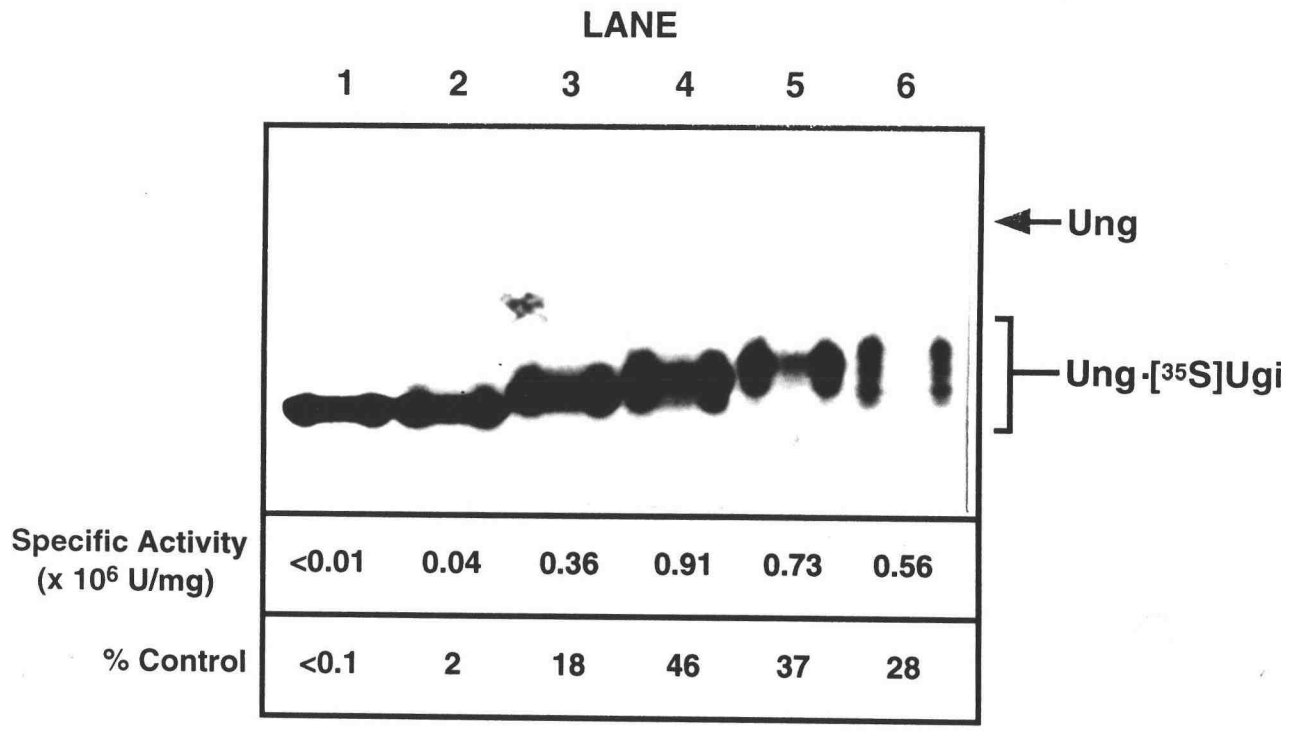
LANE
1
2
3
4
5
6
Ung
Ung·[35S]Ugi
Specific Activity
(x 10^6 U/mg)
<0.01
0.04
0.36
0.91
0.73
0.56
% Control
<0.1
2
18
46
37
28

Figure 13

Figure 14. Quantitation of various [^{35}S]Ugi forms released from the Ung•[^{35}S]Ugi complex by unmodified Ugi. Competition reaction mixtures (140 µl) each containing 228 pmol of preformed Ung•[^{35}S]Ugi complex constituted with unmodified [^{35}S]Ugi (■), form I (▨), form II (▩), form III (▨), form IV (▨), and form V (□) were incubated with buffer A (50 mM Tris-HCl (pH 7.0), 1 mM EDTA, 1 mM DTT), 684 pmol of Ugi (B), or 6,840 pmol of Ugi (C) under standard complex formation conditions. Samples were loaded onto 18% nondenaturing polyacrylamide tube gels and electrophoresis was performed. After electrophoresis, each gel was horizontally sliced (3.1 mm), dried overnight, solubilized in 30% H_2O_2 (500 µl), and analyzed for ^{35}S radioactivity. The percentage of [^{35}S]Ugi released from complex was determined as the amount of free [^{35}S]Ugi divided by the sum of free plus complexed [^{35}S]Ugi multiplied by 100.

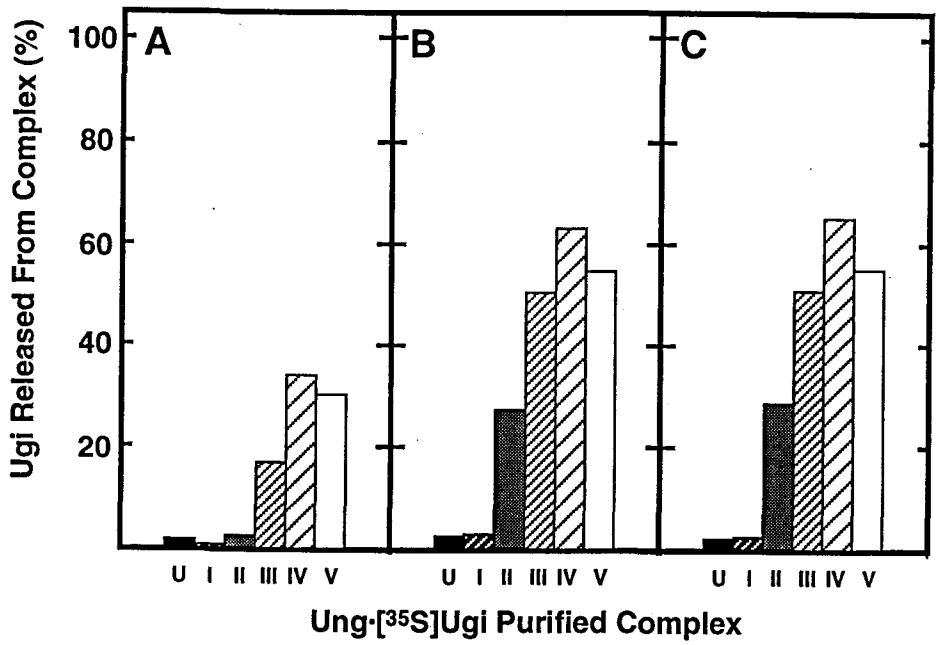
Ugi Released From Complex (%)
100
80
60
40
20
A
B
C
U I II III IV V
U I II III IV V
U I II III IV V
Ung·[35S]Ugi Purified Complex

Figure 14

Figure 15. Ability of unmodified Ugi to exchange with various [^{35}S]Ugi forms in the Ung•[^{35}S]Ugi complex. Competition reaction mixtures (140 µl) containing 228 pmol of preformed Ung•[^{35}S]Ugi constituted with unmodified [^{35}S]Ugi (*closed circles*), form I (*open circles*), form II (*closed squares*), form III (*open squares*), form IV (*closed triangles*), and form V (*open triangles*) were incubated with 684 pmol of unmodified and non-radioactive Ugi under standard complex formation conditions and then loaded onto 18% nondenaturing polyacrylamide tube gels as described under "Experimental Procedures". After electrophoresis, each gel was horizontally sliced (3.1 mm), dried overnight, solubilized in 30% H_2O_2 (500 µl), and analyzed for ^{35}S radioactivity. The direction of migration was from *left* to *right*.

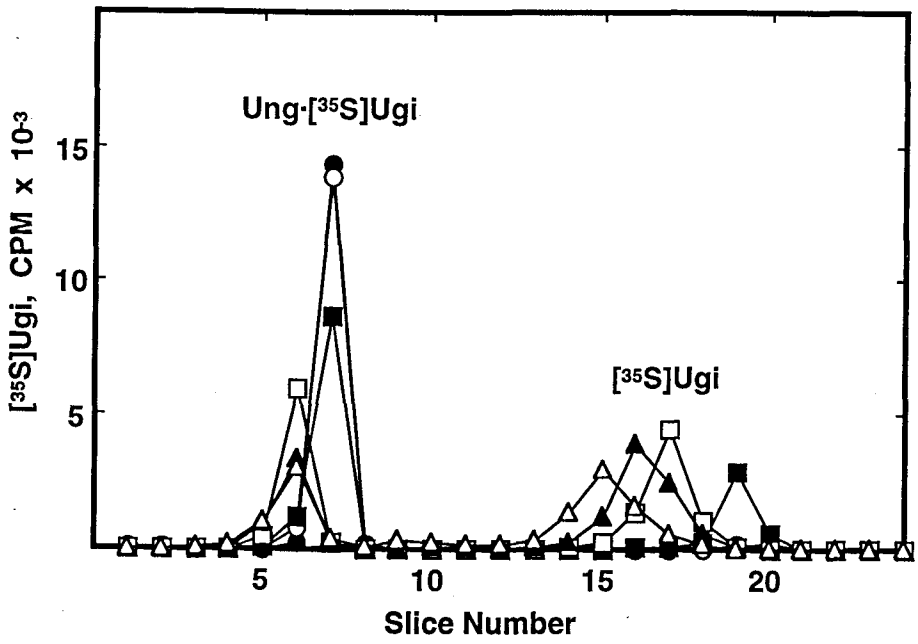
Ung·[35S]Ugi
[35S]Ugi
[35S]Ugi, CPM x 10-3
15
10
5
5
10
15
20
Slice Number

Figure 15

molar excess of Ugi promoted the release of 27, 50, 63, and 54 % of total modified Ugi forms II-V from the complex, respectively (Figure 14B). Similar increases in the amount of [^{35}S]Ugi released were observed for the exchange reactions containing the 30-fold molar excess of Ugi (Figure 14C). These results further suggest that charge neutralization due to modification leads to the destabilization of the Ung•Ugi complex.

If modification of Ugi facilitated Ung•Ugi dissociation in the presence of exogenous Ugi, then perhaps these complexes undergo dissociation in the presence of a competing uracil-containing DNA substrate. The Ung activity profiles of the DEAE-cellulose chromatography fractions containing Ung•[^{35}S]Ugi complexes II-V suggest that some free Ung was present and may have appeared as a result of a dissociated complex (Figure 12C-F). Thus, the enzymatic activity of Ung in each complex containing unmodified or modified Ugi forms I-V was determined under standard assay conditions (Figure 13). The preformed complex containing unmodified Ugi showed <0.1 % of the total uracil-DNA glycosylase activity in complex displayed catalytic activity. In contrast, Ung complexed with Ugi forms I-V, respectively, possessed 2, 18, 46, 37, and 28 % of the uracil-DNA glycosylase activity expected for completely uncomplexed and uninhibited Ung. Taken together, these results confirm that EDC/GEE- modified forms of Ugi are less capable of maintaining an irreversible and catalytically inactive Ung•Ugi complex.

3.1.7 Fluorescein 5-Isothiocyanate Labeling and Properties of F-Ung

To further investigate the properties of EDC/GEE-modified Ugi interactions with Ung, the enzyme was labeled with FITC to produce F-Ung. As previously reported (17), F-Ung fluorophores, when quenched, function as reporter groups for both Ugi and nucleic acid binding. The standard modification reaction was conducted at pH 9.5 with a 10.7-fold molar excess of FITC over Ung as described under "Experimental Procedures", and resulted in the adduction of ~2.3 FITC molecules per enzyme molecule (Table 3). Under these conditions, no significant change in the specific activity of uracil-DNA

Table 3

Effect of Various pH Conditions on Fluorescein 5-Isothiocyanate Conjugation of Uracil-DNA Glycosylase

pH	Overall $OD_{280\ nm}$	FITC $OD_{496\ nm}$	[FITC][a]	Ung $OD_{280\ nm}$[b]	[Ung]	[FITC]/[Ung][c]
			μM		*μM*	*mol/mol*
8.5	0.376	0.577	7.40	0.191	4.53	1.63
9.0	0.395	0.683	8.76	0.176	4.17	2.10
9.5	0.440	0.793	10.17	0.186	4.41	2.31
10.0	0.439	0.811	10.40	0.179	4.24	2.45

[a] The concentration of FITC in the dye-protein conjugate was determined by spectrophotometric absorbance using the extinction coefficient $\varepsilon_{496\ nm} = 7.8 \times 10^{-4}$ liters/mol•cm (99).

[b] The spectrophotometric absorbance of Ung at $OD_{280\ nm}$ was determined by subtracting the $OD_{280\ nm}$ contributed by FITC from the overall $OD_{280\ nm}$ of the dye-protein conjugate. It was experimentally determined that 1 μM FITC contributed 0.025 $OD_{280\ nm}$.

[c] The extent of fluorescein conjugation was measured by the molar ratio of FITC bound to Ung.

glycosylase or the ability of Ugi to inhibit the FITC-conjugated enzyme was observed. The excitation and emission spectra of F-Ung were determined (Figure 16) and showed two maximum excitation peaks at 472 and 496 nm and single maximum emission peak at 524 nm that are characteristic of the conjugated FITC molecule (99). Upon addition of excess Ugi and after correcting for the necessary dilution factor, the intensity of the emission spectra decreased by ~10.9 % at 520 nm.

3.1.8 Steady-state Fluorescence Measurements of Fluorescein 5-Isothiocyanate-labeled Ung Binding to Ugi Forms I-V

To determine whether fluorescence quenching was quantitative between differentially modified forms of Ugi, F-Ung was titrated with Ugi, and the relative fluorescence was monitored under steady-state conditions (Figure 17). Prior to the Ugi addition, F-Ung emitted a steady fluorescent signal which subsequently decreased proportionally to the amount of Ugi added. In the control, the addition of unmodified Ugi caused a proportional decrease in fluorescent signal and elicited a 9.4 % maximal quench achieved at a Ugi:Ung molar ratio of 0.8:1 (Figure 17A). Titration of F-Ung with modified Ugi Forms I-V also displayed a linear decrease in fluorescence intensity with maximum fluorescence quench occurring at 9.2, 7.7, 5.4, 4.9, and 5.4 %, respectively (Figure 17B-F). When the change in relative fluorescence was plotted against the molar ratio of Ugi:Ung, saturation of F-Ung occurred between Ugi:Ung ratios of 0.8:1 and 1.3:1 for each modified Ugi form I-V (Figure 18). These results are consistent with an inhibitor:enzyme stoichiometry of 1:1. We interpret the reduced levels of relative fluorescent quench for Ugi forms II-V to indicate that EDC/GEE modification either alters amino acid residues that directly interact with F-Ung fluorophores or perturbs the local structure and environment around the fluorophores in the final F-Ung•Ugi complex.

Figure 16. Excitation and emission spectra of fluoroscein 5-isothiocyanate conjugated Ung (F-Ung) and the F-Ung•Ugi complex. The excitation and emission spectra of F-Ung (*open circles*) in a volume (440 µl) containing 100 nM F-Ung in buffer DAB (30 mM Tris-HCl (pH 7.4), 1 mM EDTA, 1 mM DTT, 5 % (w/v) glycerol) supplemented with 50 mM NaCl was measured at 25°C with a LS50 luminescence spectrometer (Perkin-Elmer) as described under "Experimental Procedures". The spectrum of the F-Ung•Ugi complex (*closed circles*) in a volume (440 µl) containing 100 nM F-Ung and 1 µM Ugi was also determined.

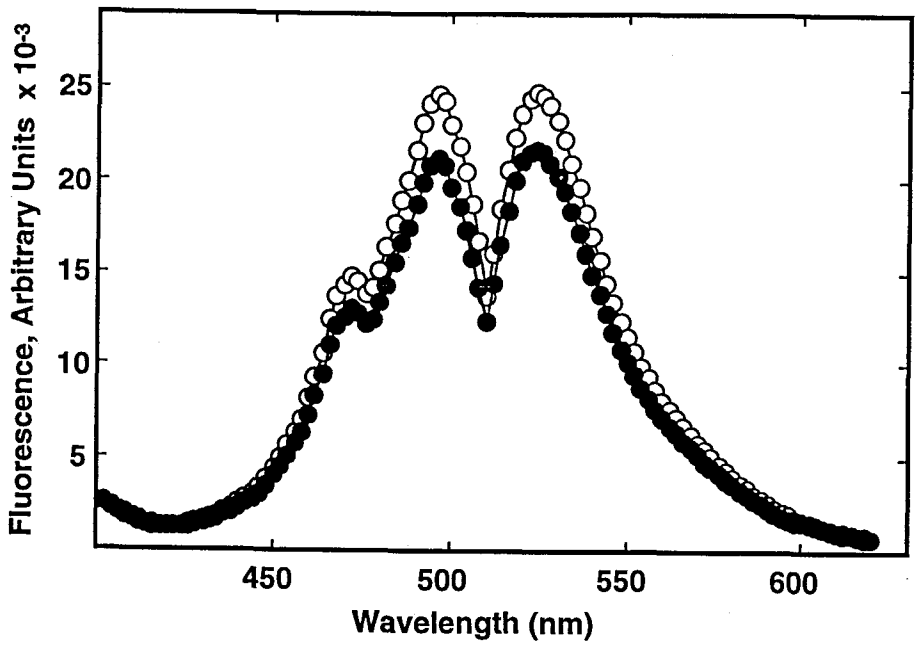
Fluorescence, Arbitrary Units x 10-3
25
20
15
10
5
450
500
550
600
Wavelength (nm)

Figure 16

Figure 17. Effect of EDC/GEE-modified Ugi binding to fluorescein-conjugated Ung on fluorescence intensity. Samples (400 µl) containing 110 nM F-Ung were equilibrated at 25°C for 5 min and placed into a thermostatted quartz minicell cuvette, and fluorescence was measured (496 nm excitation and 520 nm emission wavelengths) for 1 min to establish the F-Ung signal corresponding to 100% relative fluorescence as described under "Experimental Procedures". Following this equilibration period, additions (40 µl) containing either 0 (-●-), 138 (-○-), 275 (-■-), 413 (-□-), 550 (-▲-), 688 (-△-), 825 (-◆-), 963 (-◇-), 1,100 (-▪-), 1,238 (-▫-), 1,375 (-✱-), 5,500 (-⊡-), or 11,000 (-▣-) nM of unmodified [^{35}S]Ugi (A), form I (B), form II (C), form III (D), form IV (E), and form V (F) were added to F-Ung, and the fluorescence intensity was monitored for an additional 5.5 min. Fluorescence measurements were recorded at 5 sec intervals; however, only those taken every 15 sec have been plotted for clarity. All net decreases are plotted as a percentage relative to the F-Ung fluorescence control after correcting for dilution effects.

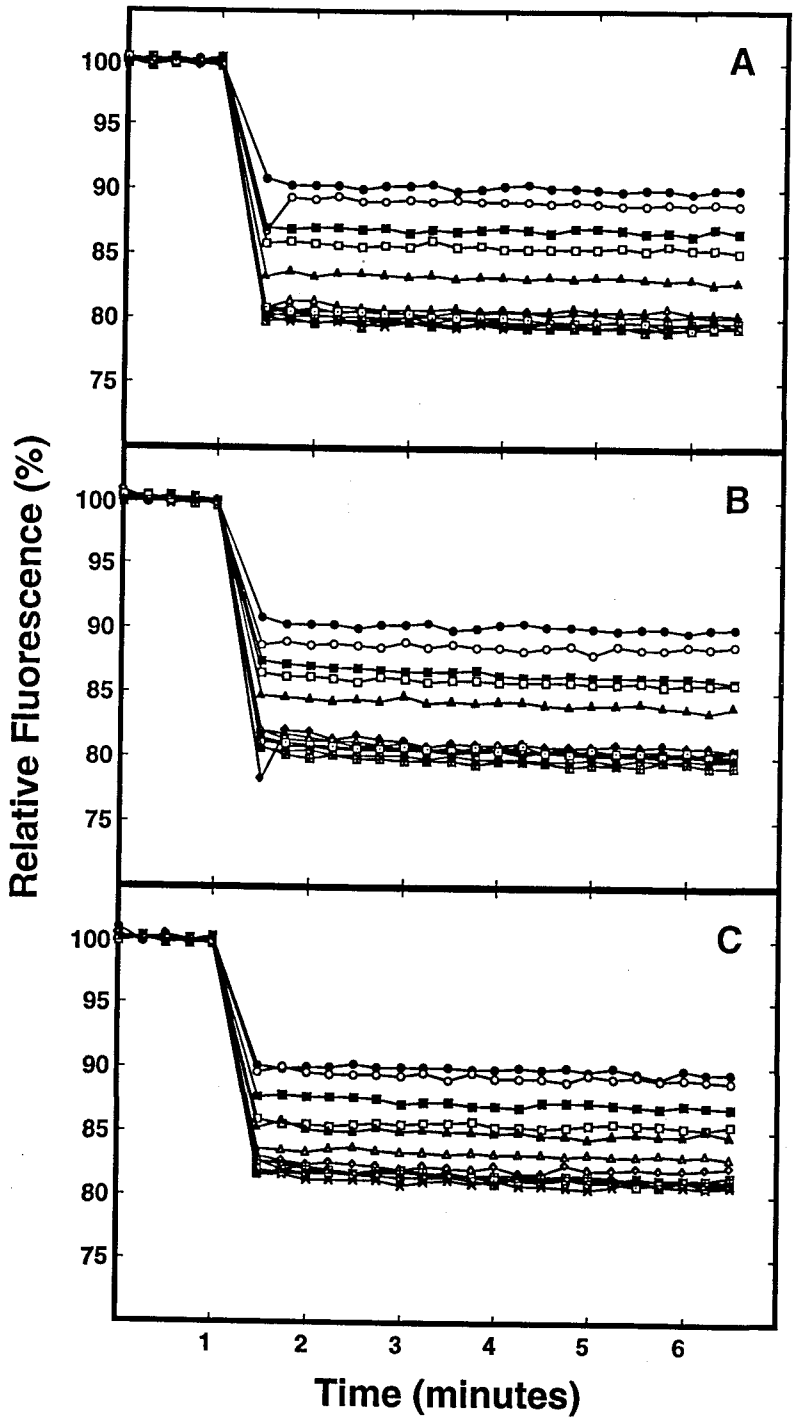
A
B
C
100
95
90
85
80
75
Relative Fluorescence (%)
1
2
3
4
5
6
Time (minutes)

Figure 17

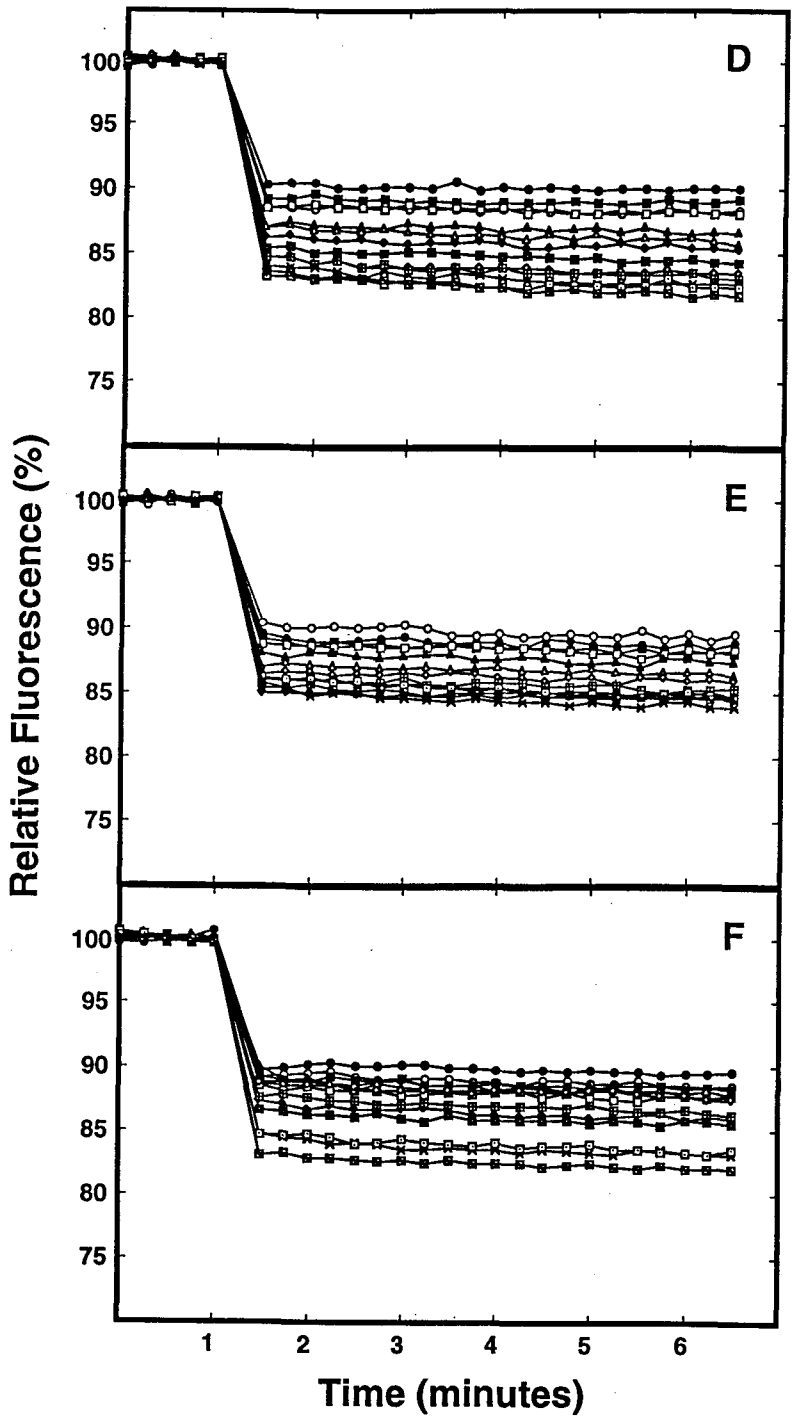

Figure 17 (continued)

Figure 18. Summary of EDC/GEE-modified Ugi forms I-V binding to fluorescein-conjugated Ung on fluorescence intensity. Samples (400 µl) containing 110 nM F-Ung and additions (40 µl) of 0, 138, 275, 413, 550, 688, 825, 963, 1,100, 1,238, 1,375, 5,500, and 11,000 nM each of unmodified [^{35}S]Ugi (*closed circles*), form I (*open circles*), form II (*closed squares*), form III (*open squares*), form IV (*closed triangles*), and form V (*open triangles*) were prepared and the fluorescence intensity was monitored as described in Figure 17. Measurements taken at 15-sec intervals were used to determine the average relative fluorescence for each Ugi concentration. After correcting for dilution effects, the percentage decrease in relative fluorescence intensity was calculated as the average relative fluorescence following the Ugi addition subtracted from the 100% relative fluorescence of F-Ung alone. Each analysis was carried out in duplicate, and the average values were plotted.

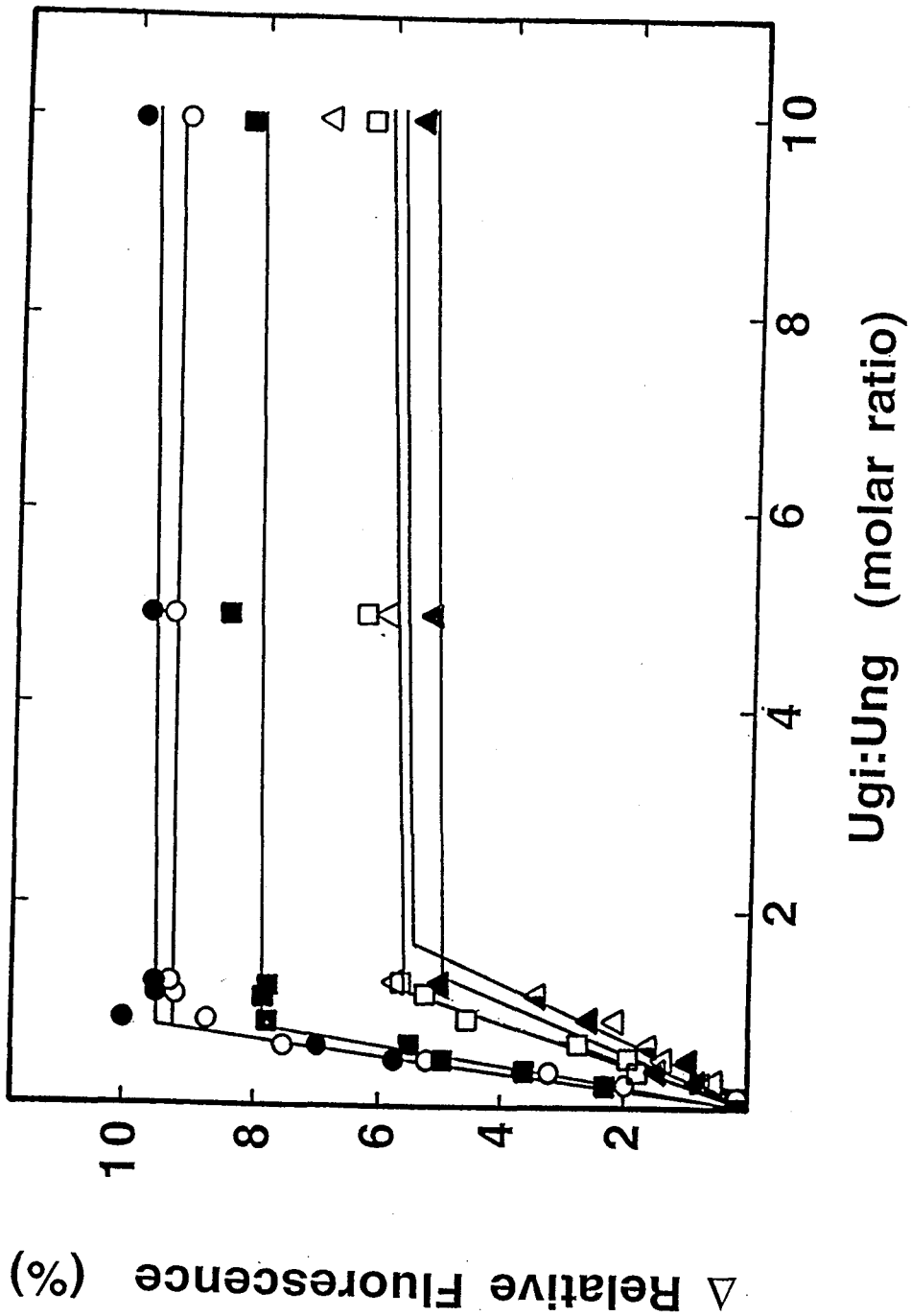

Figure 18

3.1.9 Effect of Ugi Forms I-V on F-Ung Binding to Poly(U)

The linearity of the titration curves for Ugi forms I-V binding to F-Ung (Figure 18) indicate that Ugi remains in complex with uracil-DNA glycosylase after complex formation and does not freely dissociate. This observation would appear to contradict findings showing that free Ugi will exchange with modified forms II-V in the preformed complex and that Ung demonstrates catalytic activity in these same complexes. However, an explanation for both results could be that complexes are maintained in solution but that the addition of competitor Ugi or nucleic acid present in the standard reaction mixture promotes dissociation of modified complexes. Thus, the influence of Ugi on F-Ung binding to poly(U) was investigated. When F-Ung (42 pmol) was combined with a saturating amount of poly(U), the average fluorescent intensity was quenched by 7.9 ± 0.8 % (Figure 19A, ΔRF_1). The addition of unmodified [^{35}S]Ugi (63 pmol) resulted in a further fluorescent intensity decrease of 4.5 % (Figure 19A, ΔRF_2), indicating that Ugi preferentially binds to F-Ung in the presence of poly(U) and effectively competes poly(U) out of the complex. Similar experiments were conducted using modified Ugi forms I-V in place of the unmodified Ugi. After the initial fluorescence quench (ΔRF_1 ~8 %) due to poly(U), the addition of Ugi forms I-V resulted in ΔRF_2 values of 4.3, 3.1, 1.4, 1.2, and 2.1 %, respectively (Figure 19B). Each of the EDC/GEE-modified Ugi forms, except Ugi form I, showed a significantly reduced ΔRF_2 value compared with the unmodified Ugi control (ΔRF_2 = 4.5 %).

As a second approach, an analogous experiment was conducted where F-Ung (42 pmol) was combined with either unmodified or modified Ugi forms I-V (63 pmol) prior to the poly(U) addition, and the relative fluorescence intensity was monitored after each addition to determine ΔRF_1 and ΔRF_2 (Figure 20). The initial addition of unmodified Ugi caused an 8.5 % reduction of fluorescence intensity, and no significant quenching of the

Figure 19. Effect of Ugi forms I-V on F-Ung binding to poly(U). Six samples (400 µl) containing 105 nM F-Ung were placed into a thermostatted quartz minicell cuvette and equilibrated at 25°C, and fluorescent intensity measurements were recorded as described in the legend to Figure 17. (A) To one sample, an addition (30 µl) containing 4.4 mg/ml of poly(U) was made after 1 min (*arrow*), and a second addition (30 µl) containing 2,100 nM [^{35}S]Ugi (form I) was added after 6 min (*arrow*). Fluorescence measurements were recorded at 5 sec intervals; however, only those taken every 15 sec have been plotted for clarity. ΔRF_1 represents the net decrease in fluorescent intensity caused by the first addition, and ΔRF_2 is the decrease due to the second addition. All net decreases are plotted as a percentage relative to the F-Ung fluorescence control after correcting for dilution effects. (B) Poly(U) was added to each of the six F-Ung samples (first addition), and then either 2,100 nM of unmodified [^{35}S]Ugi or 2,100 nM [^{35}S]Ugi forms I-V was added (second addition) as indicated above. Quenching of F-Ung fluorescence was measured, and ΔRF_1 was determined for the poly(U) addition (*black bars*) and ΔRF_2 for the Ugi addition (*striped bars*).

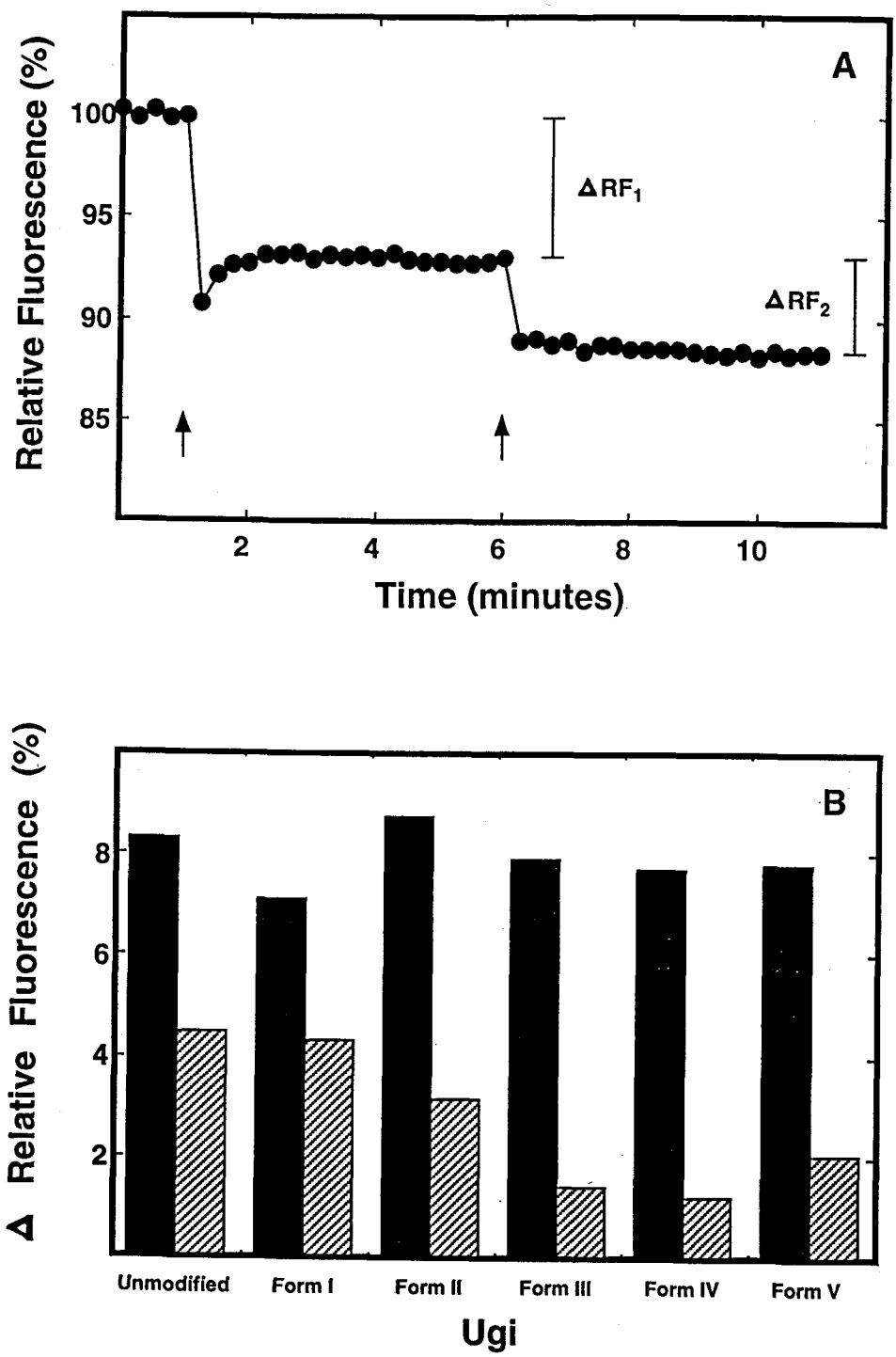
A
Relative Fluorescence (%)
100
95
90
85
ΔRF1
ΔRF2
2
4
6
8
10
Time (minutes)
B
Δ Relative Fluorescence (%)
8
6
4
2
Unmodified
Form I
Form II
Form III
Form IV
Form V
Ugi

Figure 19

Figure 20. Effect of poly(U) on F-Ung binding to Ugi forms I-V. A set of six samples (400 µl) containing 105 nM F-Ung were placed into a thermostatted quartz minicell cuvette and equilibrated at 25°C, and fluorescent intensity measurements were recorded as described in the legend to Figure 17. (A) To one sample, an addition (30 µl) containing 2,100 nM [^{35}S]Ugi (form I) was made after 1 min (*arrow*), and a second addition (30 µl) containing 4.4 mg/ml of poly(U) was added after 6 min (*arrow*). Fluorescent measurements were recorded at 5 sec intervals; however, only those taken every 15 sec have been plotted for clarity. ΔRF_1 represents the net decrease in fluorescent intensity caused by the first addition, and ΔRF_2 is the decrease due to the second addition. All net decreases are plotted as a percentage relative to the F-Ung fluorescence control after correcting for dilution effects. (B) Either 2,100 nM of unmodified [^{35}S]Ugi or 2,100 nM [^{35}S]Ugi forms I-V was added to each of the six F-Ung samples (first addition), and then poly(U) was added (second addition) as indicated above. Quenching of F-Ung fluorescence was measured, and ΔRF_1 was determined for the Ugi addition (*black bars*) and ΔRF_2 for the poly(U) addition (*striped bars*).

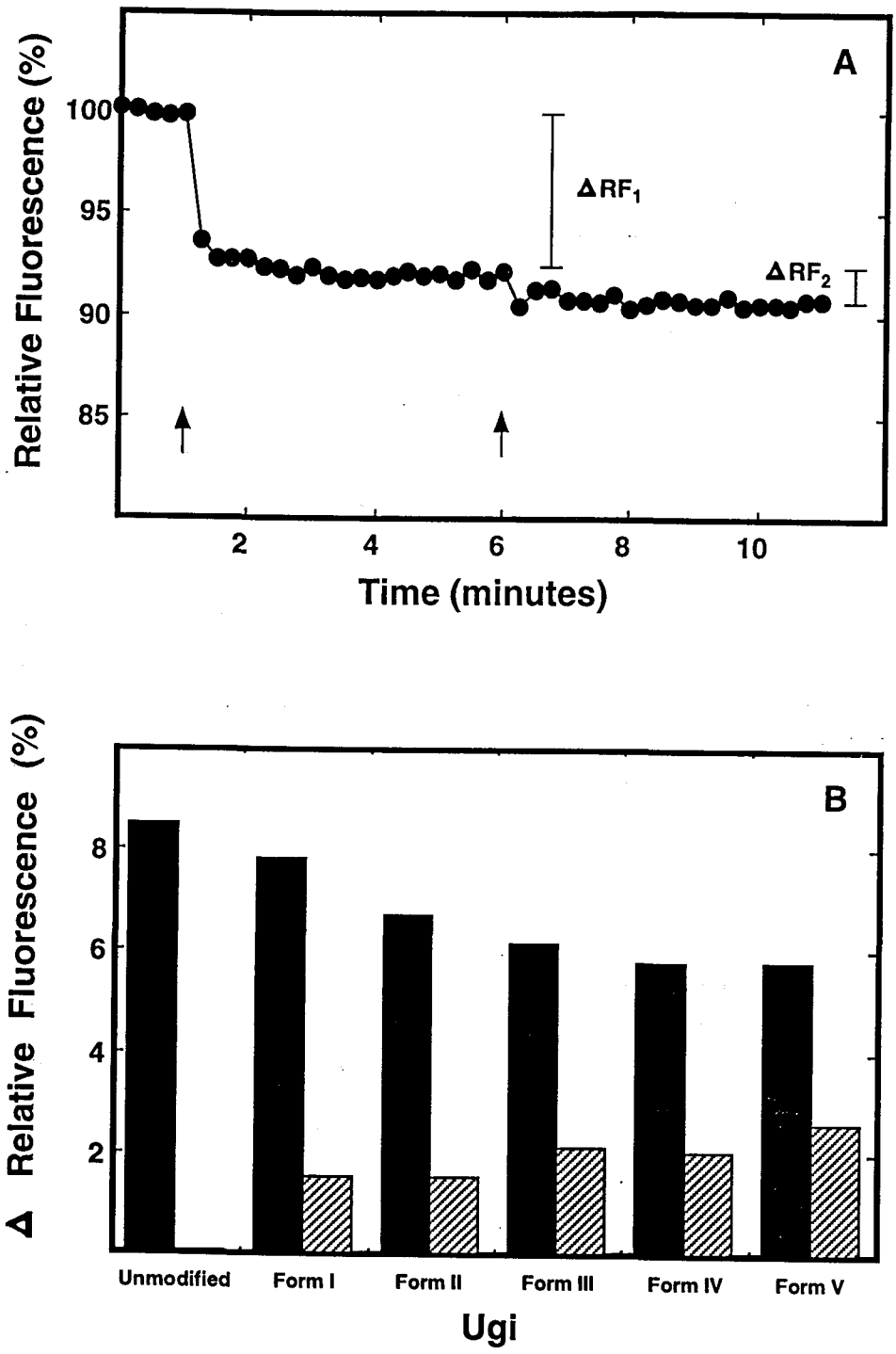
A
Relative Fluorescence (%)
100
95
90
85
ΔRF1
ΔRF2
2
4
6
8
10
Time (minutes)
B
Δ Relative Fluorescence (%)
8
6
4
2
Unmodified
Form I
Form II
Form III
Form IV
Form V
Ugi

Figure 20

fluorescent signal was observed following the poly(U) addition (ΔRF_2 <0.17 %) (Figure 20A). This observation was consistent with an interpretation that the Ung•Ugi complex was refractory to binding nucleic acid (17). Conversely, the addition of poly(U) to each of the EDC/GEE-modified Ugi forms I-V in complex with F-Ung elicited additional fluorescence quenching of 1.5, 1.5, 2.1, 2.1, and 2.6 %, respectively (Figure 20B). Collectively, these results demonstrate the reversibility of modified Ugi forms in complex with Ung when nucleic acid was present, a property not exhibited by the unmodified Ung•Ugi complex.

3.1.10 Identification of EDC/GEE-modified Amino Acid Residues in Ugi

In order to locate EDC/GEE-modified residues of Ugi forms I-V, the inhibitor protein was chemically cleaved with cyanogen bromide, and the peptide fragments were analyzed by MALDI mass spectrometry (Figure 21 and Figure 22). Ugi contains four methionine residues capable of producing five peptide fragments following complete CNBr-induced cleavage (Figure 21). Following CNBr cleavage, four peptide fragments were identified for unmodified Ugi; mass values were in excellent agreement with the predicted mass of peptides C1/2, C2, C3, and C4 (Table 4). A similar analysis was performed on EDC/GEE-modified Ugi forms I-V (Figure 22 and Table 4). As anticipated, Ugi form I generated a set of four peptides with nearly the same mass values as the unmodified control. In contrast, five peptide fragments were identified for CNBr-treated Ugi form II; four corresponded to unmodified peptides C1/2, C2, C3, and C4. The fifth peptide ($C3M_1$), comprising 82 % of C3-derived peptide fragments, had a mass of 3,643 daltons, which was 89 daltons larger than that predicted for peptide C3. These findings indicated that the major site of adduction is located on the C3 peptide. Similarly, the vast majority (92 %) of Ugi form III adducts were localized on the C3 peptide (Table 4). A second modified peptide ($C3M_2$) was identified

Figure 21. Primary amino acid sequence of bacteriophage PBS2 uracil-DNA glycosylase inhibitor protein. The four possible CNBr cleavage sites and the six potential endoproteinase Asp-N sites are indicated by *arrows* with the corresponding peptide fragments (C1-C5 and A1-A7, respectively) numbered according to amino acid sequence alignment. Negatively charged amino acid residues are denoted by a *minus sign*. Amino acid sequence analysis of peptide C3 isolated from Ugi forms II and III (*) and form IV (**) revealed unique PTH-derivatives. A third site of adduction was localized to peptide A6/7; the three potential amino acid targets are indicated (*open circles*).

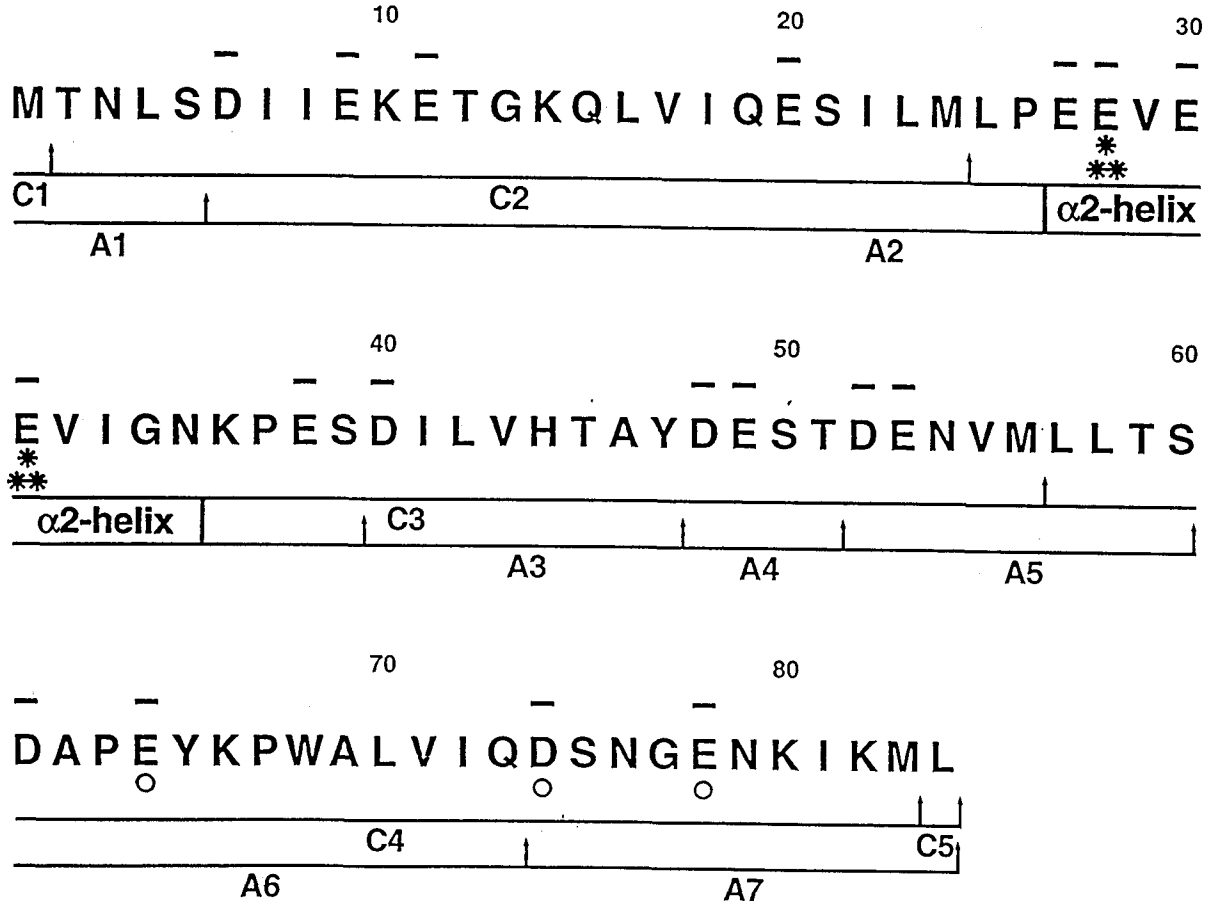
10
20
30
MTNLSDIIEKETGKQLVIQESILMLPEEVE
C1
C2
α2-helix
A1
A2
40
50
60
EVIGNKPESDILVHTAYDESTDENVMLLTS
α2-helix
C3
A3
A4
A5
70
80
DAPEYKPWALVIQDSNGENKIKML
C4
C5
A6
A7

Figure 21

Figure 22. Molecular mass determination of CNBr-generated peptides from Ugi forms I-V by MALDI mass spectrometry. [^{35}S]Ugi forms I-V were treated with CNBr, and peptide fragments were produced and analyzed by mass spectrometry as described under "Experimental Procedures". (A) Mass spectra of Ugi form I peptide fragments showed the relative intensity of singly charged ions corresponding to mass peaks of peptides C1/2, C2, C3, and C4 (Figure 21). Peptide C1/2 represents the C2 fragment containing an uncleaved amino-terminal methionine residue, and individual fragments C1 and C5 were not detected. Mass spectra on CNBr-generated peptides from [^{35}S]Ugi form II (B), form III (C), form IV (D), and form V (E) are shown, focusing on the mass peaks between 3,500 and 4,000 daltons. This region contained unmodified peptide C3 and four modified peptides, M_1 to M_4. The other mass peaks corresponding to peptides C1/2, C2, and C4 remained essentially unchanged for forms I-V.

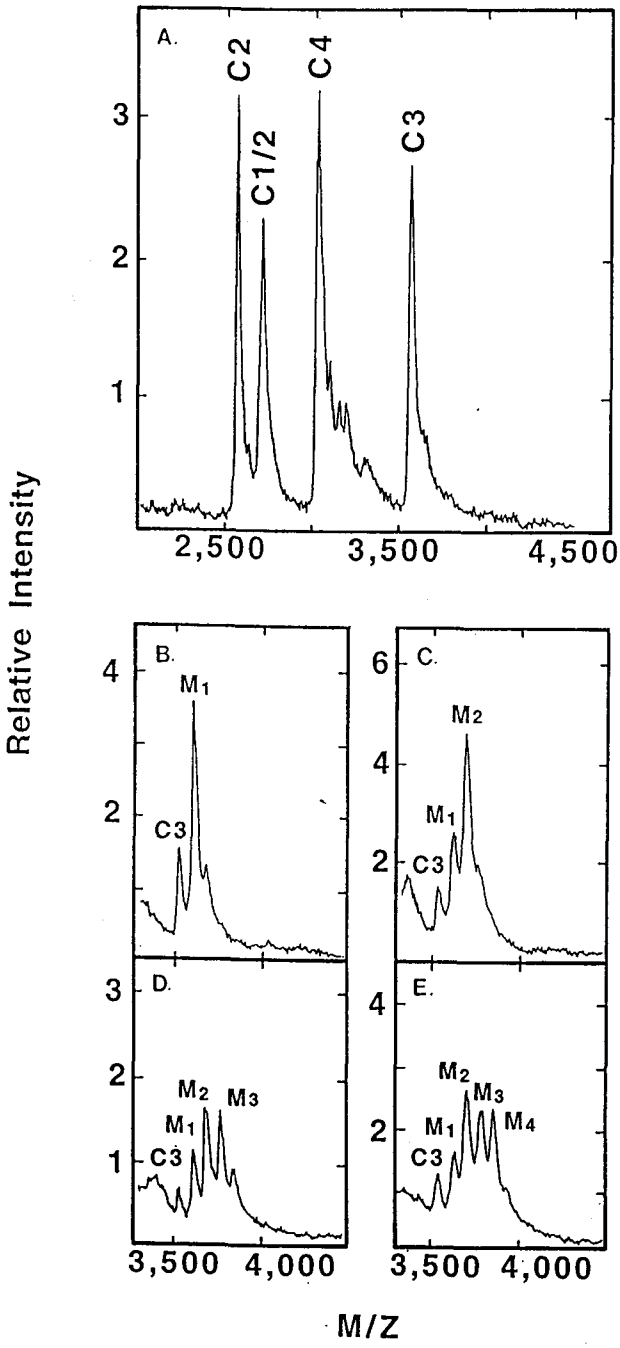
A.
C2
C4
C3
C1/2
3
2
1
2,500
3,500
4,500
B.
M1
C3
4
2
C.
M2
M1
C3
6
4
2
D.
M2
M3
M1
C3
3
2
1
E.
M2
M3
M4
M1
C3
4
2
3,500
4,000
3,500
4,000
Relative Intensity
M/Z

Figure 22

Table 4

Molecular Mass of Ugi Peptides Produced by CNBr Cleavage

Peptide	Predicted Mass[a]	Experimental Mass[b]					
		Unmodified	Form I	Form II	Form III	Form IV	Form V
				daltons			
C1/2[c]	2,674	2,700	2,696	2,701	2,703	2,706	2,707
C2	2,554	2,555	2,551	2,556	2,552	2,553	2,552
C3	3,554	3,556	3,549	3,558	3,552	3,553	3,551
$C3M_1$				3,643 (89)[d]	3,638 (84)	3,641 (87)	3,640 (86)
$C3M_2$					3,710 (156)	3,712 (158)	3,710 (156)
$C3M_3$						3,795 (241)	3,792 (238)
$C3M_4$							3,846 (310)
C4	3,012	3,015	3,008	3,018	3,011	3,013	3,011
		Relative Amounts of C3 Peptides[e]					
				%			
C3		>95	>95	18	8	5	7
$C3M_1$				82	22	17	12
$C3M_2$					70	34	29
$C3M_3$						28	25
$C3M_4$						16	27

[a] Predicted mass values of CNBr-generated peptides were determined by the computer program MacProMass, version 1.05, by Lee and Vermuri (137).

[b] Average molecular masses were determined from four independent measurements and standard errors range from 0.3 to 4.5 daltons.

[c] Peptide C1/2 contains the amino-terminal methionine residue that was neither post-translationally removed *in vivo* (284) nor cleaved by CNBr to generate peptide C2 *in vitro*, possibly due to oxidation of the methionine to the sulfone.

[d] Numbers in parentheses correspond to mass values obtained by subtracting the experimentally determined mass from the predicted mass and reflect mass increases.

[e] Relative amounts of modified or unmodified peptide C3 were determined as percentages of total peak area (3,500-4,000 daltons) for unmodified Ugi and Ugi forms I-V in Figure 7.

with a mass of 3,710 daltons, indicative of two adducts, each of ~85 daltons. Ugi form III also produced a $C3M_1$ peptide fragment (3,638 daltons), connoting a single acyl-glycine ethyl ester adduction (Table 4). Mass determination of CNBr-treated Ugi forms IV and V both included peptide fragments $C3M_1$ and $C3M_2$ and possessed additional peptides $C3M_3$ and $C3M_4$. The relative percentage of peptides $C3M_{1-4}$ detected for each Ugi form is indicated in Table 4. In all cases, the primary modification site(s) were specifically localized to peptide C3, which contained 10 Glu and Asp residues.

The location of the adducted site(s) on peptide C3 was further investigated by using the same approach but following endoproteinase Asp-N digestion of Ugi. A comparison of the molecular weights of unmodified and form II Ugi peptides revealed two modified fragments derived from peptides A2 and A6/7 (Figure 23 and Table 5). The major $A2M_1$ (~82 %) and minor $A6/7M_1$ (~23 %) modified peptide species each showed a mass increase of ~85 daltons, denoting the presence of a single acyl-glycine ethyl ester adduct. Peptide $A2M_1$ was detected in equal abundance with $C3M_1$ and overlapping amino acid sequence from Leu-25 to Ser-39 (Figure 21). Thus, it was deduced that modification by EDC/GEE likely involved Glu-27, Glu-28, Glu-30, Glu-31, and/or Glu-38. The appearance of peptide $A6/7M_1$ suggested that another site of adduction occurred with reduced frequency at Glu-64, Asp-74, Glu-78, and/or the carboxyl terminus of the Ugi protein. Unfortunately, the latter observation was not confirmed by detecting a modified peptide corresponding to peptide C4 (Table 4). We assume that the low abundance of this modified species and interference by minor mass peaks in the C4 region obscured detection following CNBr cleavage of Ugi form II. Ugi form III digested with endoproteinase Asp-N also produced peptides $A2M_1$ and $A6/7M_1$; however, an additional modified fragment ($A2M_2$) was detected with a mass increase of 162 daltons (Table 5). As observed for peptide $C3M_2$, the $A2M_2$ peptide most likely contained two acyl-glycine ethyl ester adducts among the five glutamic acid residues located between Leu-25 and Ser-39.

Figure 23. Molecular mass determination of Asp-N generated peptides from unmodified Ugi and EDC/GEE-modified Ugi forms II and III by MALDI mass spectrometry. Unmodified [^{35}S]Ugi and forms II and III were treated with endoproteinase Asp-N, and peptide fragments were produced and analyzed by mass spectrometry as described under "Experimental Procedures". (A) Mass spectra of unmodified Ugi peptide fragments showed the relative intensity of singly charged ions corresponding to mass peaks of peptides A2, A3, A6, A6/7, and A7 (Figure 21). Peptide A6/7 represents the uncleaved dipeptide of A6 plus A7, and individual fragments A1, A4, and A5 were not detected. Mass spectra of Asp-N generated peptides from [^{35}S]Ugi form II (B) and form III (C) are shown, focusing on the mass peaks between 1,000 and 5,000 daltons. This region contained both unmodified peptides A2 and A6/7 and modified peptides $A2M_1$,$A2M_2$, and $A6/7M_1$. The other mass peaks corresponding to peptides A3, A6, and A7 remained essentially unchanged between samples.

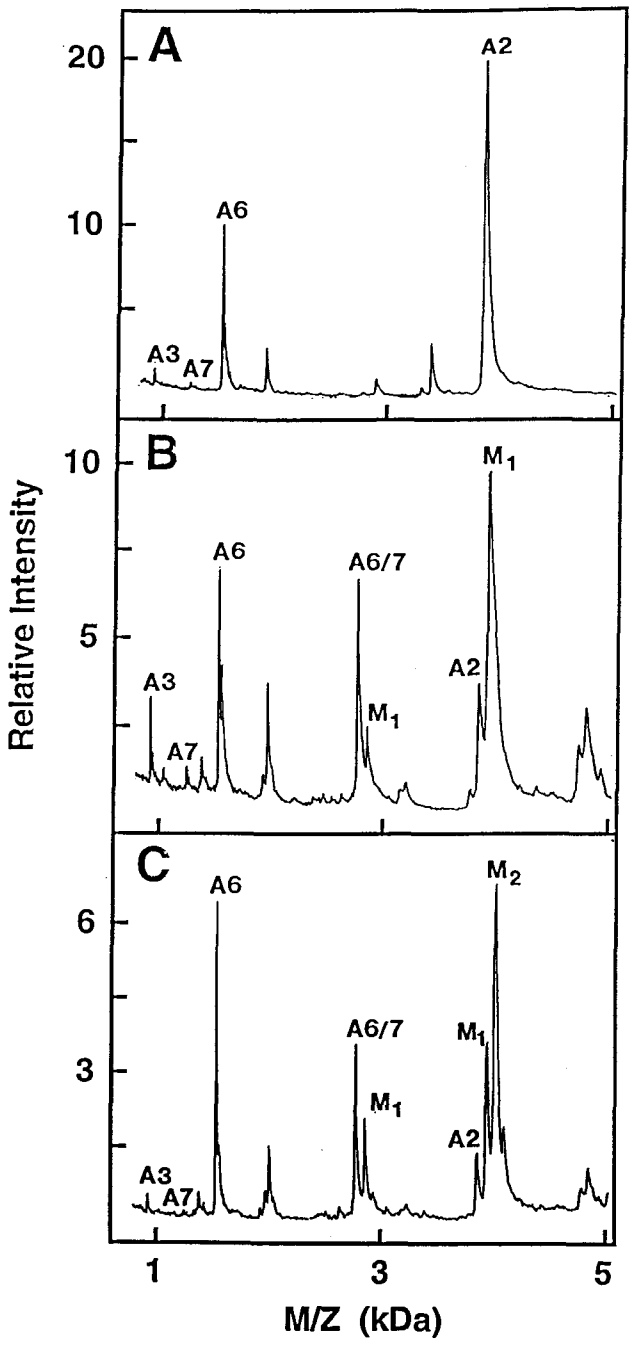
A
B
C
20
10
10
5
6
3
A2
A6
A3
A7
M1
A6/7
M2
1
3
5
Relative Intensity
M/Z (kDa)

Figure 23

Table 5

Molecular Mass of Ugi Peptides Produced by Endoproteinase Asp-N

Peptide	Predicted Mass[a]	Experimental Mass[b]		
		Unmodified	Form II	Form III
		daltons		
A1[c]	565			
A2	3,837	3,837	3,838	3,837
$A2M_1$			3,920 (83)[d]	3,923 (86)
$A2M_2$				3,999 (162)
A3	932	931	932	932
A4[c]	451			
A5[c]	1,021			
A6	1,530	1,530	1,529	1,529
A6/7[e]	2,759	2,760	2,762	2,759
$A6/7M_1$			2,846 (87)	2,844 (85)
A7	1,249	1,248	1,249	1,248
		Relative Amounts of Peptides[f]		
			%	
A2			18	10
$A2M_1$			82	25
$A2M_2$				65
A6/7			77	63
$A6/7M_1$			23	37

[a] Predicted mass values of peptides produced by Asp-N endoproteinase were determined by the computer program MacProMass, version 1.05, by Lee and Vermuri (137).

[b] Average molecular masses were determined from two to three independent measurements, and standard errors range from 0.0 to 4.5 daltons.

[c] Peptides A1, A4, and A5 were not detected, presumably due to their small size or unusual protein properties.

[d] Numbers in parentheses correspond to mass values obtained by substracting the experimentally determined mass from the predicted mass and reflect mass increases.

[e] Peptide A6/7 corresponds to the uncleaved dipeptide A6 plus A7.

[f] Relative amounts of modified or unmodified peptides A2 and A6/7 were determined by a method similar to that described in Table 4.

In order to identify the precise sites of adduction, modified and unmodified peptide C3 were purified to apparent homogeneity by DEAE-cellulose chromatography (data not shown). Amino acid sequence analysis unambiguously identified peptide C3 from CNBr-treated Ugi forms I-IV (Figure 24 and Table 6). Examination of the amino acid PTH-derivatives detected in sequencing cycles for the C3 peptide of Ugi form II revealed peaks of a unique PTH-derivitized amino acid (PTH-1) appearing at cycles 4 and 7 (Figure 25 and Figure 26A), thus identifying Glu-28 and Glu-31 as sites of modification. The unique amino acid derivative peaks concordantly appeared, corresponding to decreases in Glu-28 and Glu-31, and similar peaks were not detected at other cycles containing Glu or Asp residues. Almost equal amounts of the novel amino acid derivative were detected at cycles 4 and 7 for forms II, III, and IV (Figure 26A-C). Interestingly, an additional unique PTH-derivatized amino acid (PTH-2) was detected for Glu-28 and Glu-31 in Ugi form IV (Figure 26D), suggesting two types of adducts (Figure 21). Taken together, these results identify Glu-28 and Glu-31 as two major sites of EDC/GEE modification.

3.2 Discussion

It was determined that EDC/GEE modification of Ugi protein resulted in the selective adduction of specific glutamic acid residues that inactivated Ugi activity. Ugi form I represented unmodified inhibitor protein, since it did not exhibit any neutralization of charge, increase in mass, or reduction in inhibitor activity. Ugi form II contained a single EDC/GEE-induced adduct per protein, defining the location of the most highly reactive amino acids. The results demonstrated that 82 % of Ugi Form II adducts were located within the peptide sequence Leu-Pro-Glu-Glu-Val-Glu-Glu-Val-Ile-Gly-Asn-Lys-Pro-Glu-Ser (residues 25-39) containing the α2-helix and adjoining loop region. Of the five glutamic acid residues that reside in this sequence, only Glu-28 and Glu-31 were significantly modified and in roughly equal

Figure 24. Amino acid sequence analysis of the Ugi form II peptide C3. Amino acid sequencing was conducted using an Applied Biosystems model 475A gas phase protein sequencer as described under "Experimental Procedures". The amount (pmol) of PTH-derivatives detected for each amino acid and the unique PTH-derivative (PTH1) are plotted by amino acid residue for the first 28 cycles.

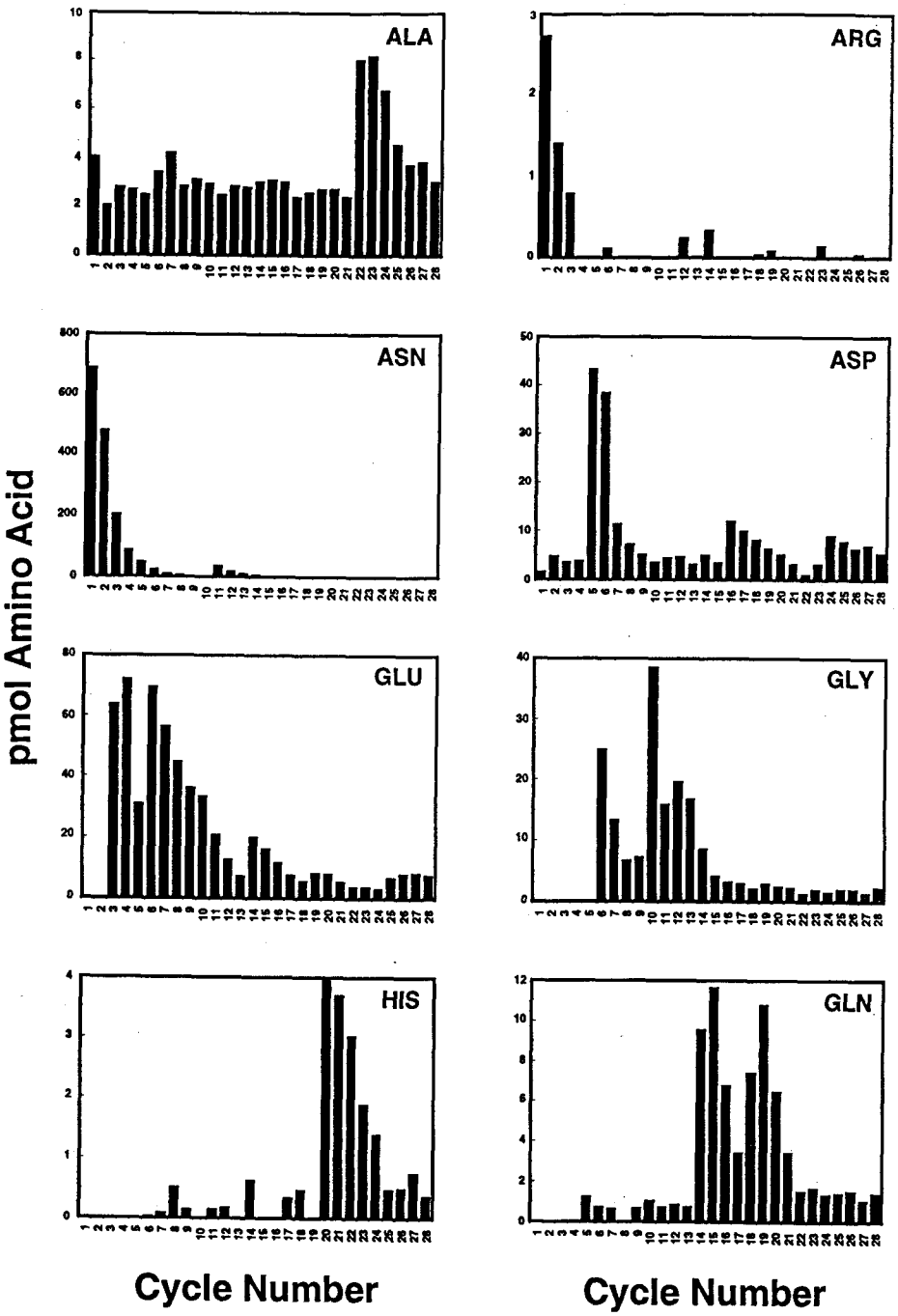
ALA
ARG
ASN
ASP
GLU
GLY
HIS
GLN
pmol Amino Acid
Cycle Number
Cycle Number

Figure 24

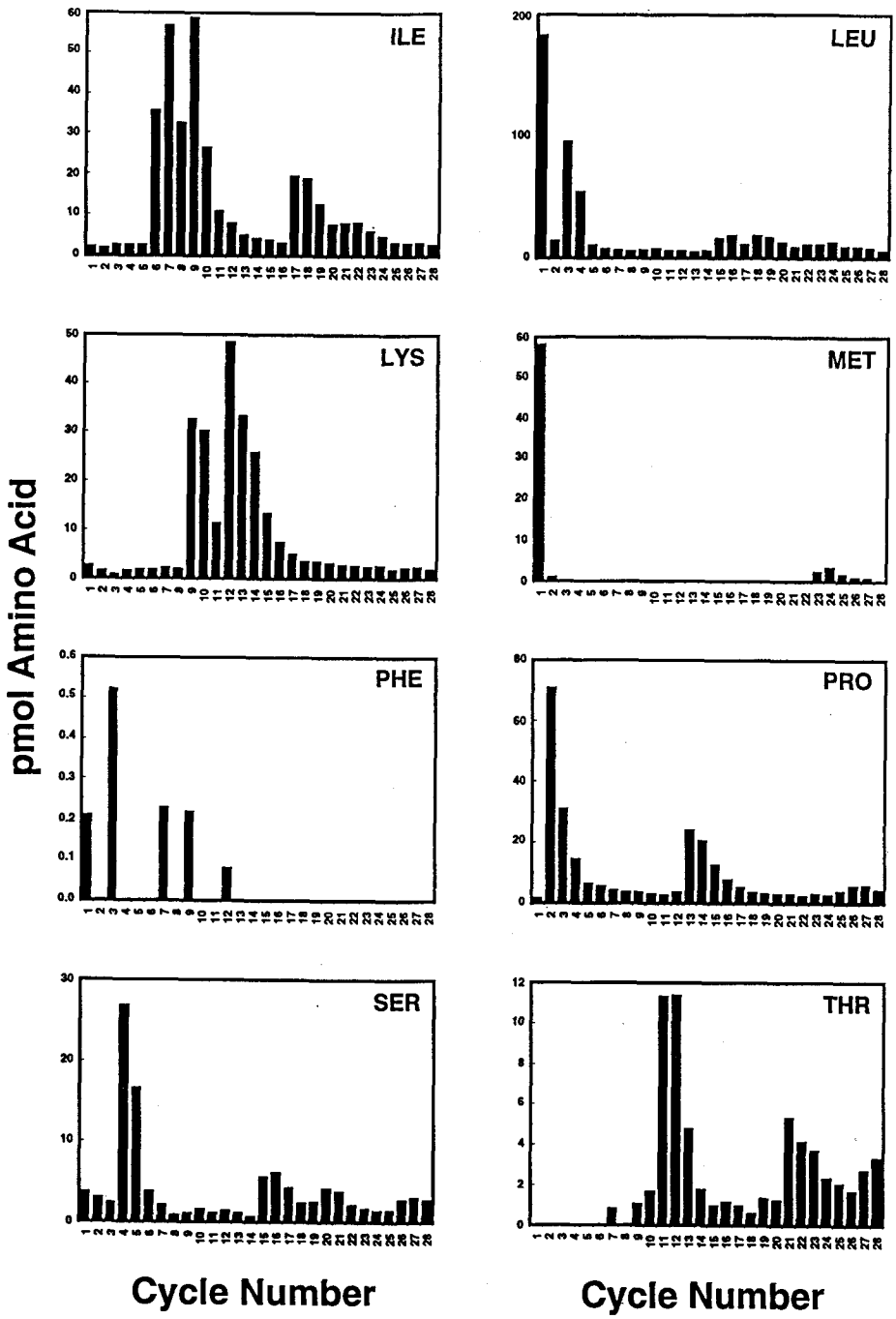

Figure 24 (continued)

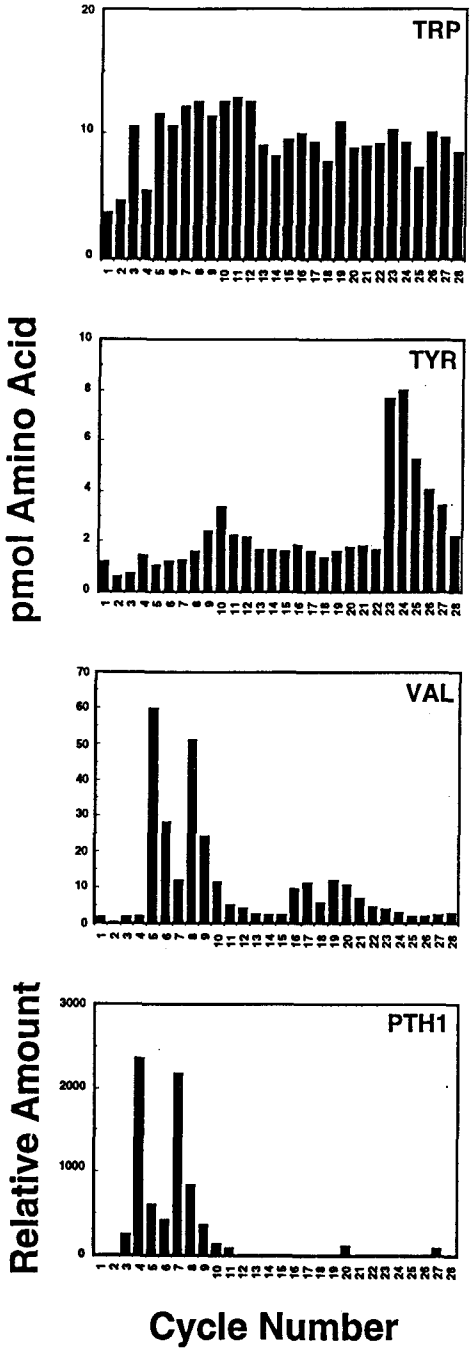

Figure 24 (continued)

Table 6

Quantitation of Gas-Phase Sequencing of the DEAE-Cellulose Purified Ugi Form II C3 Peptide

Amino Acid[a]	Cycle 1	2	3	4	5	6	7	8	9	10	11
Ala	4.0	2.1	2.8	2.7	2.5	3.4	4.2	2.8	3.1	2.9	2.5
Arg	2.7	1.4	0.8	15.6	4.0	0.1	14.5	5.6	<0.1	<0.1	0.5
Asn	687.4	480.9	204.7	86.8	48.9	24.1	10.7	6.0	4.0	2.4	33.8[b]
Asp	1.6	4.7	3.5	3.7	43.2	38.5	11.3	7.3	4.9	3.6	4.3
Glu	<0.1	<0.1	63.8[b]	71.9[b]	30.9	69.4[b]	56.4[b]	45.0	36.3	33.3	20.7
Gln	<0.1	<0.1	<0.1	<0.1	1.2	0.7	0.6	<0.1	0.6	1.1	0.7
Gly	<0.1	<0.1	<0.1	<0.1	<0.1	25.0	13.3	6.7	7.2	38.4[b]	15.9
His	<0.1	<0.1	<0.1	<0.1	<0.1	<0.1	0.1	0.5	0.2	<0.1	0.1
Ile	2.1	1.9	2.6	2.5	2.5	35.6	56.6	32.5	58.9[b]	26.4	10.9
Leu	182.4[b]	13.8	94.9	54.2	10.0	6.9	6.5	5.6	6.8	6.8	5.3
Lys	2.7	1.5	0.8	1.6	1.7	1.7	2.2	2.0	32.6	30.3	11.4
Met	58.2	1.0	0.3	0.2	<0.1	<0.1	0.1	0.1	0.3	<0.1	0.2
Phe	0.2	<0.1	0.5	<0.1	<0.1	<0.1	0.2	<0.1	0.2	<0.1	<0.1
Pro	1.7	70.7[b]	30.9	14.5	6.4	5.3	4.2	3.6	3.4	2.9	2.6
Ser	3.7	3.0	2.3	26.7	16.7	3.8	2.1	0.8	1.1	1.6	1.2
Thr	<0.1	<0.1	<0.1	<0.1	<0.1	<0.1	0.8	<0.1	1.1	1.7	11.3
Trp	3.7	4.6	10.5	5.4	11.6	10.6	12.1	12.5	11.3	12.5	12.8
Tyr	1.2	0.6	0.7	1.4	1.0	1.2	1.2	1.6	2.4	3.3	2.2
Val	1.6	0.4	1.6	2.0	59.6[b]	28.2	12.0	51.1[b]	24.4	11.4	5.0
PTH1[c]	<0.1	240.0	2354.0	597.0	422.0	2181.0	840.0	357.0	132.0	79.0	<0.1
Peptide[d]	Leu	Pro	Glu	Glu	Val	Glu	Glu	Val	Ile	Gly	Asn

Table 6 (continued)

Quantitation of Gas-Phase Sequencing of the DEAE-Cellulose Purified Ugi Form II C3 Peptide

Amino Acid[a]	Cycle 12	13	14	15	16	17	18	19	20	21	22
Ala	2.8	2.8	3.0	3.1	3.0	2.4	2.5	2.7	2.7	2.4	8.1[b]
Arg	0.2	<0.1	0.3	<0.1	<0.1	<0.1	<0.1	0.1	0.7	<0.1	<0.1
Asn	18.6	8.8	6.1	3.3	3.4	2.1	2.4	2.2	2.3	1.8	2.3
Asp	4.6	3.0	5.0	3.4	12.0[b]	9.9	8.2	6.3	5.1	3.2	1.0
Glu	12.6	7.5	20.0[b]	16.2	11.8	7.8	5.8	8.3	8.1	5.4	3.8
Gln	0.9	0.7	9.6	11.6	6.8	3.4	7.4	10.8	6.5	3.4	1.5
Gly	19.6	16.8	8.6	4.1	3.2	2.8	2.1	2.8	2.4	2.2	1.2
His	0.2	<0.1	0.6	<0.1	<0.1	0.3	0.5	<0.1	3.9[b]	3.7	3.0
Ile	7.8	5.1	4.4	3.7	3.2	19.6[b]	18.8	12.6	7.6	8.0	8.1
Leu	5.9	4.9	5.4	15.8	18.3	11.3	17.9[b]	16.7	12.5	8.9	10.9
Lys	48.5[b]	33.3	25.8	13.4	7.4	5.0	3.6	3.5	3.2	2.8	2.7
Met	0.3	<0.1	0.1	0.1	<0.1	0.2	<0.1	0.2	0.2	0.1	<0.1
Phe	0.1	<0.1	<0.1	<0.1	<0.1	<0.1	<0.1	<0.1	<0.1	<0.1	<0.1
Pro	3.6	23.8[b]	20.4	12.4	7.8	5.0	3.4	3.3	2.8	2.7	2.4
Ser	1.4	1.2	0.7	5.6[b]	6.3	4.2	2.4	2.5	4.1	3.9	2.1
Thr	11.3	4.8	1.8	1.0	1.1	0.9	0.6	1.4	1.2	5.4[b]	4.2
Trp	12.5	9.0	8.1	9.5	10.0	9.2	7.7	10.9	8.7	8.9	9.2
Tyr	2.2	1.7	1.6	1.6	1.8	1.6	1.3	1.6	1.7	1.8	1.6
Val	4.1	2.6	2.1	2.1	9.6	11.2	5.5	11.9[b]	10.6	7.1	4.5
PTH1[c]	<0.1	<0.1	<0.1	<0.1	<0.1	<0.1	<0.1	<0.1	103.0	<0.1	<0.1
Peptide[d]	Lys	Pro	Glu	Ser	Asp	Ile	Leu	Val	His	Thr	Ala

Table 6 (continued)

Quantitation of Gas-Phase Sequencing of the DEAE-Cellulose Purified Ugi Form II C3 Peptide

Amino Acid[a]	Cycle 23	24	25	26	27	28
Ala	8.2	6.8	4.6	3.7	3.8	3.0
Arg	0.1	<0.1	<0.1	<0.1	0.6	<0.1
Asn	1.9	2.6	1.8	1.6	2.8	1.7
Asp	3.2	8.9[b]	7.7	6.3	6.9	5.4[b]
Glu	3.9	3.3	6.6[b]	8.0	8.4	7.6
Gln	1.7	1.3	1.4	1.5	1.0	1.4
Gly	1.9	1.4	1.9	2.0	1.3	2.2
His	1.9	1.4	0.5	0.5	0.8	0.4
Ile	5.9	4.8	3.3	3.1	3.4	2.9
Leu	11.4	12.5	9.5	8.4	7.7	5.8
Lys	2.4	2.6	1.7	2.2	2.4	2.1
Met	2.5	3.4	1.7	1.1	0.8	0.3
Phe	<0.1	<0.1	<0.1	<0.1	<0.1	<0.1
Pro	2.8	2.6	3.9	5.3	5.7	4.2
Ser	1.7	1.5	1.4	2.8[b]	3.1	2.8
Thr	3.7	2.3	2.1	1.7	2.7[b]	3.3
Trp	10.3	9.2	7.3	10	9.6	8.4
Tyr	7.7[b]	8.0	5.3	4.0	3.4	2.2
Val	3.9	3.2	2.0	1.9	2.4	2.7
PTH1[c]	<0.1	<0.1	<0.1	<0.1	88.0	<0.1
Peptide[d]	Tyr	Asp	Glu	Ser	Thr	Asp

[a] The yield of PTH-derivatized amino acids detected in each cycle are indicated in picomols. Cytosine residues are not detected.
[b] Denotes the amino acid residue in each cycle expected to correspond to the deduced amino acid sequence of Ugi peptide C3.
[c] The yield of PTH1 detected in each cycle is indicated in arbitrary absorbance units (AAU) and not picomols because an internal amino acid standard for PTH1 is unavailable for quantitative purposes.
[d] The amino acid sequence for the C3 peptide is elucidated from the deduced amino acid sequence of the published *ugi* gene nucleotide sequence (292).

Figure 25. Amino acid sequence determination of the Ugi form II C3 peptide. A histogram shows the relative amount of a unique PTH-derivative detected during each cycle of Edman degredation of Ugi form II C3 peptide. This novel derivative appeared with a retention time of 15.54 ± 0.05 min between standards identified as Arg (~15.17 min) and Tyr (~16.13 min). The amino acid sequence determined for the C3 peptide that overlaps with the A2 peptide is indicated.

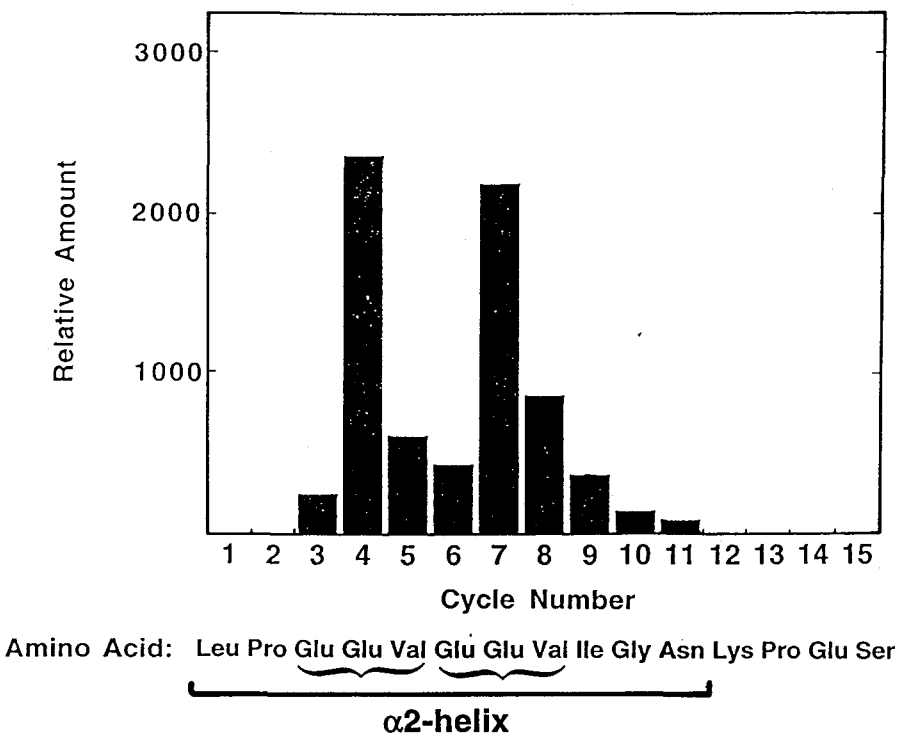
3000
2000
1000
Relative Amount
1 2 3 4 5 6 7 8 9 10 11 12 13 14 15
Cycle Number
Amino Acid: Leu Pro Glu Glu Val Glu Glu Val Ile Gly Asn Lys Pro Glu Ser
α2-helix

Figure 25

Figure 26. Quantitation of unique PTH-derivatives detected by amino acid sequenceing of peptide C3 from Ugi forms II-IV. Amino acid sequencing was conducted using an Applied Biosystems model 475A gas phase sequencer as described under "Experimental Procedures". The relative amount of unique PTH-derivatives (PTH1 and PTH2) detected for peptide C3 from Ugi forms II-IV are plotted for the first 23 cycles. PTH1 appeared with a retention time of 15.54 ± 0.05 min between standards identified as Arg (~15.17 min) and Tyr (~16.13 min). PTH2 appeared with a retention time of 19.02 ± 0.02 min between standards identified as Tyr (~16.13 min) and Pro (~20.08 min).

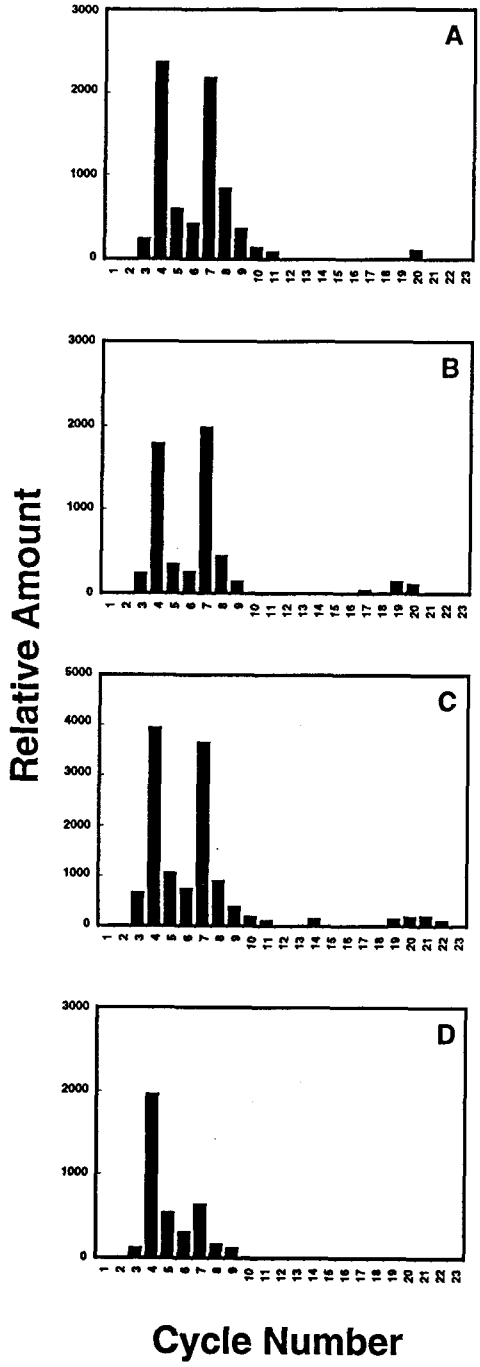

Figure 26

proportions. The preferential modification of 2 out of 19 carboxyl groups in Ugi may be facilitated by the closely spaced pairing of Glu residues (Glu-27, Glu-28 and Glu-30, Glu-31), the repeating Glu-Glu-Val sequence, and the solvent-accessible α2-helix of Ugi (12). Selective carbodiimide-mediated modification has been previously observed when acidic amino acids are clustered within a polypeptide sequence, creating a negatively charged local environment (33, 83, 160). A secondary site of modification was detected on peptide A6/7M_1 (residues 61-84) but represented only ~18 % of the total Ugi form II adducts. Ugi form III was shown to contain two acyl-glycine ethyl ester adducts, and 65-70 % of these protein molecules had adducts on both Glu-28 and Glu-31 sites. The remaining molecules of Ugi form III apparently possessed a single adduct on both peptide A2 and A6/7, since the amount of peptide A2M_1 (25 %) nearly equaled that of A6/7M_1 (37 %). The type, location, and distribution of each adduct on Ugi forms IV and V became more difficult to define due to the heterogeneity of modification. The second PTH-derivative associated with form IV peptide C3 was suspected to represent an *N*-acylurea adduct formed by an internal rearrangement of acylisourea (272). This alternative EDC-dependent modification is represented in Figure 27. Previous studies have shown that if the concentration of nucleophile is sufficiently high, the kinetics of this internal rearrangement can be reduced relative to nucleophilic attack of the O-acylisourea-activated carboxyl group (104). These results indicated that the predominant modification resulted in the formation of the terminal acyl-glycine ethyl ester reaction product.

The results presented in this investigation provide evidence that Glu-28 and Glu-31, located in the α2-helix of Ugi, play an important role in promoting stable Ung•Ugi complex formation. Involvement of these two residues was implied, since 82 and 90 % of Ugi forms II and III contained at least one adduction in the α2-helix sequence. Thus, little room is left to explain the 42 and 67 % reduction in Ugi activity by another modified site. However, the possible involvement of minor adducts in influencing the

Figure 27. Scheme for O-acylisourea adduction of Ugi by EDC/GEE modification. Activation of a protonated carboxylic acid group by EDC forms an O-acylisourea adduct which is subject to nucleophilic attack by glycine ethyl ester (GEE) to form the primary acyl-glycine ethyl ester adduct described in Figure 2. A secondary modification occurs by an internal rearrangement of the O-acylisourea adduct to form an N-acylurea adduct. Kinetic studies on carbodiimide-carboxyl-nucleophile systems have shown that formation of the N-acylurea adduct is slow as compared to nucleophilic attack if the nucleophile (GEE) concentration is sufficiently high (104). The N-acylurea adduct is positively charged and adds 156 daltons to the overall molecular weight of the Ugi protein.

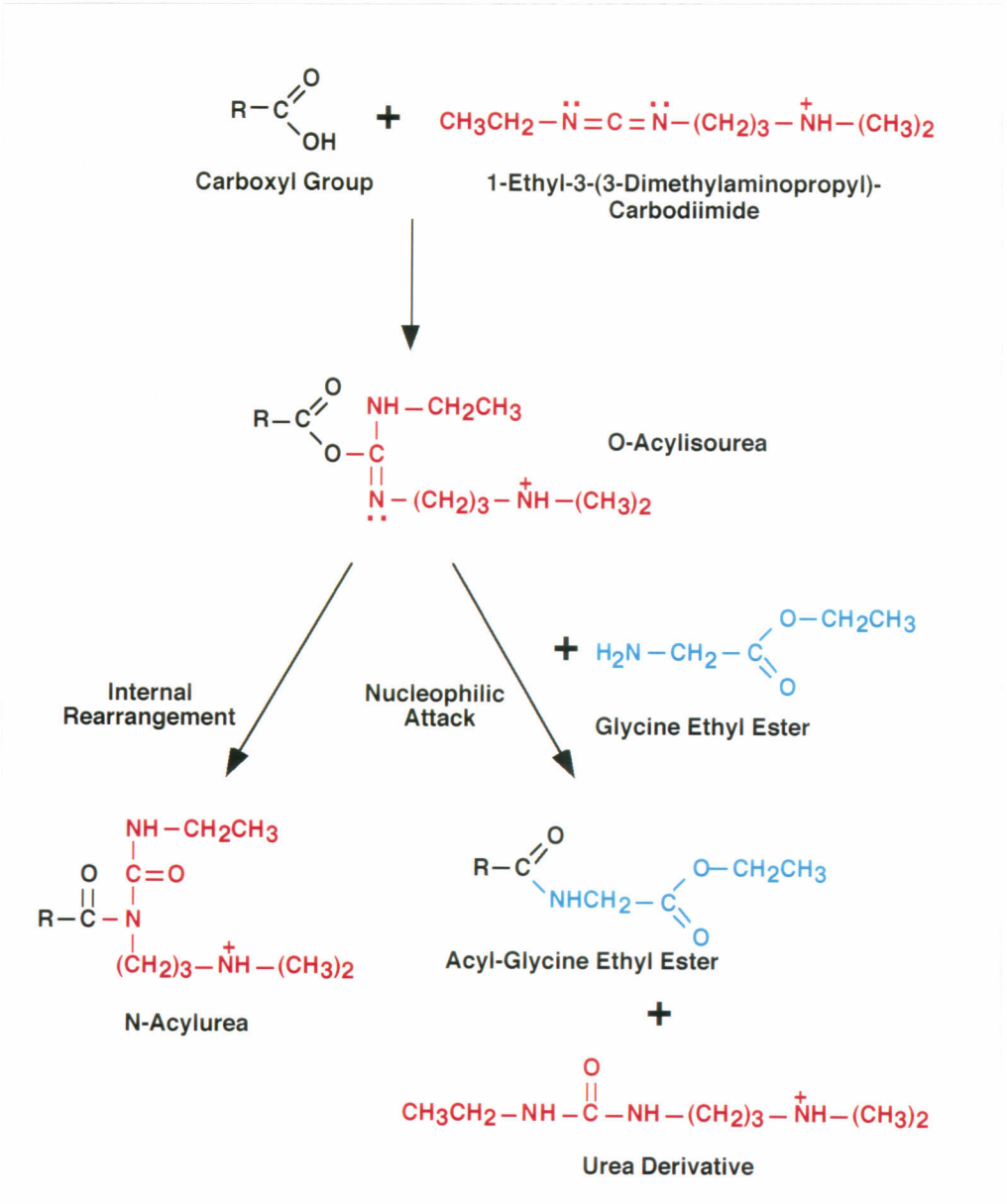
Carboxyl Group
1-Ethyl-3-(3-Dimethylaminopropyl)-Carbodiimide
O-Acylisourea
Internal Rearrangement
Nucleophilic Attack
Glycine Ethyl Ester
N-Acylurea
Acyl-Glycine Ethyl Ester
Urea Derivative

Figure 27

stability of some complexes cannot be discounted. It was postulated that both Glu-28 and Glu-31 contribute to the formation of a stable Ung•Ugi complex. This proposal is reinforced by recent x-ray crystallographic studies of the human and herpes simplex virus type-1 uracil-DNA glycosylase•Ugi complexes (167, 237). Both structures reveal that residues of the Ugi α2-helix and adjoining β1 strand dominate the interface with the enzyme and provide sites of interaction between the two proteins. The hydrophobic face of the α2-helix in conjunction with the β-sheet forms a hydrophobic pocket that surrounds the conserved Leu-272 active site loop of human uracil-DNA glycosylase (167). This pocket appears to be stabilized by Ugi Glu-28 and Glu-31 contacts with conserved residues that are shared between human and *E. coli* Ung (167, 196). These interactions have been proposed to involve the Ugi Glu-28 carboxylate forming a pair of hydrogen bonds with the Ser-247 (Ser-166 of *E. coli* Ung) backbone amide and side chain O-γ (167). In addition, Glu-28 O-ε1 also forms water-mediated hydrogen bonds with the human His-268 backbone amide and Ser-273 O-γ, corresponding to *E. coli* Ung His-187 and Ser-192, respectively (167). By the same token, Ugi Glu-31 appears to be capable of forming a salt bridge with Arg-276 of human uracil-DNA glycosylase (Arg-195 of *E. coli* Ung). Thus, EDC/GEE modification of either Glu-28 or Glu-31 might be expected to disrupt important protein/protein interactions and destabilize the complex as observed in this investigation.

Several lines of evidence suggest that the interactions between Ugi Glu-28 and Glu-31 influence the formation of a tight Ung•Ugi complex without dramatically impeding the association of the initial pre-complex. Steady-state kinetic experiments that monitored the binding of Ugi forms I-V to F-Ung demonstrated that neither modified nor unmodified Ugi freely dissociated from Ung once the final complex was achieved. However, the structures of these complexes differed since binding of Ugi forms II-V resulted

in reduced levels of maximal fluorescence quench. These observations suggest that the conjugated acyl-glycine ethyl ester adducts of Glu-28 and/or Glu-31 interact directly with F-Ung fluorophores or perturb the local structure and environment of the final F-Ung•Ugi complex. It was observed from competition binding experiments that unmodified Ugi preferably formed a complex over the modified protein species. Furthermore, unmodified Ugi was observed to replace modified Ugi (forms II-V) from a preformed complex. These properties of Ugi forms II-V were revealing, since unmodified Ugi maintains an irreversible Ung•Ugi complex (17). Thus, Ugi forms II-V appeared to be defective in achieving an irreversible association with Ung. Observations indicating that poly(U) promoted dissociation of modified Ugi from complex and that preformed Ung•Ugi (form II-V) complexes displayed uracil-DNA glycosylase activity also supported this interpretation.

The results provide new insight concerning the structural and functional relationship of the Ugi α2-helix in complex formation. Previously, stopped-flow kinetic experiments indicated that the Ung/Ugi association involved a two-step mechanism composed of a docking and locking reaction. The docking reaction was shown to involve a rapid pre-equilibrium in which Ung and Ugi associated to form a reversible complex (17). It is likely that the transition between the docking and locking steps involves an isomerization reaction. This could be achieved by a conformational change in Ung, Ugi, or both proteins. A comparison of the crystal structures of free human and herpes-simplex virus type-1 uracil-DNA glycosylase with each respective enzyme in complex with Ugi indicates that only minor changes occur within the enzyme tertiary structure upon complex formation (168, 235). A similar comparison between the NMR tertiary structure of unbound Ugi with the crystal structure of Ugi complexed with either human or herpes simplex virus type-1 enzyme reveals that significant structural changes occur in Ugi (12, 167, 237). Direct evidence that Ugi undergoes a conformational upon binding to Ung was provided by NMR

results (12). The heteronuclear multiple quantum correlation spectroscopy spectrum of free [^{15}N]Ugi compared with that of the Ung•[^{15}N]Ugi complex clearly indicates that many Ugi residues undergo a chemical shift as a consequence of forming the "locked" complex. One of the most dramatic rearrangements appears to involve the location of the Ugi α2-helix. It is speculated that movement of the α2-helix, at least in part, transforms the reversible Ung•Ugi complex to an essentially irreversible locked state. This interpretation is consistent with the observation that Ugi forms II-V were capable of successfully conducting the docking but not the locking interaction.

Conformational change in the Ugi α2-helix provides an attractive explanation that unifies the biochemical, kinetic, and structural data. However, several issues remain to be elucidated regarding the role of Glu-28, Glu-31, and other residues in the Ung/Ugi interaction. First, what is the relative involvement of Glu-28 and Glu-31 in facilitating the locking reaction? Second, does charge neutralization of these carboxyl groups alone bring about inactivation of Ugi, or does EDC/GEE modification sterically hinder α2-helix positioning? Third, what other amino acids play a role in the docking and locking interaction? In a related study, site directed mutagenesis of Glu-28 and Glu-31 in Ugi was performed to assess the individual contribution of these and other negatively charged amino acids in mediating the docking and locking interactions with *E. coli* Ung (152). The specific activity of Ugi mutants E28L and E31L were 88 % and 53 % relative to that of wild-type Ugi and were capable of associating with Ung and forming an apparently stable Ung•Ugi complex (152). However, Ugi located within a preformed Ung•Ugi complex composed of Ugi mutant E28L was reversible when challenged with wild-type [^{35}S]Ugi (~ 50 % exchange) whereas Ung complexed with Ugi E31L, for the most part, maintained an irreversible complex (~ 3.4 % exchange) (152). When taken together, these observations argue that Glu-28 was predominantly responsible for stabilizing an

irreversible Ung•Ugi complex while Glu-31 contributed only a minor role in the locking reaction. Thus, charge neutralization of Glu-28 apparently played a significant role in destabilizing the Ung•Ugi complex although potential steric hindrance by EDC/GEE-modified Glu-28 and/or Glu-31 cannot be ruled out. Three other mutant Ugi proteins (E20I, E30L, and D61G) also varied in their individual ability to inhibit Ung activity but were unaltered in their ability to form an irreversible complex (152). Together, these studies suggest that multiple Ugi amino acids are involved in mediating the Ung/Ugi docking and locking interaction but that Glu-28 plays an essential role in facilitating the "locking" reaction.

4. FIDELITY, MUTATIONAL SPECIFICITY, AND REPAIR PATCH SIZE OF URACIL-INITIATED BASE EXCISION REPAIR SYNTHESIS IN HUMAN GLIOBLASTOMA AND COLON ADENOCARCINOMA CELL EXTRACTS

Although the molecular mechanism of human uracil-initiated BER is understood in some detail, the fidelity and error specificity of DNA repair synthesis has not been adequately addressed. Thus, an M13mp2 *lacZα* DNA-based reversion assay was developed for detecting base substitution errors produced at a site-specific uracil residue during BER in human U251 and LoVo whole cell extracts. Experiments were conducted to establish that uracil-DNA repair occurred via the BER pathway. The location of DNA repair synthesis was examined to determine if dNMP incorporation was localized to the uracil target and to determine if synthesis occurred on the (-)-strand, (+)-strand, or both DNA strands. Additional experiments utilized the Ugi protein to inhibit uracil-DNA repair initiated by Ugi-sensitive uracil-DNA glycosylase(s) and to study the Ugi-insensitive uracil-DNA repair pathway. To determine if mismatch repair in human whole cell extracts might influence uracil-DNA repair, an identical set of experiments was conducted with LoVo whole cell extracts that are defective in the hMSH2 mismatch repair protein. Experiments in this chapter also evaluated the size of the repair patch produced during DNA repair synthesis associated with the Ugi-sensitive and -insensitive BER. In addition, the specific involvement of aphidicolin-sensitive and -insensitive DNA polymerases that participated in DNA repair synthesis was investigated.

The fidelity of BER synthesis at a defined uracil residue located in the *E. coli lacZα* gene of heteroduplex M13mp2 DNA was measured, and the mutation spectrum was elucidated for uracil-initiated BER in human U251 and LoVo whole cell extracts. Comparative analysis between these two cell types identified nearly identical mutation frequencies and mutation spectrums. These results are indicative of nucleotide misincorporation

events associated with uracil-initiated BER in human whole cell extracts and provide a measurement of DNA repair synthesis fidelity.

4.1 Results

4.1.1 Uracil-Initiated Base Excision DNA Repair Assay

An M13mp2 *lacZα* DNA-based reversion assay was developed to investigate the fidelity of DNA synthesis associated with uracil-initiated DNA repair in human whole cell extracts as illustrated in Figure 28. Site-directed mutagenesis was used to construct the base excision repair DNA substrate (M13mp2op14 DNA) as described under "Experimental Procedures". Substrate modifications included incorporation of a transcriptional stop codon in the *E. coli lacZα* gene of M13mp2 DNA and a downstream silent mutation that generated a unique *Sma*I restriction endonuclease site. By introducing an opal codon (TGA) in place of an arginine codon (CGT) for amino acid 14 of the *lacZα* gene product, *lacZα* was rendered inactive and incapable of α-complementation. DNA sequence analysis of isolated M13mp2op14 DNA verified the introduction of the opal codon (Asp14 CGT → TGA opal 14) at nucleotide positions 78-80 of the *lacZα* gene and also confirmed the presence of the silent point-mutation (Pro20 CCT → CCG Pro20) at nucleotide position 98 to create the novel *Sma*I restriction site (Figure 29). Circular heteroduplex M13mp2op14 DNA with a site-specific uracil at nucleotide position 78 of the (-) strand was then constructed using T4 DNA polymerase and T4 DNA ligase in a primer extension reaction and Form I DNA was purified. This DNA substrate contained a U•T base mispair at the first nucleotide of the opal codon and served as the uracil-target for repair. The uracil residue was strategically located so that faithful and unfaithful uracil-initiated DNA repair synthesis in human whole cell extracts

Figure 28. Scheme for measuring base excision DNA repair synthesis fidelity in human cell extracts. (A) M13mp2op14 DNA containing a site-specific U•T mispair at position 78 of the *lacZα* gene was constructed as described under "Experimental Procedures". Nucleotide positions 48-108 of the *lacZα* gene are depicted with position 1 corresponding to the first *lacZα* transcribed base. The uracil target for human uracil-DNA glycosylase (UDG, *vertical arrow*) and direction of DNA synthesis (*horizontal arrow*) during base excision repair are indicated. *Eco*RI and *Sma*I endonuclease recognition sequences are underlined and incision sites are indicated by *vertical arrows*. (B) Standard base excision repair reaction mixtures containing 10 μg/ml of M13mp2op14 DNA, 2 mg/ml of human whole cell extract protein, 20 μM each of dATP, dTTP, dGTP, and dCTP and other components were prepared as described under "Experimental Procedures". DNA reaction products were isolated at various times after incubation at 30°C and analyzed by 0.8% agarose gel electrophoresis. Conversion of uracil-containing Form I DNA to Form II DNA and then to Form I DNA that was resistant to cleavage by the combined treatment of *E. coli* Ung and Endo IV was indicative of DNA repair. Ung/Endo IV resistant Form I DNA was purified from the agarose gel and used for mutational analysis. *E. coli* NR9162 cells were then transfected with the recovered DNA using a Gene Pulser electroporation system. Transfected cells were diluted into SOC medium, mixed with *E. coli* CSH50 (indicator strain) and plated on M9 plates containing 0.4 mM IPTG and 1 mg/ml X-Gal as described under "Experimental Procedures". Colorless and blue (dark and light blue) plaques were counted. (C) Possible nucleotide incorporations at the uracil target site during BER. Faithful incorporation of dAMP to replace the uracil residue at position 78 in the (-) strand results in the production of an opal codon. Whereas, incorporation of dCMP, dGMP or dTMP restores a wild-type phenotype and allows α-complementation.

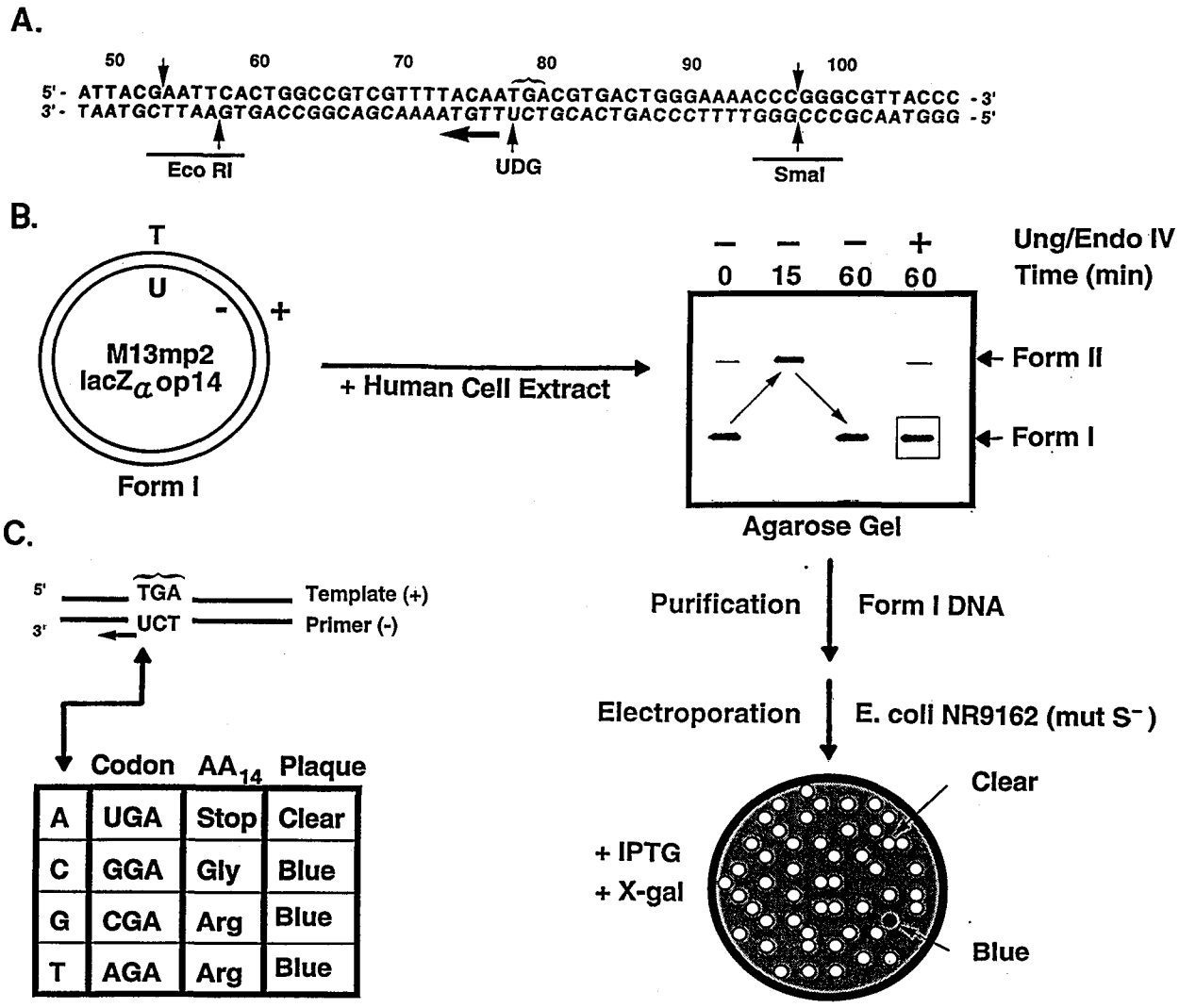
A.
50
60
70
80
90
100
5'- ATTACGAATTCACTGGCCGTCGTTTTACAATGACGTGACTGGGAAAACCCGGGCGTTACCC -3'
3'- TAATGCTTAAGTGACCGGCAGCAAAATGTTACTGCACTGACCCTTTTGGGCCCGCAATGGG -5'
Eco RI
UDG
SmaI
B.
T
U
-
+
M13mp2
lacZ$_\alpha$op14
Form I
+ Human Cell Extract
– – – +
Ung/Endo IV
0 15 60 60
Time (min)
Form II
Form I
Agarose Gel
C.
5'
3'
TGA
UCT
Template (+)
Primer (-)
Codon AA$_{14}$ Plaque
A UGA Stop Clear
C GGA Gly Blue
G CGA Arg Blue
T AGA Arg Blue
Purification
Form I DNA
Electroporation
E. coli NR9162 (mut S$^-$)
+ IPTG
+ X-gal
Clear
Blue

Figure 28

Figure 29. DNA sequence of M13mp2op14 DNA. An isolated clear plaque was used to procure single-stranded M13mp2op14 DNA and the DNA sequence was determined using an Applied Biosystems Model 373A DNA sequencer as described under "Experimental Procedures". Mutations were introduced into the nucleotide sequence of the *lacZ*α gene and resulted in the replacement of an opal codon (TGA) for an arginine codon (CGT) at codon position 14 (opal, *brackets*) and the introduction of a silent mutation to create a unique *Sma*I restriction endonuclease site (SmaI, *brackets*). The opal codon and the *Sma*I restriction site are labeled accordingly. The sequence depicted is that of the (-) DNA strand determined in the 5' to 3' direction. Unidentified bases are denoted by an 'N' in the DNA sequence.

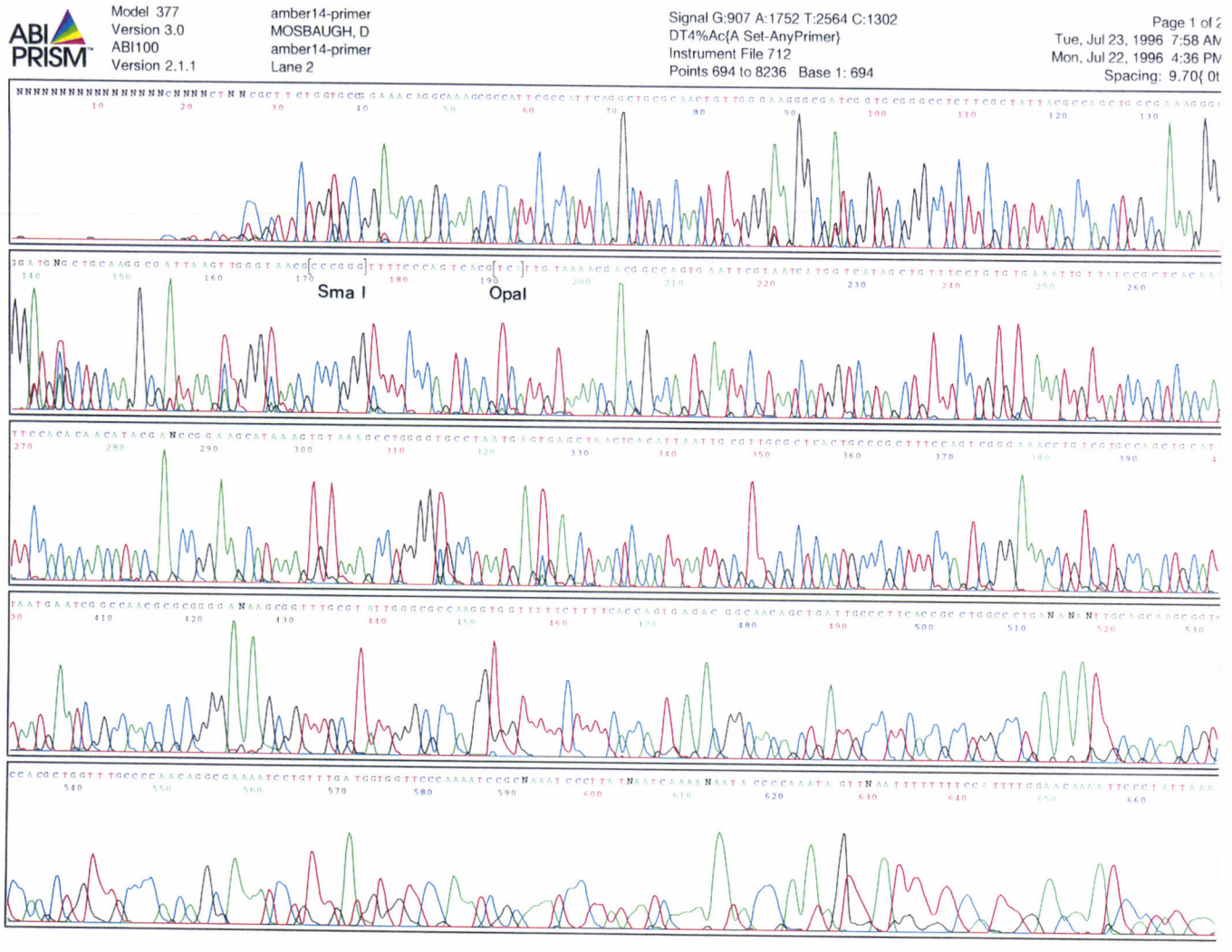
ABI PRISM
Model 377
Version 3.0
ABI100
Version 2.1.1
amber14-primer
MOSBAUGH, D
amber14-primer
Lane 2
Signal G:907 A:1752 T:2564 C:1302
DT4%Ac{A Set-AnyPrimer}
Instrument File 712
Points 694 to 8236 Base 1: 694
Page 1 of 2
Tue, Jul 23, 1996 7:58 AM
Mon, Jul 22, 1996 4:36 PM
Spacing: 9.70{ 0t
Sma I
Opal

Figure 29

could be distinguished based on reversion of the opal codon. If faithful DNA synthesis occurred with dAMP incorporation opposite thymine at nucleotide position 78, the opal codon sequence would be restored to the (-) strand (Figure 28C). Alternatively, if unfaithful DNA synthesis incorporated dGMP or dTMP, a wild type arginine codon would be generated; whereas, dCMP incorporation would introduce a glycine codon into the (-) strand. In order to preserve mispairs introduced into repaired M13mp2op14 DNA by inaccurate DNA synthesis, the substrate was transfected into *E. coli* NR9162 (*mut*S), which is methyl-directed mismatch repair defective. Transfection of *E. coli* NR9162 (*mut*S) cells with faithfully repaired M13mp2op14 DNA was expected to produce a colorless plaque on host indicator plates due to the inability of the *lacZ*α gene product to perform α-complementation (Figure 30). In contrast, unfaithful incorporation of a noncomplementary nucleotide in place of the uracil residue restored α-complementation and produced mixed burst blue plaques (colorless plus blue). These phenotypes were independently verified by transfecting *E. coli* JM109 with M13mp2 DNA containing each of the four possible nucleotide substitutions at positions 78 and plating on host indicator plates (Figure 31). As expected, M13mp2 DNA containing a *lacZ*α opal (TGA) and arginine (CGA, AGA) codon 14 produced colorless and dark blue plaques, respectively (Figure 31A-C); however, a glycine (GGA) codon was found to produce a light blue plaque (Figure 31D). These results validated the assay for detecting misincorporation events introduced at the target site during uracil-initiated DNA repair synthesis.

4.1.2 Preparation and Characterization of Uracil-Excision Repair DNA Substrates

In order to optimize primer extension reaction conditions for producing the Form I DNA uracil-excision repair substrates, 3.3 pmol of M13mp2op14 DNA was annealed to a three-fold molar excess of 5'-end phosphorylated U-23-mer and incubated with T4 DNA polymerase at ratios of

Figure 30. Detection of base excision DNA repair synthesis fidelity by *lacZα* complementation. A standard BER reaction mixture containing 10 μg/ml M13mp2op14 (U•T) DNA and 2 mg/ml human U251 whole cell extract protein was prepared, DNA was isolated, and repaired Form I DNA was purified as described under "Experimental Procedures". Competent *E. coli* NR9162 cells transfected with repaired Form I DNA were diluted into SOC media, mixed with mid-log *E. coli* CSH50 cells and plated on M9 plates containing 0.4 mM IPTG and 1 mg/ml X-Gal. Typical plating conditions were adjusted to yield approximately 1,000 to 3,000 plaque forming units (pfu) per plate and plaques were scored as either colorless or blue.

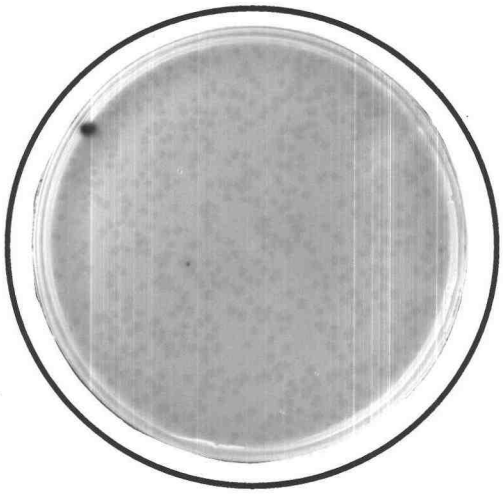

Figure 30

Figure 31. Plaque phenotype color produced by M13mp2op14 DNA and revertants. The four possible nucleotide incorporations at the uracil target site during BER in U251 whole cell extracts were analyzed for plaque phenotype color upon transfection and plating of *E. coli* NR9162 cells as described under "Experimental Procedures". M13mp2op14 DNA containing an opal codon (TGA) (plate A) produced colorless plaques while reversion of the opal codon to an arginine codon (CGA and AGA) (plates B and C, respectively) or a glycine codon (GGA) (plate D) produced dark blue or light blue plaques, respectively, and are represented accordingly. The single-base substitution generated by the original misincorporated nucleotide has been underlined for M13mp2op14 revertants.

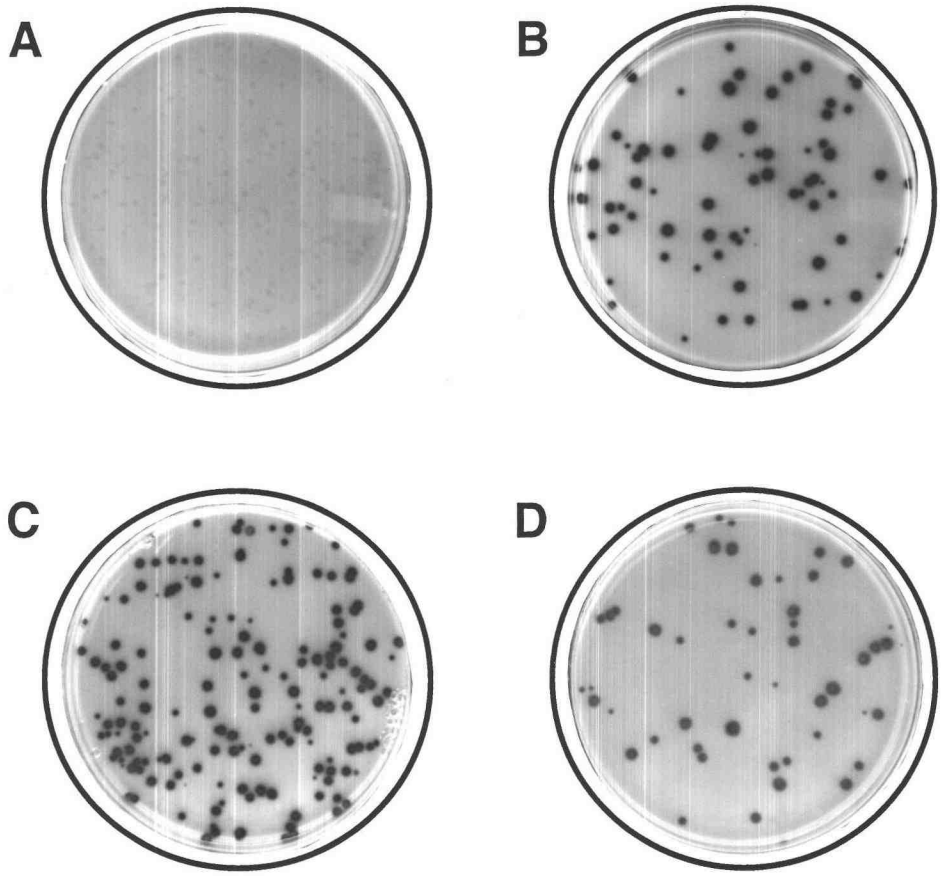

Figure 31

8:1, 2:1. 0.5:1, and 0.125:1 (polymerase unit to pmol primed template). Following DNA synthesis reactions, the reaction products were analyzed by agarose gel electrophoresis (Figure 32, lanes 3-6, respectively). As a control, 3.3 pmol of heteroduplex U-23-mer/M13mp2op14 DNA was included to indicate the position of the unextended primer/template DNA (lane 2). The addition of T4 DNA polymerase and T4 DNA ligase resulted in the extension of the primer to yield various ratios of covalently closed circular DNA (Form I), nicked circular DNA (Form II), and linearized DNA (Form III) products (lanes 3-6). Undefined reaction products accumulated at ratios of 0.5:1 and 0.125:1 (lanes 5 and 6) and may have resulted from incomplete primer extension DNA synthesis around the template. However, optimal production of Form I DNA consistently occurred at a ratio of 2:1 (lane 4) as determined by ethidium bromide staining intensity and this ratio was applied to preparative primer extension reaction mixtures in order to generate consummate amounts of Form I DNA. Similar results were also obtained with M13mp2op14 DNA annealed to 5'-end phosphorylated A-23-mer (data not shown).

To separate Form I DNA from the Form II and III DNA by-products, the terminated reaction mixture was subjected to ethidium bromide-cesium chloride gradient centrifugation. Form I DNA was purified as described under "Experimental Procedures". The purity of isolated Form I DNA was assessed by agarose gel electrophoresis (Figure 33, lane 4) and was found to contain almost exclusively Form I DNA (≥ 95 %). Samples of the heteroduplex U-23-mer/M13mp2op14 DNA primer extension reaction substrate (lane 2) and DNA reaction products from the primer extension reaction (lane 3) were analyzed for comparative purposes. Experiments were then conducted to determine the susceptibility of the uracil-containing DNA substrate to treatment with *E. coli* uracil-DNA glycosylase and endonuclease IV (Ung/Endo IV) and to treatment with the restriction endonucleases, *Eco*RI and *Sma*I (Figure 34). Isolated Form I DNA (200 ng) was treated with excess *E. coli* Ung and Endo IV (lane 3), 10 units of *Eco*RI (lane 4), or 10 units of *Sma*I

Figure 32. Effect of T4 DNA polymerase concentration on the efficiency of the primer extension reaction. Pilot primer extension reaction mixtures (50 µl) containing 3.3 pmol of M13mp2op14 DNA annealed to 5'-end phosphorylated U-23-mer, 500 µM each of dATP, dTTP, dCTP, and dGTP, and various amounts of T4 DNA polymerase were prepared as described under "Experimental Procedures". A 100-fold unit excess of T4 DNA ligase over T4 DNA polymerase was included in each reaction. After incubation for 4 h at 37°C and termination by adjustment to 15 mM EDTA, samples (2 µl, ~275 ng DNA) from reactions containing 26.4, 6.6, 1.7, and 0.4 units of T4 DNA polymerase (lanes 3-6, respectively) were analyzed by 0.8% agarose gel electrophoresis. As controls, untreated M13mp2op14 DNA annealed to U-23-mer (~150 ng) and a sample containing 2.5 µg of a 1-kb ladder (Gibco BRL) were included as reference standards (lanes 2 and 1, respectively). The location of ethidium bromide stained Form I, II, and III DNA bands and the primed template are indicated by *arrows*.

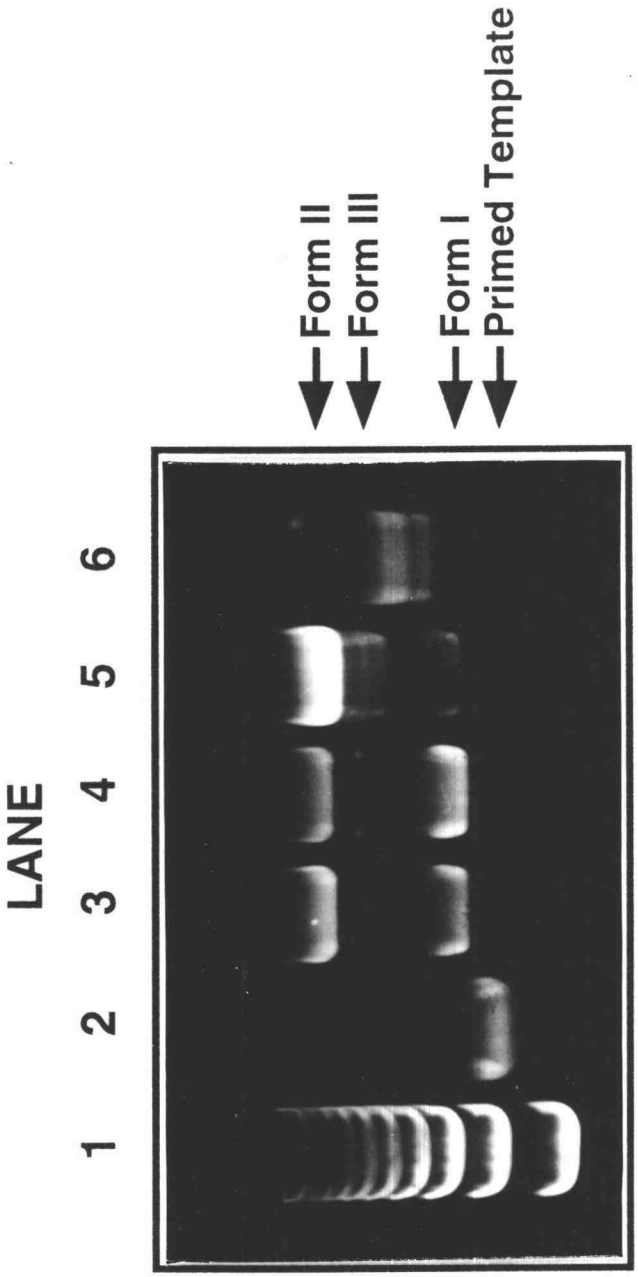

Figure 32

Figure 33. Analysis of Form I DNA isolated by ethidium bromide/cesium chloride gradient centrifugation. A primer extension reaction (3030 µl) containing 200 pmol of M13mp2op14 DNA annealed to 5'-end phosphorylated U-23-mer, 500 µM of each dNTP, 400 units of T4 DNA polymerase and 40,000 units of T4 DNA ligase was performed and Form I DNA was isolated by ethidium bromide-cesium chloride gradient centrifugation as described under "Experimental Procedures". Samples of the terminated primer extension reaction mixture (~275 ng) and ethidium bromide-cesium chloride purified Form I DNA (~100 ng) were analyzed by 0.8% agarose gel electrophoresis (lanes 3 and 4, respectively). As controls, untreated M13mp2op14 DNA annealed to U-23-mer (~150 ng) and a sample containing 2.5 µg of a 1-kb ladder (Gibco BRL) were included as reference standards (lanes 2 and 1, respectively). The location of ethidium bromide-stained Form I and II DNA bands and the primed template are indicated by *arrows*.

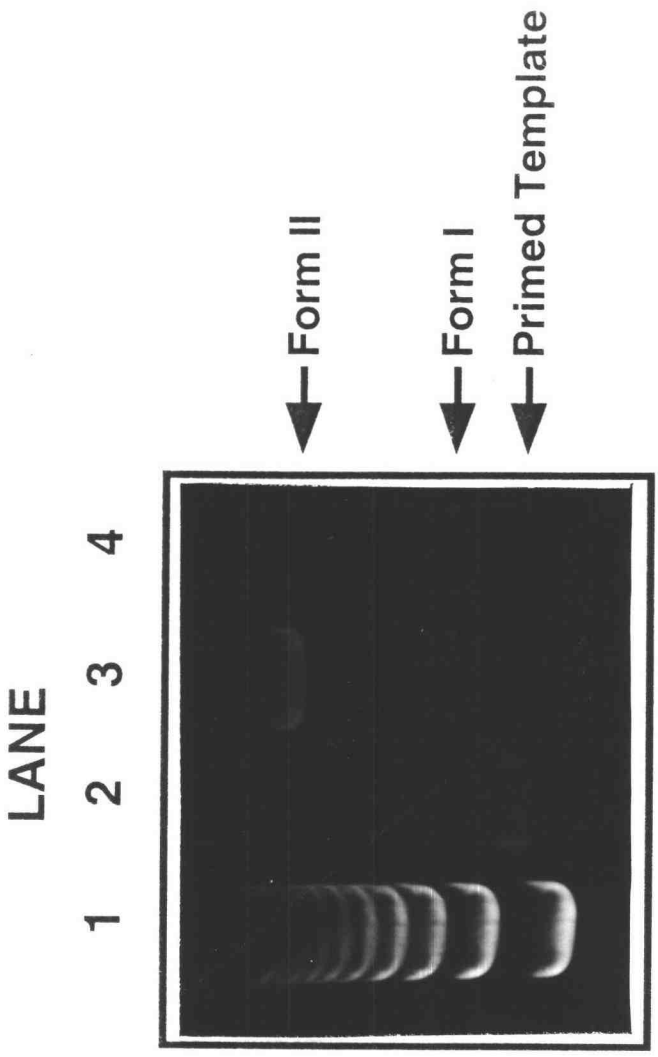

Figure 33

Figure 34. *Eco*RI and *Sma*I restriction site analysis of Form I M13mp2op14 DNA. Samples (10 µl) containing 200 ng of M13mp2op14 (U•T) Form I DNA were digested with 10 units of *Eco*RI (lane 4) or 10 units of *Sma*I (lane 5) for 1 h at 37°C and aliquots (2.5 µl, 50 ng) were analyzed by 0.8% agarose gel electrophoresis. As controls, samples (50 ng) of untreated Form I DNA and Form I DNA treated with *E. coli* Ung and Endo IV (lanes 2 and 3, respectively) and 2.5 µg of a 1-kb ladder (NEB) (lane 1) were included as reference standards. The location of ethidium bromide-stained Form I, II, and III DNA bands are indicated by *arrows*.

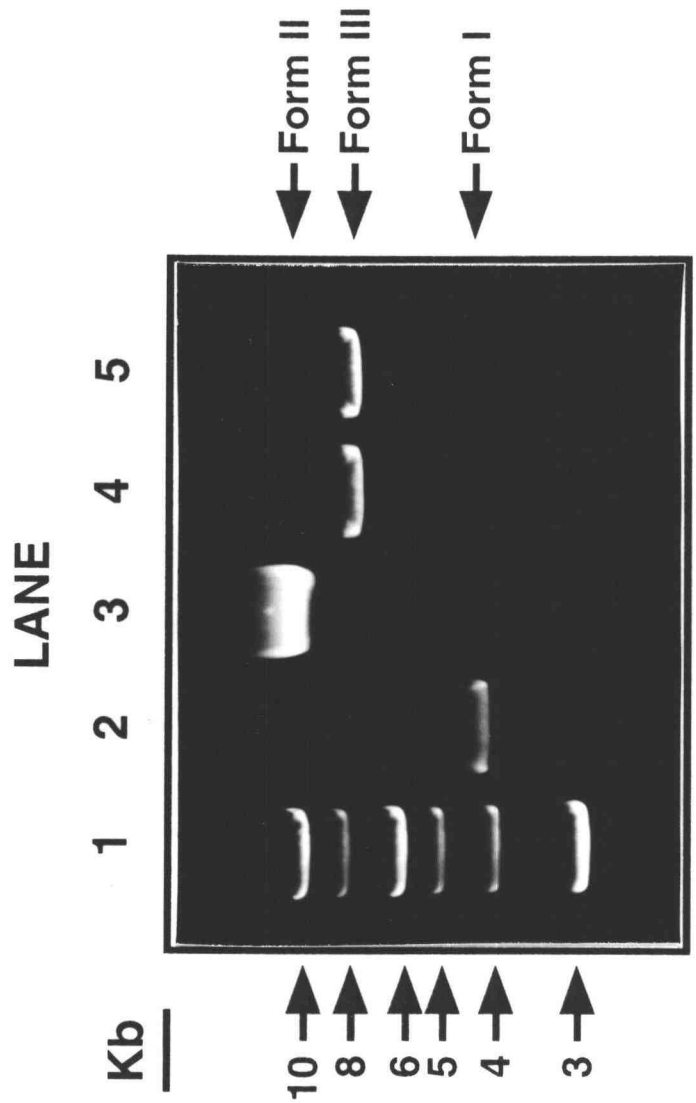

Figure 34

(lane 5) and reaction products were separated by agarose gel electrophoresis. Mock-treated Form I DNA (lane 2) was analyzed to indicate the position of the unreacted DNA substrate. As expected, removal of the site-specific uracil residue by Ung followed by apyrimidinic site incision by Endo IV converted the Form I DNA substrate into Form II DNA. No detectable Form I DNA was observed which verified that the substrate was completely susceptible to the Ung/Endo IV treatment. Individual restriction digestion reactions of Form I DNA with *Eco*RI and *Sma*I generated a single linearized DNA reaction product (Form III DNA) with an electrophoretic mobility that was roughly equidistant between the 8 kb and 6 kb bands of the DNA ladder (lane 1). This was consistent with the expected location of a linearized M13mp2op14 DNA of 7,196 bp. No other linear DNA fragments were detected. These results indicated that both restriction sites were unique and provided corroborating evidence for the introduction of the new *Sma*I restriction site by site-directed mutagenesis.

4.1.3 Detection of Uracil-DNA Repair in Human Glioblastoma U251 Whole Cell Extracts

Initial experiments were conducted using M13mp2op14 DNA to detect uracil-DNA repair in human U251 whole cell extracts. Form I DNA was mixed with whole cell extract protein, incubated for various times (0, 15, 60 min), DNA isolated, and reaction products analyzed by agarose gel electrophoresis (Figure 35). Whereas the unreacted control DNA substrate was found to contain almost exclusively (≥95 %) Form I DNA, the amount of Form I DNA was significantly reduced after incubation for 15 min with human whole cell extract. The majority of the DNA migrated as Form II DNA molecules. While some Form II DNA remained after further incubation (60 min), the amount of Form I DNA dramatically increased, suggesting that DNA repair had occurred. To establish whether the uracil residue was removed during this process, the DNA reaction products were treated with excess *E. coli* Ung and Endo IV in order to cleave uracil-

Figure 35. Agarose gel electrophoresis of M13mp2op14 DNA following base excision DNA repair in human U251 cell extracts. A standard BER reaction mixture (600 µl) containing 6 µg of M13mp2op14 (U•T) DNA (Form I) and 1.2 mg of human U251 whole cell extract protein was incubated at 30°C and aliquots (150 µl) were removed at various times (0, 15 and 60 min). DNA reaction products were then isolated, treated with (+) or without (-) *E. coli* Ung and Endo IV, and analyzed by 0.8% agarose gel electrophoresis as described under "Experimental Procedures". The position of Form I and Form II DNA is indicated by *horizontal arrows*. Form I DNA that was resistant to Ung/Endo IV treatment was isolated from the gel slice (bracket) by electroelution into 1 ml of TAE buffer and concentrated (~5-fold) using a Centricon-30 concentrator.

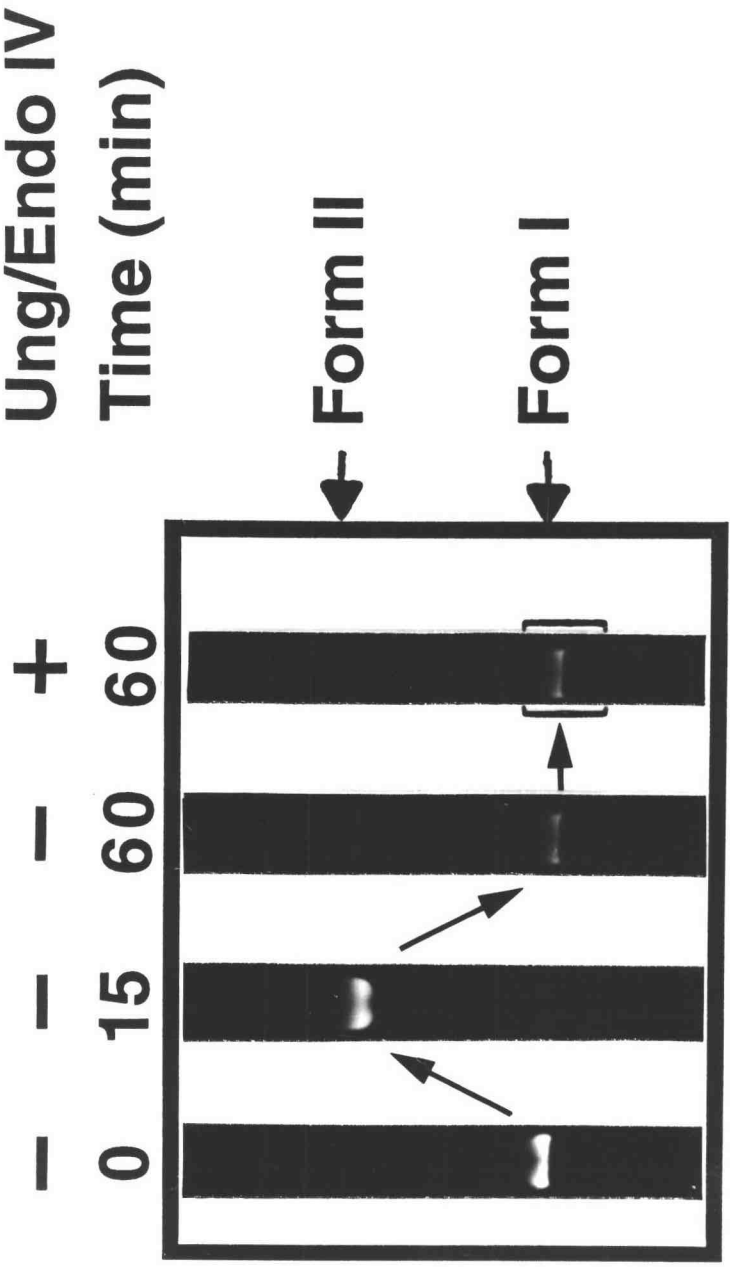

Figure 35

containing Form I DNA. Following this treatment, most of the Form I DNA was shown to be resistant to Ung/Endo IV-mediated cleavage after the 60 min repair reaction. Thus, the uracil residue was apparently removed from a significant fraction of the M13mp2op14 DNA substrate.

4.1.4 Evidence for Uracil-Initiated Base Excision DNA Repair in Human U251 Whole Cell Extracts

To establish the maximal extent of uracil-DNA repair, the M13mp2op14 DNA substrate was incubated for various times with human U251 whole cell extract (Figure 36A-B, lanes 9-14). Following the repair reaction, the recovered DNA was treated in the absence (panel A) or presence (panel B) of excess Ung and Endo IV prior to resolving the reaction products on separate 0.8 % agarose gels. As a control, the DNA substrate was also incubated with whole cell extract dialysis buffer in order to assess the stability of Form I DNA to components of the base excision repair reaction and during the DNA isolation procedure (Figure 36A, lane 8). Treatment with Ung/Endo IV demonstrated that the substrate was completely susceptible to cleavage (Figure 36B, lane 8). Untreated Form I DNA was included as a reference standard (Figure 36A-B, lane 7). Examination of DNA reaction products from time points treated without Ung/Endo IV (Figure 36A, lanes 9-14) show a direct correlation between the appearance of Form I DNA and the disappearance of Form II DNA between 15 min and 90 min of incubation. Again, this suggests that the U251 whole cell extracts are uracil-DNA repair proficient. Inspection of DNA reaction products from time points after treatment with Ung/Endo IV (Figure 36B, lanes 9-14) show a time-dependent accumulation of Form I DNA that was resistant to cleavage and indicated that removal of the uracil residue had occurred. In order to quantitate the amount of DNA reaction products, internal standards containing predetermined quantities of Form I and II M13mp2op14 DNA were prepared and separately analyzed on each agarose gel (panels A and B, lanes 1-5). Since the ethidium bromide staining intensity of Form I and II DNA varied from

Figure 36. Susceptibility of M13mp2op14 DNA repaired in human U251 cell extracts to *E. coli* Ung and Endo IV treatment. A standard BER reaction mixture (1050 µl) containing 10.5 µg of M13mp2op14 (U•T) DNA, 2.1 mg of U251 whole cell extract protein, and 210 µCi of [^{32}P]dATP was prepared. Samples (150 µl) were removed after incubation for 0, 15, 30, 45, 60, and 90 min at 30°C (panels A and B, lanes 9-14, respectively) and each reaction was terminated by addition of 2000 units of Ugi followed by adjustment to 20 mM EDTA. DNA was isolated, samples (5 µl) were mock treated (panel A) or treated with *E. coli* Ung and Endo IV (panel B), and prepared for 0.8% agarose gel electrophoresis as described under "Experimental Procedures". As a control, M13mp2op14 (U•T) DNA (1.5 µg) was incubated in the absence of whole cell extract protein and treated with or without *E. coli* Ung and Endo IV as described above (panel A and B, lane 8). Untreated M13mp2op14 (U•T) DNA (25 ng) and a sample containing 2.5 µg of a 1-kb DNA ladder (Gibco BRL) were also included as reference standards (panels A and B, lanes 7 and 6, respectively). The amount of Form I and II DNA detected in lanes 7-14 was measured relative to standards containing 100, 50, 25, 12.5, and 6.25 ng each of Form I and II DNA (panel A and B, lanes 1-5, respectively). The location of ethidium bromide-stained Form I and II DNA are indicated by *arrows*.

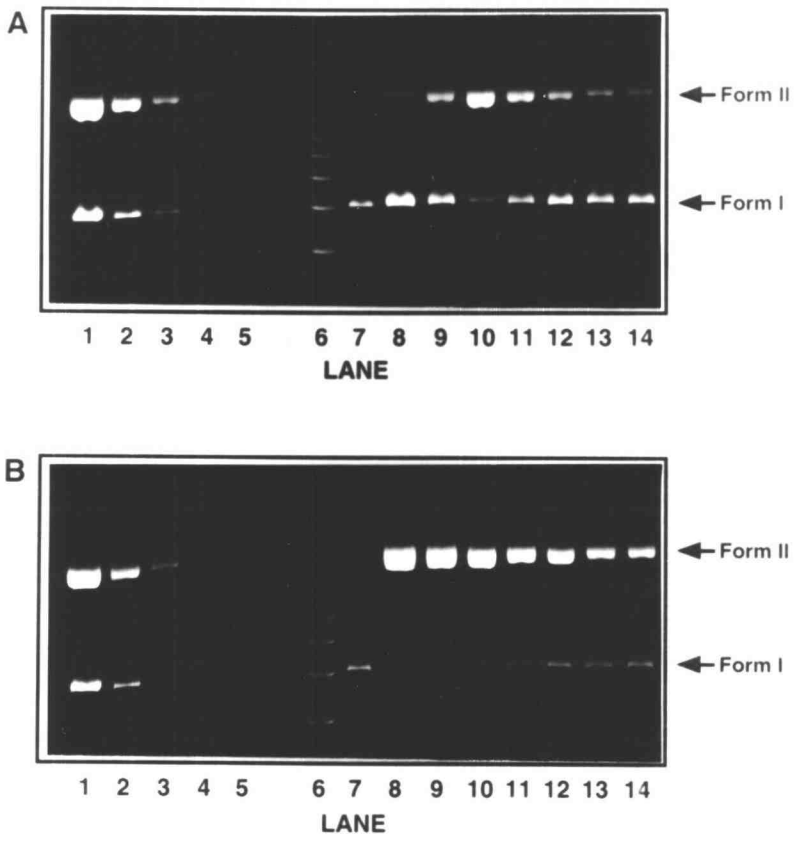
A
Form II
Form I
1 2 3 4 5 6 7 8 9 10 11 12 13 14
LANE
B
Form II
Form I
1 2 3 4 5 6 7 8 9 10 11 12 13 14
LANE

Figure 36

gel to gel, it was necessary to include a complete set of internal standards with each analysis. By using the ethidium bromide staining intensity of the internal standards, individual standard curves for Form I and II DNA were generated to correlate the staining intensity of experimental samples with defined quantities of DNA, as illustrated in Figure 37.

In order to associate the involvement of DNA repair synthesis with the removal of the uracil target, the M13mp2op14 DNA substrate was similarly incubated for various times with human U251 whole cell extract but in the presence of [α-^{32}P]dATP. The recovered DNA was treated with excess Ung and Endo IV prior to resolving the reaction products on a 0.8 % agarose gel (Figure 38A, lanes 2-7). As before, analysis of the ethidium bromide-stained gel revealed the time-dependent appearance of an Ung/Endo IV-resistant Form I DNA band. The percentage of Form I DNA detected in each lane was determined and is represented in Figure 38B. As a control, the extent of Ung/Endo IV cleavage of the M13mp2op14 DNA substrate was examined (Figure 38A, lanes C and 1). Before Ung/Endo IV treatment, ~95 % of the DNA migrated as Form I whereas after treatment, no detectable Form I DNA was observed (Figure 38B, columns C, (-) and (+)). This indicated the extent of the substrate susceptibility to the Ung/Endo IV treatment. Upon examination of the products from the reaction time course, a linear rate (~3.61 fmol/min) for the appearance of Ung/Endo IV-resistant Form I DNA was observed during the initial 30 min period. Thereafter, the rate appeared to plateau with ~50 % of the DNA being repaired. Autoradiography of the agarose gel demonstrated that the Ung/Endo IV-resistant Form I DNA appeared with concomitant incorporation of [^{32}P]dAMP (Figure 38C). Interestingly, significantly less [^{32}P]dAMP incorporation was observed in the Form I DNA as compared to Form II DNA though both represented ~50 % of the total DNA molecules after a 60-min BER reaction (Figure 38C, lane 6). This result was expected if Form I DNA was generated by BER involving DNA synthesis of only one or a few nucleotides. While these results imply that uracil-DNA

Figure 37. Standard curves used for quantitation of Form I and II DNA. The ethidium bromide staining intensity of Form I and II DNA standards in Figure 36B (lanes 1-5) were quantitated using a Gel Documentation System. The relative intensity of DNA bands containing 100, 50, 25, 12.5, and 6.25 ng of Form I (*open circles*) and II (*closed circles*) DNA were used to generate individual standard curves for quantitating the amount (ng) of Form I and II DNA in the experimental samples. The average ethidium bromide staining intensity of Form II DNA was ~2.72-fold greater than that of an equal amount (ng) of Form I DNA.

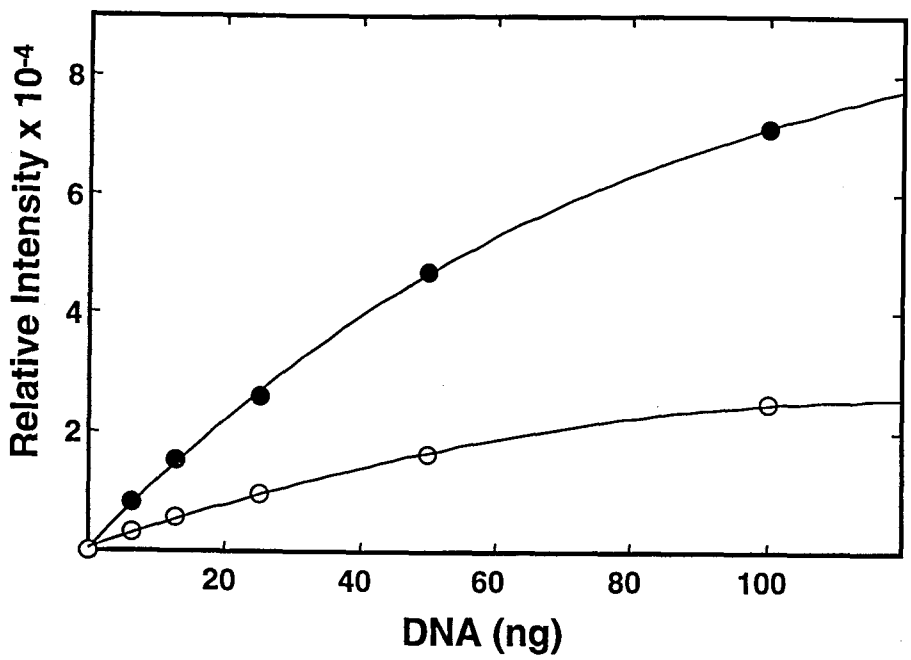

Figure 37

Figure 38. Analysis of reaction products generated by uracil-DNA base excision repair in human U251 cell extracts. (A) A standard BER reaction mixture (1050 µl) containing 10.5 µg of M13mp2op14 (U•T) DNA, 2.1 mg of U251 whole cell extract protein, and 210 µCi of [^{32}P]dATP was prepared. Samples (150 µl) were removed after incubation for 0, 15, 30, 45, 60, and 90 min at 30°C (lanes 2-7, respectively) and each reaction terminated by addition of 2000 units of Ugi followed by adjustment to 20 mM EDTA. DNA was isolated, treated with *E. coli* Ung and Endo IV, and prepared for 0.8% agarose gel electrophoresis as described under "Experimental Procedures". As a control, M13mp2op14 (U•T) DNA (1.5 µg) was mock treated without cell extract and incubated with Ung and Endo IV (lane 1). Untreated M13mp2op14 (U•T) DNA (25 ng) and a sample containing 2.5 µg of a 1-kb DNA ladder (Gibco BRL) were analyzed as reference standards (lanes C and M, respectively). The location of ethidium bromide stained Form I and II DNA bands are indicated by *arrows*. (B) DNA bands detected by ethidium bromide staining (A) were quantitatively measured using a Gel Documentation System and the percentage of Form I DNA in each sample was determined. Amounts of Form I and II DNA were measured relative to standards (6.25-100 ng) analyzed on the same gel. The percentage of Form I DNA observed before (-) or after (+) *E. coli* Ung/Endo IV treatment was determined after correcting for the ~2.72-fold greater ethidium bromide staining intensity of Form II compared to Form I DNA. The percentage of Form I DNA detected was calculated by dividing the amount of Form I DNA (ng) by that of Form I plus II DNA. (C) Autoradiography was conducted after blotting [^{32}P]DNA from the 0.8% agarose gel onto a Gene Screen Plus Membrane. (D) A standard reaction mixture (600 µl) was prepared as described under "Experimental Procedures" except that 1000 units of Ugi was added before addition of substrate. Samples (150 µl) were removed at 0, 60 and 90 min, treated with (+) or without (-) *E. coli* Ung/Endo IV as indicated, processed for gel electrophoresis, and data analyzed as described above.

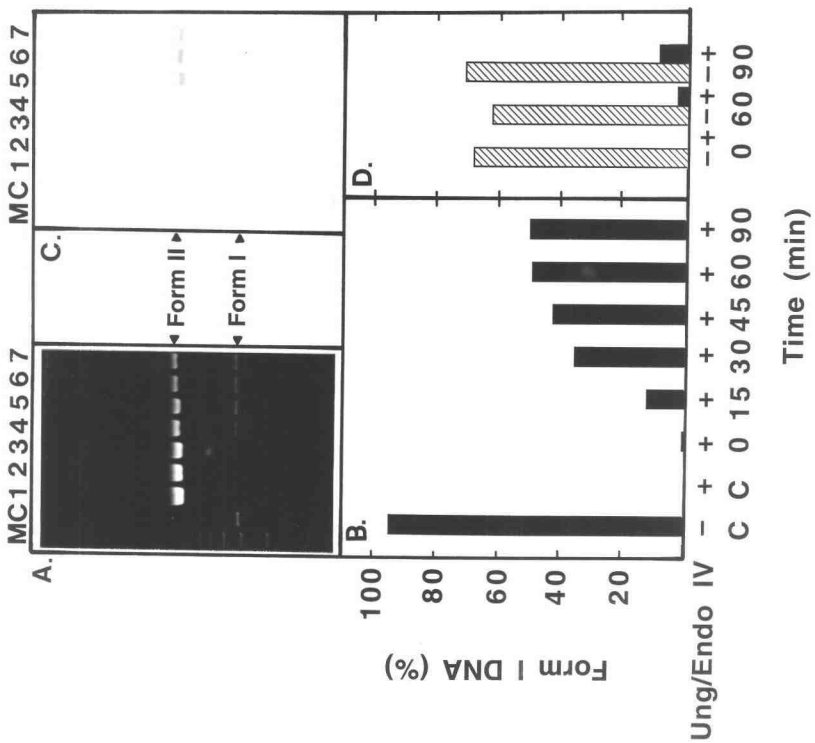
A.
MC1 2 3 4 5 6 7
B.
C.
Form II
Form I
MC 1 2 3 4 5 6 7
D.
Form I DNA (%)
100
80
60
40
20
Ung/Endo IV – + + + + + + + +
C C 0 15 30 45 60 90 0 60 90
Time (min)

Figure 38

repair involved limited DNA synthesis, these observations fell short of establishing that repair was uracil-initiated through the base excision repair pathway.

To determine if base excision repair was involved, Ugi protein was added to the whole cell extract in order to specifically inactivate human uracil-DNA glycosylase. In the absence of Ugi, U251 whole cell extracts contained ~8.6 units of Ung per mg of extract protein. However, the addition of a 45-fold unit excess of Ugi over Ung reduced the level of Ung activity to the limit of detection in the *in vitro* assay (data not shown). When the base excision repair assay was repeated in the presence of excess Ugi, the vast majority of recovered Form I DNA was sensitive to Ung/Endo IV cleavage (Figure 38D). This indicated that a Ugi-sensitive uracil-DNA glycosylase was initiating most of the repair and strongly suggested the involvement of the BER pathway. However, a small amount of Form I DNA corresponding to 3.7 % and 9.4 % of the substrate was insensitive to Ung/Endo IV cleavage after 60 and 90 min of BER reaction, respectively. Upon examination of the products from the reaction time course, an initial rate (~0.58 fmol/min) for the appearance of Ung/Endo IV-resistant Form I DNA was observed between 60 and 90 min. This implies that some repair may have occurred without the involvement of a Ugi-sensitive uracil-DNA glycosylase.

4.1.5 Analysis of Uracil-Initiated DNA Repair Synthesis in Human U251 Whole Cell Extracts

In order to localize the repair synthesis on M13mp2op14 DNA, [α-^{32}P]dATP was added to human U251 whole cell extracts and standard BER reactions were performed. At various times, reaction products were isolated and digested with the restriction endonuclease *Hin*fI, which was expected to generate a 529-bp DNA fragment that contained the uracil target (Figure 39A). Following the *Hin*fI digest, DNA fragments were resolved by nondenaturing polyacrylamide gel electrophoresis and autoradiography was performed to detect [^{32}P]dAMP incorporation (Figure 39B). While [^{32}P]dAMP incorporation

Figure 39. Analysis of uracil-initiated base excision repair-specific DNA synthesis in human U251 cell extracts. (A) Map of M13mp2 DNA indicating the location of the uracil residue (U) at position 78 in the (-) strand of the *lacZα* gene. The *hash marks* represent *Hin*fI restriction endonuclease recognition sites, and the size in base pairs (bp) of each corresponding DNA fragment is indicated. (B) After carrying out the base excision repair reactions described in Figure 38A, DNA was isolated and samples (2.5 μl, ~50 ng) were removed for digestion with 5 units of *Hin*fI for 60 min at 37°C. DNA restriction fragments were resolved by 5% nondenaturing polyacrylamide gel electrophoresis from BER reactions conducted at 0, 15, 30, 45, 60 and 90 min (lanes 1-6, respectively) and ^{32}P-labeled DNA was detected by autoradiography. The location of the uracil-containing DNA fragment (U-529 bp) and other fragments are indicated by *arrows*. (C) Two BER reaction mixtures (150 μl) were prepared as described under "Experimental Procedures" except that one reaction mixture contained M13mp2op14 DNA with an A•T basepair at position 78 (lane 1) and the other contained M13mp2op14 DNA substrate with a U•T mispair (lane 2). After incubation for 60 min at 30°C, and isolation of reaction products, *Hin*fI endonuclease reactions were conducted. Polyacrylamide gel electrophoresis and autoradiography were performed as described above. (D) The amount of [^{32}P]dAMP incorporation into DNA fragments of 253 (*striped bars*), U-529 (*black bars*), 261 (*white bars*), and 486 (*stippled bars*) base pairs in length was determined using a PhosphorImager. The relative intensity of each designated fragment (•) and U-529 was measured at the time points depicted in (B, lanes 2-6) and plotted after subtracting background values.

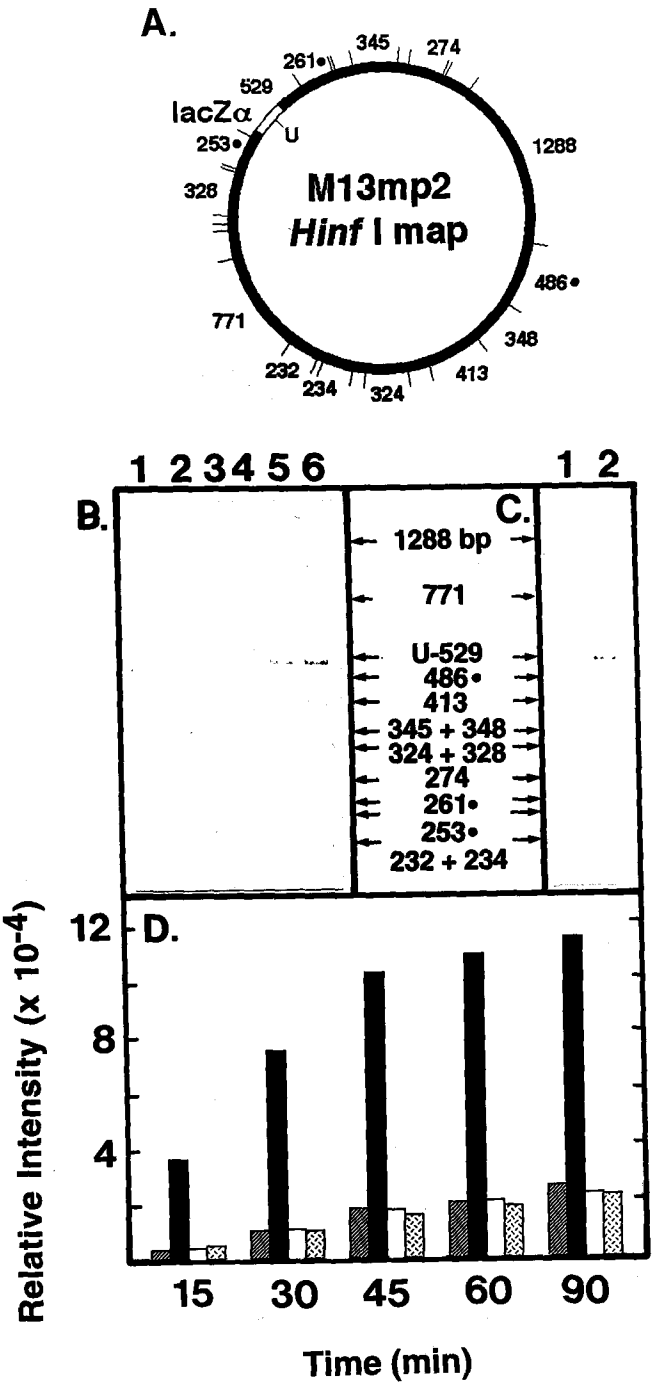
A.
M13mp2
Hinf I map
lacZα
U
529
261•
345
274
1288
253•
328
486•
348
413
324
234
232
771
B.
1 2 3 4 5 6
C.
1 2
1288 bp
771
U-529
486•
413
345 + 348
324 + 328
274
261•
253•
232 + 234
D.
12
8
4
Relative Intensity (x 10-4)
15
30
45
60
90
Time (min)

Figure 39

was detected in many of the fragments, the 529-bp fragment showed preferential incorporation that accumulated in a time-dependent manner. Control reactions were conducted with both M13mp2op14 DNA containing an A•T base pair or a U•T mispair at position 78 of the *lacZ*α gene to determine if incorporation into other fragments resulted from nonspecific DNA synthesis (Figure 39C). As before, preferential incorporation was observed specifically into the 529-bp fragment but only when containing the uracil residue. Corresponding non-uracil-containing fragments between both substrates appeared to accumulate similar levels of [^{32}P]dAMP incorporation. The level of specificity was evaluated after quantitating the amount of [^{32}P]dAMP incorporation into individual DNA fragments (Figure 39D). During the reaction time course, the relative amount of incorporation was compared for four DNA fragments (253-, U-529-, 261-, and 486-bp). A 5.2- to 7.6-fold greater [^{32}P]dAMP incorporation was observed in the U-529 bp fragment than in a similar sized 486-bp fragment located on the opposite side of the M13mp2op14 DNA molecule. Similarly, only low levels of incorporation were detected for the 253- and 261-bp fragments that flanked either side of the uracil-containing 529-bp fragment. When taken together, these results indicate that the vast majority of DNA synthesis on the 529-bp fragment was most likely uracil initiated and was limited to this fragment. Thus, most of the DNA synthesis observed was consistent with the occurrence of a uracil-initiated base excision repair mechanism.

DNA repair synthesis was further characterized to determine whether [^{32}P]dAMP incorporation occurred on the (-) strand, (+) strand, or both DNA strands. Standard BER reactions were conducted in the presence of [α-^{32}P]dATP and DNA reaction products were then digested with restriction endonucleases *Eco*RI and *Sma*I. As illustrated in Figure 28, the resulting restriction fragment contained a 44- and 40-nucleotide sequence corresponding to the (+) and (-) strands, respectively. This allowed the uracil-containing (-) strand to be distinguished from the (+) strand based on the size

of the single-stranded DNA fragments. When restriction endonuclease digested DNA products were analyzed by denaturing polyacrylamide gel electrophoresis, incorporation of [^{32}P]dAMP was observed to accumulate during the time course in association with the 40-mer fragment (Figure 40A, lanes 1-6 left). No incorporation was observed into the 44-mer fragment. To determine whether the uracil residue was removed from the 40-mer during DNA repair synthesis, a duplicate set of [^{32}P]DNA samples was treated with *E. coli* Ung and Endo IV following restriction endonuclease digestions. As before, [^{32}P]dAMP incorporation was observed in the 40-mer at nearly the same level and no smaller ^{32}P-labeled fragments were detected as a result of cleavage at the uracil site (Figure 40A, lanes 1-6 right). As a control, the activity of both Ung and Endo IV was verified using a duplex uracil-containing 34-mer substrate (Figure 40B). Collectively, these results indicate that DNA repair synthesis was directed exclusively to the (-) strand containing the uracil target.

4.1.6 Evidence for Uracil-Initiated Base Excision DNA Repair in Human LoVo Whole Cell Extracts

To determine if mismatch repair in human whole cell extracts influenced the rate of uracil-DNA repair, the experiments described above were repeated using whole cell extracts generated from human LoVo cells that are defective in the mismatch repair protein, hMSH2 (27, 282). The M13mp2op14 DNA substrate was incubated for various times with human LoVo whole cell extract supplemented with [α-^{32}P]dATP in the presence or absence of Ugi, treated with excess Ung and Endo IV, and DNA reaction products were analyzed by 0.8 % agarose gel electrophoresis (Figure 41). Analysis of the ethidium bromide-stained gel shows a time-dependent increase in Ung/Endo IV-resistant Form I DNA incubated in the absence of Ugi (Figure 41, lanes 4-9). A similar pattern was also observed for LoVo whole cell extract incubated in the presence of Ugi (Figure 41, lanes 10-15) albeit at a much reduced level. The percentage of Form I DNA at each time

Figure 40. Strand specificity of uracil-DNA repair synthesis by human U251 cell extracts. (A) A standard BER reaction mixture (700 µl) containing 7 µg of M13mp2op14 (U•T) DNA, 1.4 mg of U251 whole cell extract protein, and 140 µCi of [^{32}P]dATP was prepared. Samples (100 µl) were removed after incubation for 0, 15, 30, 45, 60 and 90 min at 30°C (lanes 1-6, respectively), the reaction terminated by addition of 2000 units of Ugi followed by adjustment to 20 mM EDTA, and DNA was isolated as described under "Experimental Procedures". DNA samples (8 µl, ~400 ng) were then simultaneously digested with 4 units each of *Eco*RI and *Sma*I for 60 min at 25°C. After terminating the restriction endonuclease reaction, equal volumes were removed, treated with (+) or without (-) *E. coli* Ung/Endo IV, and the [^{32}P]DNA products were analyzed by denaturing 12% polyacrylamide/8.3 M urea gel electrophoresis as described under "Experimental Procedures". The location of the 40-mer corresponding to the (-) strand *Eco*RI/*Sma*I restriction fragment is indicated on the autoradiogram by an *arrow*. (B) The 5'-end ^{32}P-labeled U-34-mer was annealed to a complimentary oligonucleotide (A-34-mer) forming a [^{32}P]U/A-34-mer duplex, as previously described (16, 150). Three samples of [^{32}P]U/A-34-mer (6 µl, ~20 ng) were either mock treated (lane 1), treated with *E. coli* Ung (lane 2), or treated with Ung and Endo IV (lane 3) as described under "Experimental Procedures". Following these reactions, [^{32}P]DNA products were analyzed on the identical denaturing 12% polyacrylamide/8.3 M urea gel described above. The location of the DNA substrate (34-mer) and product (15-mer) are located by *arrows* on the autoradiogram.

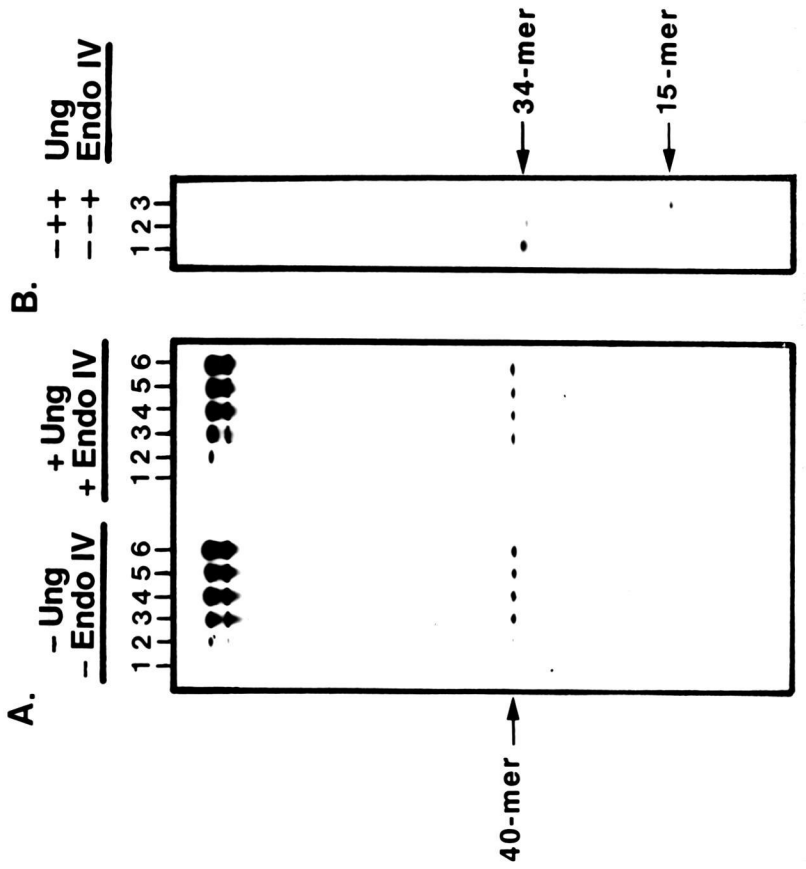
A.
- Ung
- Endo IV
1 2 3 4 5 6
+ Ung
+ Endo IV
1 2 3 4 5 6
40-mer
B.
Ung
Endo IV
- + +
- - +
1 2 3
34-mer
15-mer

Figure 40

Figure 41. Analysis of reaction products generated by uracil-DNA base excision repair in human LoVo cell extracts. Two standard BER reaction mixtures (600 µl) containing 6 µg of M13mp2op14 (U•T) DNA, 1.2 mg of LoVo whole cell extract protein and 120 µCi [^{32}P]dATP were prepared as described under "Experimental Procedures" except that one reaction mixture was supplemented with 1000 units of Ugi (+) and the other contained no Ugi (-) prior to the addition of substrate as indicated. Samples (100 µl) were removed after 0, 15, 30, 45, 60 and 90 min at 30 °C from BER reaction mixtures incubated in the absence of Ugi (lanes 4-9, respectively) and the presence of Ugi (lanes 10-15, respectively). Reactions were terminated, DNA was isolated, treated with *E. coli* Ung and Endo IV, and prepared for 0.8% agarose gel electrophoresis as described under "Experimental Procedures". As a control, M13mp2op14 (U•T) DNA (1 µg) was mock treated without cell extract and incubated with Ung and Endo IV (lane 3). Untreated M13mp2op14 (U•T) DNA (100 ng) and a sample containing 2.5 µg of a 1-kb DNA ladder (Gibco BRL) were analyzed as reference standards (lanes 2 and 1, respectively). The location of ethidium bromide-stained Form I and II DNA bands are indicated by *arrows*.

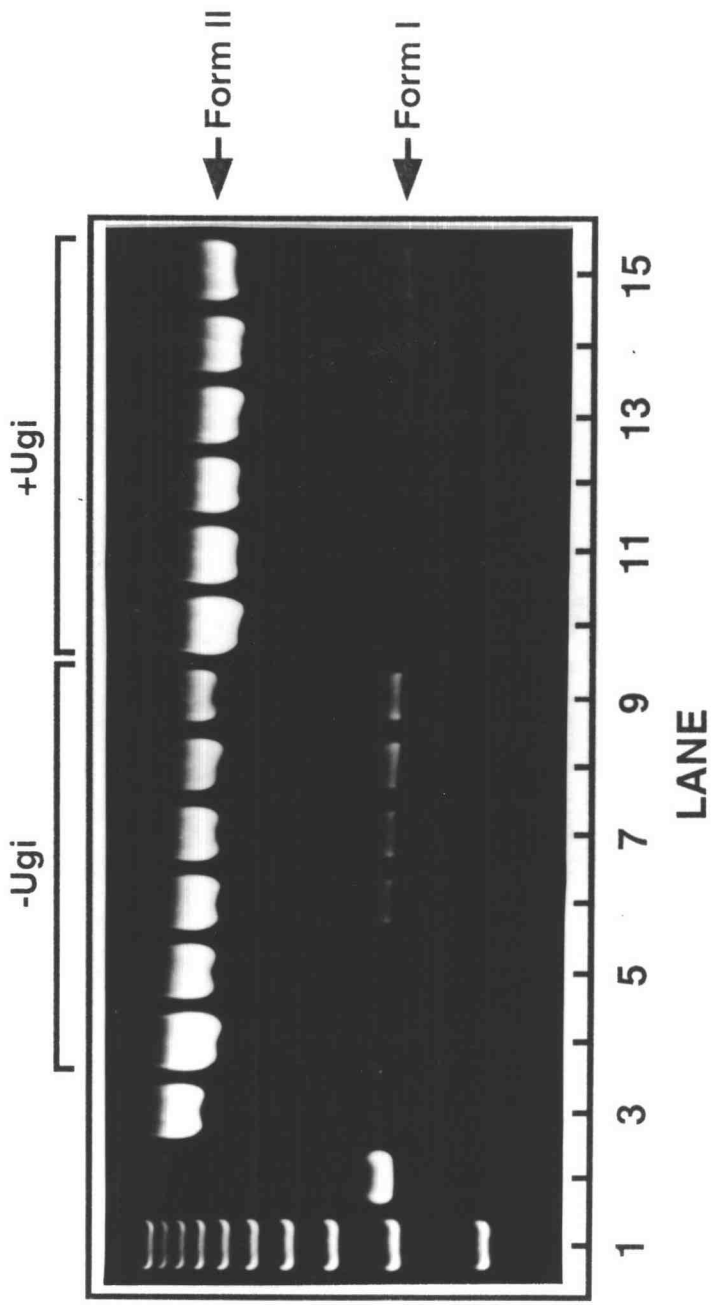

Figure 41

point was determined and was represented in Figure 42. The results do not appear to differ significantly from those observed for uracil-DNA repair in U251 whole cell extracts (Figure 38B and D). These results strongly suggest that uracil-DNA repair in LoVo whole cell extracts is predominantly mediated through the base excision repair pathway by uracil-DNA glycosylase. Under this condition where mismatch DNA repair was presumably defective, repair was again sensitive to the addition of Ugi. Thus, as previously detected in U251 whole cell extracts, some repair was initiated by a Ugi-insensitive repair pathway that was neither dependent on uracil-DNA glycosylase or the hMSH2 mismatch repair protein. On the assumption that the mechanism of Ugi insensitive uracil-DNA repair was identical between U251 and LoVo cells, the results suggest that the mismatch repair pathway was likely not involved and does not significantly contribute to uracil-DNA repair in human whole cell extracts. Upon examination of the reaction products after incubation for various times in the absence of Ugi, an initial linear rate of 1.64 fmol/min for the appearance of Ung/Endo IV resistant Form I DNA was observed after a lag time of 15 minutes. The maximal extent of repair was determined to be ~44 %. On the other hand, examination of Ung/Endo IV resistant products from the LoVo reactions incubated in the presence of Ugi showed an initial linear rate of 0.30 fmol/min for the appearance of Form I DNA. Again, a short lag period was observed and ~15 % of the DNA was repaired after 90 min. The observed rate of repair for the Ugi-insensitive uracil-DNA repair reaction was ~3-fold lower than that observed for uracil-DNA BER in LoVo whole cell extracts.

To assess the involvement and the extent of DNA repair synthesis between the Ugi sensitive and insensitive uracil-DNA repair pathways, autoradiography of the agarose gel was performed. The results illustrated that in either case, Ung/Endo IV-resistant Form I DNA appeared with concurrent incorporation of [^{32}P]dAMP (Figure 43). The extent of [^{32}P]dAMP incorporation per μg of repaired Form I DNA in the BER reaction lacking Ugi reached a maximum after 30 min whereas [^{32}P]dAMP incorporation in the

Figure 42. Quantitation of reaction products generated by uracil-DNA base excision repair in human LoVo cell extracts. DNA bands detected by ethidium bromide staining in Figure 41 were quantitated by using a Gel Documentation System and the percentage of Form I DNA from reactions supplemented with (*striped bars*) or without (*black bars*) Ugi was determined for each time point. The amount of Form I and II DNA was measured relative to standards (6.3-100 ng) analyzed on the same gel. The percentage of Form I DNA observed after *E. coli* Ung/Endo IV treatment was determined after correcting for the ~2.72-fold greater ethidium bromide staining intensity of Form II compared to Form I DNA. The percentage of Form I DNA detected was calculated by dividing the amount of Form I DNA (ng) by that of Form I plus II DNA.

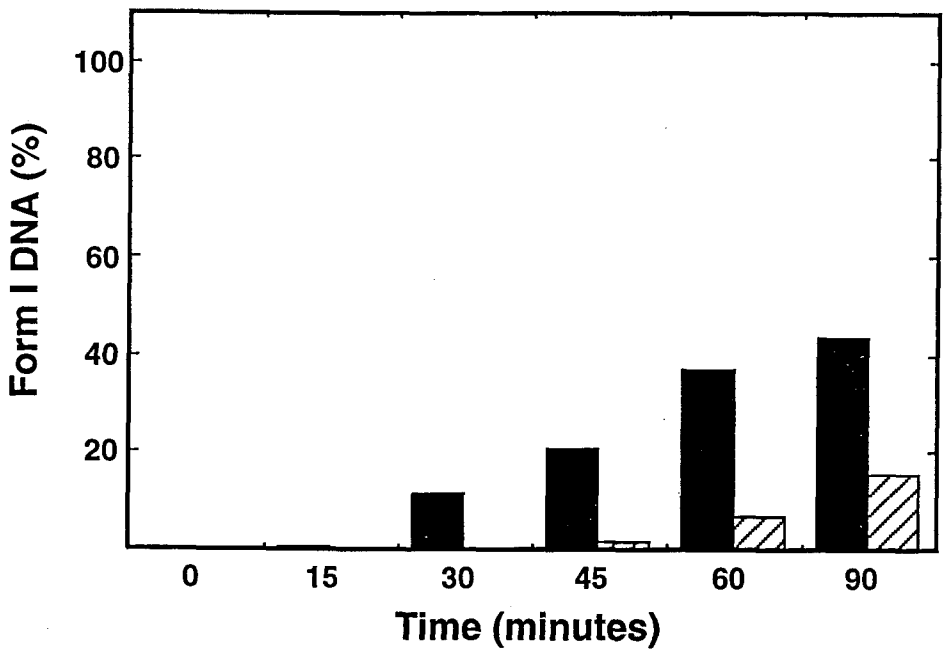

Figure 42

Figure 43. Analysis of [^{32}P]dAMP incorporation into reaction products generated by uracil-DNA base excision repair in human LoVo cell extracts. Autoradiography was performed after blotting [^{32}P]DNA from the 0.8% agarose gel described in Figure 41 onto a Gene Screen Plus nitrocellulose membrane. The location of Form I and II [^{32}P]DNA reaction products isolated after 0, 15, 30, 45, 60 and 90 min from standard LoVo BER reaction mixtures incubated in the absence of Ugi (lanes 1-6) or the presence of Ugi (lanes 7-12) are indicated by *arrows*.

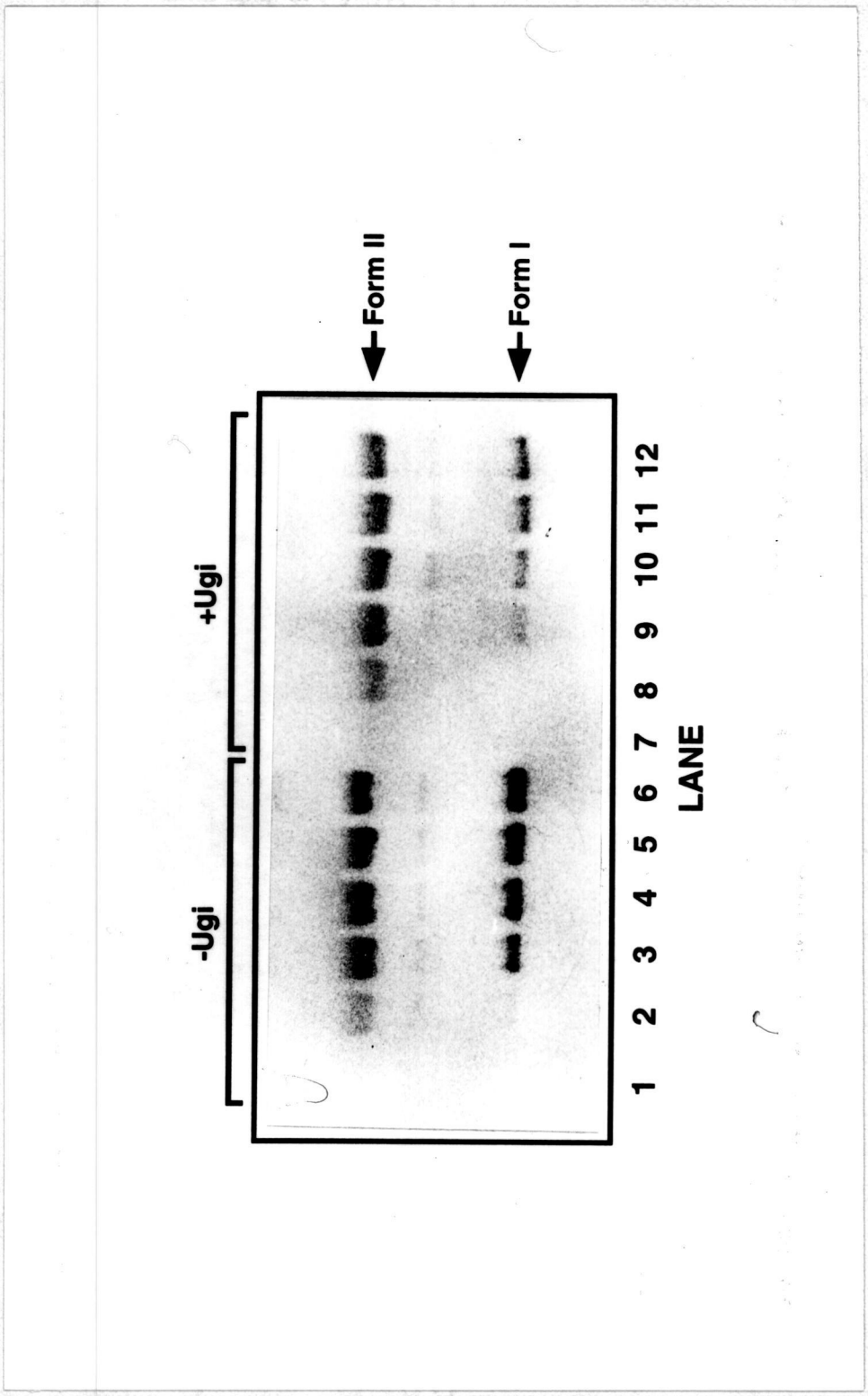

Figure 43

BER reaction containing Ugi appeared to plateau after 45 min (Figure 44). The maximal amount of [^{32}P]dAMP incorporation observed in Form I DNA generated by the Ugi insensitive repair reaction was approximately two-fold greater than that of the Ugi sensitive uracil-DNA glycosylase initiated BER pathway. This result suggested that the Ugi-insensitive uracil-DNA repair pathway involved more extensive DNA repair synthesis than that initiated by uracil-DNA glycosylase.

4.1.7 Analysis of Uracil-Initiated DNA Repair Synthesis in Human LoVo Whole Cell Extracts

In order to localize the repair synthesis on M13mp2op14 DNA, [α-^{32}P]dATP was added to human LoVo whole cell extracts in the presence and absence of Ugi and standard BER reactions were performed. Reaction products were isolated at various times, digested with the restriction endonuclease *Hin*fI, and DNA fragments were resolved by nondenaturing polyacrylamide gel electrophoresis and subjected to autoradiography to detect [^{32}P]dAMP incorporation (Figure 45). Preferential [^{32}P]dAMP incorporation was observed in a time-dependent manner into the 529-bp DNA fragment that contained the uracil residue both in the absence (lanes 1-6) and presence (lane 7-12) of Ugi. The amount of [^{32}P]dAMP incorporation was significantly reduced in all other DNA fragments for both reactions and appeared to accumulate similar low levels of incorporation. The level of specificity was evaluated after quantitating the amount of [^{32}P]dAMP incorporation into individual DNA fragments (253-, U-529-, 261-, and 486-bp) and is represented for Ugi-sensitive and -insensitive DNA repair products (Figure 46A and B, respectively). An 8.7- to 19.0-fold greater level of [^{32}P]dAMP incorporation was observed into the U-529-bp fragment than into the 486-bp fragment located on the opposite side of the M13mp2op14 DNA substrate for reaction products generated in the absence of Ugi. A similar comparison of reaction products generated in the presence of Ugi showed a 3.1- to 12.1-fold greater level of [^{32}P]dAMP incorporation. Both sets of reaction products revealed

Figure 44. Quantitation of [^{32}P]dAMP incorporation into Form I DNA generated by uracil-DNA base excision repair in human LoVo cell extracts. The amount of [^{32}P]dAMP incorporated into Form I DNA for the BER reactions described in Figure 41 was determined by using a PhosphorImager. The relative intensity of Form I DNA was measured from BER reactions conducted for 0, 15, 30, 45, 60 and 90 min in the absence of Ugi (*open circles*) or the presence of Ugi (*closed circles*) and background values were subtracted. The relative intensity of Form I [^{32}P]DNA was divided by the amount of Form I DNA (ng) as determined by ethidium bromide staining intensity and the ratio of relative intensity/μg Form I DNA was plotted versus time.

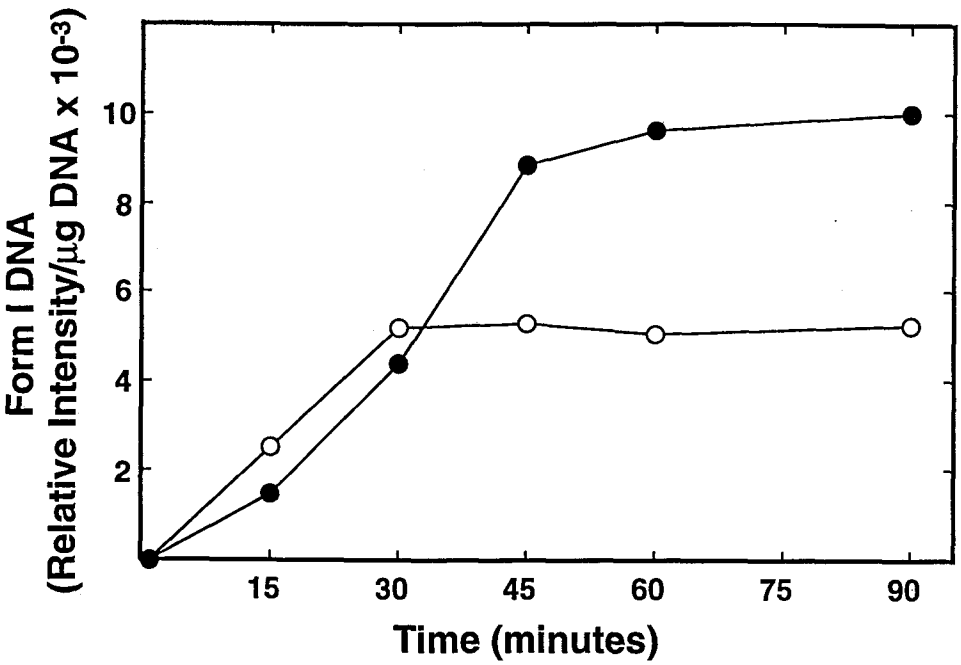
Form I DNA
(Relative Intensity/µg DNA x 10-3)
10
8
6
4
2
15
30
45
60
75
90
Time (minutes)

Figure 44

Figure 45. Analysis of base excision repair DNA synthesis associated with the uracil-containing DNA target using human LoVo cell extracts. After conducting the BER reactions described in Figure 41, M13mp2op14 DNA was isolated and samples (2.5 µl, ~50 ng) were removed for digestion with 5 units of *Hin*fI for 1 h at 37°C. DNA restriction fragments were resolved by 5% nondenaturing polyacrylamide gel electrophoresis from BER reactions conducted for 0, 15, 30, 45, 60, and 90 min in the absence of Ugi (lanes 1-6, respectively) or the presence of Ugi (lanes 7-12, respectively) and ^{32}P-labeled DNA was detected by autoradiography. The location of the uracil-containing fragment (U-529 bp) and other *Hin*fI DNA fragments are indicated by *arrows*. The uracil-containing fragment (U-529) and designated fragments (*) were quantitated.

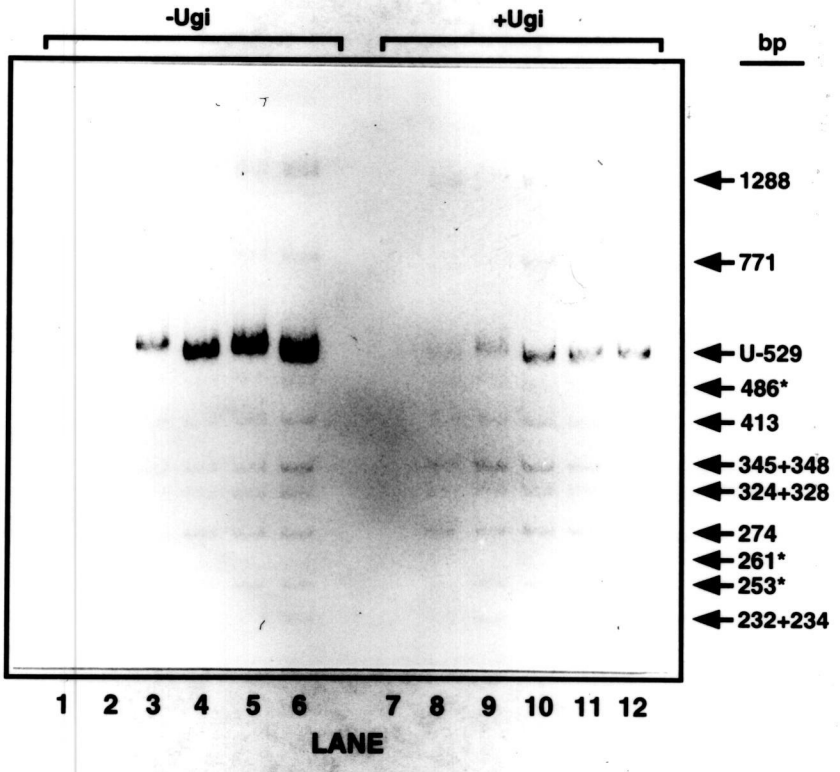
-Ugi
+Ugi
bp
1288
771
U-529
486*
413
345+348
324+328
274
261*
253*
232+234
1 2 3 4 5 6 7 8 9 10 11 12
LANE

Figure 45

Figure 46. Quantitation of base excision repair DNA synthesis associated with the uracil-containing DNA target using human LoVo cell extracts. After conducting the BER reactions described in Figure 41 and resolving *Hin*fI DNA restriction fragments by 5% nondenaturing polyacrylamide gel electrophoresis, the amount of [^{32}P]dAMP incorporation into DNA fragments of 253 (*striped bars*), 529 (*black bars*), 261 (*white bars*), and 486 (*stippled bars*) base pairs (bp) in length were determined by using a PhosphorImager. The relative intensity of each fragment was measured at the time points depicted for BER reactions containing LoVo cell extracts conducted in the absence of Ugi (A) or the presence of Ugi (B) and plotted after subtracting background values.

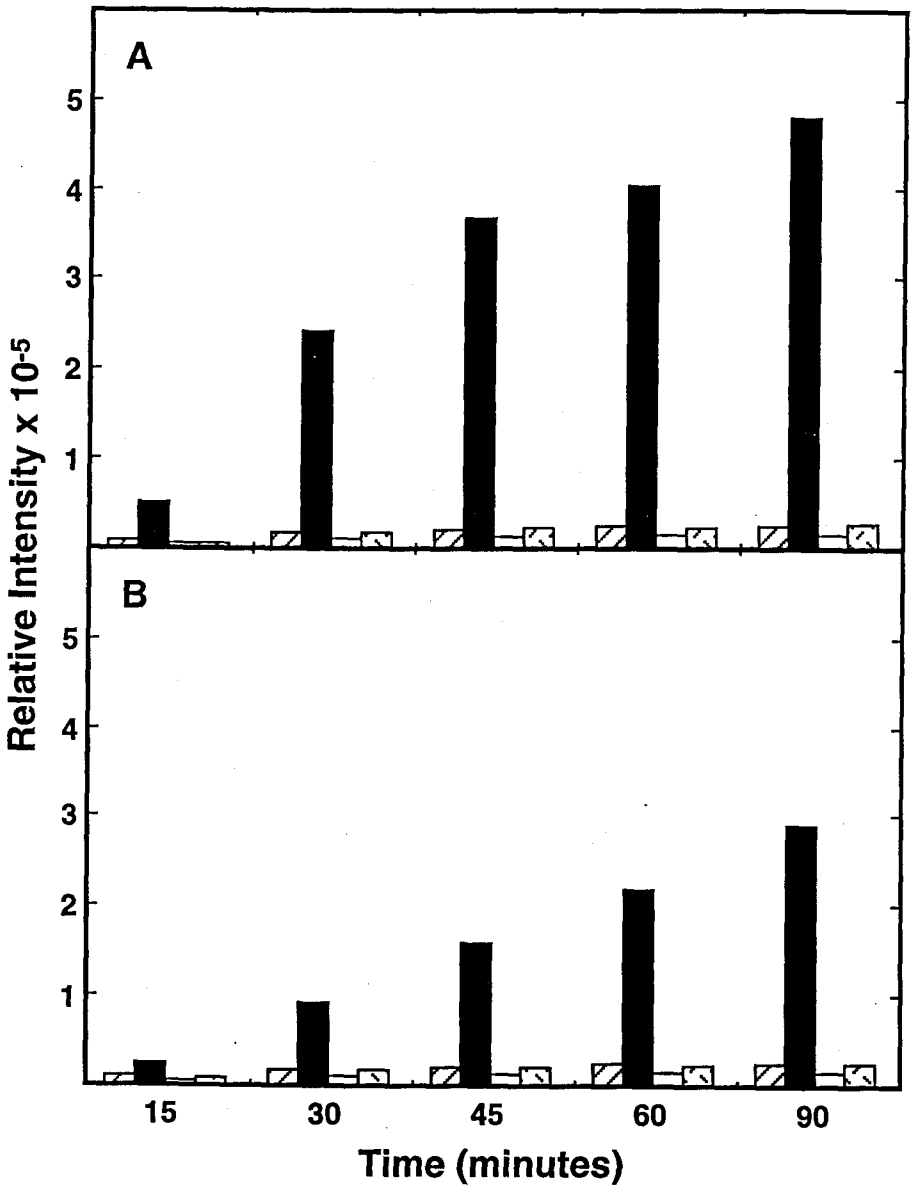

Figure 46

only low levels of incorporation into the 253-bp and 261-bp fragments flanking the uracil-containing 529-bp DNA fragment and indicated that the vast majority of DNA synthesis was uracil-initiated and limited to this fragment. As was determined for U251 whole cell extracts, most of the DNA synthesis observed was consistent with a uracil-initiated base excision repair mechanism.

DNA repair synthesis was further characterized to determine whether [^{32}P]dAMP incorporation occurred on the (-) strand, (+) strand or both DNA strands. Therefore two standard BER reaction mixtures containing [α-^{32}P]dATP were supplemented with Ugi as indicated, isolated DNA reaction products were digested with the restriction endonucleases *Eco*RI and *Sma*I , and products were analyzed by denaturing polyacrylamide gel electrophoresis (Figure 47). Autoradiography of the gel revealed a time-dependent accumulation of [^{32}P]dAMP into the 40-mer fragment for the BER reaction lacking Ugi (Figure 47, lanes 1-6). Some variations in sample loading and complete digestion with *Eco*RI and *Sma*I do apply. However, a reduced amount of [^{32}P]dAMP incorporation was observed into the 40-mer fragment for the BER reaction supplemented with Ugi (Figure 47, lanes 7-12). Under both reaction conditions, no incorporation was observed into the 44-mer fragment. Together, these results indicated that uracil-DNA repair synthesis was directed exclusively to the uracil-containing (-) strand for Ugi-sensitive and -insensitive repair pathways.

4.1.8 Comparison of Uracil-Initiated Base Excision Repair Between Human U251 and LoVo Whole Cell Extracts

To compare the amount of nonspecific DNA synthesis introduced by human U251 or LoVo whole cell extracts into the M13mp2op14 DNA substrates, [α-^{32}P]dATP was added to two sets of standard BER reactions containing either M13mp2op14 DNA with an A•T base pair or a U•T mispair at position 78 of the *lacZα* gene. Reactions were terminated after 45 and 60

Figure 47. Strand specificity of uracil-DNA repair synthesis by human LoVo cell extracts. After conducting the BER reactions described in Figure 41, DNA was isolated and samples (4 µl, ~200 ng) were removed for restriction analysis with *Sma*I and *Eco*RI. Samples from BER reactions containing LoVo cell extracts were conducted for 0, 15, 30, 45, 60, and 90 min in the absence of Ugi (lanes 1-6, respectively) or the presence of Ugi (lanes 7-12, respectively). After digestion with 10 units of *Sma*I for 1 h at 25°C and 10 units of *Eco*RI for 1 h at 25°C, the [^{32}P]DNA products were analyzed by denaturing 12% polyacrylamide/8.3 M urea gel electrophoresis as described under "Experimental Procedures." The location of the 40-mer corresponding to the (-) strand *Eco*RI/*Sma*I restriction fragment is indicated on the autoradiogram by an *arrow*.

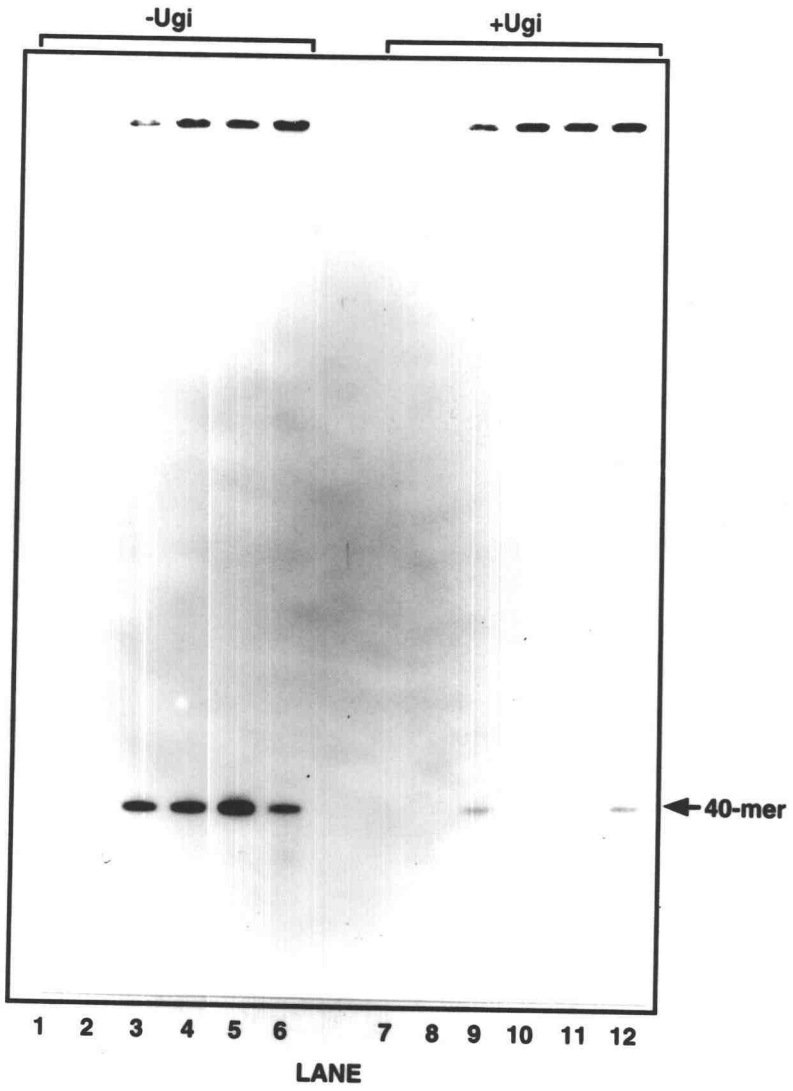

Figure 47

min for reactions containing LoVo and U251 whole cell extract protein, respectively. Following the BER reaction, the products were digested with the restriction endonuclease *Hin*fI, DNA fragments were resolved by nondenaturing polyacrylamide gel electrophoresis, and autoradiography was performed to detect [^{32}P]dAMP incorporation (Figure 48). As expected, preferential incorporation was observed specifically into the 529-bp fragment and was dependent upon the presence of the uracil residue for reactions containing both U251 and LoVo whole cell extracts (Figure 48, lanes 2 and 4, respectively). This was consistent with the occurrence of a uracil-initiated base excision repair mechanism. Corresponding non-uracil-containing fragments between both substrates appeared to accumulate similar levels of [^{32}P]dAMP incorporation when incubated with either U251 or LoVo whole cell extract. However, the amount of [^{32}P]dAMP incorporation into non-uracil-containing fragments by U251 extracts into either substrate was apparently greater than that observed for LoVo extracts. Therefore, the level of nonspecific DNA synthesis between U251 and LoVo was compared after quantitating the amount of [^{32}P]dAMP incorporation into designated DNA restriction fragments from the M13mp2op14 (A•T) and (U•T) DNA substrates (Figure 49). Incubation of M13mp2op14 (A•T) DNA with U251 whole cell extracts resulted in a 3.7- to 5.2-fold greater level of [^{32}P]dAMP incorporation into the 253-, 529-, 261-, and 486-bp DNA fragments as compared to LoVo extracts. In a similar comparison, a 3.4- to 9.9-fold greater level of [^{32}P]dAMP incorporation by U251 was observed into DNA fragments of 253-, 261-, and 486-bp in length generated from the M13mp2op14 (U•T) DNA substrate. However, the level of incorporation into the 529-bp fragment containing the uracil target was observed to be similar (~1.4-fold greater [^{32}P]dAMP incorporation by U251) between U251 and LoVo extracts. Non-uracil containing *Hin*fI DNA fragments exhibited a 4.8- to 6.6-fold reduced level of [^{32}P]dAMP following incorporation and repair by U251 extracts. For LoVo extracts, this value exhibited a 16.2- to 42.6-fold reduction. These results

Figure 48. Comparison of specific and nonspecific DNA synthesis associated with uracil-initiated base excision repair in human U251 and LoVo cell extracts. Standard BER reaction mixtures (200 µl) containing 0.4 mg of human U251 (lanes 1 and 2) or LoVo (lanes 3 and 4) whole cell extract protein, 2 µg of M13mp2op14 (A•T) DNA (lanes 1 and 3) or M13mp2op14 (U•T) DNA (lane 2 and 4), and 40 µCi of [^{32}P]dATP were prepared. Samples containing U251 or LoVo whole cell extract protein were incubated at 30 °C for 60 min or 45 min, respectively. Each reaction was terminated with 2000 units of Ugi protein followed by adjustment to 20 mM EDTA, DNA was isolated, and samples (2.5 µl, ~50 ng) were removed for digestion with 5 units of *Hin*fI for 1 h at 37°C. DNA restriction fragments were resolved by 5% nondenaturing polyacrylamide gel electrophoresis and ^{32}P-labeled DNA was detected by autoradiography. The location of the uracil-containing fragment (U-529 bp) and other *Hin*fI DNA fragments are indicated by *arrows*. The uracil-containing fragment (U-529) and designated fragments (*) were quantitated.

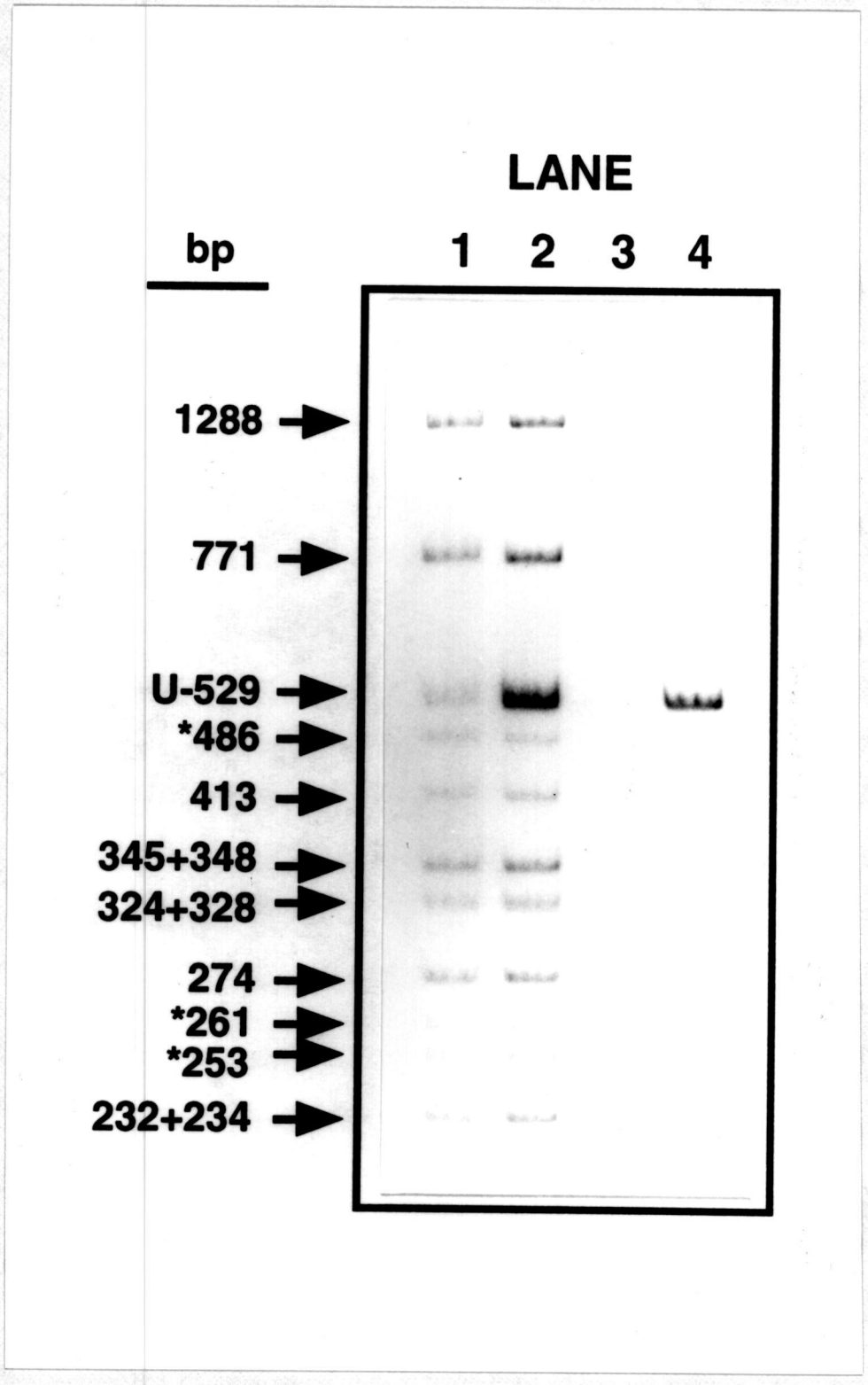
LANE
bp
1
2
3
4
1288
771
U-529
*486
413
345+348
324+328
274
*261
*253
232+234

Figure 48

Figure 49. Quantitation of specific and nonspecific DNA synthesis associated with uracil-initiated base excision repair in human U251 and LoVo cell extracts. The amount of [^{32}P]dAMP incorporation into DNA fragments of 253 (*striped bars*), 529 (*black bars*), 261 (*white bars*), and 486 (*stippled bars*) base pairs (bp) in length from the autoradiogram depicted in Figure 48 were determined by using a PhosphorImager. The relative intensities of each designated fragment from U251 and LoVo BER reaction mixtures containing the M13mp2op14 (A•T) DNA or M13mp2op14 (U•T) DNA substrates were plotted after subtracting background values.

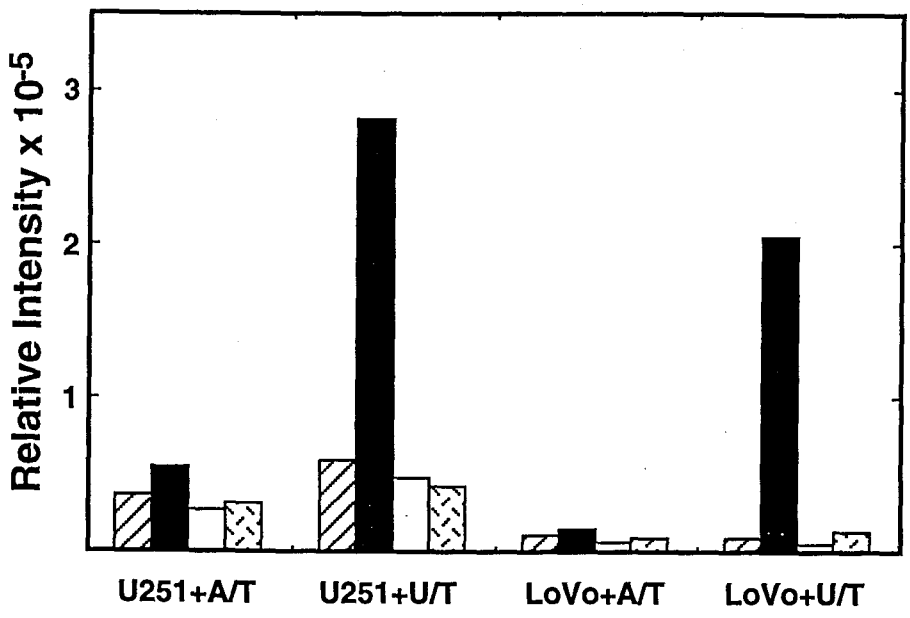

Figure 49

indicate a decreased level of nonspecific DNA synthesis by LoVo whole cell extract preparations. As previously observed, [^{32}P]dAMP incorporation profiles for both extract preparations are consistent with a uracil-initiated base excision repair mechanism.

To determine if the amount of nonspecific [^{32}P]dAMP incorporation into designated *Hin*fI restriction fragments was influenced by the presence of Form II DNA repair intermediates, a standard BER reaction containing M13mp2op14 (U•T) DNA and LoVo whole cell extract protein was performed and the recovered DNA was divided into two aliquots. One sample was designated the Form I/II DNA mixture. The second sample was treated with Ung/Endo IV and Ung/Endo IV-resistant Form I DNA was purified by agarose gel electrophoresis. Both samples were subsequently digested with *Hin*fI and analyzed for [^{32}P]dAMP incorporation, as described above. For comparative purposes, the relative intensity of the 529-bp fragment from the Form I/II DNA mixture (~38,000 arbitrary units) was normalized to that of the 529-bp fragment from the isolated Form I DNA (~156,000 arbitrary units). Hence, the relative intensities of designated fragments (253-, 261- , and 486-bp) from the Form I/II DNA mixture were multiplied by the normalization constant (4.1) and plotted (Figure 50). A 3.0- to 3.7-fold increase in nonspecific [^{32}P]dAMP incorporation into DNA fragments of 253-, 261-, and 486-bp in length was observed for the Form I/II DNA mixture as compared to the isolated Form I DNA. These results suggest that the extent of DNA synthesis associated with uracil-initiated repair into the 529-bp fragment was previously underestimated due to the presence of unrepaired or repair intermediate DNA molecules that remained as Form II DNA.

Figure 50. Quantitation of nonspecific DNA synthesis associated with Form II DNA present in Form I/II DNA mixtures. Two standard BER reaction mixtures (500 µl) containing 5 µg of M13mp2op14 (U•T) DNA, 1 mg of LoVo whole cell extract protein, 100 µCi [^{32}P]dATP, and 1000 units of Ugi were prepared and incubated for 1 h at 30°C. Reactions were terminated by addition of 2000 units of Ugi followed by adjustment to 20 mM EDTA. DNA was isolated and treated with or without *E.coli* Ung and Endo IV. Untreated M13mp2op14 (U•T) DNA was designated Form I/II DNA mixture. Repaired Form I DNA from the sample treated with Ung and Endo IV was isolated by 0.8% agarose gel elctrophoresis as described under "Experimental Procedures" and designated Form I DNA. Samples of Form I/II DNA mixture and Form I DNA (2.5 µl, ~50 ng) were removed for digestion with 5 units of *Hinf* I for 1 h at 37°C. DNA restriction fragments were resolved by 5% nondenaturing polyacrylamide gel electrophoresis and ^{32}P-labeled DNA was detected by autoradiography. The amount of [^{32}P]dAMP incorporated into DNA fragments of 253 (*striped bars*), 529 (*black bars*), 261 (*white bars*), and 486 (*stippled bars*) base pairs (bp) in length were determined by using a PhosphorImager. The relative intensities of the 529 bp fragment from each sample were normalized and normalization constants were generated for each sample set. The relative intensity of DNA fragments of 253, 486, and 261 base pairs in length were adjusted by multiplying the relative intensity of each with the derived normalization constant and values were plotted.

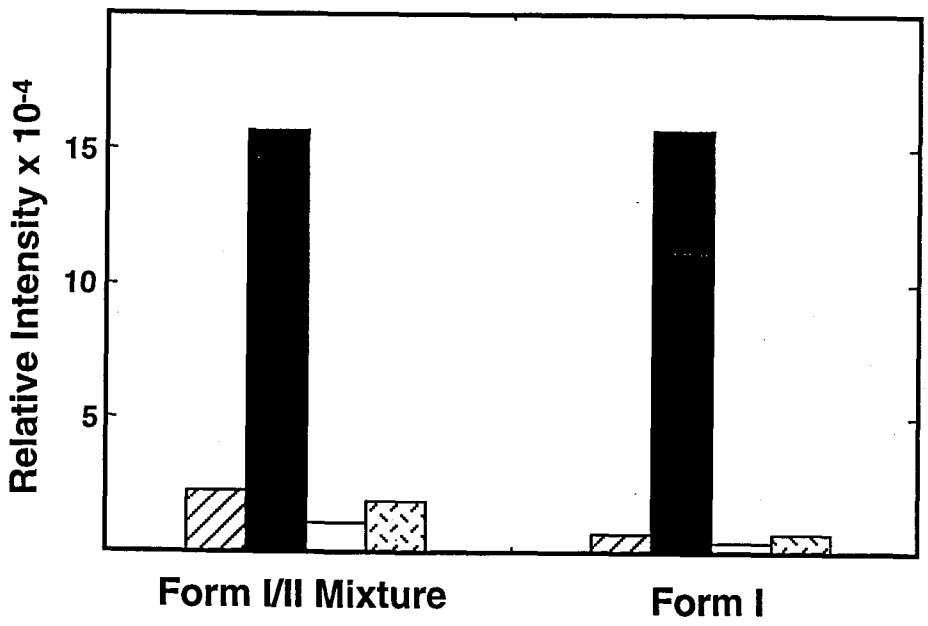

Figure 50

4.1.9 Mutational Frequency of Base Excision DNA Repair Synthesis in Human U251 Whole Cell Extracts

Using the M13mp2op14 *lacZα* DNA-based reversion assay, the fidelity of BER synthesis was examined in U251 whole cell extracts. Standard BER reactions containing either M13mp2op14 DNA with a U•T mispair or an A•T base pair at position 78 were conducted and Ung/Endo IV resistant Form I DNA was purified from the reaction products. DNA was subsequently transfected into either *E. coli* NR9162 (*mutS*$^-$) or the isogenic strain MC1061 (*mutS*$^+$) for comparative purposes. The reversion frequency of opal codon 14 was determined by the analysis of M13 plaque phenotype color as a result of proficient or deficient α-complementation detected on host indicator plates. The appearance of light or dark blue plaques was indicative of putative mismatches at the opal codon introduced during inaccurate DNA repair synthesis. Background reversion frequencies for M13mp2op14 (A•T) DNA substrate incubated in the absence of whole cell extract protein were determined to be 0.079×10^{-4} and 0.78×10^{-4} when transfected into *E. coli* MC1061 and NR9162 cells, respectively (Table 7). The observed ~10-fold difference in reversion frequency was attributed to the correction of endogenous errors by *E. coli* MC1061 cells capable of conducting methyl-directed mismatch repair. The background reversion frequency for M13mp2op14 (U•T) incubated in the absence of whole cell extract protein was also determined and yielded significantly higher reversion frequencies of 4.6×10^{-4} and 2.1×10^{-4}, respectively, when transfected into MC1061 and NR9162 cells. The ~2-fold difference in reversion frequency observed between MC1061 and NR9162 cells was also attributed to methyl-directed mismatch repair by *E. coli* MC1061. However, it must be noted that these reversion frequencies do not directly reflect the true α-complementation status of the substrate since the (-) strand DNA correctly encodes a wild-type *lacZα* gene. Additionally, the presence of uracil in transformed DNA would elicit *in vivo*

Table 7

Frequency of Mutations Produced by Uracil-Initiated Base Excision Repair in Human U251 Whole Cell Extracts

Standard base excision DNA repair reaction mixtures (500 µl) were prepared containing 1 mg of human U251 whole cell extract protein and either 5 µg of M13mp2op14 (U•T) or (A•T) DNA. After incubation at 30°C for 1 h, reactions were terminated, DNA products recovered, and Form I DNA that was resistant to *E. coli* Ung/Endo IV treatment was isolated by 0.8% agarose gel electrophoresis as described under "Experimental Procedures". Form I DNA was then transfected into *E. coli* NR9162 and MC1061 cells as indicated below and the M13mp2 lacZα DNA-based reversion assay was performed as described by Kunkel (130).

	NR9162 (mutS$^-$)			MC1061 (mutS$^+$)		
	Plaques Scored			Plaques Scored		
DNA (-/+)[b]	Total	Blue	Reversion Frequency[a] ($x10^{-4}$)	Total	Blue	Reversion Frequency ($x10^{-4}$)
Control[c]						
A/T	216,840	17	0.78	251,680	2	0.079
U/T	176,540	81	4.6	211,770	44	2.1
U251 WCE						
A/T	532,480	13	0.24	309,218	8	0.26
U/T	150,705	78	5.2	150,355	19	1.3
U251 WCE + Ugi[d]						
U/T	350,428	993	28.3	59,748	162	27.1

[a] Reversion frequencies were calculated by dividing the number of blue plaques scored by the total number of blue plus colorless plaques. Revertants included dark blue and light blue phenotypes.

[b] Denotes the (-) and (+) strand nucleotide at the target site.

[c] Control reaction mixtures (500 µl) contained 5 µg of M13mp2op14 (U•T) or (A•T) DNA and substituted whole cell extract (WCE) dialysis buffer (25 mM Hepes-KOH, 100 mM KCl, 2 mM DTT, 12 mM $MgCl_2$, 1 mM EDTA, and 17% (w/v) glycerol adjusted to pH 7.9) instead of human whole cell extract protein in standard BER reaction mixtures.

[d] A standard reaction mixture (500 µl) was prepared as described under "Experimental Procedures" except that 1000 units of Ugi (~100-fold unit excess over whole cell extract UDG) was added before the substrate addition.

BER by the transfected host cells. Thus, the observed increase in reversion frequency relative to the M13mp2op14 (A•T) substrate is not a direct or accurate measurement of the background reversion frequency of the M13mp2op14 (U•T) substrate but a measurement of α-complementation influenced by unrepaired uracil residues in the (-) strand and the fidelity of *in vivo* uracil-initiated BER in the transfected host.

Experiments were subsequently conducted to measure the fidelity of uracil-initiated DNA repair synthesis using U251 whole cell extracts in the presence or absence of Ugi. When M13mp2op14 (U•T) DNA was incubated with U251 whole cell extract in the absence of Ugi and processed, a reversion frequency of 5.2×10^{-4} was observed after transfection of repaired Form I DNA into *E. coli* NR9162 (*mut*S) cells. This value was ~22-fold greater than that of M13mp2op14 (A•T) DNA incubated with U251 whole cell extract. As expected, this value was reduced (~4-fold) when the same repaired Form I DNA was transfected into *E. coli* MC1061 cells capable of removing mispairs from the unmethylated (-) strand. These results are indicative of nucleotide misincorporation events associated with uracil-initiated base excision repair in human whole cell extracts and provide a measurement of DNA repair synthesis fidelity. When M13mp2op14 (U•T) DNA was incubated with U251 whole cell extract protein in the presence of Ugi, a reversion frequency of 28.3×10^{-4} was observed following transfection of repaired Form I DNA into *E. coli* NR9162 (*mut*S). This value was ~5-fold higher than that of M13mp2op14 (U•T) DNA repaired by U251 whole cell extract in the absence of Ugi and ~36-fold greater than that of the U251 whole cell extract treated M13mp2op14 (A•T) DNA control. Interestingly, transfection of the same repaired Form I DNA into *E. coli* MC1061 yielded a nearly identical reversion frequency of 27.1×10^{-4} and implied that endogenous errors introduced by human whole cell extracts were not repaired by the methyl-directed mismatch repair in the transfected host. These results indicated that the Ugi-insensitive repair

pathway in U251 cells is more error prone than that of the uracil-DNA glycosylase-initiated uracil-base excision repair pathway.

4.1.10 Mutational Spectrum of Human U251 Cells

Mutational analysis was performed on individual revertant M13 phage DNA to define the type of misincorporation that occurred during uracil-initiated base excision DNA repair synthesis in U251 whole cell extracts. Single-stranded DNA was isolated and sequenced from the 78 blue plaques obtained from repaired DNA produced in human U251 whole cell extracts incubated in the absence Ugi. The DNA sequence analysis of three revertants representing each of the three possible nucleotide misincorporation events at the site of the uracil are shown in Figure 51A-C. The distribution and specificity of single-base substitutions located within the opal codon are shown in Figure 52 and Table 8, respectively. Seventy-four (95 %) of the mutations occurred at the first nucleotide of the opal codon while one mutation (1 %) was detected at the second nucleotide position and three (4 %) were observed at the third nucleotide position. Thus, almost all of the base substitutions occurred at the location of the uracil target. Interestingly, the major class of these base substitutions were transversion mutations (~94 %) and were nearly equally divided between T to G and T to A changes in the (+) strand template. Only four mutations were scored as T to C transitions at this site. These results define the uracil-initiated repair-mediated mutation spectrum at this target site.

4.1.11 Mutational Frequency of Base Excision DNA Repair Synthesis in Human LoVo Whole Cell Extracts

To determine if mismatch repair in human whole cell extracts might influence the determination of reversion frequency, the fidelity of BER synthesis was examined in LoVo whole cell extracts using the M13mp2op14 *lacZ*α DNA-based reversion assay, as described above. Upon transfection of

Figure 51. DNA sequence analysis of M13mp2op14 DNA *lacZα* gene revertants. Isolated dark blue and light blue plaques were used to procure single-stranded M13mp2op14 DNA and the DNA sequences were determined using an Applied Biosystems Model 373A DNA sequencer as described under "Experimental Procedures". The DNA sequence analysis of M13mp2op14 DNA containing an arginine codon (CGA, AGA) (pp. 255 and 256, respectively) or a glycine codon (GGA) (pp. 257) are indicative of (A) T→G, (B) T→A, and (C) T→C mutations at the site of the uracil, respectively. The codon containing the single-base substitution generated by the original mispair is indicated by *brackets* for each revertant. The sequences depicted are those of the (-) DNA strand determined in the 5' to 3' direction. Unidentified bases are denoted by an 'N' in the DNA sequence.

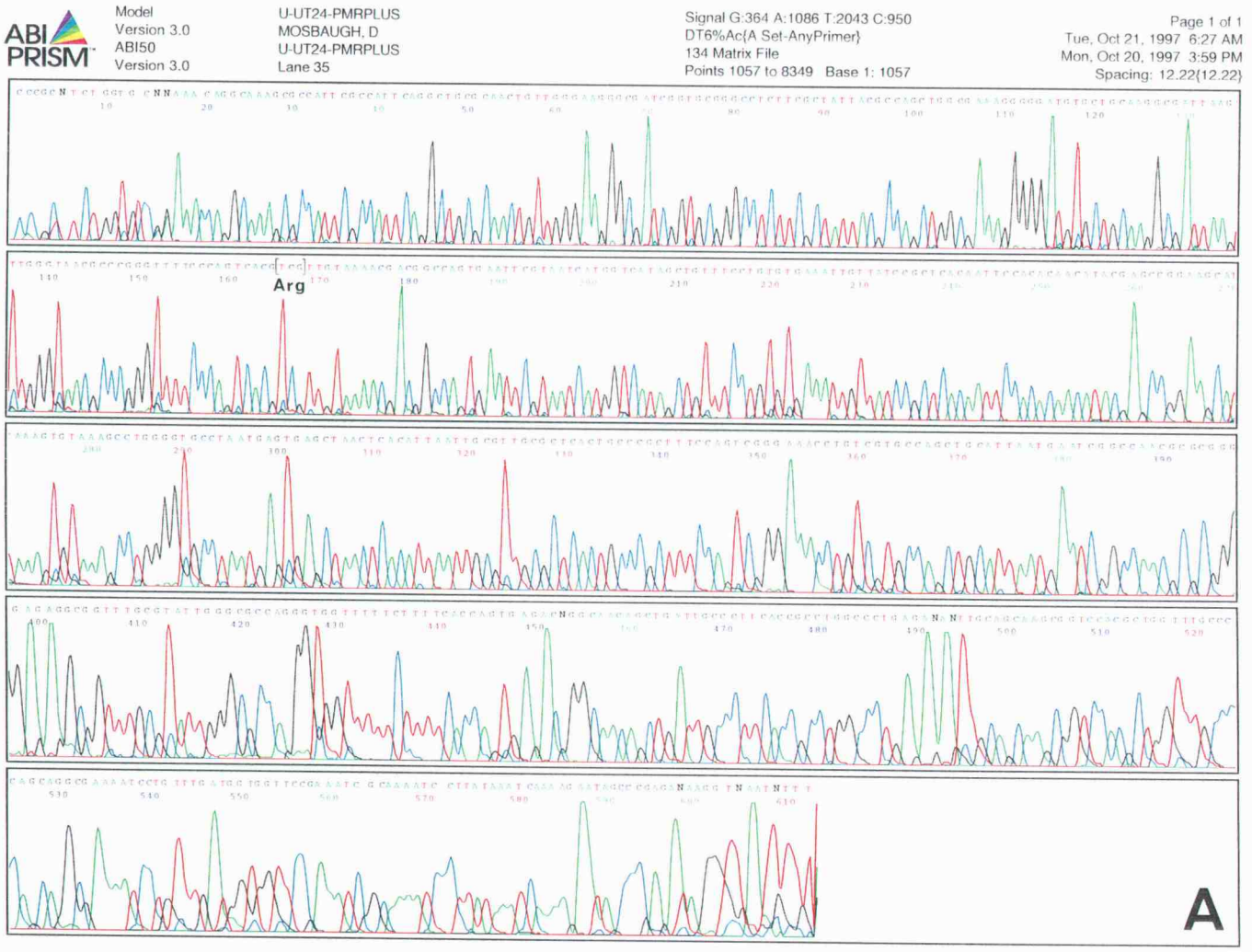
ABI PRISM
Model
Version 3.0
ABI50
Version 3.0
U-UT24-PMRPLUS
MOSBAUGH, D
U-UT24-PMRPLUS
Lane 35
Signal G:364 A:1086 T:2043 C:950
DT6%Ac{A Set-AnyPrimer}
134 Matrix File
Points 1057 to 8349 Base 1: 1057
Page 1 of 1
Tue, Oct 21, 1997 6:27 AM
Mon, Oct 20, 1997 3:59 PM
Spacing: 12.22{12.22}
Arg
A

Figure 51

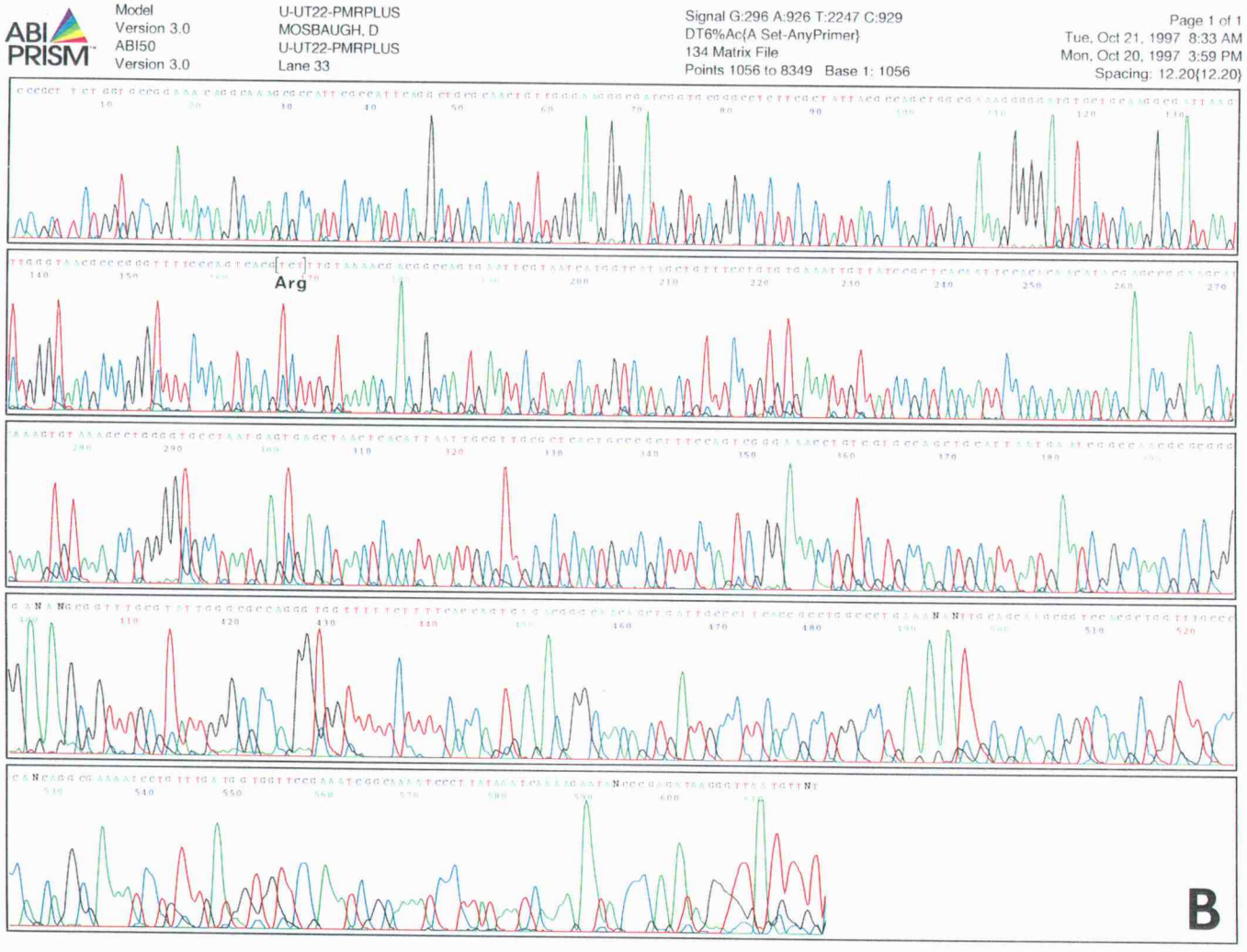

Figure 51 (continued)

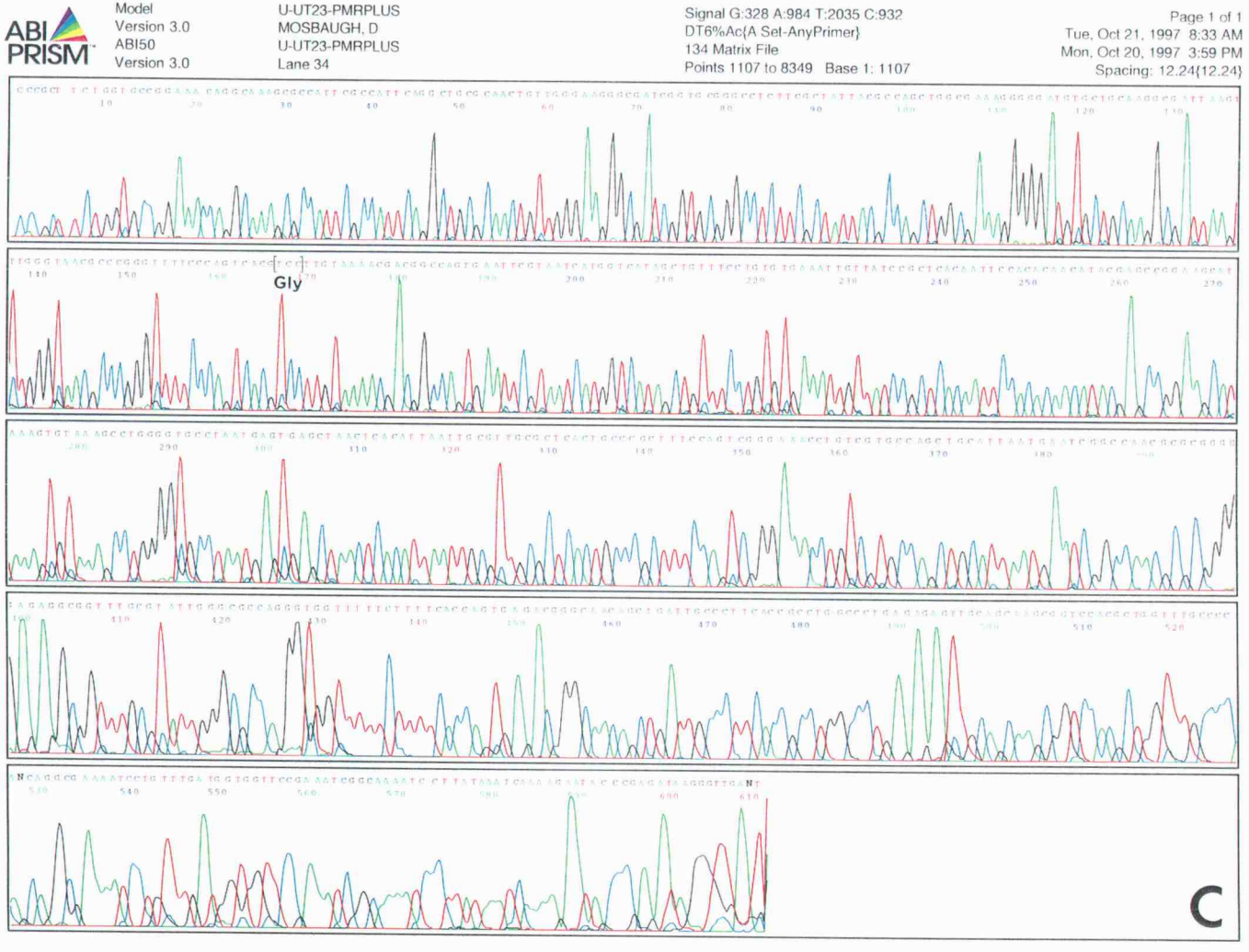

Figure 51 (continued)

Figure 52. Mutation spectrum of uracil-initiated base excision DNA repair synthesis in human U251 cell extracts. A standard BER reaction was performed using M13mp2op14 (U•T) DNA and human U251 whole cell extract as described in Table 7. Following transfection of Ung/Endo IV resistant Form I DNA into *E. coli* NR9162 cells, 78 blue plaques were isolated, single-stranded DNA purified and DNA sequenced over the *lacZα* gene target as described under "Experimental Procedures". The nucleotide sequence (TGA) for the opal codon opposite the transcribed (-) strand serves as the template strand for uracil-initiated base excision DNA repair synthesis and is indicated. Above each template nucleotide, the four possible deoxyribonucleotide triphosphates used for nucleotide incorporation are indicated with the coded amino acid (parenthesis). The number of individual base-substitution mutations observed from DNA sequence analysis are plotted.

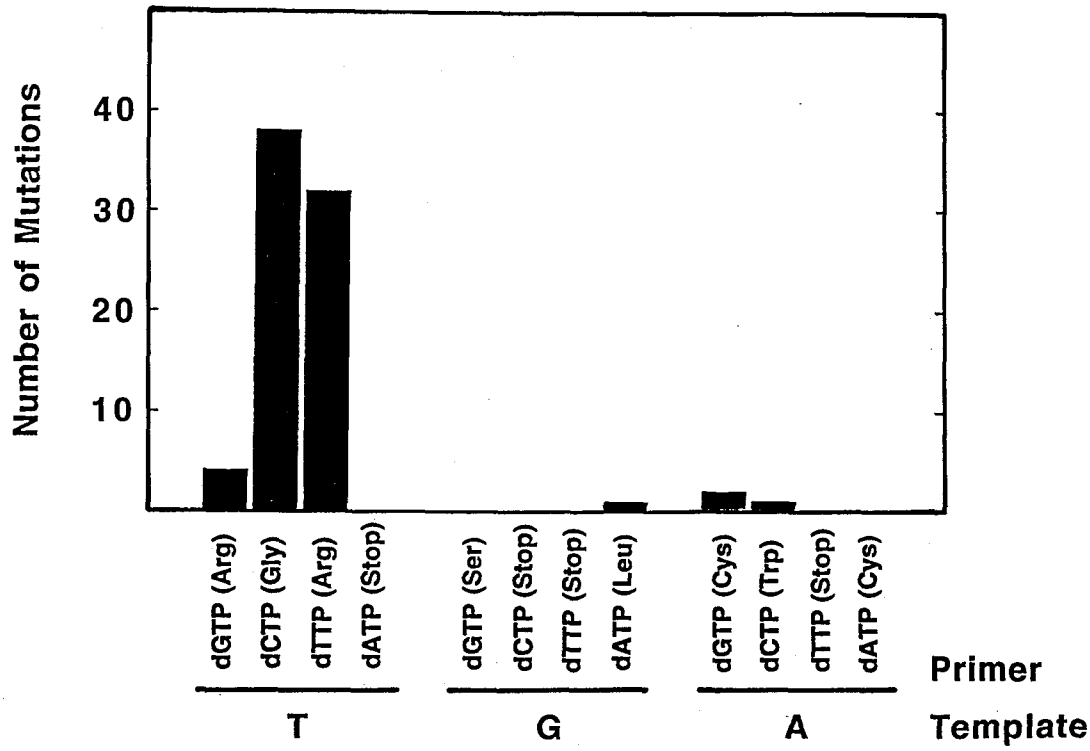
Number of Mutations
40
30
20
10
dGTP (Arg)
dCTP (Gly)
dTTP (Arg)
dATP (Stop)
dGTP (Ser)
dCTP (Stop)
dTTP (Stop)
dATP (Leu)
dGTP (Cys)
dCTP (Trp)
dTTP (Stop)
dATP (Cys)
Primer
T
G
A
Template

Figure 52

Table 8

Specificity of Mutations Produced by Uracil-Initiated Base Excision Repair in Human U251 Whole Cell Extracts

Revertant	Mispair (+/-)[a]	Codon Change[b]	Phenotype[c]
1	T/G	CGA (Arg)[d]	Dark
2	T/C	GGA (Gly)	Light
3	T/T	AGA (Arg)	Dark
4	A/G	TGC (Cys)	Dark
5	T/C	GGA (Gly)	Light
6	T/C	GGA (Gly)	Light
7	T/T	AGA (Arg)	Dark
8	T/T	AGA (Arg)	Dark
9	T/T	AGA (Arg)	Dark
10	T/T	AGA (Arg)	Dark
11	T/T	AGA (Arg)	Dark
12	T/T	AGA (Arg)	Dark
13	T/C	GGA (Gly)	Light
14	T/T	AGA (Arg)	Dark
15	T/C	GGA (Gly)	Light
16	T/T	AGA (Arg)	Dark
17	G/A	TTA (Leu)	Light
18	T/T	AGA (Arg)	Dark
19	T/C	GGA (Gly)	Light
20	T/C	GGA (Gly)	Light
21	T/C	GGA (Gly)	Light
22	T/T	AGA (Arg)	Dark
23	T/C	GGA (Gly)	Light
24	T/G	CGA (Arg)	Dark
25	T/C	GGA (Gly)	Light
26	T/C	GGA (Gly)	Light
27	T/T	AGA (Arg)	Dark
28	T/C	GGA (Gly)	Light
29	T/C	GGA (Gly)	Light
30	T/C	GGA (Gly)	Light
31	T/C	GGA (Gly)	Light
32	T/T	AGA (Arg)	Dark
33	T/T	AGA (Arg)	Dark
34	T/T	AGA (Arg)	Dark
35	T/C	GGA (Gly)	Light
36	T/C	GGA (Gly)	Light
37	T/T	AGA (Arg)	Dark
38	T/G	CGA (Arg)	Dark
39	T/T	AGA (Arg)	Dark
40	T/C	GGA (Gly)	Light
41	T/T	AGA (Arg)	Dark
42	T/C	GGA (Gly)	Light

Table 8 (continued)

Specificity of Mutations Produced by Uracil-Initiated Base Excision Repair in Human U251 Whole Cell Extracts

Revertant	Mispair (+/-)[a]	Codon Change[b]	Phenotype[c]
43	T/T	AGA (Arg)[d]	Dark
44	T/C	GGA (Gly)	Light
45	T/T	AGA (Arg)	Dark
46	T/G	CGA (Arg)	Dark
47	T/T	AGA (Arg)	Dark
48	T/T	AGA (Arg)	Dark
49	T/T	AGA (Arg)	Dark
50	T/C	GGA (Gly)	Light
51	T/C	GGA (Gly)	Light
52	T/C	GGA (Gly)	Light
53	T/T	AGA (Arg)	Dark
54	T/C	GGA (Gly)	Light
55	A/G	TGC (Cys)	Dark
56	T/C	GGA (Gly)	Light
57	T/C	GGA (Gly)	Light
58	T/C	GGA (Gly)	Light
59	T/T	AGA (Arg)	Dark
60	T/C	GGA (Gly)	Light
61	T/C	GGA (Gly)	Light
62	A/C	TGG (Trp)	Dark
63	T/C	GGA (Gly)	Light
64	T/T	AGA (Arg)	Dark
65	T/C	GGA (Gly)	Light
66	T/C	GGA (Gly)	Light
67	T/C	GGA (Gly)	Light
68	T/T	AGA (Arg)	Dark
69	T/C	GGA (Gly)	Light
70	T/T	AGA (Arg)	Dark
71	T/C	GGA (Gly)	Light
72	T/C	GGA (Gly)	Light
73	T/T	AGA (Arg)	Dark
74	T/T	AGA (Arg)	Dark
75	T/T	AGA (Arg)	Dark
76	T/C	GGA (Gly)	Light
77	T/T	AGA (Arg)	Dark
78	T/C	GGA (Gly)	Light

[a] Denotes the mispair produced by uracil-initiated base excision DNA repair synthesis as extrapolated from the DNA sequence analysis of individual revertants. The template (+) strand nucleotide and the misincorporated opposite (-) strand nucleotide within opal (TGA) codon 14 are indicated.
[b] The nucleotide sequence of the opal codon for individual revertants was determined by DNA sequence analysis as described under "Experimental Procedures" and the single-base substitution generated by the original mispair is underlined.
[c] Revertants included dark blue and light blue phenotypes.
[d] The amino acid for each codon change is indicated in parenthesis.

repaired M13mp2op14 (U•T) DNA into *E. coli* NR9162, a reversion frequency of 5.4 x 10^{-4} was observed which closely matched that obtained from human U251 whole cell extracts (Table 7 and 9). Interestingly, similar reversion frequencies were also measured for control M13mp2op14 (A•T) DNA after incubation with U251 or LoVo whole cell extracts and transfection into either *E. coli* MC1061 or NR9162 cells. Thus, incubation of this substrate with either extract apparently created a background level of mutation that does not differ between U251 and LoVo cells. Together, these results suggest that mismatch repair in both human whole cell extracts does not appear to influence the detection of misincorporations that occurred during the BER reaction.

Experiments were also conducted to measure the fidelity of Ugi-insensitive uracil-DNA repair using LoVo whole cell extracts supplemented with Ugi (Table 9). When Ung/Endo IV resistant Form I DNA was transfected into *E. coli* NR9162, a reversion frequency of 11.7 x 10^{-4} was observed which was ~2-fold greater than that observed for M13mp2op14 (U•T) DNA repaired by LoVo whole cell extract in the absence of Ugi. This value was also ~2.4-fold less than that of M13mp2op14 (U•T) DNA repaired by U251 whole cell extract in the presence of Ugi. Interestingly, transfection of the repaired Form I DNA into MC1061 cells yielded a reversion frequency of 2.4 x 10^{-4} and exhibited the 4- to 5-fold reduction previously observed following transfection of repaired Form I DNA substrates into cells capable of removing mispairs from the unmethylated (-) strand. Comparison of this result to those obtained for U251 whole cell extracts suggests that the repaired Form I DNA from U251 extracts did not contain endogenous mispairs for the MC1061 methyl-directed mismatch repair machinery to correct, perhaps due to the fixation of potential mispairs during incubation with the whole cell extract protein. Overall, these results suggest that the Ugi-insensitive uracil-DNA repair pathway in LoVo cells is also more error prone than that of the predominantly uracil-DNA glycosylase initiated uracil BER pathway.

Table 9

Frequency of Mutations Produced by Uracil-Initiated Base Excision Repair in Human LoVo Whole Cell Extracts

Standard base excision DNA repair reaction mixtures (500 µl) were prepared containing 1 mg of human LoVo whole cell extract protein and either 5 µg of M13mp2op14 (U•T) or (A•T) DNA. After incubation at 30°C for 45 minutes, reactions were terminated, DNA products recovered, and Form I DNA that was resistant to *E. coli* Ung/Endo IV treatment was isolated by 0.8% agarose gel electrophoresis as described under "Experimental Procedures". Form I DNA was then transfected into *E. coli* NR9162 and MC1061 cells as indicated below and the M13mp2 lacZα DNA-based reversion assay was performed as described by Kunkel (130).

	NR9162 (mutS$^-$)			MC1061 (mutS$^+$)		
	Plaques Scored			Plaques Scored		
DNA (-/+)[b]	Total	Blue	Reversion Frequency[a] (x10^{-4})	Total	Blue	Reversion Frequency (x10^{-4})
Control[c]						
A/T	216,840	17	0.78	251,680	2	0.079
U/T	176,540	81	4.6	211,770	44	2.1
LoVo WCE						
A/T	222,820	7	0.31	48,490	2	0.41
U/T	121,290	66	5.4	162,240	28	1.7
LoVo WCE + Ugi[d]						
U/T	163,670	191	11.7	141,960	34	2.4

[a] Reversion frequencies were calculated by dividing the number of blue plaques scored by the total number of blue plus colorless plaques. Revertants included dark blue and light blue phenotypes.

[b] Denotes the (-) and (+) strand nucleotide at the target site.

[c] Control reaction mixtures (500 µl) contained 5 µg of M13mp2op14 (U•T) or (A•T) DNA and substituted whole cell extract (WCE) dialysis buffer (25 mM Hepes-KOH, 100 mM KCl, 2 mM DTT, 12 mM $MgCl_2$, 1 mM EDTA, and 17% (w/v) glycerol adjusted to pH 7.9) instead of human whole cell extract protein in standard BER reaction mixtures.

[d] A standard reaction mixture (500 µl) was prepared as described under "Experimental Procedures" except that 1000 units of Ugi (~100-fold unit excess over whole cell extract UDG) was added before the substrate addition.

4.1.12 Mutational Spectrum of Human LoVo Cells

A preliminary mutational analysis of individual revertant M13 phage DNA was performed to define the types of misincorporation events that occurred during uracil-initiated base excision DNA repair synthesis in LoVo whole cell extracts. Single-stranded DNA was isolated and sequenced from 59 of the 66 blue plaques obtained from repaired DNA produced in LoVo whole cell extracts in the absence of Ugi. The distribution and specificity of single-base substitutions located within the opal codon are shown in Figure 53A and Table 10, respectively. Fifty four (90 %) mutations occurred at the first nucleotide of the opal codon while six (10 %) mutations were detected at the third nucleotide position. One double mutant containing base substitutions at both the first and third nucleotide positions of the opal codon was detected. As observed for repaired DNA in U251 whole cell extracts, almost all of the base substitutions were detected at the location of the uracil target. Similarly, ~91 % of the base substitution at this site promoted transversion mutations and were represented by T to G (~61 %) and T to A (~39 %) changes in the (+) strand template. Five mutations (~9 %) were scored as T to C transitions. These results defined the uracil-initiated base excision repair-mediated mutation spectrum at this site and did not appear to differ significantly between U251 and LoVo cells.

A limited investigation of mutations introduced during the Ugi-insensitive uracil-DNA repair pathway in LoVo whole cell extracts was also conducted. Single-stranded DNA was isolated from 24 of the 191 blue plaques obtained from repaired Form I DNA transfected into *E. coli* NR9162 cells and DNA sequence analysis was performed. The distribution and specificity of single-base substitutions located within the opal codon are shown in Figure 53B and Table 11, respectively. All of the mutations were detected at the first nucleotide position of the opal codon. All base substitutions were scored as transversion mutations and were represented as T to G (71 %) and T to A (29 %) changes in the (+) strand template. These results define the mutation

Figure 53. Mutation spectrum of uracil-initiated base excision DNA repair synthesis in human LoVo cell extracts. Standard BER reactions were performed using M13mp2op14 (U•T) DNA and human LoVo whole cell extract as described in Table 9. Following transfection of Ung/Endo IV resistant Form I DNA into *E. coli* NR9162 cells, blue plaques were isolated, single-stranded DNA purified and DNA sequenced over the *lacZ*α gene target as described under "Experimental Procedures". The nucleotide sequence (TGA) for the opal codon opposite the transcribed (-) strand serves as the template strand for uracil-initiated base excision DNA repair synthesis and is indicated. Above each template nucleotide, the four possible deoxyribonucleoside triphosphates used for nucleotide incorporation are indicated with the coded amino acid (parenthesis). The number of individual base-substitution mutations observed from DNA sequence analysis from standard BER reaction mixtures incubated in the absence of Ugi (A) and the presence of Ugi (B) are plotted. The DNA sequences of 59 and 24 revertants from standard BER reaction mixtures containing LoVo whole cell extract and LoVo whole cell extract supplemented with Ugi, respectively, were analyzed.

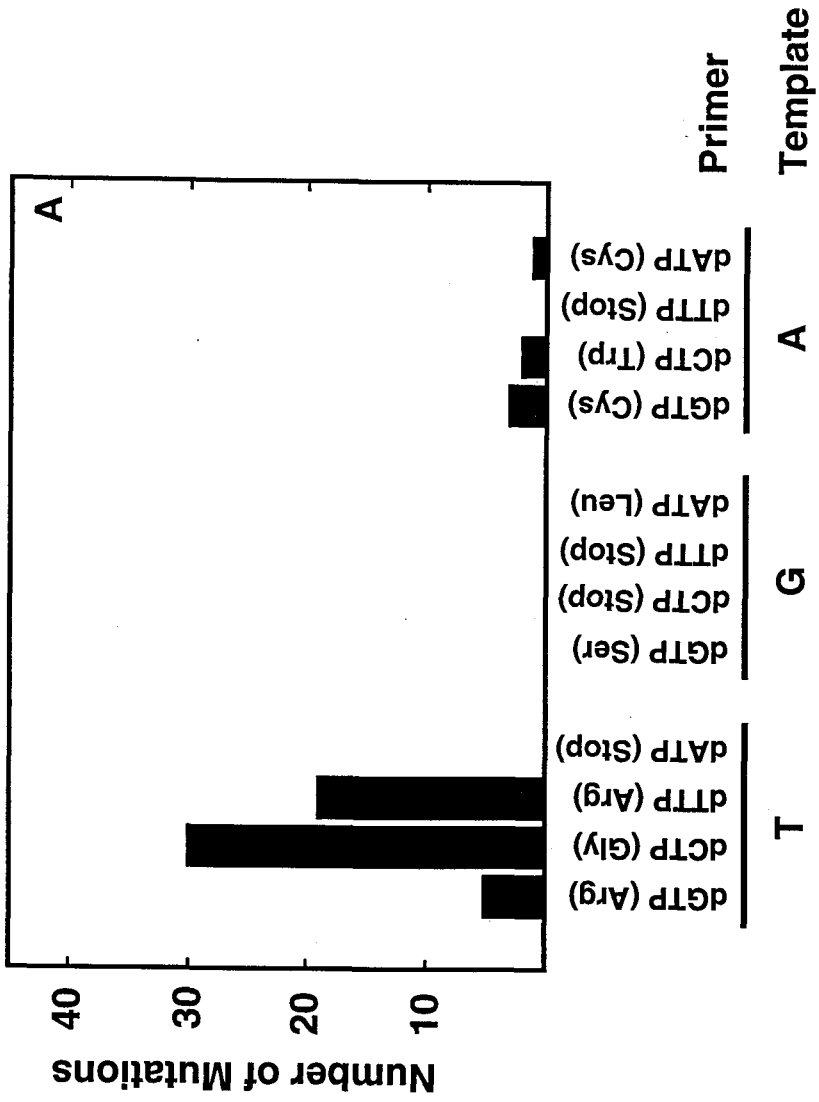
A
Number of Mutations
40
30
20
10
Template
Primer
T
dGTP (Arg)
dCTP (Gly)
dTTP (Arg)
dATP (Stop)
G
dGTP (Ser)
dCTP (Stop)
dTTP (Stop)
dATP (Leu)
A
dGTP (Cys)
dCTP (Trp)
dTTP (Stop)
dATP (Cys)

Figure 53

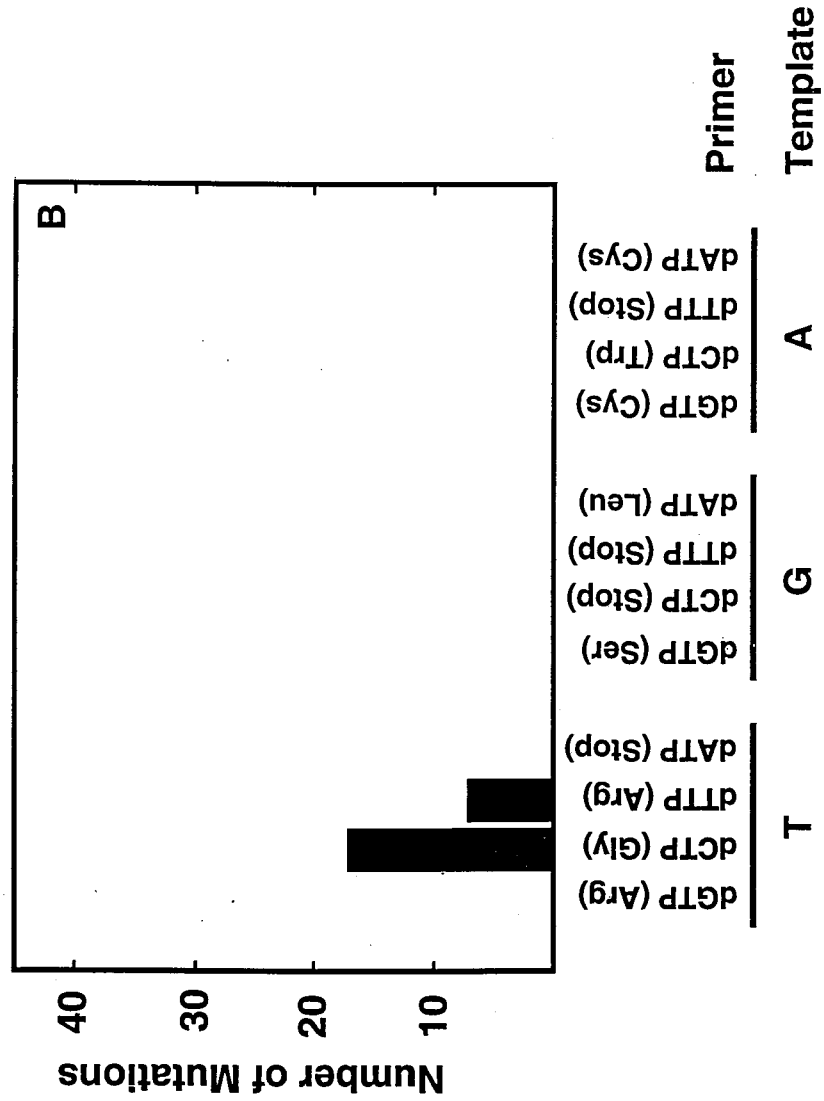

Figure 53 (continued)

Table 10

Specificity of Mutations Produced by Uracil-Initiated Base Excision Repair in Human LoVo Whole Cell Extracts

Revertant	Mispair (+/-)[a]	Codon Change[b]	Phenotype[c]
1	T/C	GGA (Gly)[d]	Light
2	A/G	TGC (Cys)	Dark
3	T/C	GGA (Gly)	Light
4	T/T	AGA (Arg)	Dark
5	T/C	GGA (Gly)	Light
6	T/T	AGA (Arg)	Dark
7	T/C	GGA (Gly)	Light
8	T/T, A/A	AGT (Ser)	Dark
9	T/C	GGA (Gly)	Light
10	T/G	CGA (Arg)	Dark
11	T/C	GGA (Gly)	Light
12	T/C	GGA (Gly)	Light
13	T/C	GGA (Gly)	Light
14	T/C	GGA (Gly)	Light
15	T/C	GGA (Gly)	Light
16	A/G	TGC (Cys)	Dark
17	T/C	GGA (Gly)	Light
18	T/G	CGA (Arg)	Dark
19	T/C	GGA (Gly)	Light
20	T/C	GGA (Gly)	Light
21	T/C	GGA (Gly)	Light
22	T/T	AGA (Arg)	Dark
23	T/T	AGA (Arg)	Dark
24	T/C	GGA (Gly)	Light
25	T/C	GGA (Gly)	Light
26	T/C	GGA (Gly)	Light
27	T/T	AGA (Arg)	Dark
28	T/G	CGA (Arg)	Dark
29	T/T	AGA (Arg)	Dark
30	T/C	GGA (Gly)	Light
31	T/G	CGA (Arg)	Dark
32	T/T	AGA (Arg)	Dark
33	T/C	GGA (Gly)	Light
34	T/C	GGA (Gly)	Light
35	T/T	AGA (Arg)	Dark
36	T/C	GGA (Gly)	Light
37	T/C	GGA (Gly)	Light
38	T/T	AGA (Arg)	Dark
39	T/C	GGA (Gly)	Light
40	T/C	GGA (Gly)	Light
41	T/C	GGA (Gly)	Light
42	T/G	CGA (Arg)	Dark

Table 10 (continued)

Specificity of Mutations Produced by Uracil-Initiated Base Excision Repair in Human LoVo Whole Cell Extracts

Revertant	Mispair (+/-)[a]	Codon Change[b]	Phenotype[c]
43	A/C	TG**G** (Trp)	Dark
44	T/T	**A**GA (Arg)	Dark
45	T/T	**A**GA (Arg)	Dark
46	T/C	**G**GA (Gly)	Light
47	T/T	**A**GA (Arg)	Dark
48	T/T	**A**GA (Arg)	Dark
49	A/G	TG**C** (Cys)	Dark
51	T/T	**A**GA (Arg)	Dark
52	T/C	**G**GA (Gly)	Light
53	T/T	**A**GA (Arg)	Dark
54	T/C	**G**GA (Gly)	Light
59	T/T	**A**GA (Arg)	Dark
60	T/T	**A**GA (Arg)	Dark
62	T/C	**G**GA (Gly)	Light
63	T/T	**A**GA (Arg)	Dark
64	A/C	TG**G** (Trp)	Dark
65	T/C	**G**GA (Gly)	Light

[a] Denotes the mispair produced by uracil-initiated base excision DNA repair synthesis as extrapolated from the DNA sequence analysis of individual revertants. The template (+) strand nucleotide and the misincorporated opposite (-) strand nucleotide within opal (TGA) codon 14 are indicated.

[b] The nucleotide sequence of the opal codon for individual revertants was determined by DNA sequence analysis as described under "Experimental Procedures" and the single-base substitution generated by the original mispair is underlined.

[c] Revertants included dark blue and light blue phenotypes.

[d] The amino acid for each codon change is indicated in parenthesis.

Table 11

Specificity of Mutations Produced by Uracil-Initiated Base Excision Repair in Human LoVo Whole Cell Extracts in the Presence of Ugi

Revertant	Mispair (+/-)[a]	Codon Change[b]	Phenotype[c]
1	T/C	GGA (Gly)	Light
2	T/C	GGA (Gly)	Light
3	T/C	GGA (Gly)	Light
4	T/C	GGA (Gly)	Light
5	T/C	GGA (Gly)	Light
6	T/C	GGA (Gly)	Light
7	T/T	AGA (Arg)	Dark
8	T/C	GGA (Gly)	Light
89	T/C	GGA (Gly)	Light
90	T/C	GGA (Gly)	Light
91	T/C	GGA (Gly)	Light
92	T/T	AGA (Arg)	Dark
93	T/T	AGA (Arg)	Dark
94	T/C	GGA (Gly)	Light
95	T/T	AGA (Arg)	Dark
96	T/C	GGA (Gly)	Light
149	T/C	GGA (Gly)	Light
150	T/T	AGA (Arg)	Dark
151	T/T	AGA (Arg)	Dark
152	T/C	GGA (Gly)	Light
153	T/C	GGA (Gly)	Light
154	T/C	GGA (Gly)	Light
155	T/T	AGA (Arg)	Dark
156	T/C	GGA (Gly)	Light

[a] Denotes the mispair produced by uracil-initiated base excision DNA repair synthesis as extrapolated from the DNA sequence analysis of individual revertants. The template (+) strand nucleotide and the misincorporated opposite (-) strand nucleotide within opal (TGA) codon 14 are indicated.

[b] The nucleotide sequence of the opal codon for individual revertants was determined by DNA sequence analysis as described under "Experimental Procedures" and the single-base substitution generated by the original mispair is underlined.

[c] Revertants included dark blue and light blue phenotypes.

[d] The amino acid for each codon change is indicated in parenthesis.

spectrum of the Ugi-insensitive uracil-DNA repair pathway at this site. The overall distribution of mutations across the opal codon does not significantly differ from distributions observed for Ugi-sensitive uracil-initiated base excision DNA repair synthesis in U251 and LoVo cells. The frequency of each individual type of transition and transversion mutation introduced during Ugi sensitive and insensitive uracil-initiated DNA repair in human whole cell extracts was represented in Table 12.

4.1.13 Sensitivity of Uracil-DNA Repair Synthesis in Human Whole Cell Extracts to Aphidicolin

To determine the effect of aphidicolin on the activity of α-like DNA polymerases present in U251 or LoVo whole cell extracts, DNA synthesis reactions containing activated calf thymus DNA and [^{3}H]dTTP were supplemented with increasing concentrations of aphidicolin and standard DNA polymerase assays were conducted as described under "Experimental Procedures". Polymerase activity in both U251 and LoVo whole cell extracts exhibited similar levels of sensitivity to aphidicolin and incorporation of [^{3}H]dTMP decreased as a function of increasing aphidicolin concentration (Figure 54). The inhibitory effect of aphidicolin appeared to reach saturation at concentrations of 25 and 50 μM as exhibited by the reduction of DNA polymerase activity by ~80 % and ~83 %, respectively, relative to the control reactions lacking aphidicolin. These results confirm the presence of α-like DNA polymerase activity in U251 and LoVo whole cell extracts under standard BER reaction conditions and their susceptibility to the inhibitory effects of aphidicolin.

To determine if α-like DNA polymerase(s) participated in the DNA repair synthesis step associated with uracil-initiated base excision repair in U251 or LoVo whole cell extracts, standard BER reactions containing increasing concentrations of aphidicolin were incubated with M13mp2op14 (U•T) DNA. As before, the recovered DNA was treated with excess Ung and

Table 12

Frequency of Transition and Transversion Mutations Introduced by Uracil-Initiated Base Excision Repair in Human Whole Cell Extracts

	U251		LoVo		LoVo + Ugi	
	Mutations[a]	Reversion Frequency[b] ($x10^{-4}$)	Mutations	Reversion Frequency[c] ($x10^{-4}$)	Mutations	Reversion Frequency[c] ($x10^{-4}$)
Transition Mispairs						
T→C	4	0.27	5 (~5)[d]	0.41	-	-
G→A	-	-	-	-	-	-
A→G	1	0.07	2 (~2)	0.16	-	-
Transversion Mispairs						
T→G	38	2.5	30 (~34)	2.8	17 (~135)	8.2
T→A	32	2.1	19 (~21)	1.7	7 (~56)	3.4
G→C	-	-	-	-	-	-
G→T	1	0.07	-	-	-	-
A→C	2	0.13	3 (~3)	0.25	-	-
A→T	-	-	1 (~1)	0.08	-	-

[a] The number of specific transition and transversion mutation types are derived from the mutation spectrum generated by the transfection of repaired M13mp2op14 (U•T) Form I DNA into *E. coli* NR9162 cells.

[b] Reversion frequencies for each category of mutation were calculated by dividing the number of specific mutations by the total number of blue plus colorless plaques indicated on Table 7.

[c] Reversion frequencies for each category of mutation were calculated by dividing the estimated number of specific mutations by the total number of blue plus colorless plaques indicated on Table 9.

[d] Numbers in parenthesis correspond to the predicted number of specific mutations for each category since all revertants have not been sequenced. This value was obtained by dividing the number of mutations for each type of mutation by the total number of revertants sequenced and then multiplying by the total number of revertants scored.

Figure 54. *In vitro* inhibition of DNA polymerase activity by aphidicolin in U251 and LoVo cell extracts. DNA polymerase activity was assayed under standard BER reaction conditions in reaction mixtures (100 µl) containing 20 µg of U251 or LoVo whole cell extract protein, 10 µg of activated calf thymus DNA and [^{3}H]dTTP (1700 cpm/pmol). Reaction mixtures were supplemented with 0, 1, 5, 10, 25, and 50 µM aphidicolin in DMSO prior to the addition of substrate and incubated for 60 min (U251) or 45 min (LoVo) at 30°C. Reactions were terminated on ice by the addition of 1 mg/ml BSA in 0.1 M sodium pyrophosphate (200 µl), DNA precipitated with 10% (saturated) trichloroacetic acid, and acid-insoluble DNA was collected on #30 glass fiber filters and analyzed for [^{3}H]dTMP incorporation. The percentage of polymerase activity detected in U251 (*closed circles*) and LoVo (*open circles*) whole cell extracts for each aphidicolin concentration was determined as the amount of [^{3}H]dTMP incorporated in the presence of aphidicolin divided by the amount of [^{3}H]dTMP incorporated in the absence of aphidicolin and multiplied by 100. The amount of [^{3}H]dTMP (1,700 cpm/pmol) incorporated into activated calf thymus DNA that represents 100 % DNA polymerase activity for U251 and LoVo cell extracts was 19.9 and 9.8 pmol of [^{3}H]dTMP, respectively.

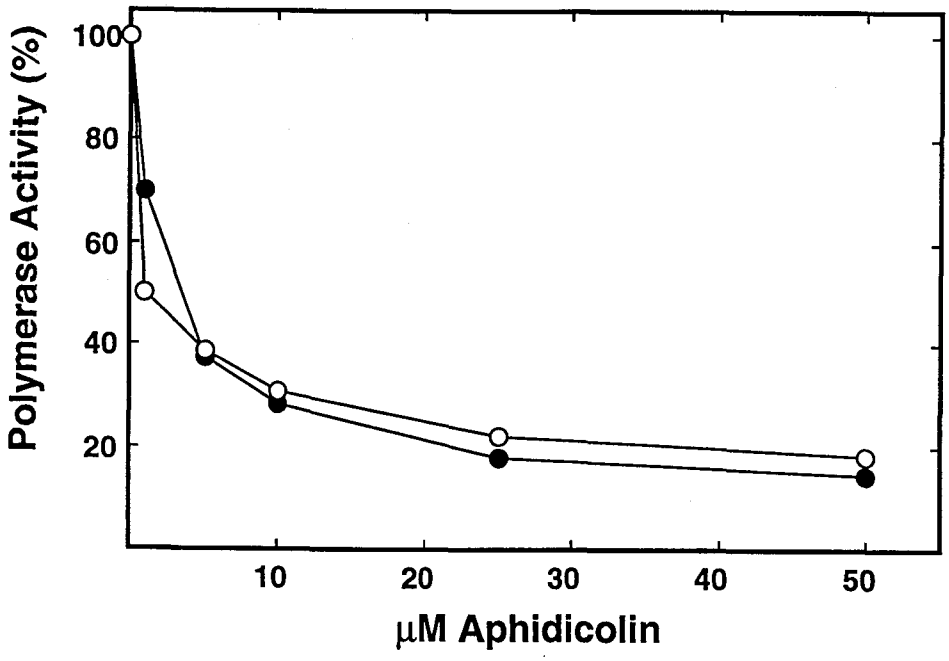
Polymerase Activity (%)
100
80
60
40
20
10
20
30
40
50
μM Aphidicolin

Figure 54

Endo IV prior to resolving the reaction products by agarose gel electrophoresis (Figure 55A and B). Analysis of the ethidium bromide stained gels revealed similar ratios of Ung/Endo IV resistant Form I DNA to Form II DNA in each BER reaction containing U251 (Figure 55A, lanes 6-10) or LoVo (Figure 55B, lanes 6-10) whole cell extract proteins. As controls, standard BER reactions lacking aphidicolin (Figure 55A and B, lane 5) or the aphidicolin solubilization reagent, DMSO (Figure 55A and B, lane 4), were similarly analyzed. The percentage of Form I DNA detected in lanes 5-10 was determined and was represented for U251 and LoVo whole cell extracts (Figure 56A and B, respectively). The percentage of repaired Form I DNA between aphidicolin concentrations of 1 and 50 μM did not significantly differ for U251 (50 % and 40 %, respectively) and LoVo (55 % and 48 %, respectively) cell extracts. Together, these results suggest that the α-like DNA polymerase(s) present in U251 and LoVo whole cell extracts contribute only a minor percentage (20 % and 13 %, respectively) of the DNA repair synthesis activity associated with uracil-initiated base excision repair under these reaction conditions.

4.1.14 Determination of the Repair Patch Size Generated During Uracil-Initiated DNA Repair in Human U251 and LoVo Whole Cell Extracts

A radioactively labeled [^{32}P]M13mp2op14 (U•T) DNA substrate was constructed by introducing a site-specific [^{32}P]dCMP residue at nucleotide position 90 (corresponding the 5'-terminal nucleotide of the [^{32}P]U-23-mer primer) during the primer extension reaction as described under "Experimental Procedures". Thus, the location of the [^{32}P]dCMP residue in the (-) strand between the uracil-target and the *Sma*I restriction site enabled autoradiographic detection of DNA bands following restriction with endonucleases *Eco*RI and *Sma*I. Standard BER reactions containing [^{32}P]M13mp2op14 (U•T) DNA and all four dNTP[αS] precursors were prepared in order to detect the 3' boundary of the repair patch introduced during uracil-

Figure 55. Effect of aphidicolin on uracil-DNA base excision repair in human U251 and LoVo cell extracts. (A) Standard BER reaction mixtures (100 µl) containing 1 µg of M13mp2op14 (U•T) DNA, 200 µg of U251 whole cell extract protein, and 20 µCi of [^{32}P]dATP were supplemented with 0, 1, 5, 10, 25, and 50 µM aphidicolin in DMSO (lanes 5-10, respectively). Samples were incubated for 60 min at 30°C and terminated by addition of 2000 units of Ugi followed by adjustment to 20 mM EDTA. As controls, M13mp2op14 (U•T) DNA (1 µg) was supplemented with whole cell extract dialysis buffer (lane 3) or with 200 µg of U251 whole cell extract protein (lane 4) in reaction mixtures lacking DMSO. DNA was isolated, treated with *E. coli* Ung and Endo IV, and analyzed by 0.8% agarose gel electrophoresis as described under "Experimental Procedures". Untreated M13mp2op14 (U•T) DNA (100 ng) and a sample containing 2.5 µg of a 1-kb DNA ladder (Gibco BRL) were analyzed as reference standards (lanes 2 and 1, respectively). (B) Standard BER reaction mixtures containing LoVo whole cell extract protein were analyzed as described above except samples were incubated for 45 min at 30°C. The locations of ethidium bromide-stained Form I and II DNA are indicated by *arrows*.

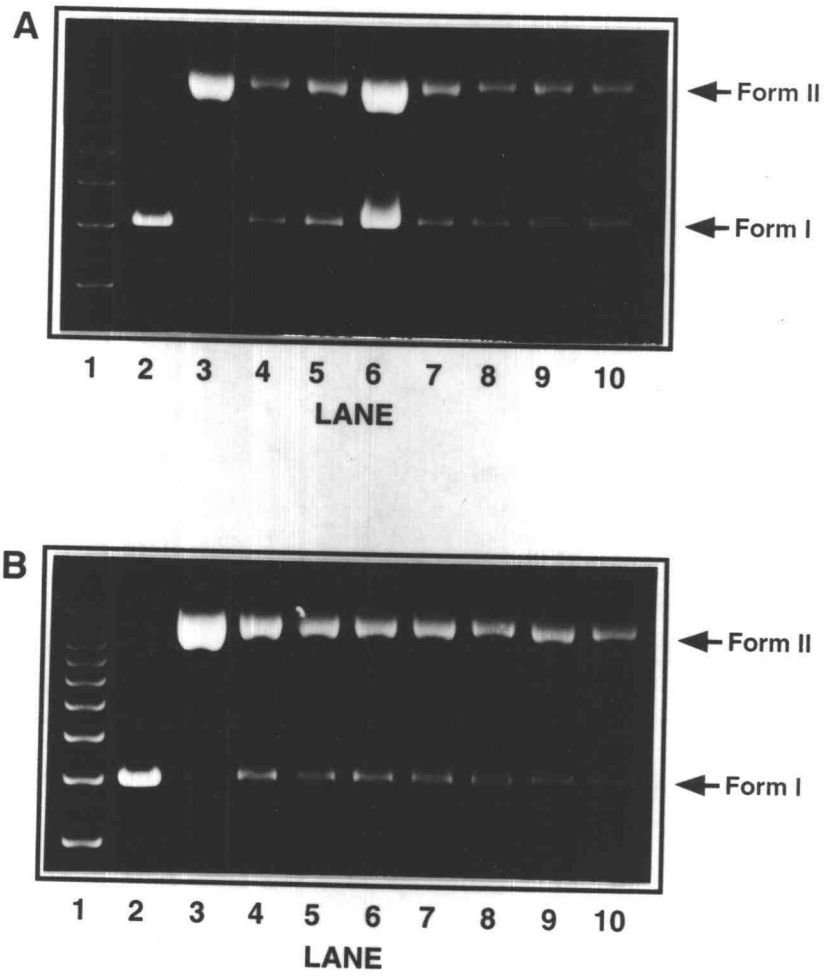
A
Form II
Form I
1 2 3 4 5 6 7 8 9 10
LANE
B
Form II
Form I
1 2 3 4 5 6 7 8 9 10
LANE

Figure 55

Figure 56. Quantitation of uracil-DNA base excision repair reaction products following aphidicolin treatment in human U251 and LoVo cell extracts. DNA bands detected by ethidium bromide staining in Figure 55 (A and B) were quantitated using a Gel Documentation System and the percentage of Form I DNA in the U251/aphidicolin titration series (A) and the LoVo/aphidicolin titration series (B) were determined. Amounts of Form I and II DNA were measured relative to standards (6.3-100 ng) analyzed on the same gel. After correcting for the ~0.38-fold reduction in ethidium bromide staining intensity of Form I DNA relative to Form II DNA, the percentage of Form I DNA was determined by dividing the amount of Form I DNA (ng) by that of Form I plus II DNA.

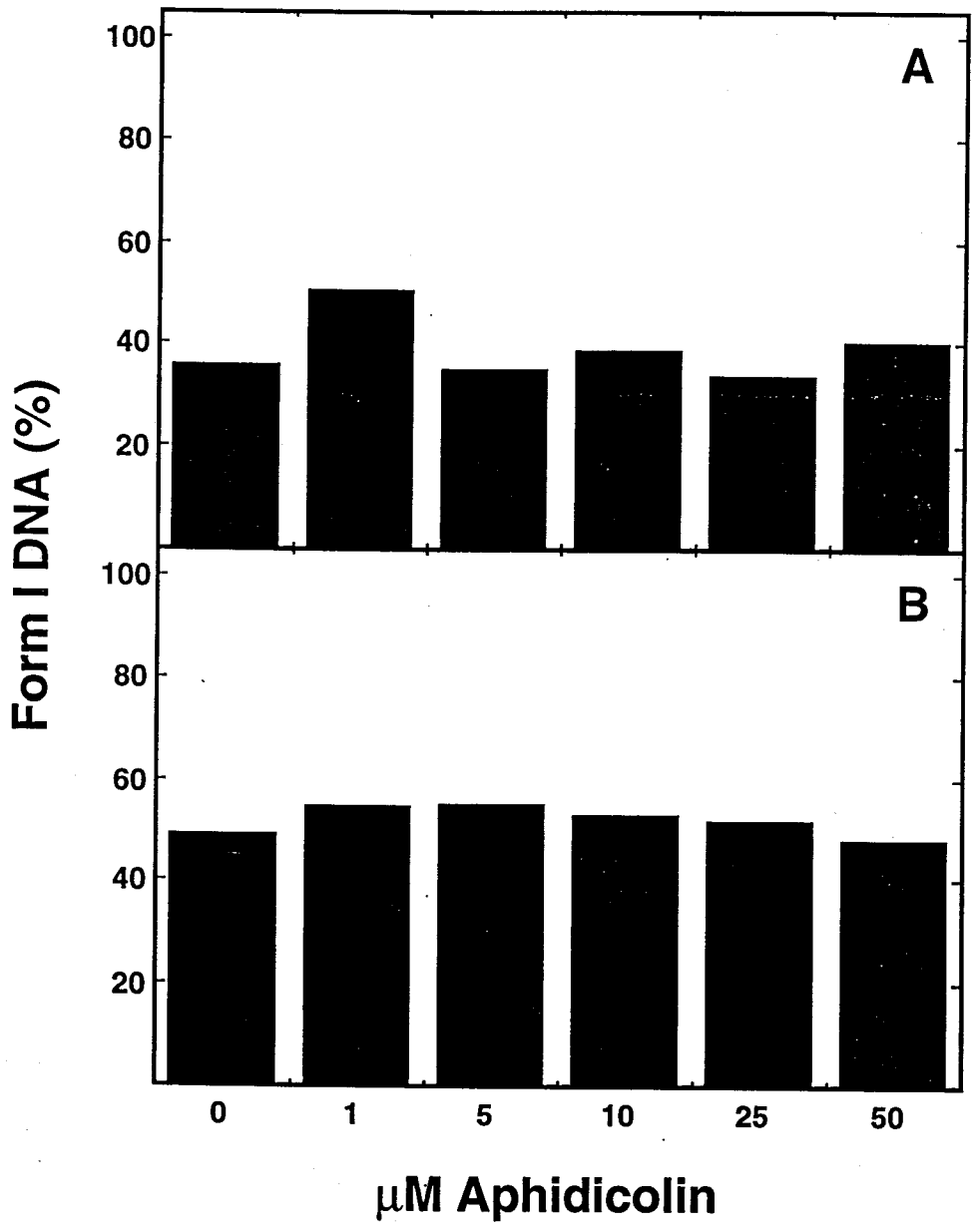

Figure 56

initiated base excision DNA repair synthesis in human whole cell extracts. Recovered DNA reaction products were restricted with *Eco*RI, which cuts after nucleotide position 57 in the (-) strand of the *lacZ*α gene, to generate linear DNA with a recessed 3' terminus located twenty nucleotides downstream from the uracil target. Linearized DNA reaction products were subsequently digested with *E. coli* exonuclease III (Exo III). This 3' to 5' exonuclease reportedly does not hydrolyze phosphorothioate DNA linkages (107, 218) and as a consequence, was expected to stop at the 3' border of the repair patch. Digested reaction products were subsequently restricted with *Sma*I, which cuts after nucleotide position 97 in the (-) strand, to generate small DNA fragments with 5' DNA termini located nineteen nucleotides upstream from the uracil target. DNA fragments were subsequently analyzed by denaturing 12 % polyacrylamide/8.3 M urea gel electrophoresis and autoradiography. Repair patches of one nucleotide in length were expected to produce a 20-bp DNA band following the *Eco*RI/Exo III/*Sma*I treatment since the incorporation of a single dNTP[αS] at the site of the uracil target blocked further digestion by Exo III. Thus, repair patches of two or more nucleotides in length were expected to produce corresponding DNA fragments of 21 or greater nucleotides in length due to the inability of Exo III to hydrolyze dNTP[αS] nucleotides incorporated during associated uracil-initiated DNA repair synthesis.

To optimize the amount of Exo III required to measure the 3' base excision repair patch boundary, samples (~200 ng) of LoVo BER reaction products (Form I and II DNA) recovered from a standard BER reaction mixture containing [^{32}P]M13mp2op14 (U•T) DNA and dNTP[αS] precursors were linearized with *Eco*RI and digested with various amounts of Exo III (0.16 - 1.6 x 10^{-8} units). After incubation with *Sma*I, [^{32}P]DNA fragments were resolved by denaturing 12 % polyacrylamide/8.3 M urea gel electrophoresis and the gel was subjected to autoradiography. Analysis of [^{32}P]DNA products digested with 0.16 and 0.016 units of Exo III resulted in the production of eight

predominant DNA bands that extended sequentially from 20 to 27 nucleotides in length (Figure 57, lanes 1 and 2). This result indicated that base excision repair patches of one to eight nucleotides in length were generated. The distribution of DNA fragments did not differ significantly between these two treatments and indicated that complete digestion of the substrate had occurred using an Exo III:DNA ratio of greater than 0.08:1 (units:μg DNA). However, incubation with smaller unit amounts of Exo III resulted in the production of incomplete Exo III digestion products (Figure 57, lanes 3-8). The 40-bp [^{32}P]DNA fragment was the expected result for a completely undigested *Eco*RI/*Sma*I restriction fragment corresponding to the (-) DNA strand. The 19-bp [^{32}P]DNA fragment was the expected product from an unsynthesized Form II DNA base excision repair intermediate containing an incised apyrimidinic site at the location of the uracil target. This DNA fragment appeared to represent ~50 % of the DNA repair products. Furthermore, this 19-bp DNA fragment was expected to be susceptible to Exo III digestion since dNMP[αS] incorporation had not occurred. Supporting this interpretation, the 19-bp DNA fragment was observed to be degraded by Exo III (Figure 57, lanes 1-3). Interestingly, base excision repair intermediates exhibiting limited DNA repair synthesis were not observed.

Experiments were conducted to determine the size and distribution of the DNA repair patches introduced during uracil-initiated DNA repair synthesis in U251 whole cell extracts. The influence of aphidicolin on the size and distribution of the repair patch was also investigated. Standard BER reactions containing all four dNTP[αS] precursors and [^{32}P]M13mp2op14 (U•T) DNA were prepared and samples (500 ng) of DNA reaction products isolated from standard BER reactions supplemented with no addition, 2000 units of Ugi, 50 μM aphidicolin, or 2000 units of Ugi and 50 μM aphidicolin were incubated with *Eco*RI (Figure 58). Linearized DNA was mock-digested or digested with 20, 2, or 0.2 units of Exo III as indicated in the figure legend, incubated with *Sma*I, and reaction products were analyzed by denaturing 12 %

Figure 57. Effect of exonuclease III concentration on determining the size of the uracil-initiated base excision repair patch. A standard BER reaction mixture (500 µl) containing 5 µg of [^{32}P]M13mp2op14 (U•T) DNA, 1 mg of human LoVo whole cell extract protein, and 20 µM each of dATPαS, dTTPαS, dCTPαS and dGTPαS was incubated at 30°C for 45 min and DNA reaction products were isolated and resuspended in TE buffer (80 µl). Samples (3.2 µl, ~200 ng) were removed for digestion with 10 units of *Eco*RI for 1 h at 25°C and then incubated with 0.16, 1.6 x 10^{-2}, 1.6 x 10^{-3}, 1.6 x 10^{-4}, 1.6 x 10^{-5}, 1.6 x 10^{-6}, 1.6 x 10^{-7}, and 1.6 x 10^{-8} units of *E. coli* exonuclease III (lanes 1-8, respectively) for 30 min at 37°C. Following Exo III digestion, reaction products were restricted with 10 units of *Sma*I for 1 h at 25°C. DNA reaction products were resolved by 12% polyacrylamide/8.3 M urea gel electrophoresis as described under "Experimental Procedures". The location of the 40-mer corresponding to the (-) strand *Eco*RI/*Sma*I restriction fragment and the 19-mer through 27-mer BER reaction products are located by *arrows* on the autoradiogram.

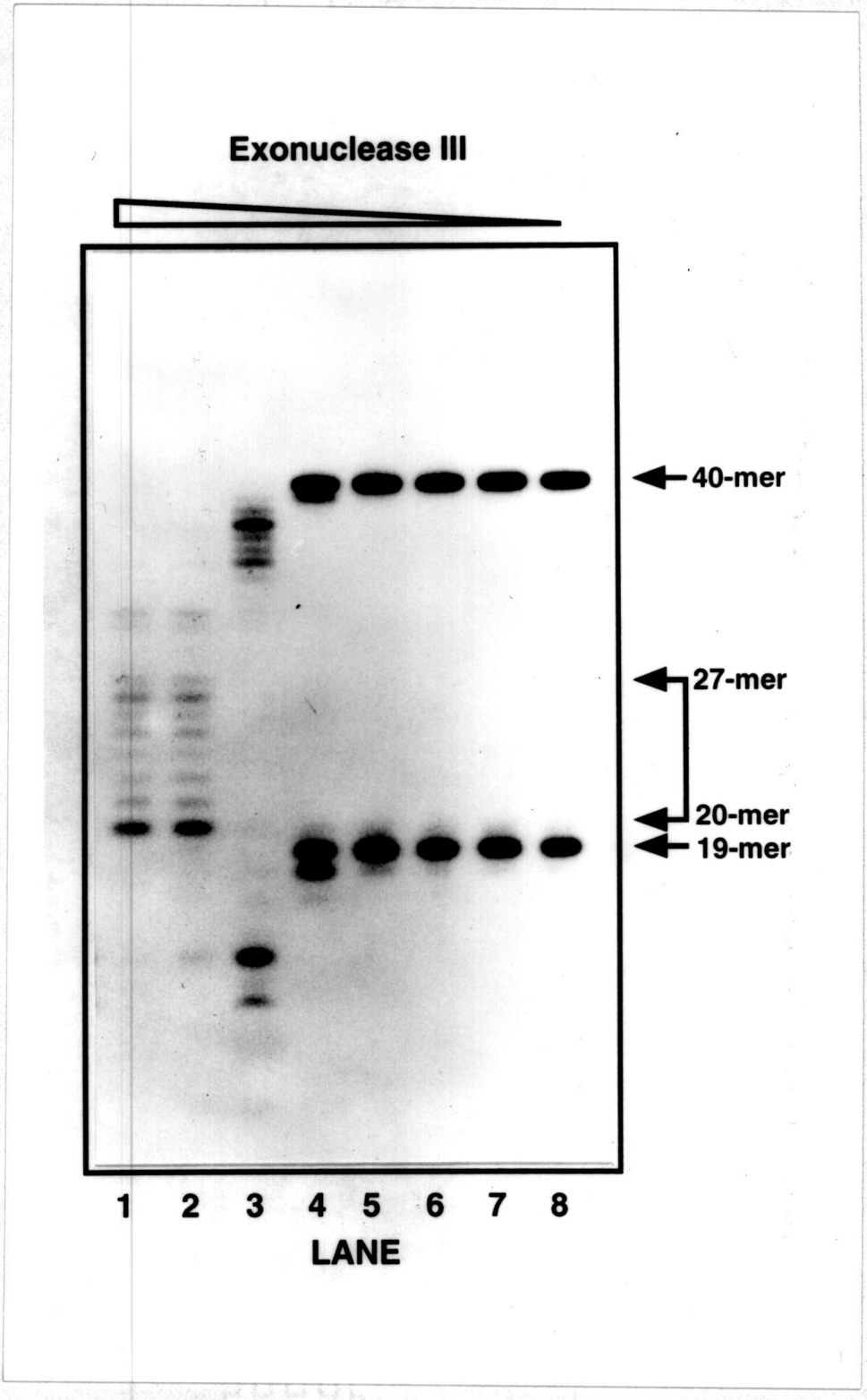

Figure 57

Figure 58. Effect of Ugi and aphidicolin on the 3' boundary of the repair patch introduced by uracil-initiated base excision repair in U251 cell extracts. Standard BER reaction mixtures (500 µl) containing 5 µg of [^{32}P]M13mp2op14 (U•T) DNA, 1 mg of human U251 whole cell extract protein, and 20 µM each of dATPαS, dTTPαS, dCTPαS and dGTPαS were supplemented with either no addition (lanes 3-6), 2000 units of Ugi (lanes 7-10), 50 µM aphidicolin (lanes 11-14), or 2000 units of Ugi and 50 µM aphidicolin (lanes 15-18). Reactions were incubated at 30°C for 60 min and DNA reaction products were isolated. Samples (8 µl, ~500 ng) were removed for digestion with 25 units of *Eco*RI for 1 h at 25°C. The linearized DNA was then incubated with no addition (lanes 3/7/11/15) or the addition of 20 units (lanes 4/8/12/16), 2 units (lanes 5/9/13/17), or 0.2 units (lanes 6/10/14/18) of *E. coli* Exo III for 30 min at 37°C. Following Exo III digestion, reaction products were treated with 25 units of *Sma*I for 1 h at 25°C. As controls, unreacted [^{32}P]M13mp2op14 (U•T) DNA (~500 ng) was incubated with *Eco*RI and *Sma*I (lane 1) or *Eco*RI, Exo III (0.2 units), and *Sma*I (lane 2). Following these reactions, DNA reaction products were resolved by 12% polyacrylamide/8.3 M urea gel electrophoresis as described under "Experimental Procedures". The location of the 40-mer corresponding to the (-) strand *Eco*RI/*Sma*I restriction fragment and the 19-mer through 27-mer BER reaction products are located by *arrows* on the autoradiogram.

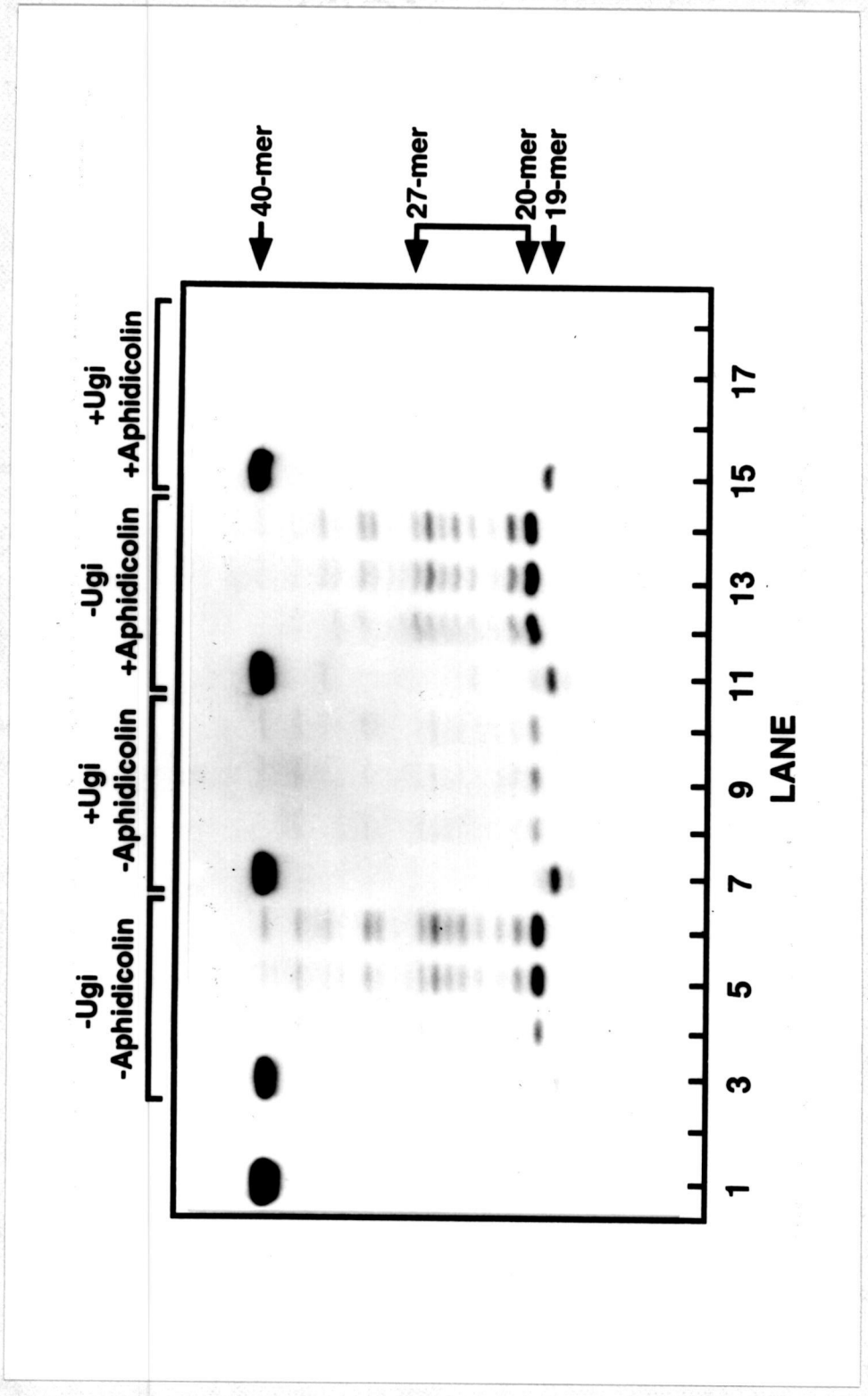
40-mer
27-mer
20-mer
19-mer
-Ugi
-Aphidicolin
+Ugi
-Aphidicolin
-Ugi
+Aphidicolin
+Ugi
+Aphidicolin
1
3
5
7
9
11
13
15
17
LANE

Figure 58

polyacrylamide/8.3 M urea gel electrophoresis and autoradiography was performed. As controls, unreacted [^{32}P]M13mp2op14 (U•T) DNA was incubated with *Eco*RI and *Sma*I (Figure 58, lane 1) or *Eco*RI, Exo III, and *Sma*I (Figure 58, lane 2). Incubation of the unreacted control with Exo III resulted in the complete digestion of the 40-mer [^{32}P]DNA fragment (lane 2). Thus, the incorporation of dNTP[αS] at and after the site of the uracil-target during uracil-DNA repair synthesis in whole cell extracts was required for resistance to Exo III digestion (Figure 58, lanes 4-6, 8-10, 12-14, 16-18). The relative intensity of DNA fragments of 20 to 27 nucleotides in length, which corresponded to DNA repair patches of one to eight nucleotides, respectively, were quantitated and plotted (Figure 59) for each reaction condition. The percentage of short patch BER (one nucleotide) and long patch BER (two to eight nucleotides) associated with uracil-DNA repair synthesis was also determined under these conditions (Table 13). Several observations can be derived from these results. First, the Ugi-sensitive uracil-DNA repair pathway initiated by uracil-DNA glycosylase produced repair patches consistent with a base excision repair mechanism since 36-38 % of the repair DNA synthesis involved short patch BER and 62-64 % involved long patch BER (Figure 58, lanes 4-6 and 12-14, Figure 59A and C, and Table 13). These results are similar for Ugi-insensitive uracil-DNA BER (Figure 58, lanes 8-10 and 16-18, Figure 59A and C, and Table 13). Second, standard BER reaction mixtures containing Ugi (Figure 59B and D) exhibited a 3.2- to 3.8-fold reduction in the relative intensity of Exo III resistant DNA reaction products as compared to equivalent BER reactions lacking Ugi (Figure 59A and C). Reduced levels of uracil-DNA repair were previously observed for the Ugi-insensitive BER pathway and are consistent with these results (Figure 38D). Third, the presence of a 19-mer in samples treated with *Eco*RI and *Sma*I but not Exo III (Figure 58, lanes 7 and 15) suggested that the Ugi-insensitive uracil-DNA BER reaction is initiated by a DNA glycosylase activity. The 19-mer [^{32}P]DNA product is the expected reaction intermediate following uracil base

Figure 59. Quantitation of repair patch sizes introduced by uracil-initiated base excision repair in U251 cell extracts under various conditions. Relative amounts of DNA reaction products detected by autoradiography in Figure 58 were determined using a PhosphorImager. The relative intensity of DNA bands of 20 to 27 nucleotides in length corresponded to BER repair patches of 1 to 8 nucleotides in length, respectively, and were measured for U251 whole cell extract reaction products digested with 20 units (*black bars*), 2 units (*white bars*) and 0.2 units (*grey bars*) of *E. coli* exonuclease III as described under "Experimental Procedures". Relative intensity values of individual DNA bands were plotted after subtracting background values for standard BER reactions containing no addition (A), 2000 units of Ugi (B), 50 μM aphidicolin (C), and 2000 units of Ugi and 50 μM aphidicolin (D).

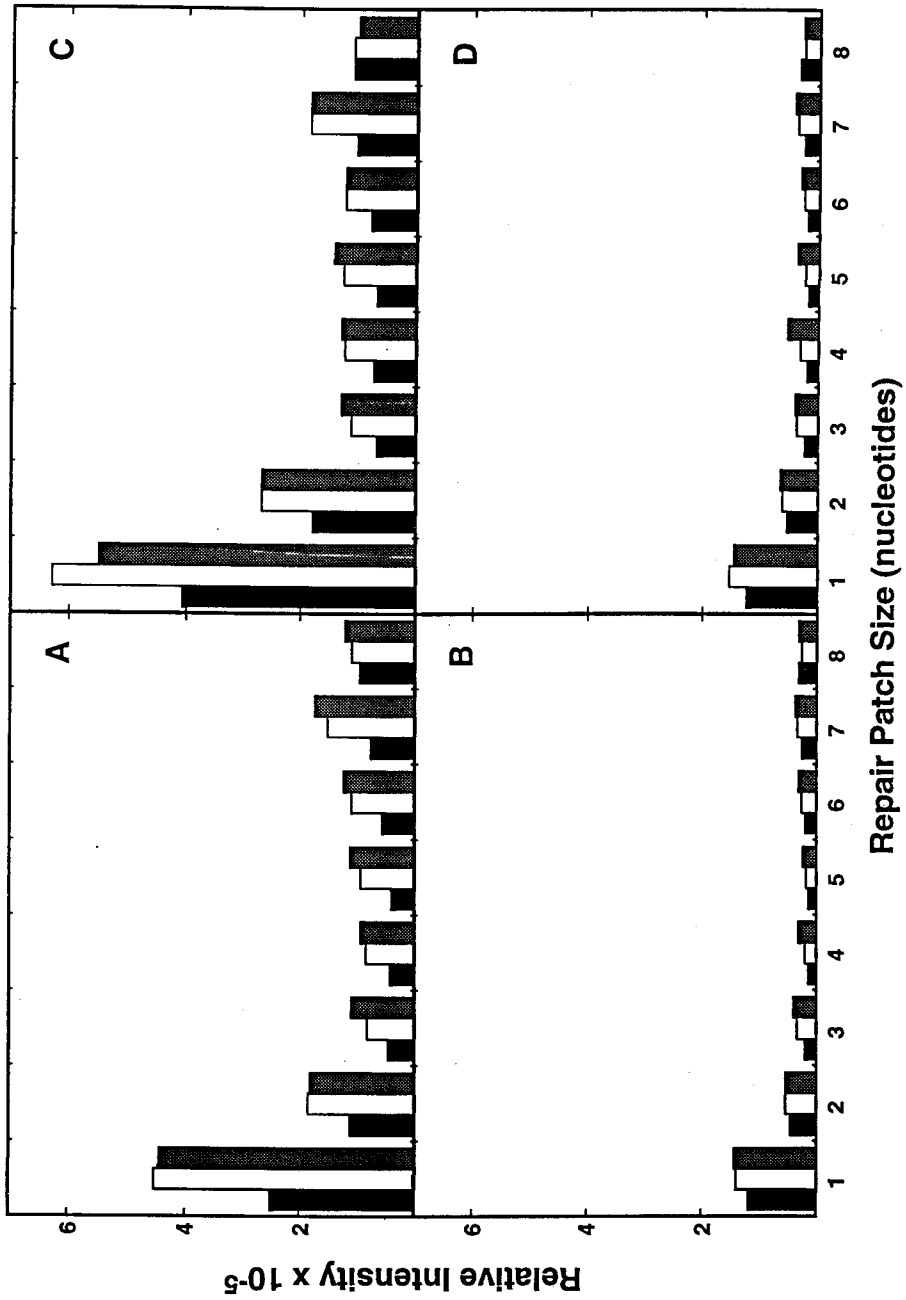
A
B
C
D
Relative Intensity x 10-5
Repair Patch Size (nucleotides)

Figure 59

Table 13

Effect of Various Conditions on the Size of the Repair Patch Introduced by Uracil-Initiated Base Excision Repair in Human Whole Cell Extracts[a]

Repair Patch (nucleotides)	-Ugi -Aphidicolin	+Ugi -Aphidicolin	-Ugi +Aphidicolin	+Ugi +Aphidicolin
	%	%	%	%
U251				
1	35.7	40.4	37.5	39.4
2	14.7	15.0	16.0	15.8
3	6.4	9.9	6.7	9.0
4	6.6	5.5	7.3	7.8
5	7.2	5.1	7.6	6.1
6	8.7	6.9	7.4	6.3
7	12.0	9.6	11.0	9.1
8	8.7	7.6	6.4	6.5
Short Patch	35.7	40.4	37.5	39.4
Long Patch	64.3	59.6	62.5	60.6
LoVo				
1	31.8	46.3	29.0	26.6
2	19.0	19.0	17.8	15.7
3	9.2	12.5	9.8	11.9
4	7.6	4.5	12.6	14.7
5	8.2	4.3	8.9	8.9
6	7.6	3.7	6.8	7.2
7	10.4	6.7	9.5	8.0
8	6.2	3.0	5.6	7.0
Short Patch	31.8	46.3	29.0	26.6
Long Patch	68.2	53.7	71.0	73.4

[a] Represented repair patch sizes correlate to data collected from human whole cell extract reaction products digested with 2 units of *E. coli* exonuclease III as described under "Experimental Procedures".

removal and AP-site incision. Fourth, the addition of aphidicolin did not significantly influence the size or distribution of the DNA repair patches produced by either BER pathway. This implies that the α-like DNA polymerase(s) are not specifically required for long patch BER (Figure 58 and Figure 59C and D, and Table 13) . Thus, the majority of DNA synthesis did not appear to involve an aphidicolin-sensitive DNA polymerase that was capable of supporting both short- and long-patch BER. Fifth, base excision repair intermediates exhibiting limited DNA repair synthesis were observed for standard BER reactions supplemented with aphidicolin (Figure 58, lanes 11 and 15). Taken together, these results imply that all uracil-DNA repair detected in U251 whole cell extracts involves a base excision repair mechanism that predominantly involves one-nucleotide DNA repair synthesis mediated by an aphidicolin-insensitive DNA polymerase.

To determine the size and distribution of repair patches introduced during uracil-initiated BER in a mismatch repair-deficient cell line, an identical set of experiments was conducted using LoVo whole cell extract protein. As before, reactions were conducted both in the presence and absence of aphidicolin. Standard BER reactions supplemented with no addition, 2000 units of Ugi, 50 μM aphidicolin, or 2000 units of Ugi and 50 μM aphidicolin were incubated for 45 min, reaction products isolated, and treated with *Eco*RI, various amounts of Exo III, and *Sma*I. DNA products were resolved by denaturing 12 % polyacrylamide/8.3 M urea gel electrophoresis and autoradiography was performed (Figure 60). The relative intensity of DNA fragments of 20 to 27 nucleotides in length were quantitated and plotted (Figure 61) and expressed as a percentage in Table 13. Results detected for LoVo cells were similar to those observed for U251 cells and suggest that the presence or absence of mismatch repair does not influence the size or distribution of uracil-initiated DNA repair synthesis. Uracil-DNA BER initiated by uracil-DNA glycosylase resulted in short- and long-patch DNA synthesis constituting 29-32 % and 68-71 % of the total repair synthesis and

Figure 60. Effect of Ugi and aphidicolin on the 3' boundary of the repair patch introduced by uracil-initiated base excision repair in LoVo cell extracts. Standard BER reaction mixtures (500 µl) containing 5 µg of [^{32}P]M13mp2op14 (U•T) DNA, 1 mg of human LoVo whole cell extract protein, and 20 µM each of dATPαS, dTTPαS, dCTPαS and dGTPαS were supplemented with no addition (lanes 3-6), 2000 units of Ugi (lanes 7-10), 50 µM aphidicolin (lanes 11-14), or 2000 units of Ugi and 50 µM aphidicolin (lanes 15-18). Reactions were incubated at 30°C for 45 min and DNA reaction products were isolated. Samples (8 µl, ~500 ng) were removed for digestion with 25 units of *Eco*RI for 1 h at 25°C. The linearized DNA was then supplemented with no addition (lanes 3/7/11/15) or the addition of 20 units (lanes 4/8/12/16), 2 units (lanes 5/9/13/17), or 0.2 units (lanes 6/10/14/18) of *E. coli* Exo III for 30 min at 37°C. Following Exo III digestion, reaction products were restricted with 25 units of *Sma*I for 1 h at 25°C. As controls, unreacted [^{32}P]M13mp2op14 (U•T) DNA (~500 ng) was incubated with *Eco*RI and *Sma*I (lane 1) or *Eco*RI, Exo III (0.2 units), and *Sma*I (lane 2). Following these reactions, DNA reaction products were resolved by 12% polyacrylamide/8.3 M urea gel electrophoresis as described under "Experimental Procedures". The location of the 40-mer corresponding to the (-) strand *Eco*RI/*Sma*I restriction fragment and the 19-mer through 27-mer BER reaction products are located by *arrows* on the autoradiogram.

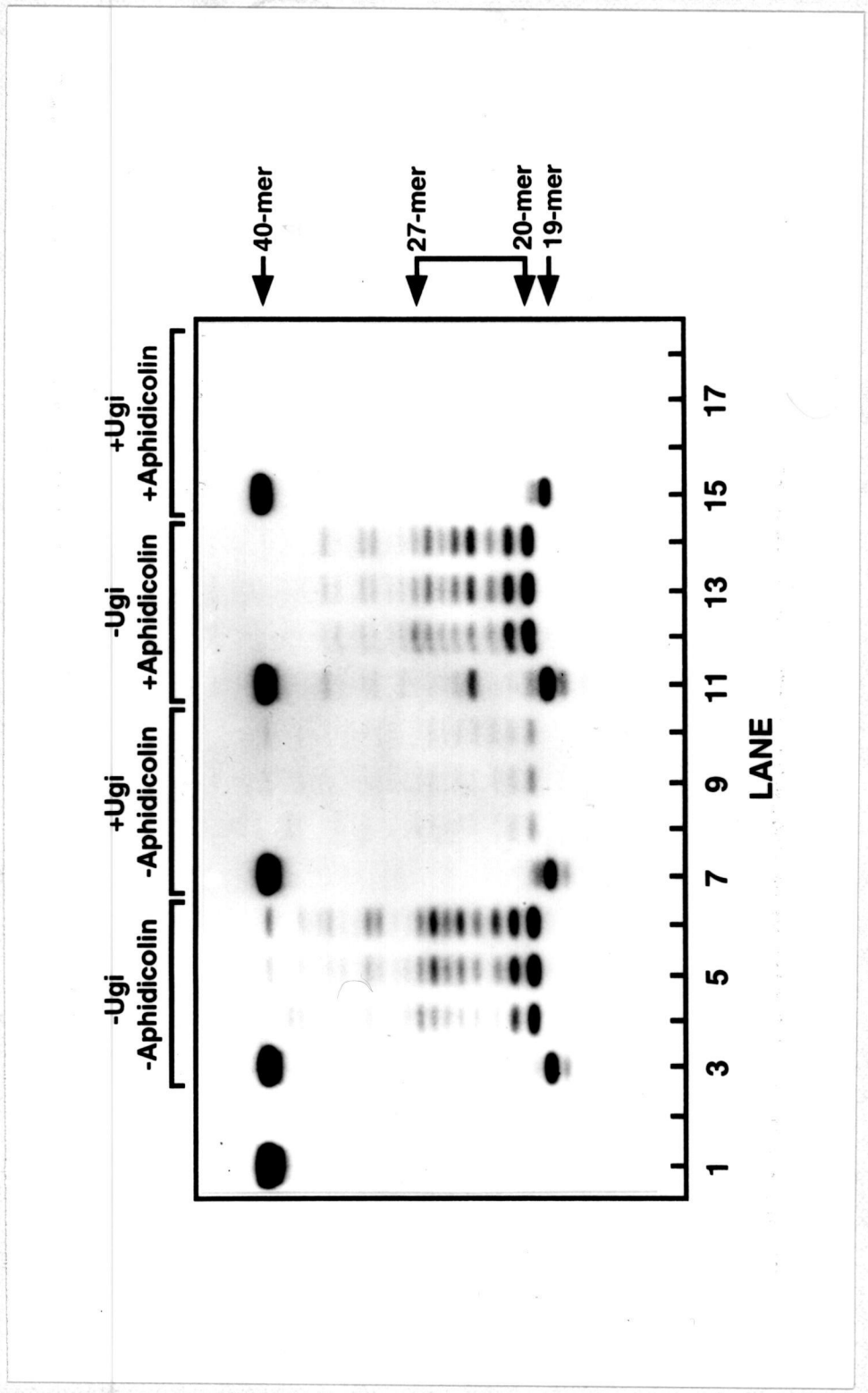
40-mer
27-mer
20-mer
19-mer
-Ugi
-Aphidicolin
+Ugi
-Aphidicolin
-Ugi
+Aphidicolin
+Ugi
+Aphidicolin
1
3
5
7
9
11
13
15
17
LANE

Figure 60

Figure 61. Quantitation of repair patch sizes introduced by uracil-initiated base excision repair in LoVo cell extracts under various conditions. Relative amounts of DNA reaction products detected by autoradiography in Figure 64 were determined using a PhosphorImager. The relative intensity of DNA bands of 20 to 27 nucleotides in length corresponded to repair patches of 1 to 8 nucleotides in length, respectively, and were measured for LoVo whole cell extract reaction products following digestion with 20 units (*black bars*), 2 units (*white bars*) and 0.2 units (*grey bars*) of *E. coli* exonuclease III as described under "Experimental Procedures". Relative intensity values of individual DNA bands were plotted after subtracting background values for standard BER reactions containing no addition (A), 2000 units of Ugi (B), 50 μM aphidicolin (C), and 2000 units of Ugi and 50 μM aphidicolin (D).

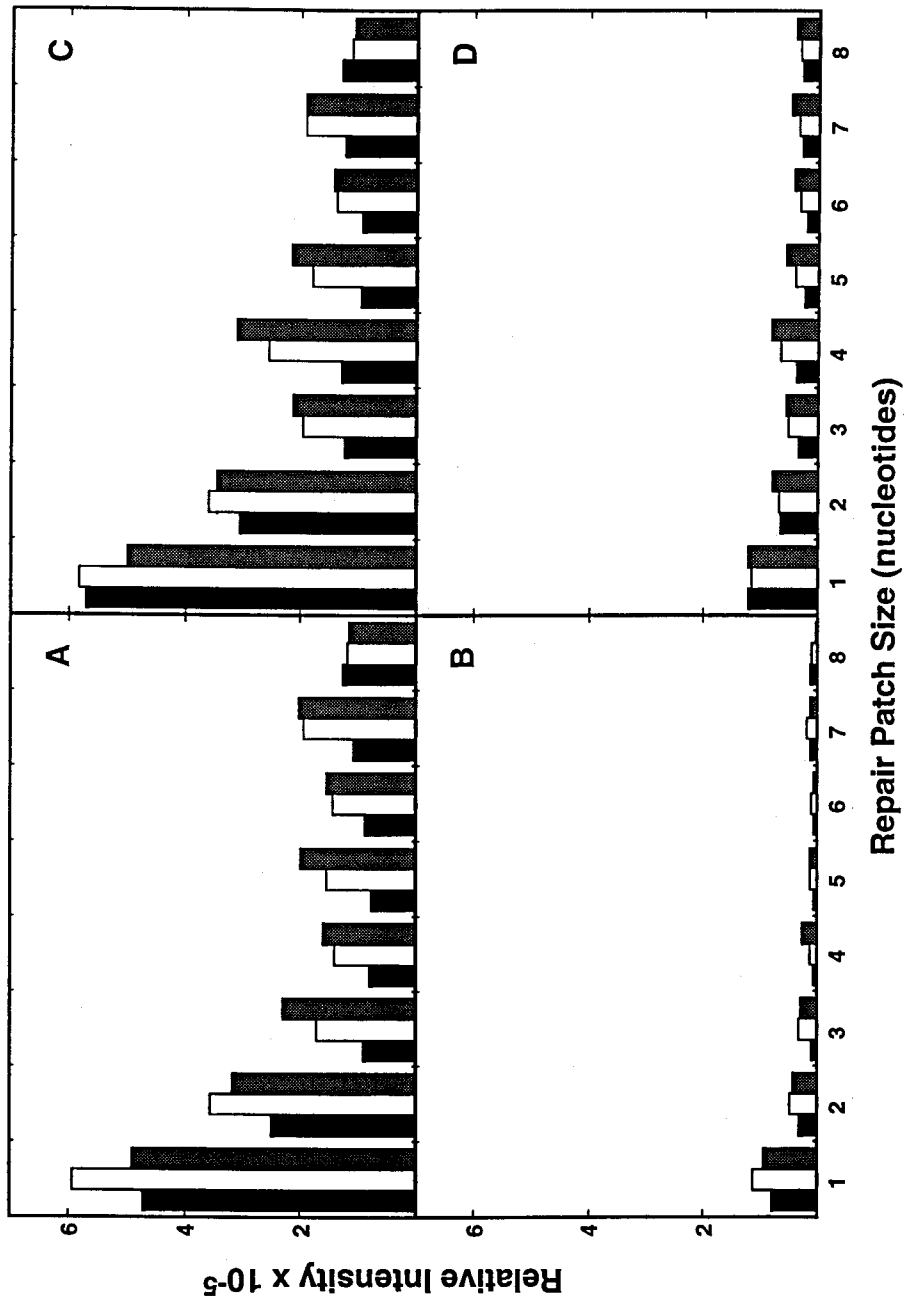
A
B
C
D
Relative Intensity x 10-5
Repair Patch Size (nucleotides)

Figure 61

was not significantly influenced by aphidicolin. These results were also similar to those observed for U251 cells. As expected, standard BER reaction mixtures containing Ugi (Figure 61B and D) exhibited a 4.3- to 8.2-fold reduction in the relative intensity of Exo III-resistant DNA reaction products as compared to BER reactions lacking Ugi (Figure 61A and C). These results imply that an aphidicolin-insensitive DNA polymerase promotes both short- and long-patch DNA repair synthesis in uracil-initiated base excision repair in LoVo whole cell extracts.

4.2 Discussion

The ability of human glioblastoma U251 and human colon adenocarcinoma LoVo whole cell extracts to conduct uracil-DNA repair using an M13mp2 *lacZ*α DNA-derived substrate containing a site-specific uracil residue was examined. Unlike several recent investigations that have utilized uracil-containing oligonucleotides to characterize BER reactions in eukaryotic cell extracts (54, 247, 253, 295), a covalently closed circular duplex DNA substrate with a defined uracil target was used in this study to facilitate DNA synthesis fidelity measurements and to mimic the natural DNA substrate (20). Since a PCNA-dependent base excision repair pathway has previously been observed in eukaryotic *in vitro* repair systems (77, 158) and reports indicate that PCNA and PCNA-dependent DNA polymerases δ and ε are loaded more stably on circular DNA than on linear DNA *in vitro* (205, 206), a linear DNA substrate was considered inappropriate for this study.

Under the conditions examined in this system, most of the uracil-DNA repair in U251 and LoVo whole cell extracts occurred via the uracil-initiated BER pathway. Several observations support this conclusion: i) DNA synthesis was preferentially localized to the *Hinf* I DNA fragment (529-bp) that contained the uracil target; ii) repair DNA synthesis within the 529-bp fragment was almost exclusively dependent on the presence of the uracil residue; iii) DNA synthesis was specifically confined to the (-) strand DNA

that initially contained the uracil target; iv) addition of Ugi to the whole cell extract significantly inhibited repair DNA synthesis; and v) Ugi-sensitive and -insensitive uracil-DNA repair synthesis produced repair patches that predominantly involved the incorporation of a single nucleotide. In contrast, these results were not consistent with a mismatch DNA repair pathway since DNA synthesis was confined to a region significantly <1000 nucleotides, occurred preferentially on only one of the two DNA strands containing the mispair, and efficient repair was observed in LoVo whole cell extracts that are defective in the mismatch repair protein, hMSH2 (27, 282).

An examination of the BER reaction kinetics in human U251 whole cell extracts revealed that ~50 % of the uracil-DNA substrate was repaired and repair had reached equilibrium after 60 min of incubation whereas ~37 % of the substrate was repaired by human LoVo whole cell extracts after the same amount of time. The ability to achieve this relatively high efficiency of completed repair suggested that a coordinated set of repair reactions occurred without significant accumulation of side products or repair intermediates. This would be consistent with the notion that a concerted BER reaction occurred (209). Inclusion of Ugi protein in the standard BER reaction containing U251 whole cell extract protein reduced the amount of repaired Form I DNA from 50 % to 3.7 % after 60 min. Thus, approximately 93 % of the observed BER appeared to be initiated by a Ugi-sensitive uracil-DNA glycosylase. The small but detectable amount (~7 %) of repair that was insensitive to Ugi inhibition suggests that a back-up enzyme or repair pathway exists. By an alternative comparison, the initial rates of repair for the Ugi-sensitive (3.61 fmol/min) *versus* the Ugi-insensitive (0.58 fmol/min) reactions suggests that the back-up enzyme or repair pathway could contribute as much as 16 % of the uracil-DNA repair. However, this is most likely an overestimate since the accumulation of repaired Form I DNA as initiated by uracil-DNA glycosylase was essentially completed after 60 min. The BER reaction in LoVo whole cell extracts supplemented with Ugi also yielded a reduction in the amount of repaired Form I DNA from 37 % to 6.5 % after 60

min. This result indicated that approximately 82 % of the observed repair activity appeared to be initiated by a Ugi-sensitive uracil-DNA glycosylase. By this measurement, ~18 % of the uracil-DNA repair in LoVo whole cell extracts involved a Ugi-insensitive system. When the initial rates of repair by the Ugi-sensitive (1.64 fmol/min) and the Ugi-insensitive (0.30 fmol/min) reactions were compared, ~18 % of the repair could have been initiated by an activity other than that of uracil-DNA glycosylase. Again, this might be expected to represent an overestimate since a significant accumulation of repaired Form I DNA initiated by the Ugi-insensitive repair reaction is not observed until 60 min. A potential candidate for this alternate activity might be the human TDG protein, which is insensitive to Ugi and capable of excising uracil from G•U mispairs (80, 186). Recently, the ability of hTDG to recognize and excise uracil from a T•U mispair has been established (298). Hence, it seems conceivable that hTDG may be capable of removing uracil from a T•U mispair. Another formal possibility would be that GAPDH functions as a back-up enzyme. However, the inability of several laboratories to confirm that purified human GAPDH possesses significant uracil-DNA glycosylase activity casts doubt on this possibility (36, 190, 249). The biological significance of two uracil-DNA repair systems within human cells remains to be elucidated.

In experiments designed to measure the distribution of repair patch sizes affiliated with uracil-initiated BER, the rate-limiting step appeared to occur subsequent to uracil removal and AP-site hydrolysis and prior to DNA synthesis for both the Ugi-sensitive and Ugi-insensitive repair activities. This observation was deduced from an examination of the DNA repair products treated with *Eco*RI and *Sma*I but not with Exo III. DNA fragments of 19 nucleotides in length indicated that uracil-DNA glycosylase and AP endonuclease had removed the uracil residue and incised the AP site but DNA synthesis had not occurred. The absence of repair intermediates ≥20 nucleotide in length and the presence of full length 40-mer *Eco*RI/*Sma*I

restriction DNA fragments indicated that ligation was achieved in repair events where DNA repair synthesis had occurred. This implies that the rate-limiting step is not associated with DNA ligation but with the interaction of the DNA polymerase with the nicked AP-site as it involves release of the 5'-terminal deoxyribose phosphate moiety and DNA synthesis. Fortini and co-workers (69) witnessed a similar accumulation of UDG/HAP1 reaction intermediates (incised DNA molecules) and suggested that the release of the 5'-terminal deoxyribose phosphate moiety as free dRp or as part of a short oligonucleotide preceded the DNA synthesis step. An additional observation that supports this conclusion emerges from the results of Srivastava *et al.* (256) that reported the rate-determining step of a reconstituted BER reaction involving AP-endonuclease, pol β, and DNA ligase I was the dRp lyase activity associated with pol β (256). Interestingly, the presence of the 5'-terminal dRp moiety of the nicked AP site did not disrupt DNA synthesis and DNA ligase I activity was inhibited by the dRp flap intermediate presumably created during strand displacement (256). Contrary to our observations and those of Fortini *et al.* (69), the model proposed for AP site BER involved the sequential enzymatic activities of AP endonuclease, DNA polymerase, dRp lyase activity, and DNA ligase (256). These differences could be attributed to the use of a whole cell extract *versus* a reconstituted system and DNA repair of a uracil-containing circular DNA substrate *versus* an AP site-containing linear DNA substrate.

Several independent studies have reported that the short-patch BER provides the dominant pathway for mammalian cells (69, 118). Analysis of short- and long-patch DNA repair synthesis in human U251 and LoVo whole cell extracts revealed that 32 % to 46 % of the repaired uracil-containing DNA substrate involved incorporation of a single nucleotide. Thus, longer DNA repair patches (2 to 8 nucleotides) appeared to be the predominant route for uracil-initiated BER under our assay conditions. Approximately 70-80 % of the newly synthesized DNA repair patches in human lymphoblastoid cell

extracts after uracil excision contained one nucleotide. This difference might reflect the fact that the uracil-containing linear duplex oligonucleotide used by Dianov *et al.* (54) was a poor substrate for the assembly of the RF-C-PCNA sliding clamp which might be expected to influence the amount of long-patch DNA repair synthesis. Previously, Podust *et al.*(205, 206) have demonstrated that RF-C-PCNA associates with the stable assembly of pol δ and/or pol ε onto the linear substrate. Thus, the use of a covalently closed circular duplex DNA substrate in this study might facilitate the stable assembly of BER enzymes that influence the balance between short- and long-patch DNA repair synthesis.

An examination of the DNA polymerase(s) involved in uracil-initiated BER in human cell extracts was conducted using the α-like DNA polymerase inhibitor, aphidicolin. Inclusion of aphidicolin into standard BER reactions containing U251 and LoVo whole cell extracts reduced the amount of BER by 20 % and 13 %, respectively. Similar levels (~20 %) of uracil-initiated BER inhibition by aphidicolin were also observed in HeLa cell extracts (183). Together, these observations suggest that pol β plays a predominant role in BER in human cells. However, these results do not rule out the possibility that other DNA polymerases, particularly pol δ and/or pol ε, potentially contribute to DNA repair synthesis. In particular, pol δ and ε may function in synthesis involving long-patch BER. Several other studies have previously implicated a role for pol δ and/or pol ε in BER using eukaryotic whole cell extracts (54, 77, 123, 158, 294). Examination of the repair patch size distribution during DNA repair synthesis in U251 and LoVo cell extracts illustrated that aphidicolin did not interfere with the repair kinetics of short- or long-patch BER. This provided evidence that pol β can participate in DNA repair synthesis of both short and long DNA patches under our assay conditions. Klungland and Lindahl (118) have described a BER pathway that repairs reduced AP sites. This pathway generates repair patches of 2-6 nucleotides by

pol β or pol δ. Experiments using cell extracts from mouse fibroblasts derived from embryos harboring a homozygous pol β-deletion mutation suggested that the rate of short-patch BER initiated at AP-sites was dramatically reduced but not completely eliminated in the absence of pol β activity (69). In contrast, the rate of long-patch BER was apparently unaffected in these pol β-deficient extracts (69). These observations infer that short-patch BER is largely pol β-dependent and constitutes the major pathway for repair whereas DNA polymerase(s) other than pol β are specifically involved in long-patch BER. Interestingly, the kinetic rate of long-patch repair observed by Fortini *et al.* (69) was significantly slower than that of short-patch repair and was attributed to a strand displacement reaction mechanism. Thus, the faster rate of short-patch DNA synthesis by pol β coupled with its processivity on short gaps and ability to conduct strand displacement DNA synthesis could presumably influence its role in the synthesis of longer DNA tracts (118, 248). In a separate study, the addition of pol β antibodies to human lymphoblastoid cell-free extracts inhibited long-patch BER, suggesting that pol δ and pol ε were inefficient in substituting for pol β during long-patch BER (118). Altogether, these results imply that pol β is definitively involved in short- and long-patch DNA repair synthesis but the contributing role of other DNA polymerases in long-patch DNA repair synthesis remains to be clearly determined.

Using the *lacZα* reversion assay, we observed that uracil-initiated BER in human U251 whole cell extracts occurred with a reversion frequency of 5.2 x 10^{-4} (~1 misincorporation per 1900 repaired uracil residues). Uracil-initiated BER in human LoVo whole cell extracts yielded a reversion frequency of 5.4 x 10^{-4} (~1 misincorporation per 1850 repaired uracil residues). Although the presence of a functional mismatch DNA repair pathway in U251 whole cell extracts has not been determined under our assay conditions, the similarity of the reversion frequencies between U251 and LoVo cells implies that the

fidelity of the BER reaction in U251 cells was not influenced by the mismatch DNA repair pathway. Inclusion of Ugi into standard BER reactions with U251 and LoVo whole cell extracts resulted in considerably greater reversion frequencies of 28.3 x 10^{-4} (~1 misincorporation per 350 repaired uracil residues) and 11.7 x 10^{-4} (~1 misincorporation per 850 repaired uracil residues), respectively. The Ugi-insensitive BER pathway was 2 to 5 times more error prone than uracil-BER initiated by the uracil DNA glycosylases. Elucidation of the pathway involving this Ugi-resistant uracil-DNA glycosylase activity must await further characterization.

In all cases, the uracil-DNA BER reaction was considerably more error-prone than DNA synthesis associated with leading or lagging strand replication in human cell extracts (111). For example, the reported average replication error rates for G•dGTP, T•dGTP, and A•dGTP mispairs occurred between 0.25 x 10^{-4} and 0.03 x 10^{-4} errors per detectable nucleotide incorporated (111). The error-prone nature of the BER reaction may necessitate that the repair patch size be kept to a minimum to avoid mutations from being introduced during DNA repair synthesis. Thus, it is not surprising that the repair patch size associated with BER (1-8 nucleotides) is considerably smaller than that associated with nucleotide excision repair (27-29 nucleotides) or mismatch repair (>1000 nucleotides) in human cells (269). The latter two repair pathways do not appear to utilize pol β for the DNA repair synthesis step (229, 269).

The studies reported here present the first fidelity measurements associated with BER DNA synthesis in mammalian whole cell extracts. The analysis utilized a *lacZα* reversion assay capable of detecting 8 out of 9 possible base substitutions within the opal (TGA) codon, including all 3 misinsertions at the uracil target site. Only a misincorporation of dTMP opposite G at position 79 in the (+) strand template was undetectable since this created a TAA stop codon that would not be scored as a revertant with a blue plaque phenotype. As expected, most (~95 %) of the 78 revertants sequenced

following the BER reaction in U251 whole cell extracts contained a base substitution at the first position of the opal codon (nucleotide 78) corresponding to the site of the uracil residue. In BER reactions containing LoVo whole cell extract protein, ~92 % of the 24 revertants sequenced similarly contained a base substitution at the site of the uracil residue. Of the 24 revertants sequenced following uracil-DNA repair in standard BER reactions containing LoVo whole cell extract and Ugi, all of the base substitutions were found to occur at the site of the uracil. In all cases, these results are consistent with DNA repair synthesis being initiated at the uracil target site on the (-) strand and proceeding in the 5' to 3' direction away from the opal codon. However, the results do not distinguish between BER involving a short- or long-patch mechanism since the fidelity assay was specifically designed to detect misincorporations only at the uracil target and not downstream (5' to 3') along the (-) strand. Consequently, the error frequencies represent those of short-patch BER and the first nucleotide incorporated during long-patch BER.

A considerable amount of evidence implicates pol β as playing a major role in uracil-initiated BER in mammalian cells (171) (13, 69, 157, 158, 174, 200, 209, 247). Recently, the fidelity of *in vitro* gap filling DNA synthesis by purified pol β was evaluated (11). Beard *et al.* (11), using a *lacZα* opal codon reversion assay to assess the DNA synthesis fidelity on a substrate containing a five-nucleotide gap, demonstrated that purified human pol β produced one revertant per 370 filled gaps (reversion frequency of 27×10^{-4}). This value reflects a somewhat lower fidelity (~5-fold) than that observed for the completed uracil-DNA glycosylase-initiated BER reaction in either U251 or LoVo whole cell extracts. However, this value was similar to the reversion frequencies observed for the Ugi-insensitive BER reaction in U251 (28.3×10^{-4}) and LoVo (11.7×10^{-4}) whole cell extracts. Thus, the decreased DNA repair synthesis fidelity associated with the Ugi-insensitive DNA glycosylase could have resulted from the formation of a gapped DNA substrate. Supporting the

concept of lowered fidelity on gapped DNA substrates, Chagovetz *et al.* (40) observed that the nucleotide insertion fidelity of purified rat pol β was considerably higher (>10-fold) on a DNA substrate containing a 5'-phosphorylated single-nucleotide gap as compared to a gap of six nucleotides. Additionally, the catalytic efficiency of pol β on a 5'-phosphorylated gap was ≥500 times greater than on a six-nucleotide gapped DNA substrate (40). Clearly, other factors such as DNA sequence context and accessory proteins associated with the BER reaction potentially contribute to the observed fidelity of DNA repair synthesis and mutation fixation. In particular, the ability of DNA ligase to act on nicks containing specific 3'-mismatched nucleotides juxtaposed to a 5'-end could significantly influence the mutation spectrum derived from BER. In this regard, recent evidence indicates that bovine DNA ligase III seals a nick containing a 3'-C•T mispair with nearly the same efficiency as one containing base-paired termini, whereas a 3'-G•T mispair was recognized with ~5-fold less efficiency (109). A similar preference for 3'-terminal mispairs (3'-C•T > 3'-G•T) was also observed for bovine DNA ligase I; however, the overall efficiency of DNA joining was reduced 5-10-fold for each individual mispaired termini compared with DNA ligase III (109). These results may provide a partial explanation for the high frequency of C•T *versus* G•T mispairs detected following the BER assay.

The results observed by Husain *et al.* (109) potentially reflect the fidelity of ligation associated with one-nucleotide repair patches but not ligation of DNA repair patches involving two or more nucleotides. Thus, in long-patch BER, the initial misinsertion event at the site of the uracil target must be followed by primer extension from the 3'-terminal mispair. Approximately 54 % to 68 % of the uracil-initiated BER in U251 and LoVo whole cell extracts involved repair patches of two or more nucleotides. Interestingly, the ability of pol β to efficiently utilize template-primers containing up to three nucleotide mispaired termini has been reported (25,

120). Specifically, the ability of pol β to conduct primer extension from a 3'-C•T and 3'-T•T terminal mispairs was observed (25). This could also provide a partial explanation for the 'fixation' of these types of mispairs in light of the extensive long-patch DNA repair synthesis observed in this study. Currently, it is unclear whether the error frequencies measured for U251 and LoVo uracil-initiated BER represent errors associated with short- or long-patch DNA repair synthesis.

DNA polymerase-mediated base substitutions occur as a consequence of either direct nucleotide misincorporation or template-directed dislocation events (25, 223). The mutational spectrum observed for BER in human U251 whole cell extracts included 73 transversion mutations (~94 %) and only five transition mutations (~6 %). The transversion mutations were almost equally distributed between T to G (38/73) and T to A (32/73) changes resulting from dCMP and dTMP incorporation opposite thymine at position 78 in the DNA (+)-strand, respectively. In human LoVo whole cell extracts, similar proportions of transversion mutations were observed for repair reactions conducted in the absence (~88 %) and presence (~86 %) of Ugi. Again, transversion mutations were distributed between T to G (30/53) and T to A (19/53) changes for repair initiated by uracil-DNA glycosylase in the absence of Ugi. Similarly, T to G (17/24) and T to A (7/24) changes in the DNA (+)-strand constituted the transversion mutation spectrum for the Ugi-insensitive BER reaction. In all cases, T to G changes were the dominant type of transversion mutation. Transition mutations involving a T to C change for BER reactions containing U251 (4/5) or LoVo (5/7) whole cell extracts occurred as a consequence of dGMP being inserted opposite the template thymine residue. Misincorporation of dCMP and dGMP opposite a template thymine were recently reported to be the most kinetically favorable misinsertions for purified rat pol β, while misincorporation of dTMP ranked among the least favorable events (2). Inspection of the DNA template sequence around the target site suggested that dTMP incorporation could

have occurred via a dislocation mechanism. This could occur during the DNA synthesis process as depicted in Figure 62. If the thymine at position 78 in the template strand was looped out prior to nucleotide incorporation, this would allow the adenine at position 77 to base pair with the incoming dTTP. Under this condition, primer extension would occur due to the next nucleotide effect, and incorporation of two dTMPs might be expected to follow because of the adenine dinucleotide sequence of the template strand. Upon realignment of the primer-template, a T•T mispair would be created at position 78, and the 3' terminal nucleotide of the primer would form an A•T base pair at position 77. While this interpretation provides a plausible explanation, further experimentation would be required to elucidate the mutagenic mechanism. Additional studies will be required to determine the fidelity and mutational specificity of uracil-initiated BER within other sequence contexts.

Figure 62. Model for base substitution errors introduced by dislocation of the M13mp2op14 primer-template. A theoretical mechanism for introducing single-base substitutions during DNA repair synthesis is diagrammed and based upon the dislocation mutagenesis theory. After excision of the uracil and incision at the 5'-end of the resultant apyrimidinic site, slippage of the template or primer strand can result in the looping out of a single nucleotide to generate a 3' terminal mispair. If nucleotide incorporation and realignment of the template strand occur, the incorporated T will align with a template T to create a T:T mispair. The incorporated base leading to the mispair after realignment is *outlined*. In this model, mispairs are introduced, not by direct misinsertion, but by transient misalignment of the template strand. For clarity, the DNA sequence located to the 3' side of the uracil residue of the uracil-containing DNA strand has been omitted.

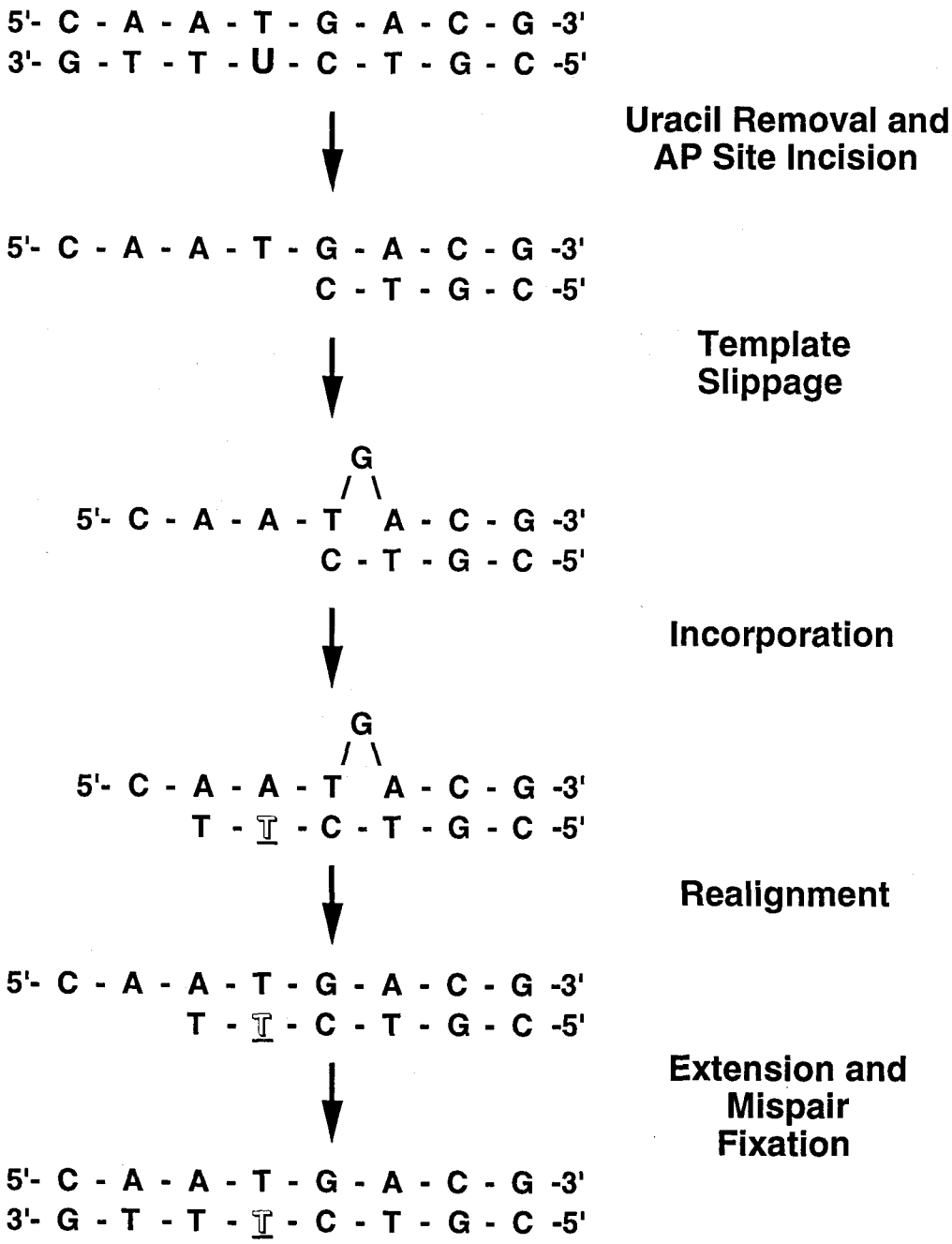
5'- C - A - A - T - G - A - C - G -3'
3'- G - T - T - U - C - T - G - C -5'
Uracil Removal and
AP Site Incision
5'- C - A - A - T - G - A - C - G -3'
C - T - G - C -5'
Template
Slippage
G
5'- C - A - A - T A - C - G -3'
C - T - G - C -5'
Incorporation
G
5'- C - A - A - T A - C - G -3'
T - I - C - T - G - C -5'
Realignment
5'- C - A - A - T - G - A - C - G -3'
T - I - C - T - G - C -5'
Extension and
Mispair
Fixation
5'- C - A - A - T - G - A - C - G -3'
3'- G - T - T - I - C - T - G - C -5'

Figure 62

5. INACTIVATION OF URACIL-DNA GLYCOSYLASE ACTIVITY IN HUMAN CELLS EXPRESSING THE UGI PROTEIN

The use of the Ugi protein to create a uracil-DNA glycosylase defective cell was initially explored in *E. coli* and resulted in the inactivation of Ung activity and production of bacteria with phenotypic properties equivalent to *ung* mutants (62, 291). Since *ung* mutants have not yet been isolated from mammalian cells, a similar approach was applied to human U251 glioblastoma cells by Dr. E. Radany (University of Michigan) and human cell lines stably expressing the *ugi* gene were characterized in this laboratory. This dissertation specifically characterizes the effect of *ugi* expression on the human uracil-DNA glycosylase activity of transduced cells *in vitro*. The approach utilizes synthetic oligonucleotide substrates containing site-specific uracil residues and the extent of uracil removal by crude cell extract protein was assessed. The findings establish that U251 cells stably transfected with the *ugi* gene express Ugi protein at a high level and have undetectable levels of uracil-DNA glycosylase activity in crude cellular extracts. In the process, the results indicated that a novel secondary uracil-DNA glycosylase activity exists that is insensitive to Ugi.

5.1 Results

5.1.1 Expression of the *ugi* Gene in Human U251 Glioblastoma Cells

Expression of the *ugi* gene in intact human cells was explored as a method to create a uracil-DNA glycosylase defective cell line. The *ugi* gene contained in pZWtac was modified and subcloned into a eukaryotic expression vector to facilitate the protein synthesis of Ugi in human cells. Construction of the mammalian expression vector and transduction of human U251 cells were conducted by Eric Radany (University of Michigan). The essential components of the mammalian expression vector,

pvBiPNeo1001-m*ugi*, are summarized in Figure 63 and consist of the retroviral long terminal repeat (LTR) elements and extended packaging signal (ψ^+) (163), strong CMV early promoter (26), *ugi* gene (219), and internal ribosome entry signal (IRES) of the human BiP/GRP70 gene (153) linked to the wild type prokaryotic Tn5 neomycin phosphotransferase gene (315). Transcription of the transgene (*ugi*) and drug resistance gene (Neo) were both under the control of the same CMV early promoter. As a result, a single bicistronic mammalian mRNA was expected to be transcribed with an internal ribosome entry signal (IRES) sequence from the BiP/GRP70 locus located between the individual gene sequences. This vector obligatorily links expression of *ugi* to Neo (153). Following transient transfection of pvBiPNeo-*ugi* into packaging cells, infectious retroviral vector containing supernatant samples were produced for infection of human U251 cells. Infections were conducted and G418 selection resulted in 51 independent drug-resistant colonies of different sizes. Subsequently, 25 clones were expanded to stably transduced cell lines.

Crude cell extracts were prepared from one of the G418-resistant transductants, U251*ugi*17, and unmodified parental U251 cells to specifically characterize the effect of *ugi* gene expression on the human uracil-DNA glycosylase (UDG) activity of transduced cells *in vitro*. Cell extracts from parental cells contained 11.7 units of UDG per mg of extract protein and no detectable Ugi activity (Figure 63). In contrast, crude cell extracts derived from U251*ugi*17 cells showed significantly reduced UDG activity (<0.08 units/mg) and also expressed Ugi activity (0.7 units/mg). Thus, essentially complete inhibition of endogenous UDG occurred in U251*ugi*17 cell extracts as determined by the uracil-DNA glycosylase assay.

Figure 63. Construction of Ugi-expressing human glioma cell lines. The plasmid map (*top*) depicts the structure of the *ugi*-containing retroviral vector used for transient infection of BOSC packaging cells to generate infectious amphitropic supernatants. Components include the retroviral long terminal repeat (5'LTR and 3'LTR) elements and extended packaging signal (ψ^+), the strong CMV early promoter (pCMV), *ugi*, and the internal ribosome entry signal (IRES) of the human BiP/GRP70 gene linked to the wild type prokaryotic Tn5 neomycin phosphotransferase gene (Neo). Below is a flow diagram showing the steps used for selection and cloning of human glioma cell lines carrying the pvBiPNeo-*ugi* provirus. Standard uracil-DNA glycosylase and uracil-DNA glycosylase inhibitor assays were conducted on U251 and U251*ugi*17 crude extract protein as described under "Experimental Procedures" to determine levels of Ung and Ugi activity in control and transformed cells.

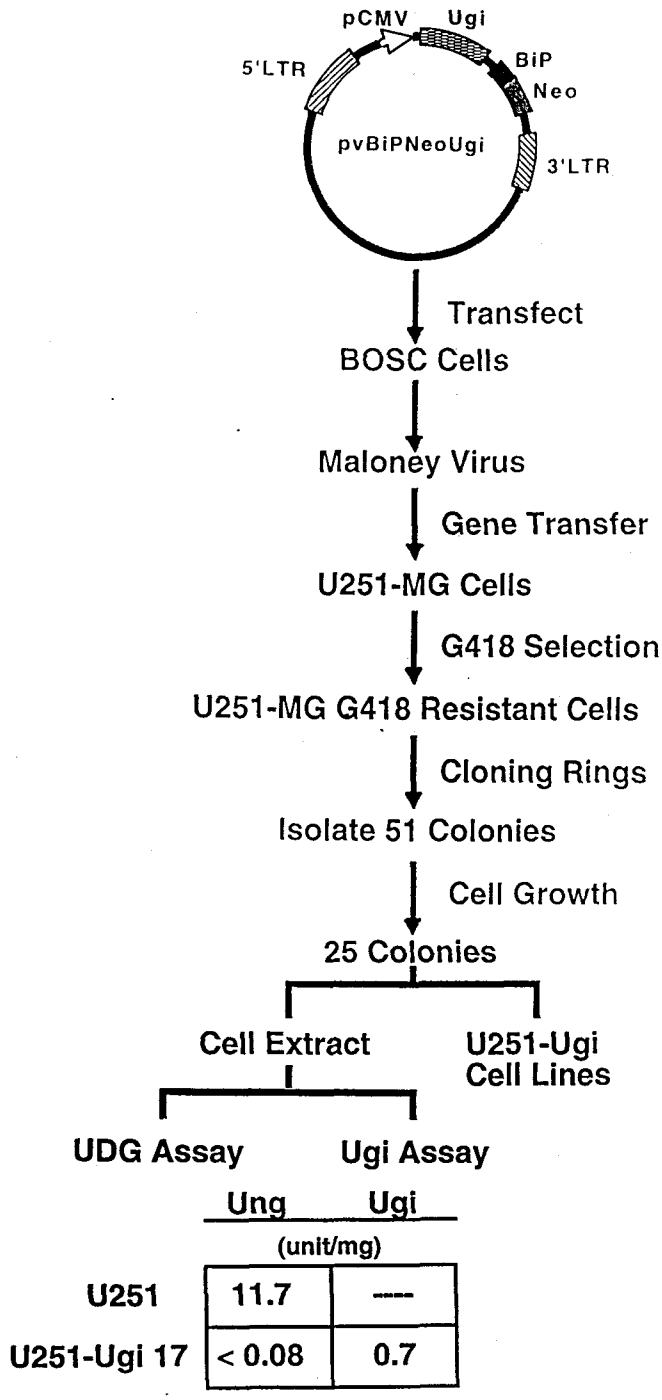

	Ung (unit/mg)	Ugi (unit/mg)
U251	11.7	----
U251-Ugi 17	< 0.08	0.7

Figure 63

5.1.2 Detection of UDG Activity in Human U251*ugi*17 Cell Extracts Using Various Uracil-Containing DNA Substrates

A more detailed investigation of the substrate specificity of UDG activity was conducted since recent evidence has indicated that HeLa cells contain a mismatch-specific thymine-DNA glycosylase (TDG) capable of removing thymine and uracil from T:G and U:G mispairs, respectively (80, 186). Parental U251 and U251*ugi*17 crude cell extracts were examined for uracil-DNA glycosylase activity using three 5'-end ^{32}P-labeled uracil-containing oligonucleotide substrates as indicated (Figure 64A). Increasing amounts of crude cell extract from either the control (U251) or *ugi*-expressing (U251*ugi*17) cells were incubated with each DNA substrate (U-34-mer, U/A-34-mer, and U/G-34-mer). Following these reactions, DNA reaction products were treated with alkali to hydrolyze the phosphodiester backbone on the 3'-side of the resultant apyrimidinic sites. A product ([^{32}P]15*-mer) containing a 3'-terminal deoxyribose-phosphate residue was anticipated as a result of this treatment. The products and substrate were resolved by denaturing polyacrylamide gel electrophoresis to assess the extent of uracil removal (Figure 64B-D, lanes 3-8). Control reactions were supplemented with no addition or exogenous *E. coli* uracil-DNA glycosylase to determine the efficiency of alkali-mediated AP-site cleavage (Figure 64B-D, lanes 1 and 2). In each case, >98 % of the 34-mer (U, U/A, U/G) was shown to be susceptible to cleavage by the combination of *E. coli* uracil-DNA glycosylase and alkali treatments.

As expected, the reaction mixtures containing the single-stranded U-34-mer and U251 cell extract produced a single reaction product ([^{32}P]15*-mer) corresponding to uracil removal by uracil-DNA glycosylase (Figure 64B). In an analogous experiment using the U251*ugi*17 cell extract, no UDG activity was detected due to the expression of the *ugi* gene product. Similar results were also observed in reaction mixtures containing either the double-stranded U/A- or U/G-34-mer substrate (Figure 64C and D). In both cases, no detectable UDG activity was observed with the U251*ugi*17 cell extract whereas

Figure 64. Substrate specificity of uracil-DNA glycosylase activity of human U251 and U251*ugi*17 cell extracts. (A) Three 5'-end ^{32}P-labeled oligonucleotides each containing a site-specific uracil residue located at position 16 were prepared as single-stranded [^{32}P]U-34-mer, double-stranded [^{32}P]U/A-34-mer, and [^{32}P]U/G-34-mer as described under "Experimental Procedures". The *arrows* flanking the uracil designate the 5'- and 3'-cleavage sites produced by AP-endonuclease and AP-lyase activities, respectively. The *asterisk* denotes the position of the 5'-end ^{32}P-label. (B) Two sets of uracil-DNA glycosylase reaction mixtures (100 µl) each containing 0.16, 0.63, 2.5, 10, 40, and 160 µg of U251 or U251*ugi*17 crude extract protein (lanes 3-8, respectively) were incubated with 4 pmol of [^{32}P]U-34-mer at 30°C for 30 min. Control reactions were similarly prepared but lacked cellular extract protein (lane 1) or contained 400 units of *E. coli* uracil-DNA glycosylase (lane 2). The order of these two controls was inverted in panel C for the U251 cell extract. After incubation, the reactions were terminated, DNA was isolated, and AP-sites were hydrolyzed. Reaction products were analyzed by electrophoresis using a denaturing 12% polyacrylamide gel containing 8.3 M urea and autoradiography was performed as described under "Experimental Procedures". Identical sets of reactions were prepared using 4 pmol of duplex [^{32}P]U/A-34-mer (C) or [^{32}P]U/G-34-mer (D) as substrate. The location of the DNA substrate (U-, U/A-, and U/G-34-mer) and reaction products (15*-mer and 16-mer) are indicated by *arrows*. The 15*-mer corresponds to the location of a 15-mer containing a 3'-terminal deoxyribose phosphate residue.

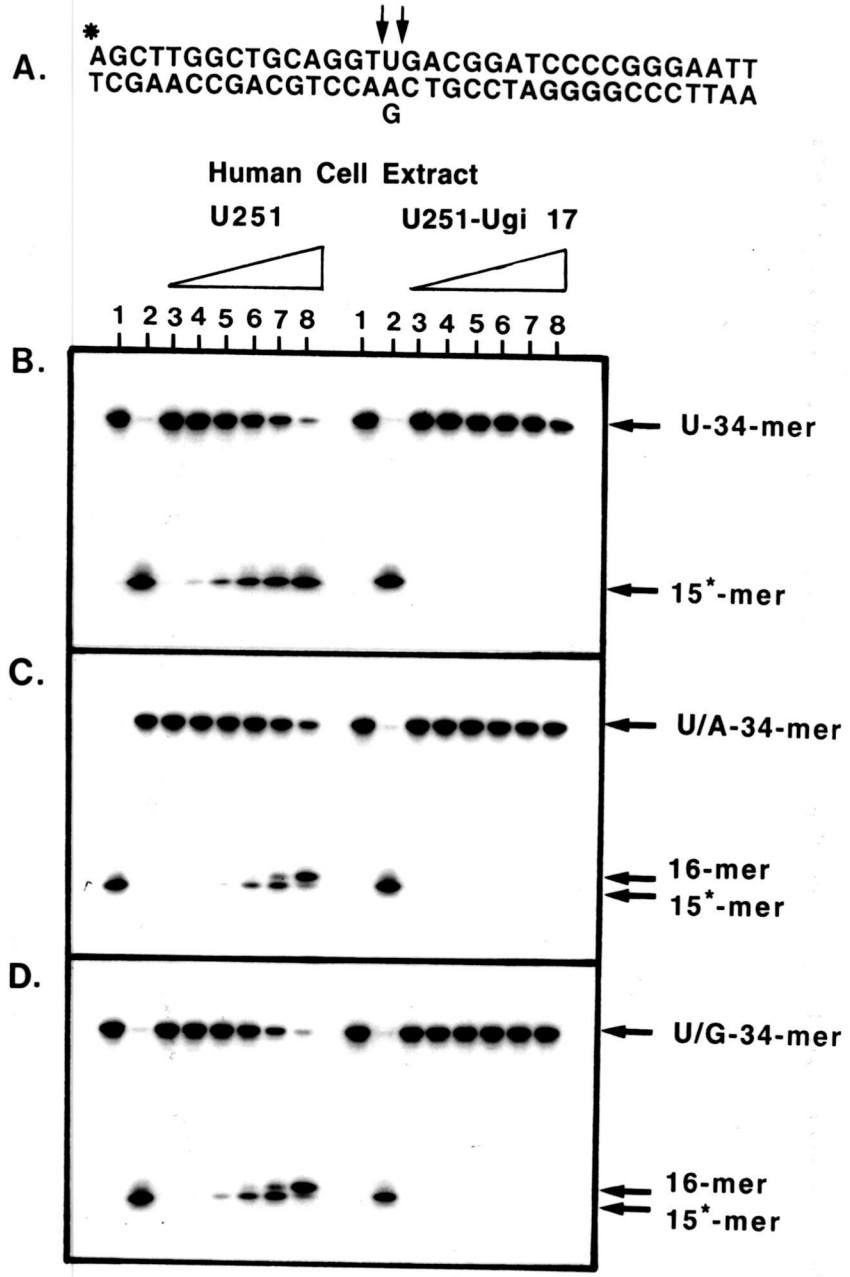
A.
*
AGCTTGGCTGCAGGTUGACGGATCCCCGGGAATT
TCGAACCGACGTCCAACTGCCTAGGGGCCCTTAA
G
Human Cell Extract
U251
U251-Ugi 17
1 2 3 4 5 6 7 8 1 2 3 4 5 6 7 8
B.
U-34-mer
15*-mer
C.
U/A-34-mer
16-mer
15*-mer
D.
U/G-34-mer
16-mer
15*-mer

Figure 64

significant cleavage of both duplex substrates occurred in extracts from parental U251 cell lines. The appearance of the [^{32}P]16-mer exclusively detected in reactions containing the duplex substrate was consistent with DNA synthesis that extended the 15-mer by one nucleotide. This product could be explained as a predicted intermediate in the uracil-initiated base excision DNA repair pathway (247). Taken together, these results imply that Ugi production in U251*ugi*17 cells effectively eliminated uracil-DNA glycosylase activity. After quantitating the amount of 15*-mer and 16-mer detected for each of the three uracil-containing 34-mer substrates, the percentage of product formed in each reaction was plotted as a function of U251 crude cell extract protein (Figure 65A-C). The relationship between the extent of uracil excision and the amount of cell extract protein was determined for the initial 10 % of the reaction. Under these conditions, the activity of crude cell extract protein from parental U251 cells for the removal of uracil from each substrate was determined to be 317, 72, and 147 fmol of uracil removed per μg of extract protein for U-, U/A-, and U/G-34-mer substrates, respectively. Thus, the DNA substrate containing U/G was preferred ~2.0-fold over U/A whereas single-stranded U-34-mer was preferred 4.4- and 2.2-fold over both U/A and U/G substrates, respectively.

The observation that uracil-DNA glycosylase activity was not detected under these assay conditions using the U/G-34-mer substrate inferred that U251 and U251*ugi*17 cell extracts contained little, if any, TDG activity. Since TDG has previously been detected in some human cell extracts, the experiment was repeated using a T/G-34-mer DNA substrate under reaction conditions specifically described for detecting TDG activity (246). U251 or U251*ugi*17 cell extract protein (160 μg) was incubated with 5'-end ^{32}P-labeled oligonucleotides (U-, U/A-, U/G-, T/G-34-mer), treated with alkali, and analyzed by denaturing polyacrylamide gel electrophoresis. Reactions were conducted both in the presence (Figure 66A-D, lanes 5 and 7) and absence (Figure 66A-D, lanes 4 and 6) of exogenous Ugi and the results obtained are shown following polyacrylamide/urea gel electrophoresis and

Figure 65. Quantitation of the substrate specificity of uracil-DNA glycosylase activity of human U251 and m*ugi* cell extracts. [^{32}P]DNA bands detected by autoradiography in Figure 64 (lanes 3-8) were excised from the dried gel and the amount of ^{32}P radioactivity was measured for reaction mixtures containing U251 (*closed circles*) and U251*ugi*17 crude extract protein (*open circles*). The percentage of product formed was calculated by dividing the amount of product ([^{32}P]15*-mer and [^{32}P]16-mer) by the amount of product plus substrate ([^{32}P]34-mer) detected for single-stranded [^{32}P]U-34-mer (A), [^{32}P]U/A-34-mer (B), and [^{32}P]U/G-34-mer (C).

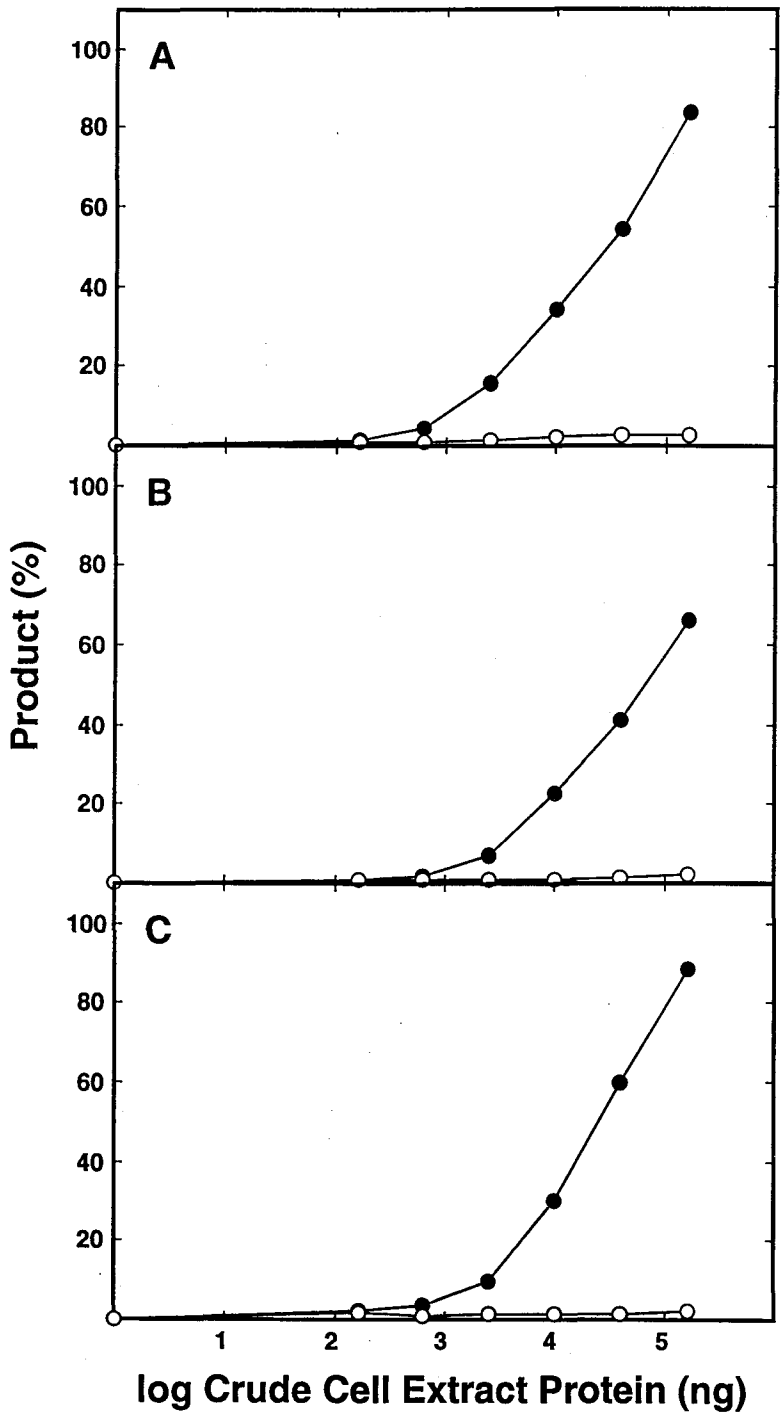
A
B
C
100
80
60
40
20
Product (%)
1
2
3
4
5
log Crude Cell Extract Protein (ng)

Figure 65

Figure 66. Analysis of thymine-DNA glycosylase activity in human U251 cell extracts. Four sets of uracil- or thymine-DNA glycosylase reaction mixtures (100 µl) each containing 160 µg of crude extract protein from either U251 (lanes 4 and 5) or U251*ugi*17 (lanes 6 and 7) cells were incubated with 4 pmol of [^{32}P]U-34-mer (A), [^{32}P]U/A-34-mer (B), [^{32}P]U/G-34-mer (C), or [^{32}P]T/G-34-mer (D), as indicated above in the presence (lanes 5 and 7) and the absence (lanes 4 and 6) of 1000 units of Ugi protein. In addition, each reaction mixture contained 25 mM Hepes-KOH (pH 7.9), 50 mM KCl, 1 mM DTT, 0.5 mM EDTA, 0.01 mM $ZnCl_2$, and 100 µl/ml acetylated BSA. Control reaction mixtures either lacked crude extract protein (lane 1), contained 400 units of *E. coli* Ung (lane 2), or 400 units of *E. coli* Ung plus 1000 units of Ugi protein (lane 3). Each reaction was terminated after 30 min at 30°C and the mixtures processed as described in Figure 64. Unreacted substrate (34-mer) and reaction products (15*- and 16-mer) were resolved by denaturing 12 % polyacrylamide/8.3 M urea gel electrophoresis, detected by autoradiography, and are located by the *arrows*.

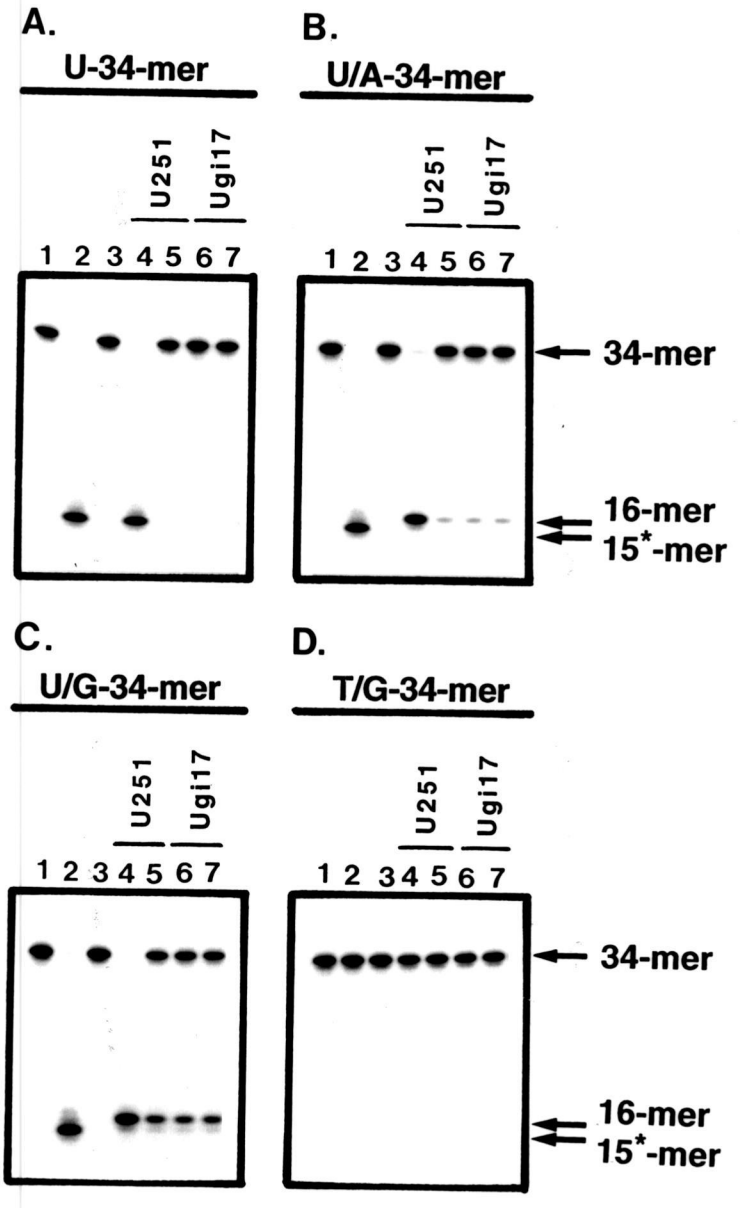
A.
U-34-mer
U251
Ugi17
1 2 3 4 5 6 7
B.
U/A-34-mer
U251
Ugi17
1 2 3 4 5 6 7
34-mer
16-mer
15*-mer
C.
U/G-34-mer
U251
Ugi17
1 2 3 4 5 6 7
D.
T/G-34-mer
U251
Ugi17
1 2 3 4 5 6 7
34-mer
16-mer
15*-mer

Figure 66

autoradiography. Control reactions for each DNA substrate containing the appropriate [^{32}P]34-mer supplemented with no addition, *E. coli* uracil-DNA glycosylase, or uracil-DNA glycosylase plus Ugi are shown for comparison (Figure 66A-D, lanes 1-3, respectively). The results indicate that TDG activity was not detectable in either the U251 or U251*ugi*17 cell extracts (Figure 66D). However, a novel activity was detected under these conditions that i) preferentially recognized the U/G-34-mer over the U/A-34-mer by a factor of ~3.5-fold; ii) did not appear to recognize the single-stranded U-34-mer substrate; iii) was insensitive to inhibition by Ugi; and iv) was expressed in both U251 and U251*ugi*17 cell lines. Virtually identical results were obtained for parental U251 and U251*ugi*17 cell extracts examined in the presence of exogenous Ugi. This, in conjunction with the observations that Ugi efficiently inhibited *E. coli* uracil-DNA glycosylase under identical reaction conditions, essentially negates the trivial explanation that the activity arose due to an inefficiency to inhibit UDG activity under these conditions. Together, these results suggest that TDG activity was not detectable but that a Ugi-insensitive double-strand specific uracil-DNA glycosylase (ds-UDG) existed in the extract.

Since ds-UDG activity was detected in human cell extracts using TDG but not UDG buffering conditions, an experiment was conducted to determine the buffer component(s) required to detect the Ugi-insensitive uracil-DNA glycosylase. Both buffers contained 25 mM Hepes-KOH (pH 7.8 or 7.9), 0.5 mM EDTA, and 0.5 mM or 1.0 mM DTT but buffer conditions described for detecting TDG activity also included 50 mM KCl, 10 μM $ZnCl_2$, and 100 μg/ml acetylated bovine serum albumin (BSA) protein. Therefore, U251 whole cell extract protein (160 μg) supplemented with and without exogenous Ugi was incubated with 5'-end ^{32}P-labeled oligonucleotides (U-, U/A-, U/G-, T/G-34-mer) under UDG buffering conditions containing various combinations of 50 mM KCl, 10 μM $ZnCl_2$, and/or 100 μg/ml acetylated BSA, treated with alkali, and analyzed by denaturing polyacrylamide gel electrophoresis (Figure 67A-D). Control reactions for each

Figure 67. Effect of various buffer conditions on uracil-DNA glycosylase activities in human U251 cell extracts. Four sets of uracil-DNA glycosylase reaction mixtures (100 µl) each containing 160 µg of U251 crude extract protein were incubated with 4 pmol of [^{32}P]U-34-mer (A), [^{32}P]U/A-34-mer (B), [^{32}P]U/G-34-mer (C), or [^{32}P]T/G-34-mer (D) under various buffer conditions (KCl, $ZnCl_2$, BSA) and in the presence or absence of 1000 units of Ugi protein as indicated. Control reaction mixtures either lacked crude cell extract protein (lane 1), contained 400 units of *E. coli* Ung (lane 2), or 400 units of *E. coli* Ung plus 1000 units of Ugi protein (lane 3). Each reaction was terminated after 30 min at 30°C, DNA was isolated, and AP-sites were hydrolyzed. Unreacted substrate (34-mer) and reaction products (15*- and 16-mer) were resolved by denaturing 12% polyacrylamide/8.3 M urea gel electrophoresis followed by autoradiography. The location of the substrate and reaction products are located by *arrows*.

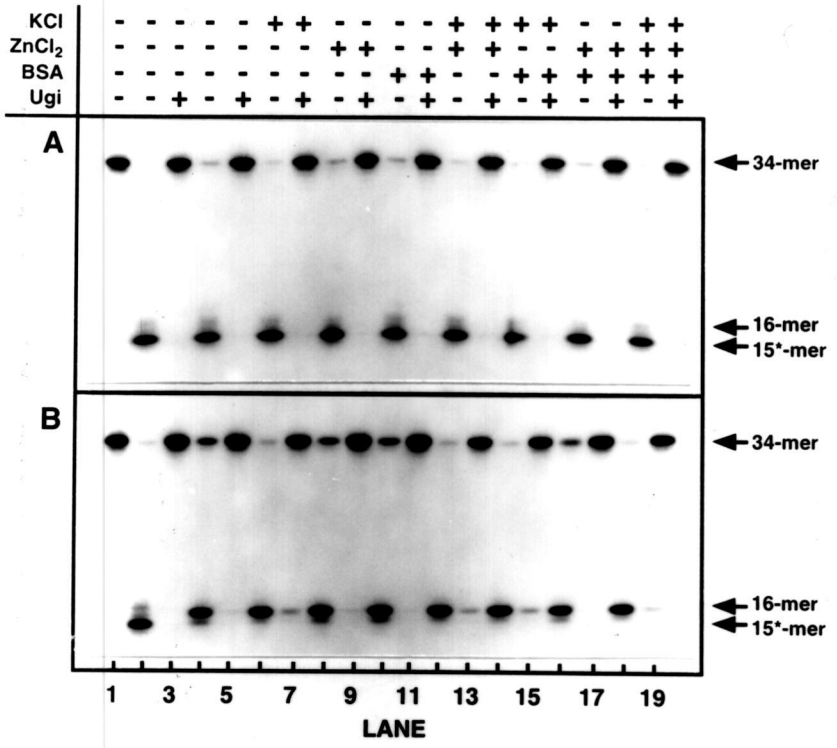
KCl
ZnCl2
BSA
Ugi
A
B
34-mer
16-mer
15*-mer
34-mer
16-mer
15*-mer
1 3 5 7 9 11 13 15 17 19
LANE

Figure 67

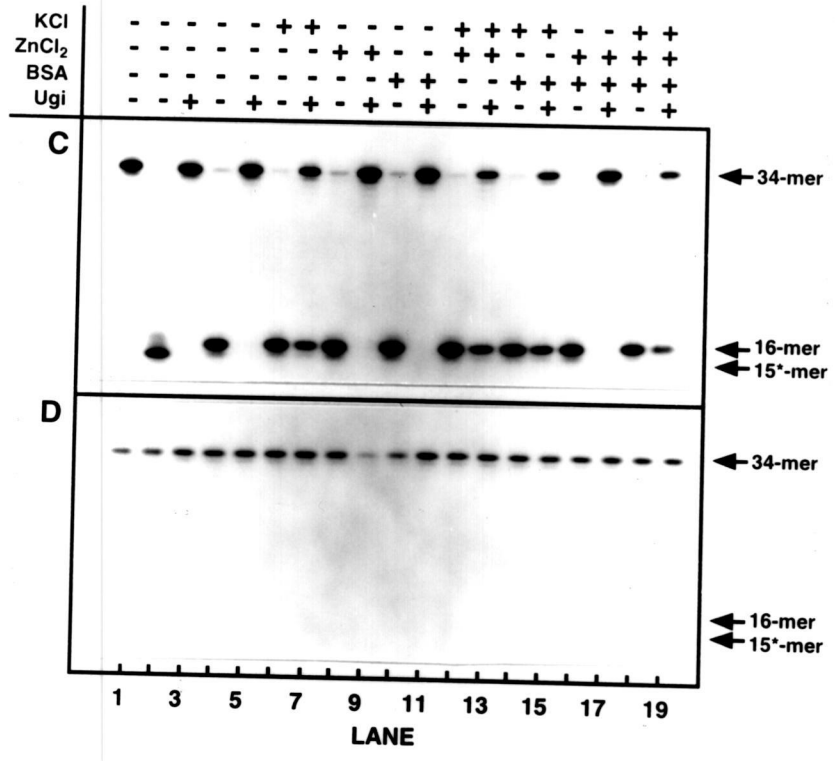

Figure 67 (continued)

DNA substrate containing the appropriate [^{32}P]34-mer supplemented with no addition, *E. coli* uracil-DNA glycosylase, or uracil-DNA glycosylase plus Ugi were analyzed for comparative purposes using UDG buffer (Figure 67A-D, lanes 1-3, respectively). As previously demonstrated, ds-UDG activity was not detected on single-stranded [^{32}P]U-34-mer or duplex [^{32}P]T/G-34-mer using any combination of buffer components (Figure 67A and D). However, ds-UDG activity was detected using buffer conditions that included 50 mM KCl and duplex [^{32}P]U/A- or [^{32}P]U/G-34-mer (Figure 67B and C, lanes 7, 13, 15, and 19). Importantly, UDG buffer supplemented with acetylated bovine serum albumin (BSA) did not yield a positive result and eliminated BSA as a potential source for this novel activity (Figure 67B and C, lane 11). These results suggest that monovalent ions are influential in stimulating ds-UDG activity.

To compare the amount of ds-UDG and uracil-DNA glycosylase activity present in U251 and U251*ugi*17 cell extracts, various amounts of cell extract were incubated with oligonucleotides [^{32}P]U/A- and [^{32}P]U/G-34-mer under reaction conditions previously used to detect TDG activity, treated with alkali, and analyzed by denaturing polyacrylamide gel electrophoresis. In addition, duplex oligonucleotides [^{32}P]A/U- and [^{32}P]G/U-34-mer, which contained the ^{32}P-label on the non-uracil-containing strand, were incubated with cell extract (160 μg) and similarly processed. Reactions were conducted both in the presence and absence of exogenous Ugi and results obtained with U251 and U251*ugi*17 cell extracts are represented in Figures 68 and 69 and Figures 70 and 71, respectively. As controls, each [^{32}P]34-mer substrate was incubated with no addition, uracil-DNA glycosylase, or uracil-DNA glycosylase plus Ugi under identical reaction conditions for comparative purposes (Figure 68 and Figure 70, A-D, lanes 1-3, respectively). As before, addition of Ugi to parental U251 cell extracts inhibited uracil-DNA glycosylase activity but did not inhibit the Ugi-insensitive double-strand specific uracil-DNA glycosylase activity which exhibited preferential activity toward U:G mispairs (Figure 68C) over U:A base pairs (Figure 68A). This novel activity was also shown to be specific for the

Figure 68. Effect of Ugi on uracil-DNA glycosylase activities detected in human U251 cell extracts. (A) Two sets of uracil-DNA glycosylase reaction mixtures (100 µl) each containing 160, 40, 10, 2.5, 0.63, and 0.16 µg of U251 crude extract protein were incubated in the absence (lanes 4-9, respectively) or the presence (lanes 10-15, respectively) of 1000 units of Ugi protein with 4 pmol of [^{32}P]U/A-34-mer at 30°C for 30 min. Each reaction mixture contained 25 mM Hepes-KOH (pH 7.9), 50 mM KCl, 1 mM DTT, 0.5 mM EDTA, 0.01 mM $ZnCl_2$, and 100 µg/ml acetylated BSA. Control reaction mixtures either lacked crude extract protein (lane 1), contained 400 units of *E. coli* Ung (lane 2), or 400 units of *E. coli* Ung plus 1000 units of Ugi protein (lane 3). Reactions were terminated, DNA isolated, AP-sites hydrolyzed, and reaction products analyzed by denaturing 12% polyacrylamide/8.3 M urea gel electrophoresis and autoradiography. The locations of unreacted substrate (34-mer) and reaction products (15*- and 16-mer) are located by *arrows*. (B) Two uracil-DNA glycosylase reaction mixtures (100 µl) containing 160 µg of U251 crude extract protein supplemented with (lane 5) or without (lane 4) 1000 units of Ugi were incubated with 4 pmol of [^{32}P]A/U-34-mer at 30°C for 30 min and buffered as described above. Control reaction mixtures either lacked crude extract protein (lane 1), contained 400 units of *E. coli* Ung (lane 2), or 400 units of *E. coli* Ung plus 1000 units of Ugi protein (lane 3). Samples were processed and analyzed as described above. (C) The effect of Ugi on uracil-DNA glycosylase activities in human U251 cell extracts was examined under identical reaction conditions with [^{32}P]U/G-34-mer substrate as described above. (D) The effect of Ugi on uracil-DNA glycosylase activities in human U251 cell extracts was examined under identical reaction conditions with the [^{32}P]G/U-34-mer substrate as described above.

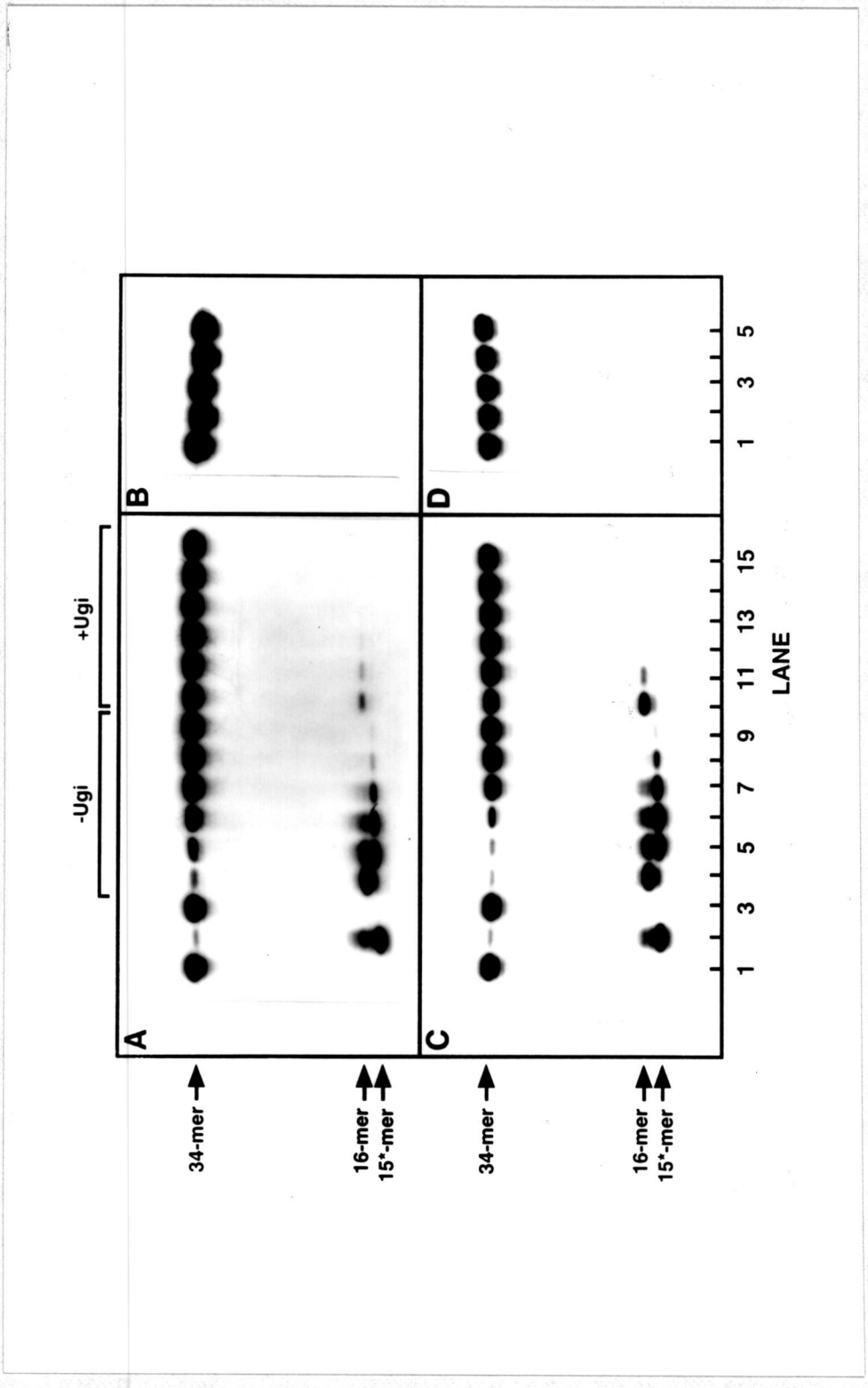
-Ugi
+Ugi
A
B
C
D
34-mer
16-mer
15*-mer
34-mer
16-mer
15*-mer
1 3 5 7 9 11 13 15
1 3 5
LANE

Figure 68

Figure 69. Quantitation of reaction products generated by U251 cell extracts in the presence and absence of Ugi. [^{32}P]DNA bands detected by autoradiography in Figure 67 (A and C, lanes 4-15) were excised from the dried gel and the amount of ^{32}P radioactivity was measured for reactions containing U251 crude extract protein incubated with [^{32}P]U/A-34-mer in the absence (*closed circles*) or presence (*open circles*) of Ugi and with [^{32}P]U/G-34-mer in the absence (*closed squares*) or presence (*open squares*) of Ugi. The percentage of product formed was calculated by dividing the amount of product ([^{32}P]15*-mer and [^{32}P]16-mer) by the amount of product plus substrate ([^{32}P]34-mer) and multiplying by 100.

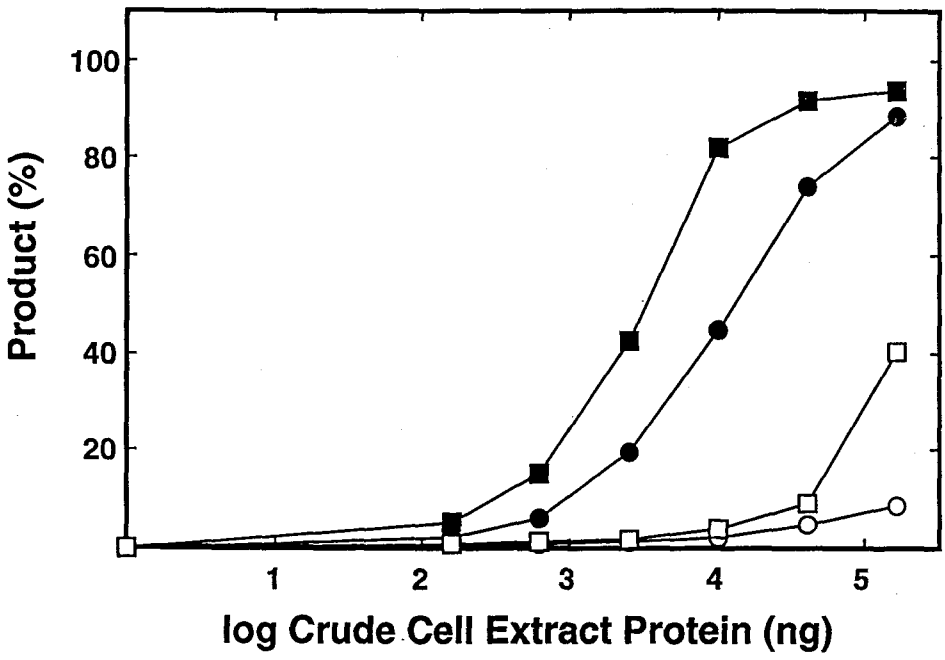
Product (%)
100
80
60
40
20
1
2
3
4
5
log Crude Cell Extract Protein (ng)

Figure 69

Figure 70. Effect of Ugi on uracil-DNA glycosylase activities detected in U251*ugi*17 cell extracts. (A) Two sets of uracil-DNA glycosylase reaction mixtures (100 µl) each containing 160, 40, 10, 2.5, 0.63, and 0.16 µg of U251*ugi*17 crude extract protein were incubated in the absence (lanes 4-9, respectively) or the presence (lanes 10-15, respectively) of 1000 units of Ugi protein with 4 pmol of [^{32}P]U/A-34-mer at 30°C for 30 min. Each reaction mixture contained 25 mM Hepes-KOH (pH 7.9), 50 mM KCl, 1 mM DTT, 0.5 mM EDTA, 0.01 mM $ZnCl_2$, and 100 µg/ml acetylated BSA. Control reaction mixtures either lacked crude extract protein (lane 1), contained 400 units of *E. coli* Ung (lane 2), or 400 units of *E. coli* Ung plus 1000 units of Ugi protein (lane 3). Reactions were terminated, DNA isolated, AP-sites hydrolyzed, and reaction products analyzed by denaturing 12% polyacrylamide/8.3 M urea gel electrophoresis and autoradiography. The location of unreacted substrate (34-mer) and reaction products (15*- and 16-mer) are located by *arrows*. (B) Two uracil-DNA glycosylase reaction mixtures (100 µl) containing 160 µg each of U251*ugi*17 crude extract protein supplemented with (lane 5) or without (lane 4) 1000 units of Ugi were incubated with 4 pmol of [^{32}P]A/U-34-mer at 30°C for 30 min and buffered as described above. Control reaction mixtures either lacked crude extract protein (lane 1), contained 400 units of *E. coli* Ung (lane 2), or 400 units of *E. coli* Ung plus 1000 units of Ugi protein (lane 3). Samples were processed and analyzed as described above. (C) The effect of Ugi on uracil-DNA glycosylase activities in human U251*ugi*17 cell extracts was examined under identical reaction conditions with [^{32}P]U/G-34-mer substrate as described above. (D) The effect of Ugi on uracil-DNA glycosylase activities in human U251*ugi*17 cell extracts was examined under identical reaction conditions with the [^{32}P]G/U-34-mer substrate as described above.

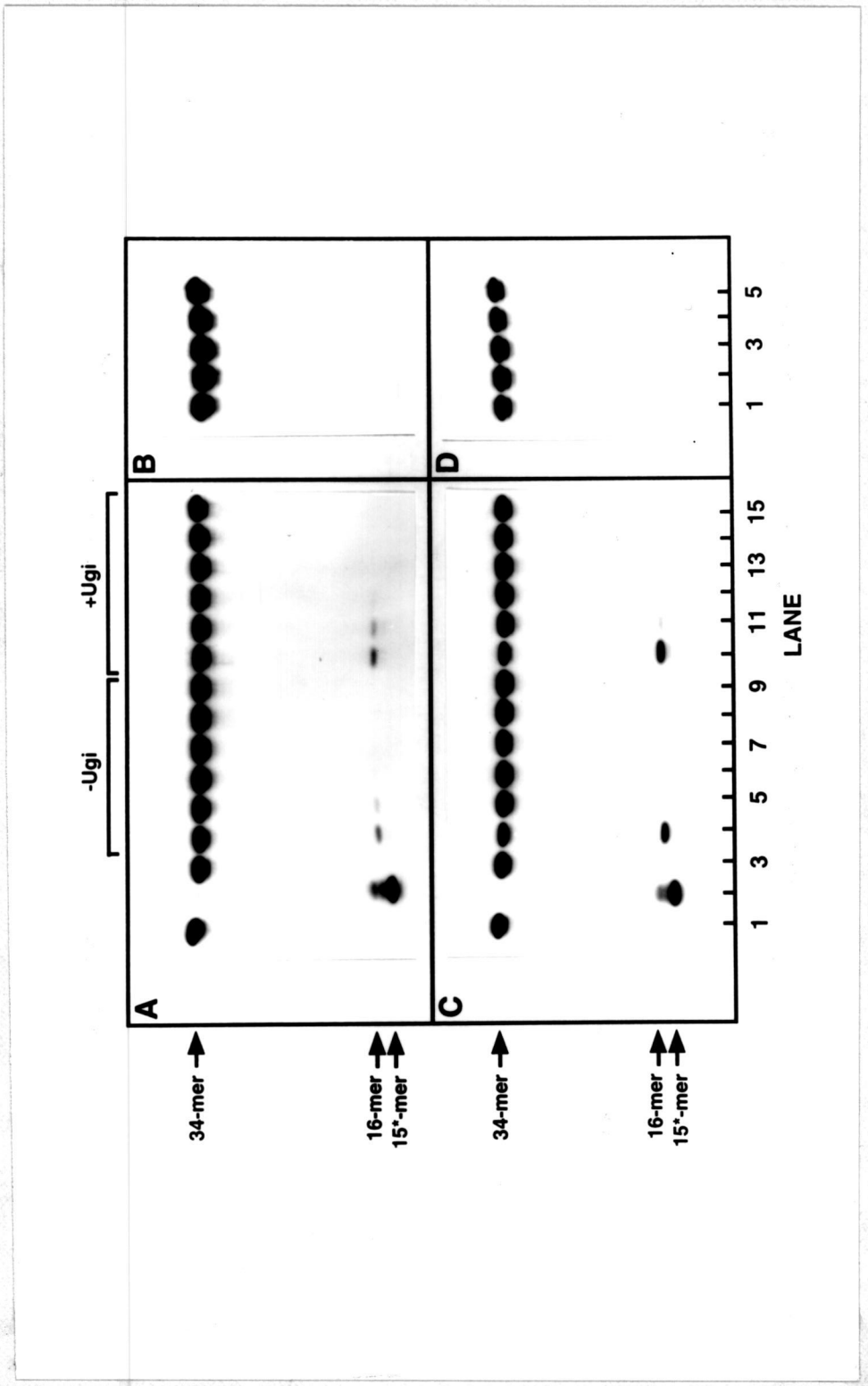
-Ugi
+Ugi
A
B
C
D
1 3 5 7 9 11 13 15
1 3 5
LANE
34-mer
16-mer
15*-mer
34-mer
16-mer
15*-mer

Figure 70

Figure 71. Quantitation of reaction products generated by U251*ugi*17 cell extracts in the presence and absence of Ugi. [^{32}P]DNA bands detected by autoradiography in Figure 69 (A and C, lanes 4-15) were excised from the dried gel and the amount of ^{32}P radioactivity was measured for reactions containing U251*ugi*17 crude extract protein incubated with [^{32}P]U/A-34-mer in the absence (*closed circles*) or presence (*open circles*) of Ugi and with [^{32}P]U/G-34-mer in the absence (*closed squares*) or presence (*open squares*) of Ugi. The percentage of product formed was calculated by dividing the amount of product ([^{32}P]15*-mer and [^{32}P]16-mer) by the amount of product plus substrate ([^{32}P]34-mer) and multiplying by 100.

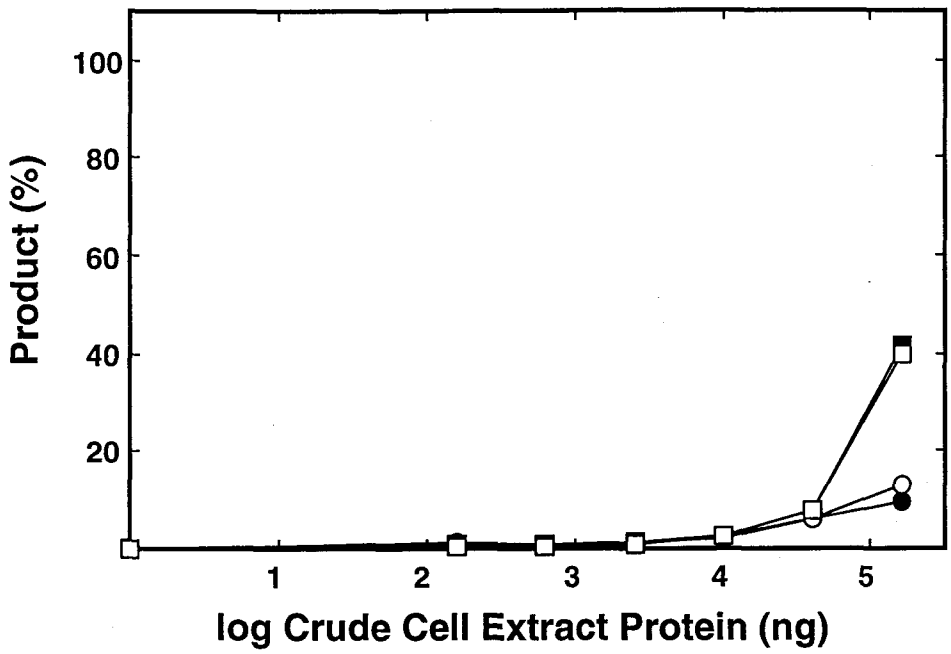
Product (%)
100
80
60
40
20
1
2
3
4
5
log Crude Cell Extract Protein (ng)

Figure 71

uracil-containing strand of both the U:A and U:G substrates as verified by the presence of intact [^{32}P]A- and [^{32}P]G-34-mer DNA bands incubated under identical conditions (Figure 68B and D, respectively, lane 5). Virtually identical results were obtained for U251*ugi*17 cell extracts (Figure 70A-D) although the presence or absence of Ugi did not affect the amount of uracil removal since Ugi production in U251*ugi*17 cells effectively eliminated endogenous uracil-DNA glycosylase activity.

After quantitating the amount of 15*-mer and 16-mer detected for the [^{32}P]U/A- and [^{32}P]U/G-34-mer substrates, the percentage of product formed in each reaction was plotted as a function of crude cell extract protein for U251 and U251*ugi*17 cells (Figure 69 and Figure 71, respectively). Again, the extent of uracil excision was determined for the initial 10 % of the product formed. For parental U251 cells, the activity of crude cell extract protein in the absence of exogenous Ugi for the removal of uracil from the U/A and U/G substrates was determined to be 433 and 1324 fmol of uracil removed per μg of extract protein, respectively. In the presence of Ugi, these values decreased to 1.5 and 9.7 fmol of uracil removed per μg of extract protein for U/A and U/G substrates, respectively. Thus, the double-strand-specific uracil-DNA glycosylase activity appears to contribute only a minor percentage of the overall uracil excision activity present in parental U251 cells under the conditions tested. For U251 m*ugi*-17 cells, the activity of crude cell extract protein in the absence of exogenous Ugi for the removal of uracil from the U/A and U/G substrates was determined to be 2.1 and 6.0 fmol of uracil removed per μg of extract, respectively, whereas these values were calculated to be 4.5 and 6.2 in the presence of exogenous Ugi. Thus, double-strand specific uracil-DNA glycosylase activity is present at similar levels in both U251 and U251*ugi*17 cell extracts but appears to contribute a relatively minor role in uracil-initiated BER as compared to the Ugi-sensitive UDGs.

5.2 Discussion

Ugi has been previously demonstrated to inhibit various forms of uracil-DNA glycosylase isolated from human cells, including the nuclear (UNG2 or UDG1A), mitochondrial (UNG1 or UDG1), and cyclin-like (UDG2) enzymes (36, 46, 167, 178, 292). Since *in vitro* observations have indicated that the UDG•Ugi complex is essentially irreversible under physiological conditions (15, 17, 231), it seemed feasible that expression of the *ugi* gene in human cells might lead to a uracil-DNA glycosylase defective phenotype. A similar strategy utilizing the *in vivo* expression of the *ugi* gene in *E. coli* previously resulted in bacteria with phenotypic properties that were reflective of *ung* mutants (291). Thus, a eukaryotic expression vector containing the *ugi* gene designed by Dr. E. Radany (University of Michigan) was developed to simultaneously knock out the three human UDG activities. This strategy circumvented the need to individually disrupt the expression of at least two UDG genes by a more complicated genetic approach. The results presented here demonstrated that U251 glioma cells transformed with the pvBiPNeo1001-m*ugi* vector produced active Ugi *in vivo* which in turn inactivated the uracil-DNA glycosylase. This observation was supported by the apparent absence of uracil-DNA glycosylase activity (>775-fold reduction) in U251*ugi*17 cell extracts when assayed on either activated calf-thymus DNA containing U•A base pairs or on U-34-mer, U/A-34-mer, and U/G-34-mer synthetic DNA substrates.

A detailed investigation of UDG activity in U251 and U251*ugi*17 cell extracts was conducted using defined uracil-containing oligonucleotide (U-, U/A-, and U/G-34-mer) substrates. UDG activity was not detected in U251*ugi*17 cell extracts, which was consistent with previous reports indicating that the three major UDG activities in human cells are inhibited by Ugi (36, 167, 292). This observation was confirmed by the detection of excess Ugi in extracts that lacked a detectable amount of uracil-DNA glycosylase activity. Contrary to our expectations, the U251*ugi*17 cell extract did not exhibit activity

toward the U/G-34-mer substrate. Recently, a human mismatch-specific thymine-DNA glycosylase (TDG) activity was reported to excise uracil from U•G mispairs more efficiently than it excises thymine from T•G mispairs (186). Unlike UDGs, TDG has been shown to be Ugi-resistant and does not recognize uracil residues in either single-stranded DNA or double-stranded DNA containing U•A base pairs (80, 186). Thus, it was anticipated that this activity might appear in both the human U251*ugi*17 cell extracts and the U251 cell extracts treated with Ugi *in vitro*. The inability to detect TDG could not be attributed to DNA substrate differences since the identical oligonucleotide substrate previously reported for detecting TDG activity (186) was used in this study. However, it was recognized that the standard reaction conditions used for detecting uracil-DNA glycosylase differed somewhat from those reported for optimal TDG activity. In an attempt to examine this difference, U251 and U251*ugi*17 cell extracts were assayed under conditions specifically defined for detecting TDG activity *in vitro* (246). Under these conditions, a Ugi-resistant uracil-DNA glycosylase activity was detected that catalyzed the removal of uracil from the U/A- and U/G-34-mer substrates but not thymine from the T/G-34-mer substrate. In contrast to the UDG enzyme, a 50 mM KCl buffer component was required in order to detect this Ugi-resistant activity. Additional experiments demonstrated that the removal of the uracil base was indicative of glycosylase action and the activity was specific for the uracil-containing strand. The inability of this Ugi-insensitive activity to remove uracil from the single-stranded DNA substrate clearly distinguished this activity from the conventional UDG activities. This observation eliminated the trivial possibility that the observed activity was derived from a sub-population of UDG that had escaped inhibition by Ugi. On the basis of these results, it seemed most likely that U251 and U251*ugi*17 cell extracts contained little, if any, TDG activity. However, this is not to indicate that the TDG gene product was excluded as a potential candidate for the activity detected in the presence of Ugi. For example, deletion mutant analysis of the N-terminal

and C-terminal regions of human TDG resulted in a mutant TDG enzyme that could effectively remove uracil but not thymine from U•G and T•G mispairs, respectively (80). Thus, it remains a formal possibility that post-translational proteolysis of TDG in U251 and U251*ugi*17 cell extracts or expression of a mutated form of TDG by these cell types could yield defective TDG polypeptides capable of processing U•G but not T•G mispairs. These results must be interpreted with considerable caution since the findings are based on a complex mixture of cell extract protein. Nevertheless, the observed substrate specificity clearly points to the existence of an alternative Ugi-resistant UDG enzyme(s).

Subsequent to this study, a detailed report of the kinetics of substrate recognition and excision by recombinant human TDG was published (298). The results indicated that the initial rate of uracil removal from a U•G mispair (k_{cat}=11 min^{-1}) was over 10-fold greater than that for the removal of thymine from a T•G mispair (k_{cat}=0.91 min^{-1}) (298). Coincidentally, the buffer conditions used in the study by Waters and Swann (298) were nearly identical to those of the present study and the 34-mer oligonucleotide substrates were identical. Thus, if TDG activity were present in the human U251 cell extracts, its detection should have been possible. When considering the limit of detection of the assay, a 10-fold reduction in product formation with the T/G-34-mer substrate should have been detectable.

In addition to the removal of uracil from U•G mispairs, the Ugi-resistant UDG activity in U251 cell extracts removed uracil from U•A base pairs at an approximately 3-fold reduced rate. The initial rate for uracil removal from a U•A base pair by purified human TDG was observed (k_{cat}=0.047 min^{-1}) that was ~234-fold lower than the initial rate observed for removal of uracil from a U•G mispair (298). Comparatively, the observed activity toward U•A base pairs of purified human TDG suggests that in U251 cells, an alternative enzyme other than TDG exists. Again, a comparison of

the substrate specificities and catalytic rates observed for purified TDG to those present in a cell extract are complicated due to the complex mixture of proteins present in these cell extracts.

Further elucidation of this Ugi-resistant double-strand specific uracil-DNA glycosylase activity must await the purification and characterization of this enzyme(s). The significance of an alternative uracil-DNA glycosylase activity requires further investigation. Experiments conducted to determine the initial rate of uracil removal indicated that U251 cell extracts removed 433 and 1324 fmol of uracil per μg of extract protein from U/A and U/G substrates, respectively. This was in sharp contrast to the ~2 and 6 fmol of uracil removed when incubated with U251*ugi*17 cell extracts. A comparison between U251 and U251*ugi*17 cell extracts for each of these respective substrates indicated an approximate 216- and 220-fold reduction in both activities for the Ugi-resistant double-strand specific UDG activity. Thus, the *in vitro* assays presented here suggests that the Ugi-insensitive activity most likely plays a relatively minor role in uracil-initiated BER as compared to the Ugi-sensitive UDGs. As a consequence, pvBiPNeo1001-m*ugi* transduction resulting in *ugi* expression and inactivation of UDGs provide a valuable model system for further understanding the physiological importance of uracil-DNA repair.

BIBLIOGRAPHY

1. Abbotts, J., SenGupta, D.N., Zmudzka, B., Widen, S.G., Notario, V., and Wilson, S.H. (1988) Expression of human DNA polymerase beta in *Escherichia coli* and characterization of the recombinant enzyme. *Biochemistry* 27, 901-909.

2. Ahn, J., Werneburg, B.G., and Tsai, M.-D. (1997) DNA polymerase beta: structure-fidelity relationship from pre-steady-state kinetic analysis of all possible correct and incorrect base pairs for wild type and R283A mutant. *Biochemistry* 36, 1100-1107.

3. Anderson, C.T., and Friedberg, E.C. (1980) The presence of nuclear and mitochondrial uracil-DNA glycosylase in extracts of human KB cells. *Nucleic Acids Res.* 8, 875-888.

4. Aspinwall, R., Rothwell, D.G., Roldan-Arjona, T., Anselmino, C., Ward, C.J., Cheadle, J.P., Sampson, J.R., Lindahl, T., Harris, P.C., and Hickson, I.D. (1997) Cloning and characterization of a functional human homolog of *Escherichia coli* endonuclease III. *Proc. Natl. Acad. Sci. U.S.A.* 94, 109-114.

5. Au, K.G., Clark, S., Miller, J.H., and Modrich, P. (1989) *Escherichia coli* mutY gene encodes an adenine glycosylase active on G-A mispairs. *Proc. Natl. Acad. Sci. U.S.A.* 86, 8877-8881.

6. Bailly, V., and Verly, W.G. (1988) Possible roles of beta-elimination and delta-elimination reactions in the repair of DNA containing AP (apurinic/apyrimidinic) sites in mammalian cells. *Biochem. J.* 253, 553-559.

7. Balasubramanian, S., Beger, R.D., Bennett, S.E., Mosbaugh, D.W., and Bolton, P.H. (1995) Secondary structure of uracil-DNA glycosylase inhibitor protein. *J. Biol. Chem.* 270, 296-303.

8. Barak, Y., Cohen-Fix, O., and Livneh, Z. (1995) Deamination of cytosine-containing pyrimidine photodimers in UV-irradiated DNA. *J. Biol. Chem.* 270, 24174-24179.

9. Barrett, T.E., Savva, R., Panayotou, G., Barlow, T., Brown, T., Jiricny, J., and Pearl, L.H. (1998) Crystal structure of a G:T/U mismatch-specific DNA glycosylase: mismatch recognition by complementary-strand interactions. *Cell* 92, 117-129.

10. Baxi, M.D., and Vishwanatha, J.K. (1995) Uracil DNA-glycosylase/glyceraldehyde-3-phosphate dehydrogenase is an Ap_4A binding protein. *Biochemistry* 34, 9700-9707.

11. Beard, W.A., Osheroff, W.P., Prasad, R., Sawaya, M.R., Jaju, M., Wood, T.G., Kraut, J., Kunkel, T.A., and Wilson, S.H. (1996) Enzyme-DNA interactions required for efficient nucleotide incorporation and discrimination in human DNA polymerase beta. *J. Biol. Chem.* 271, 12141-12144.

12. Beger, R.D., Balasubramanian, S., Bennett, S.E., Mosbaugh, D.W., and Bolton, P.H. (1995) Tertiary structure of uracil-DNA glycosylase inhibitor protein. *J. Biol. Chem.* 270, 16840-16847.

13. Bennett, R.A.O., Wilson, D.M. III, Wong, D., and Demple, B. (1997) Interaction of human apurinic endonuclease and DNA polymerase beta in the base excision repair pathway. *Proc. Natl. Acad. Sci. U.S.A.* 94, 7166-7169.

14. Bennett, S.E., Jensen, O.N., Barofsky, D.F., and Mosbaugh, D.W. (1994) UV-catalyzed cross-linking of *Escherichia coli* uracil-DNA glycosylase to DNA. *J. Biol. Chem.* 269, 21870-21879.

15. Bennett, S.E., and Mosbaugh, D.W. (1992) Characterization of the Escherichia coli uracil-DNA glycosylase/inhibitor protein complex. *J. Biol. Chem.* 267, 22512-22521.

16. Bennett, S.E., Sanderson, R.J., and Mosbaugh, D.W. (1995) Processivity of Escherichia coli and rat liver mitochondrial uracil-DNA glycosylase is affected by NaCl concentration. *Biochemistry* 34, 6109-6119.

17. Bennett, S.E., Schimerlik, M.I., and Mosbaugh, D.W. (1993) Kinetics of the uracil-DNA glycosylase/inhibitor protein association. *J. Biol. Chem.* 268, 26879-26885.

18. Berg, O.G., Winter, R.B., and von Hippel, P.H. (1981) Diffusion-driven mechanisms of protein translocation on nucleic acids. 1. Models and theory. *Biochemistry* 20, 6929-6948.

19. Bessman, M.J., Lehman, I.R., Adler, J., Zimmerman, S., Simms, E.S., and Kornberg, A. (1958) Enzymatic synthesis of deoxyribonucleic acid. III. The incorporation of pyrimidine and purine analogues into deoxyribonucleic acid. *Proc. Natl. Acad. Sci. U.S.A.* 44, 633-640.

20. Biade, S., Sobol, R.W., Wilson, S.H., and Matsumoto, Y. (1998) Impairment of proliferating cell nuclear antigen-dependent apurinic/apyrimidinic site repair on linear DNA. *J. Biol. Chem.* 273, 898-902.

21. Bjursell, G., Gussander, E., and Lindahl, T. (1979) Long regions of single-stranded DNA in human cells. *Nature* 280, 420-423.

22. Blount, B.C., Mack, M.M., Wehr, C.M., MacGregor, J.T., Hiatt, R.A., Wang, G., Wickramasinghe, S.N., Everson, R.B., and Ames, B.N. (1997) Folate deficiency causes uracil misincorporation into human DNA and chromosome breakage: implications for cancer and neuronal damage. *Proc. Natl. Acad. Sci. U.S.A.* 94, 3290-3295.

23. Boorstein, R.J., Hilbert, T.P., Cadet, J., Cunningham, R.P., and Teebor, G.W. (1989) UV-induced pyrimidine hydrates in DNA are repaired by bacterial and mammalian DNA glycosylase activities. *Biochemistry* 28, 6164-6170.

24. Boorstein, R.J., Hilbert, T.P., Cunningham, R.P., and Teebor, G.W. (1990) Formation and stability of repairable pyrimidine photohydrates in DNA. *Biochemistry* 29, 10455-10460.

25. Boosalis, M.S., Mosbaugh, D.W., Hamatake, R., Sugino, A., Kunkel, T.A., and Goodman, M.F. (1989) Kinetic analysis of base substitution mutagenesis by transient misalignment of DNA and by miscoding. *J. Biol. Chem.* 264, 11360-11366.

26. Boshart, M., Weber, F., Hahn, G., Dorsch-Hsler, K., Fleckenstein, B., and Schaffner, W. (1985) A very strong enhancer is located upstream of an immediate early gene of human cytomegalovirus. *Cell* 41, 521-530.

27. Branch, P., Hampson, R., and Karran, P. (1995) DNA mismatch binding defects, DNA damage tolerance, and mutator phenotypes in human colorectal carcinoma cell lines. *Cancer Res.* 55, 2304-2309.

28. Bridges, B.A., and Woodgate, R. (1985) The two-step model of bacterial UV mutagenesis. *Mutat. Res.* 150, 133-139.

29. Brown, T.C., and Jiricny, J. (1987) A specific mismatch repair event protects mammalian cells from loss of 5-methylcytosine. *Cell* 50, 945-950.

30. Brutlag, D., and Kornberg, A. (1972) Enzymatic synthesis of deoxyribonucleic acid. XXXVI. A proofreading function for the 3' to 5'exonuclease activity in deoxyribonucleic acid polymerases. *J. Biol. Chem.* 247, 241-248.

31. Brynolf, K., Eliasson, R., and Reichard, P. (1978) Formation of Okazaki fragments in polyoma DNA synthesis caused by misincorporation of uracil. *Cell* 13, 573-580.

32. Budd, M.E., and Campbell, J.L. (1995) Purification and enzymatic and functional characterization of DNA polymerase beta-like enzyme, POL4. expressed during yeast meiosis. *Methods Enzymol.* 262, 108-130.

33. Buechler, J.A., and Taylor, S.S. (1990) Differential labeling of the catalytic subunit of cAMP-dependent protein kinase with a water-soluble carbodiimide: identification of carboxyl groups protected by MgATP and inhibitor peptides. *Biochemistry* 29, 1937-1943.

34. Burgers, P.M. (1991) *Saccharomyces cerevisiae* replication factor C. II. Formation and activity of complexes with the proliferating cell nuclear antigen and with DNA polymerases delta and epsilon. *J. Biol. Chem.* 266, 22698-22706.

35. Caldecott, K.W., McKeown, C.K., Tucker, J.D., Ljungquist, S., and Thompson, L.H. (1994) An interaction between the mammalian DNA repair protein XRCC1 and DNA ligase III. *Mol. Cell. Biol.* 14, 68-76.

36. Caradonna, S., Ladner, R., Hansbury, M., Kosciuk, M., Lynch, F., and Muller, S. (1996) Affinity purification and comparative analysis of two distinct human uracil-DNA glycosylases. *Exp. Cell. Res.* 222, 345-359.

37. Caradonna, S.J., and Adamkiewicz, D.M. (1984) Purification and properties of the deoxyuridine triphosphate nucleotidohydrolase enzyme derived from HeLa S3 cells. *J. Biol. Chem.* 259, 5459-5464.

38. Caradonna, S.J., and Cheng, Y.-C. (1980) Uracil DNA-glycosylase. Purification and properties of this enzyme isolated from blast cells of acute myelocytic leukemia patients. *J. Biol. Chem.* 255, 2293-2300.

39. Carraway, K.L., and Koshland, D.E. (1972) Carbodiimide modification of proteins. *Methods Enzymol.* 25, 616-623.

40. Chagovetz, A. M., Sweasy, J.B., and Preston, B.D. (1997) Increased activity and fidelity of DNA polymerase beta on single-nucleotide gapped DNA. *J. Biol. Chem.* 272, 27501-27504.

41. Chang, L.M.S. (1973) Low molecular weight deoxyribonucleic acid polymerase from calf thymus chromatin. *J. Biol. Chem.* 248, 3789-3795.

42. Chen, H., and Shaw, B.R. (1993) Kinetics of bisulfite-induced cytosine deamination in single-stranded DNA. *Biochemistry* 32, 3535-3539.

43. Chen, H., and Shaw, B.R. (1994) Bisulfite induces tandem double CC to TT mutations in double-stranded DNA. 2. Kinetics of cytosine deamination. *Biochemistry* 33, 4121-4129.

44. Chung, D.W., Zhang, J.A., Tan, C.K., Davie, E.W., So, A.G., and Downey, K.M. (1991) Primary structure of the catalytic subunit of human DNA polymerase delta and chromosomal location of the gene. *Proc. Natl. Acad. Sci. U.S.A.* 88, 11197-11201.

45. Collins, K.L., Russo, A.A., Tseng, B.Y., and Kelly, T.J. (1993) The role of the 70 kDa subunit of human DNA polymerase alpha in DNA replication. *EMBO J.* 12, 4555-4566.

46. Cone, R., Bonura, T., and Friedberg, E.C. (1980) Inhibitor of uracil-DNA glycosylase induced by bacteriophage PBS2. Purification and preliminary characterization. *J. Biol. Chem.* 255, 10354-10358.

47. Coulondre, C., Miller, J.H., Farabaugh, P.J., and Gilbert, W. (1978) Molecular basis of base substitution hotspots in *Escherichia coli. Nature* 274, 775-780.

48. Cullmann, G., Hindges, R., Berchtold, M.W., and Hubscher, U. (1993) Cloning of a mouse cDNA encoding DNA polymerase delta: refinement of the homology boxes. *Gene* 134, 191-200.

49. Date, T., Yamaguchi, M., Hirose, F., Nishimoto, Y., Tanihara, K., and Matsukage, A. (1988) Expression of active rat DNA polymerase beta in *Escherichia coli. Biochemistry* 27, 2983-2990.

50. Davis, B.J. (1964) Disc electrophoresis. II. Method and application to human serum protein. *Ann. N. Y. Acad. Sci.* 121, 404-427.

51. Delort, A.M., Duplaa, A.M., Molko, D., Teoule, R., Leblanc, J.P., and Laval, J. (1985) Excision of uracil residues in DNA: mechanism of action of *Escherichia coli* and *Micrococcus luteus* uracil-DNA glycosylases. *Nucleic Acids Res.* 13, 319-335.

52. DeLucia, P., and Cairns, J. (1969) Isolation of an *E. coli* strain with a mutation affecting DNA polymerase. *Nature* 224, 1164-1166.

53. Dianov, G., and Lindahl, T. (1994) Reconstitution of the DNA base excision-repair pathway. *Curr. Biol.* 4, 1069-1076.

54. Dianov, G., Price, A., and Lindahl, T. (1992) Generation of single-nucleotide repair patches following excision of uracil residues from DNA. *Mol. Cell. Biol.* 12, 1605-1612.

55. Dianov, G., Sedgwick, B., Daly, G., Olsson, M., Lovett, S., and Lindahl, T. (1994) Release of 5'-terminal deoxyribose-phosphate residues from incised abasic sites in DNA by the *Escherichia coli* RecJ protein. *Nucleic Acids Res.* 22, 993-998.

56. Dimitriadis, E.K., Prasad, R., Vaske, M.K., Chen, L., Tomkinson, A.E., Lewis, M.S., and Wilson, S.H. (1998) Thermodynamics of human DNA ligase trimerization and association with DNA polymerase beta. *J. Biol. Chem.* 273, 20540-20550.

57. Domena, J.D., and Mosbaugh, D.W. (1985) Purification of nuclear and mitochondrial uracil-DNA glycosylase from rat liver. Identification of two distinct subcellular forms. *Biochemistry* 24, 7320-7328.

58. Domena, J.D., Timmer, R.T., Dicharry, S.A., and Mosbaugh, D.W. (1988) Purification and properties of mitochondrial uracil-DNA glycosylase from rat liver. *Biochemistry* 27, 6742-6751.

59. Dube, D.K., Kunkel, T.A., Seal, G., and Loeb, L.A. (1979) Distinctive properties of mammalian DNA polymerases. *Biochim. Biophys. Acta* 561, 369-382.

60. Duncan, B.K., and Chambers, J.A. (1984) The cloning and overproduction of *Escherichia coli* uracil-DNA glycosylase. *Gene* 28, 211-219.

61. Duncan, B.K., and Miller, J.H. (1980) Mutagenic deamination of cytosine residues in DNA. *Nature* 287, 560-561.

62. Duncan, B.K., Rockstroh, P.A., and Warner, H.R. (1978) *Escherichia coli* K-12 mutants deficient in uracil-DNA glycosylase. *J. bacteriol.* 134, 1039-1045.

63. Duncan, B.K., and Weiss, B. (1982) Specific mutator effects of *ung* (uracil-DNA glycosylase) mutations in *Escherichia coli. J. Bacteriol.* 151, 750-755.

64. Echols, H., and Goodman, M.F. (1991) Fidelity mechanisms in DNA replication. *Annu. Rev. Biochem.* 60, 477-511.

65. Eftedal, I., Guddal, P.H., Slupphaug, G., Volden, G., and Krokan, H.E. (1993) Consensus sequences for good and poor removal of uracil from double stranded DNA by uracil-DNA glycosylase. *Nucleic Acids Res.* 21, 2095-2101.

66. Ehrlich, M., Zhang, X.-Y., and Inamdar, N.M. (1990) Spontaneous deamination of cytosine and 5-methylcytosine residues in DNA and replacement of 5-methylcytosine residues with cytosine residues. *Mutation Res.* 238, 277-286.

67. Fix, D., and Bockrath, R. (1981) Thermal resistance to photoreactivation of specific mutations potentiated in *E. coli* B/r *ung* by ultraviolet light. *Mol. Gen. Genet.* 182, 7-11.

68. Focher, F., Mazzarello, P., Verri, A., Hubscher, U., and Spadari, S. (1990) Activity profiles of enzymes that control the uracil incorporation into DNA during neuronal development. *Mutation Res.* 237, 65-73.

69. Fortini, P., Pascucci, B., Parlanti, E., Sobol, R.W., Wilson, S.H., and Dogliotti, E. (1998) Different DNA polymerases are involved in the short- and long-patch base excision repair in mammalian cells. *Biochemistry* 37, 3575-3580.

70. Franklin, W.A., and Lindahl, T. (1988) DNA deoxyribophosphodiesterase. *EMBO J.* 7, 3617-3622.

71. Frederico, L.A., Kunkel, T.A., and Shaw, B.R. (1990) A sensitive genetic assay for the detection of cytosine deamination: determination of rate constants and the activation energy. *Biochemistry* 29, 2532-2537.

72. Frederico, L.A., Kunkel, T.A., and Shaw, B.R. (1993) Cytosine deamination in mismatched base pairs. *Biochemistry* 32, 6523-6530.

73. Freshney, R.I. (1987) *Culture of Animal Cells: A Manual of Basic Techniques,* Alan R. Liss, Inc., New York, NY.

74. Friedberg, E.C., Ganesan, A.K., and Minton, K. (1975) *N*-glycosidase activity in extracts of *Bacillus subtilis* and its inhibition after infection with bacteriophage PBS2. *J. Virol.* 16, 315-321.

75. Friedberg, E.C., Walker, G.C., and Siede, W. (1995) *DNA Repair and Mutagenesis,* American Society for Microbiology, Washington, D.C.

76. Frosina, G., Fortini, P., Rossi, O., Carrozzino, F., Abbondandolo, A., and Dogliotti, E. (1994) Repair of abasic sites by mammalian cell extracts. *Biochem. J.* 304, 699-705.

77. Frosina, G., Fortini, P., Rossi, O., Carrozzino, F., Raspaglio, G., Cox, L.S., Lane, D.P., Abbondandolo, A., and Dogliotti, E. (1996) Two pathways for base excision repair in mammalian cells. *J. Biol. Chem.* 271, 9573-9578.

78. Fry, M., and Loeb, L.A. (1986) *Animal Cell DNA Polymerases.*, CRC Press, Inc., Boca Raton, FL.

79. Gale, E.F., Cundliffe, E., Reynolds, P.E., Richmond, M.H., and Waring, M.J. (1981) *The Molecular Basis of Antibiotic Action,* Wiley/Interscience, New York, N.Y.

80. Gallinari, P., and Jiricny, J. (1996) A new class of uracil-DNA glycosylase related to human thymine-DNA glycosylase. *Nature* 383, 735-738.

81. Gates, F.T. III, and Linn, S. (1977) Endonuclease V of *Escherichia coli. J. Biol. Chem.* 252, 1647-1653.

82. Geider, K. (1972) DNA synthesis in nucleotide-permeable *Escherichia coli* cells. The effect of nucleotide analogues on DNA synthesis. *Eur. J. Biochem.* 27, 554-563.

83. Geren, L.M., O'Brien, P., Stonehuerner, J., and Millett, F. (1984) Identification of specific carboxylate groups on adrenodoxin that are involved in the interaction with adrenodoxin reductase. *J. Biol. Chem.* 259, 2155-2160.

84. Gibbs, P.E.M., McGregor, W.G., Maher, V.M., Nisson, P., and Lawrence, C.W. (1998) A human homolog of the *Saccharomyces cerevisiae REV3* gene, which encodes the catalytic subunit of DNA polymerase zeta. *Proc. Natl. Acad. Sci. U.S.A.* 95, 6876-6880.

85. Goulian, M., Bleile, B., and Tseng, B.Y. (1980) The effect of methotrexate on levels of dUTP in animal cells. *J. Biol. Chem.* 255, 10630-10637.

86. Goulian, M., Bleile, B., and Tseng, B.Y. (1980) Methotrexate-induced misincorporation of uracil into DNA. *Proc. Natl. Acad. Sci. U.S.A.* 77, 1956-1960.

87. Goulian, M., Herrmann, S.M., Sackett, J.W., and Grimm, S.L. (1990) Two forms of DNA polymerase delta from mouse cells. Purification and properties. *J. Biol. Chem.* 265, 16402-16411.

88. Graves, S.W., Johnson, A.A., and Johnson, K.A. (1998) Expression, purification, and initial charcterization of the large subunit of the human mitochondrial DNA polymerase. *Biochemistry* 37, 6050-6058.

89. Gray, H., and Wong, T.W. (1992) Purification and identification of subunit structure of the human mitochondrial DNA polymerase. *J. Biol. Chem.* 267, 5835-5841.

90. Grossman, L., and Rodgers, E. (1968) Evidence for the presence of cytosine photohydrates in UV irradiated nucleic acids. *Biochem. Biophys. Res. Commun.* 33, 975-983.

91. Gruskin, E.A., and Lloyd, R.S. (1986) The DNA scanning mechanism of T4 endonuclease V. Effect of NaCl concentration on processive nicking activity. *J. Biol. Chem.* 261, 9607-9613.

92. Gupta, P.K., and Sirover, M.A. (1981) Stimulation of the nuclear uracil DNA glycosylase in proliferating human fibroblasts. *Cancer Res.* 41, 3133-3136.

93. Gupta, P.K., and Sirover, M.A. (1984) Altered temporal expression of DNA repair in hypermutable Bloom's syndrome cells. *Proc. Natl. Acad. Sci. U.S.A.* 81, 757-761.

94. Harrington, J.J., and Lieber, M.R. (1994) The characterization of a mammalian DNA structure-specific endonuclease. *EMBO J.* 13, 1235-1246.

95. Hatahet, Z., Kow, Y.W., Purmal, A.A., Cunningham, R.P., and Wallace, S.S. (1994) New substrates for old enzymes. 5-hydroxy-2'-deoxycytidine and 5-hydroxy-2'-deoxyuridine are substrates for *Escherichia coli* endonuclease III and formamidopyrimidine DNA *N*-glycosylase, while 5-hydroxy-2'-deoxyuridine is a substrate for uracil DNA *N*-glycosylase. *J. Biol. Chem.* 269, 18814-18820.

96. Haug, T., Skorpen, F., Aas, P.A., Malm, V., Skjelbred, C., and Krokan, H.E. (1998) Regulation of expression of nuclear and mitochondrial forms of human uracil-DNA glycosylase. *Nucleic Acids Res.* 26, 1449-1457.

97. Haug, T., Skorpen, F., Kvaloy, K., Eftedal, I., Lund, H., and Krokan, H.E. (1996) Human uracil-DNA glycosylase gene: sequence organization, methylation pattern, and mapping to chromosome 12q23-q24.1. *Genomics* 36, 408-416.

98. Haug, T., Skorpen, F., Lund, H., and Krokan, H.E. (1994) Structure of the gene for human uracil-DNA glycosylase and analysis of the promoter function. *FEBS Lett.* 353, 180-184.

99. Haugland, R.P. (1992) *Handbook of Fluorescent Probes and Research Chemicals* (L. K.D.) 22, Molecular Probes Inc., Eugene, OR.

100. Hayatsu, H. (1976) Bisulfite modification of nucleic acids and their constituents. *Prog. Nucleic Acids Res. Mol. Biol.* 16, 75-124.

101. Higley, M., and Lloyd, R.S. (1993) Processivity of uracil DNA glycosylase. *Mutat. Res.* 294, 109-116.

102. Hindges, R., and Hubscher, U. (1997) Cloning, chromosomal localization, and interspecies interaction of mouse DNA polymerase delta small subunit (PolD2). *Genomics* 44, 45-51.

103. Hindges, R., and Hubscher, U. (1997) DNA polymerase delta, an essential enzyme for DNA transactions. *Biol. Chem.* 378, 345-362.

104. Hoare, D.G., and Koshland, D.E. (1967) A method for the quantitative modification and estimation of carboxylic acid groups in proteins. *J. Biol. Chem.* 242, 2447-2453.

105. Hochhauser, S.J., and Weiss, B. (1978) *Escherichia coli* mutants deficient in deoxyuridine triphosphatase. *J. Bacteriol.* 134, 157-166.

106. Holbeck, S.L., and Strathern, J.N. (1997) A role for *REV3* in mutagenesis during double-strand break repair in *Saccharomyces cerevisiae. Genetics* 147, 1017-1024.

107. Huang, J.-C., Svoboda, D.L., Reardon, J.T., and Sancar, A. (1992) Human nucleotide excision nuclease removes thymine dimers from DNA by incising the 22nd phosphodiester bond 5' and the 6th phosphodiester bond 3' to the photodimer. *Proc. Natl. Acad. Sci. U.S.A.* 89, 3664-3668.

108. Hunter, B.I., Yamagishi, H., and Takahashi, I. (1967) Molecular weight of bacteriophage PBS1 deoxyribonucleic acid. *J. Virol.* 9, 841-842.

109. Husain, I., Tomkinson, A.E., Burkhart, W.A., Moyer, M.B., Ramos, W., Mackey, Z.B., Besterman, J.M., and Chen, J. (1995) Purification and characterization of DNA ligase III from bovine testes. *J. Biol. Chem.* 270, 9683-9690.

110. Impellizzeri, K.J., Anderson, B., and Burgers, P.M.J. (1991) The spectrum of spontaneous mutations in a *Saccharomyces cerevisiae* uracil-DNA-glycosylase mutant limits the function of this enzyme to cytosine deamination repair. *J. Bacteriol.* 173, 6807-6810.

111. Izuta, S., Roberts, J.D., and Kunkel, T.A. (1995) Replication error rates for G-dGTP, T-dGTP, and A-dGTP mispairs and evidence for differential proofreading by leading and lagging strand DNA replication complexes in human cells. *J. Biol. Chem.* 270, 2595-2600.

112. Jensen, O.N., Barofsky, D.F., Young, M.C., von Hippel, P.H., Swenson, S., and Seifried, S.E. (1993) Direct observation of UV-crosslinked protein-nucleic acid complexes by matrix-assisted laser desorption ionization mass spectrometry. *Rapid Commun. Mass Spectrom.* 7, 496-501.

113. Jiang, N., and Taylor, J.-S. (1993) *In vivo* evidence that UV-induced C to T mutations at dipyrimidine sites could result from the replicative bypass of *cis-syn* cyclobutane dimers or their deamination products. *Biochemistry* 32, 472-481.

114. Johnson, K.A. (1993) Conformational coupling in DNA polymerase fidelity. *Annu. Rev. Biochem.* 62, 685-713.

115. Kahan, F.M. (1963) Novel enzymes formed by *Bacillus subtilis* infected with bacteriophage. *Fed. Proc.* 22, 406.

116. Karran, P., Cone, R., and Friedberg, E.C. (1981) Specificity of the bacteriophage PBS2 induced inhibitor of uracil-DNA glycosylase. *Biochemistry* 20, 6092-6096.

117. Kavli, B., Slupphaug, G., Mol, C.D., Arvai, A.S., Petersen, S.B., Tainer, J.A., and Krokan, H.E. (1996) Excision of cytosine and thymine from DNA by mutants of human uracil-DNA glycosylase. *EMBO J.* 15, 3442-3447.

118. Klungland, A., and Lindahl, T. (1997) Second pathway for completion of human DNA base excision-repair: reconstitution with purified proteins and requirement for DNase IV (FEN1). *EMBO J.* 16, 3341-3348.

119. Koetsier, P.A., Schorr, J., and Doerfler, W. (1993) A rapid optimized protocol for downward alkaline southern blotting of DNA. *BioTechniques* 15, 260-262.

120. Korn, D., Fisher, P.A., and Wang, T. S.-F. (1983) Enzymological characterization of human DNA polymerases alpha and beta. *New Approaches in Eukaryotic DNA Replication* (A. M. de Recondo) 17-55, Plenum Press, New York, NY.

121. Krokan, H., and Wittwer, C.U. (1981) Uracil DNA-glycosylase from HeLa cells: general properties, substrate specificity and effect of uracil analogs. *Nucleic Acids Res.* 9, 2599-2613.

122. Krokan, H.E., Standal, R., and Slupphaug, G. (1997) DNA glycosylases in the base excision repair of DNA. *Biochem. J.* 325, 1-16.

123. Kubota, Y., Nash, R.A., Klungland, A., Schar, P., Barnes, D.E., and Lindahl, T. (1996) Reconstitution of DNA base excision-repair with purified human proteins: interaction between DNA polymerase beta and the XRCC1 protein. *EMBO J.* 15, 6662-6670.

124. Kumar, N.V., and Varshney, U. (1994) Inefficient excision of uracil from loop regions of DNA oligomers by *E. coli* uracil DNA glycosylase. *Nucleic Acids Res.* 22, 3737-3741.

125. Kumar, N.V., and Varshney, U. (1997) Contrasting effects of single stranded DNA binding protein on the activity of uracil DNA glycosylase from *Escherichia coli* towards different DNA substrates. *Nucleic Acids Res.* 25, 2336-2343.

126. Kunkel, T.A. (1984) Mutational specificity of depurination. *Proc. Natl. Acad. Sci. USA* 81, 1494-1498.

127. Kunkel, T.A. (1985) The mutational specificity of DNA polymerase-beta during *in vitro* DNA synthesis. *J. Biol. Chem.* 260, 5787-5796.

128. Kunkel, T.A. (1990) Misalignment-mediated DNA synthesis errors. *Biochemistry* 29, 8003-8011.

129. Kunkel, T.A., and Alexander, P.S. (1986) The base substitution fidelity of eucaryotic DNA polymerases. *J. Biol. Chem.* 261, 160-166.

130. Kunkel, T.A., Roberts, J.D., and Zakour, R.A. (1987) Rapid and efficient site-specific mutagenesis without phenotypic selection. *Methods Enzymol.* 154, 367-382.

131. Kunkel, T.A., Sabatino, R.D., and Bambara, R.A. (1987) Exonucleolytic proofreading by calf thymus DNA polymerase delta. *Proc. Natl. Acad. Sci. U.S.A.* 84, 4865-4869.

132. Kunkel, T.A., and Soni, A. (1988) Exonucleolytic proofreading enhances the fidelity of DNA synthesis by chick embryo DNA polymerase-gamma. *J. Biol. Chem.* 263, 4450-4459.

133. Kunkel, T.A., and Soni, A. (1988) Mutagenesis by transient misalignment. *J. Biol. Chem.* 263, 14784-14789.

134. Laemmli, U.K. (1970) Cleavage of structural proteins during the assembly of the heads of bacteriophage T4. *Nature* 227, 680-685.

135. Leblanc, J.-P., and Laval, J. (1982) Comparison at the molecular level of uracil-DNA glycosylases from different origins. *Biochimie* 64, 735-738.

136. Lecomte, P., Boiteux, S., and Doubleday, O. (1981) Mechansim of ultraviolet-induced mutagenesis: the coding properties of ultraviolet-irradiated poly(dC) replicated by *E. coli* DNA polymerase I. *Nucleic Acids Res.* 9, 3491-3501.

137. Lee, T.D., and Vemuri, S. (1989) *Proceedings of the 37th American Society of Mass Spectrometry Conference, May 21-26, Miami Beach, FL*

138. Levin, J.D., and Demple, B. (1990) Analysis of class II (hydrolytic) and class I (beta-lyase) apurinic/apyrimidinic endonucleases with a synthetic DNA substrate. *Nucleic Acids Res.* 18, 5069-5075.

139. Lewis, D.L., Farr, C.L., Wang, Y., Lagina, A.T., and Kaguni, L.S. (1996) Catalytic subunit of mitochondrial DNA polymerase from *Drosophila* embryos. Cloning, bacterial overexpression, and biochemical characterization. *J. Biol. Chem.* 271, 23389-23394.

140. Li, X., Li, J., Harrington, J., Lieber, M.R., and Burgers, P.M. (1995) Lagging strand DNA synthesis at the eukaryotic replication fork antigen. *J. Biol. Chem.* 270, 22109-22112.

141. Lin, T.-C., Rush, J., Spicer, E.K., and Konigsberg, W.H. (1987) Cloning and expression of T4 DNA polymerase. *Proc. Natl. Acad. Sci. U.S.A.* 84, 7000-7004.

142. Lindahl, T. (1979) DNA glycosylases, endonucleases for apurinic/apyrimidinic sites, and base excision-repair. *Prog. Nucleic Acid Res. Mol. Biol.* 22, 135-192.

143. Lindahl, T. (1980) Uracil-DNA glycosylase from *Escherichia coli. Methods Enzymol.* 65, 284-290.

144. Lindahl, T. (1982) DNA repair enzymes. *Annu. Rev. Biochem.* 51, 61-87.

145. Lindahl, T., and Barnes, D.E. (1992) Mammalian DNA ligases. *Annu. Rev. Biochem.* 61, 251-281.

146. Lindahl, T., Ljungquist, S., Siegert, W., Nyberg, B., and Sperens, B. (1977) DNA N-glycosidases. Properties of a uracil-DNA glycosidase from *Escherichia coli*. *J. Biol. Chem.* 252, 3286-3294.

147. Lindahl, T., and Nyberg, B. (1974) Heat-induced deamination of cytosine residues in deoxyribonucleic acid. *Biochemistry* 13, 3405-3410.

148. Ljungquist, S. (1977) A new endonuclease from *Escherichia coli* acting at apurinic sites in DNA. *J. Biol. Chem.* 252, 2808-2814.

149. Lloyd, R.S., Hanawalt, P.C., and Dodson, M.L. (1980) Processive action of T4 endonuclease V on ultraviolet-irradiated DNA. *Nucleic Acids Res.* 8, 5113-5127.

150. Longley, M.J., and Mosbaugh, D.W. (1993) In situ detection of DNA-metabolizing enzymes following polyacrylamide gel electrophoresis. *Methods Enzymol.* 218, 587-609.

151. Lovett, S.T., and Clark, A.J. (1984) Genetic analysis of the *recJ* gene of *Escherichia coli* K-12. *J. Bacteriol.* 157, 190-196.

152. Lundquist, A.J., Beger, R.D., Bennett, S.E., Bolton, P.H., and Mosbaugh, D.W. (1997) Site-directed mutagenesis and characterization of uracil-DNA glycosylase inhibitor protein. *J. Biol. Chem.* 272, 21408-21419.

153. Macejak, D.G., and Sarnow, P. (1991) Internal initiation of translation mediated by the 5' leader of a cellular mRNA. *Nature* 353, 90-94.

154. Makino, F., and Munakata, N. (1977) Isolation and characterization of a *Bacillus subtilis* mutant with a defective *N*-glycosidase activity for uracil-containing deoxyribonucleic acid. *J. Bacteriol.* 131, 438-445.

155. Matsumoto, Y., and Bogenhagen, D.F. (1989) Repair of a synthetic abasic site in DNA in a *Xenopus laevis* oocyte extract. *Mol. Cell. Biol.* 9, 3750-3757.

156. Matsumoto, Y., and Bogenhagen, D.F. (1991) Repair of a synthetic abasic site involves concerted reactions of DNA synthesis followed by excision and ligation. *Mol. Cell. Biol.* 11, 4441-4447.

157. Matsumoto, Y., and Kim, K. (1995) Excision of deoxyribose phosphate residues by DNA polymerase beta during DNA repair. *Science* 269, 699-702.

158. Matsumoto, Y., Kim, K., and Bogenhagen, D.F. (1994) Proliferating cell nuclear antigen-dependent abasic site repair in *Xenopus laevis* oocytes: an alternative pathway of base excsion DNA repair. *Mol. Cell. Biol.* 14, 6187-6197.

159. Mauro, D.J., De Riel, J.K., Tallarida, R.J., and Sirover, M.A. (1993) Mechanisms of excision of 5-fluorouracil by uracil DNA glycosylase in normal human cells. *Mol. Pharmacol.* 43, 854-857.

160. Medina, M., Peleato, M.L., Mendez, E., and Gomez-Moreno, C. (1992) Identification of specific carboxyl groups on *Anabaena* PCC 7119 flavodoxin which are involved in the interaction with ferredoxin-$NADP^+$ reductase. *Eur. J. Biochem.* 203, 373-379.

161. Merchant, K., Chen, H., Gonzales, T.C., Keefer, L.K., and Shaw, B.R. (1996) Deamination of single-stranded DNA cytosine residues in aerobic nitric oxide solution at micromolar total NO exposures. *Chem. Res. Toxicol.* 9, 891-896.

162. Meyer-Siegler, K., Mauro, D.J., Seal, G., Wurzer, J., deRiel, J.K., and Sirover, M.A. (1991) A human nuclear uracil DNA glycosylase is the 37-kDa subunit of glyceraldehyde-3-phosphate dehydrogenase. *Proc. Natl. Acad. Sci. U.S.A.* 88, 8460-8464.

163. Miller, A.D., and Rosman, G.J. (1989) Improved retroviral vectors for gene transfer and expression. *BioTechniques* 7, 980-990.

164. Miller, J.H., Ganem, D., Lu, P., and Schmitz, A. (1977) Genetic studies of the lac repressor. I. Correlation of mutational sites with specific amino acid residues: construction of a colinear gene-protein map. *J. Mol. Biol.* 109, 275-298.

165. Miller, J.H., Lebkowski, J.S., Greisen, K.S., and Calos, M.P. (1984) Specificity of mutations induced in transfected DNA by mammalian cells. *EMBO J.* 3, 3117-3121.

166. Mitchell, D.L., Jen, J., and Cleaver, J.E. (1991) Relative induction of cyclobutane dimers and cytosine photohydrates in DNA irradiated *in vitro* and *in vivo* with ultraviolet-C and ultraviolet-B light. *Photochem. Photobiol.* 54, 741-746.

167. Mol, C.D., Arvai, A.S., Sanderson, R.J., Slupphaug, G., Kavli, B., Krokan, H.E., Mosbaugh, D.W., and Tainer, J.A. (1995) Crystal structure of human uracil-DNA glycosylase in complex with a protein inhibitor: protein mimicry of DNA. *Cell* 82, 701-708.

168. Mol, C.D., Arvai, A.S., Slupphaug, G., Kavli, B., Alseth, I., Krokan, H.E., and Tainer, J.A. (1995) Crystal structure and mutational analysis of human uracil-DNA glycosylase: structural basis for specificity and catalysis. *Cell* 80, 869-878.

169. Morrison, A., Christensen, R.B., Alley, J., Beck, A.K., Bernstine, E.G., Lemontt, J.F., and Lawrence, C.W. (1989) *REV3*, a *Saccharomyces cerevisiae* gene whose function is required for induced mutagenesis, is predicted to encode a nonessential DNA polymerase. *J. Bacteriol.* 171, 5659-5667.

170. Mosbaugh, D.W. (1988) Purification and characterization of porcine liver DNA polymerase gamma: utilization of dUTP and dTTP during *in vitro* DNA synthesis. *Nucleic Acid Res.* 16, 5645-5659.

171. Mosbaugh, D.W., and Bennett, S.E. (1994) Uracil-excision DNA repair. *Prog. Nucleic Acid Res. Mol. Biol.* 48, 315-370.

172. Mosbaugh, D.W., and Linn, S. (1980) Further characterization of human fibroblast apurinic/apyrimidinic DNA endonucleases. The definition of two mechanistic classes of enzyme. *J. Biol. Chem.* 255, 11743-11752.

173. Mosbaugh, D.W., and Linn, S. (1982) Characterization of the action of *Escherichia coli* DNA polymerase I at incisions produced by repair endodeoxyribonucleases. *J. Biol. Chem.* 257, 575-583.

174. Mosbaugh, D.W., and Linn, S. (1983) Excision repair and DNA synthesis with a combination of HeLa DNA polymerase beta and DNase V. *J. Biol. Chem.* 258, 108-118.

175. Moyer, R., Briley, D., Johnsen, A., Stewart, U., and Shaw, B.R. (1993) Echinomycin, a bis-intercalating agent, induces C to T mutations via cytosine deamination. *Mutat. Res.* 288, 291-300.

176. Muller, S.J., and Caradonna, S. (1991) Isolation and characterization of a human cDNA encoding uracil-DNA glycosylase. *Biochim. Biophys. Acta* 1088, 197-207.

177. Muller, S.J., and Caradonna, S. (1993) Cell cycle regulation of a human cyclin-like gene encoding uracil-DNA glycosylase. *J. Biol. Chem.* 268, 1310-1319.

178. Muller-Weeks, S., Mastran, B., and Caradonna, S. (1998) The nuclear isoform of the highly conserved human uracil-DNA glycosylase is an M_r 36,000 phosphoprotein. *J. Biol. Chem.* 273, 21909-21917.

179. Muller-Weeks, S.J., and Caradonna, S. (1996) Specific association of cyclin-like uracil-DNA glycosylase with the proliferating cell nuclear antigen. *Exp. Cell Res.* 226, 346-355.

180. Myers, K.A., Saffhill, R., and O'Connor, P.J. (1988) Repair of alkylated purines in the hepatic DNA of mitochondria and nuclei in the rat. *Carcinogenesis* 9, 285-292.

181. Nagelhus, T.A., Slupphaug, G., Lindmo, T., and Krokan, H.E. (1995) Cell cycle regulation and subcellular localization of the major human uracil-DNA glycosylase. *Exp. Cell. Res.* 220, 292-297.

182. Nash, R.A., Caldecott, K.W., Barnes, D.E., and Lindahl, T. (1997) XRCC1 protein interacts with one of two distinct forms of DNA ligase III. *Biochemistry* 36, 5207-5211.

183. Nealon, K., Nicholl, I.D., and Kenny, M.K. (1996) Characterization of the DNA polymerase requirement of human base excision repair. *Nucleic Acid Res.* 24, 3763-3770.

184. Neddermann, P., Gallinari, P., Lettieri, T., Schmid, D., Truong, O., Hsuan, J.J., Wiebauer, K., and Jiricny, J. (1996) Cloning and expression of human G/T mismatch-specific thymine-DNA glycosylase. *J. Biol. Chem.* 271, 12767-12774.

185. Neddermann, P., and Jiricny, J. (1993) The purification of a mismatch-specific thymine-DNA glycosylase from HeLa cells. *J. Biol. Chem.* 268, 21218-21224.

186. Neddermann, P., and Jiricny, J. (1994) Efficient removal of uracil from G:U mispairs by the mismatch-specific thymine DNA glycosylase from HeLa cells. *Proc. Natl. Acad. Sci. U.S.A.* 91, 1642-1646.

187. Nelson, J.R., Lawrence, C.W., and Hinkle, D.C. (1996) Thymine-thymine dimer bypass by yeast DNA polymerase zeta. *Science* 272, 1646-1649.

188. Neuhard, J., and Thomassen, E. (1976) Altered deoxyribonucleotide pools in P2 eductants of *Escherichia coli* K-12 due to deletion of the *dcd* gene. *J. Bacteriol.* 126, 999-1001.

189. Nevins, J.R. (1992) Transcriptional regulation. A closer look at E2F. *Nature* 358, 375-376.

190. Nicholl, I.D., Nealon, K., and Kenny, M.K. (1997) Reconstitution of human base excision repair with purified proteins. *Biochemistry* 36, 7557-7566.

191. Nilsen, H., Otterlei, M., Haug, T., Solum, K., Nagelhus, T.A., Skorpen, F., and Krokan, H.E. (1997) Nuclear and mitochondrial uracil-DNA glycosylases are generated by alternative splicing and transcription from different positions in the *UNG* gene. *Nucleic Acids Res.* 25, 750-755.

192. Nilsen, H., Yazdankhah, S.P., Eftedal, I., and Krokan, H.E. (1995) Sequence specificity for removal of uracil from U:A pairs and U:G mismatches by uracil-DNA glycosylase from *Escherichia coli*, and correlation with mutational hotspots. *FEBS Lett.* 362, 205-209.

193. O'Donnell, R.E., Boorstein, R.J., Cunningham, R.P., and Teebor, G.W. (1994) Effect of pH and temperature on the stability of UV-induced repairable pyrimidine hydrates in DNA. *Biochemistry* 33, 9875-9880.

194. O'Donovan, G.A., Edlin, G., Fuchs, J.A., Neuhard, J., and Thomassen, E. (1971) Deoxycytidine triphosphate deaminase: characterization of an *Escherichia coli* mutant deficient in the enzyme. *J. Bacteriol.* 105, 666-672.

195. Olivera, B.M. (1978) DNA intermediates at the *Escherichia coli* replication fork: effect of dUTP. *Proc. Natl. Acad. Sci. U.S.A.* 75, 238-242.

196. Olsen, L.C., Aasland, R., Wittwer, C.U., Krokan, H.E., and Helland, D.E. (1989) Molecular cloning of human uracil-DNA glycosylase, a highly conserved DNA repair enzyme. *EMBO J.* 8, 3121-3125.

197. Panayotou, G., Brown, T., Barlow, T., Pearl, L.H., and Savva, R. (1998) Direct measurement of the substrate preference of uracil-DNA glycosylase. *J. Biol. Chem.* 273, 45-50.

198. Patel, D.J., Kozlowski, S.A., Ikuta, S., and Itakura, K. (1984) Dynamics of DNA duplexes containing internal G.T, G.A, A.C, and T.C pairs: hydrogen exchange at and adjacent to mismatch sites. *Fed. Proc.* 43, 2663-2670.

199. Patrick, M.H., and Rahn, R.O. (1976) Photochemistry of DNA and Polynucleotides: Photoproducts. *Photochemistry and Photobiology of Nucleic Acids* (S. Y. Wang) 35-95, Academic Press, New York, N.Y.

200. Pelletier, H., Sawaya, M.R., Wolfle, W., Wilson, S.H., and Kraut, J. (1996) Crystal structures of human DNA polymerase beta complexed with DNA: implications for catalytic mechanism, processivity, and fidelity. *Biochemistry* 35, 12742-12761.

201. Peng, W., and Shaw, B.R. (1996) Accelerated deamination of cytosine residues in UV-induced cyclobutane pyrimidine dimers leads to CC to TT transitions. *Biochemistry* 35, 10172-10181.

202. Perlman, D., and Huberman, J.A. (1977) Asymmetric Okazaki piece synthesis during replication of simian virus 40 DNA *in vivo*. *Cell* 12, 1029-1043.

203. Piersen, C.E., Prasad, R., Wilson, S.H., and Lloyd, R.S. (1996) Evidence for an imino intermediate in the DNA polymerase beta deoxyribose phosphate excision reaction. *J. Biol. Chem.* 271, 17811-17815.

204. Pinz, K.G., and Bogenhagen, D.F. (1998) Efficient repair of abasic sites in DNA by mitochondrial enzymes. *Mol. Cell. Biol.* 18, 1257-1265.

205. Podust, L.M., Podust, V.N., Floth, C., and Hubscher, U. (1994) Assembly of DNA polymerase delta and epsilon holoenzymes depends on the geometry of the DNA template. *Nucleic Acids Res.* 22, 2970-2975.

206. Podust, L.M., Podust, V.N., Sogo, J.M., and Hubscher, U. (1995) Mammalian DNA polymerase auxillary proteins: analysis of replication factor C-catalyzed proliferating cell nuclear antigen loading onto circular double-stranded DNA. *Mol. Cell. Biol.* 15, 3072-3081.

207. Podust, V.N., Podust, L.M., Muller, F., and Hubscher, U. (1995) DNA polymerase delta holoenzyme: action on single-stranded DNA and on double-stranded DNA in the presence of replicative DNA helicases. *Biochemistry* 34, 5003-5010.

208. Prasad, R., Beard, W.A., Strauss, P.R., and Wilson, S.H. (1998) Human DNA polymerase beta deoxyribose phosphate lyase. Substrate specificity and catalytic mechanism. *J. Biol. Chem.* 273, 15263-15270.

209. Prasad, R., Singhal, R.K., Srivastava, D.K., Molina, J.T., Tomkinson, A.E., and Wilson, S.H. (1996) Specific interaction of DNA polymerase beta and DNA ligase I in a multiprotein base excision repair complex from bovine testis. *J. Biol. Chem.* 271, 16000-16007.

210. Prasad, R., Widen, S.G., Singhal, R.K., Watkins, J., Prakash, L., and Wilson, S.H. (1993) Yeast open reading frame YCR14C encodes a DNA beta-polymerase-like enzyme. *Nucleic Acids Res.* 21, 5301-5307.

211. Price, A., and Lindahl, T. (1991) Enzymatic release of 5'-terminal deoxyribose phosphate residues from damaged DNA in human cells. *Biochemistry* 30, 8631-8637.

212. Price, A.R., and Cook, S.J. (1972) New deoxyribonucleic acid polymerase induced by *Bacillus subtilis* bacteriophage PBS2. *J. Virol.* 9, 602-610.

213. Price, A.R., and Fogt, S.M. (1973) Deoxythymidylate phosphohydrolase induced by bacteriophage PBS2 during infection of *Bacillus subtilis*. *J. Biol. Chem.* 248, 1372-1380.

214. Price, A.R., and Frato, J. (1975) *Bacillus subtilis* deoxyuridinetriphosphatase and its bacteriophage PBS2-induced inhibitor. *J. Biol. Chem.* 250, 8804-8811.

215. Prigent, C., Satoh, M.S., Daly, G., Barnes, D.E., and Lindahl, T. (1994) Aberrant DNA repair and DNA replication due to an inherited enzymatic defect in human DNA ligase I. *Mol. Cell. Biol.* 14, 310-317.

216. Purmal, A.A., Lampman, G.W., Pourmal, E.I., Melamede, R.J., Wallace, S.S., and Kow, Y.W. (1994) Uracil DNA *N*-glycosylase distributively interacts with duplex polynucleotides containing repeating units of either TGGCCAAGCU or TGGCCAAGCTTGGCCAAGCU. *J. Biol. Chem.* 269, 22046-22053.

217. Purmal, A.A., Wallace, S.S., and Kow, Y.W. (1996) The phosphodiester bond 3' to a deoxyuridine residue is crucial for substrate binding for uracil-DNA glycosylase. *Biochemistry* 35, 16630-16637.

218. Putney, S.D., Benkovic, S.J., and Schimmel, P.R. (1981) A DNA fragment with an alpha-phosphorothioate nucleotide at one end is assymetrically blocked from digestion by exonuclease III and can be replicated *in vivo*. *Proc. Natl. Acad. Sci. U.S.A.* 78, 7350-7354.

219. Radany, E.H., Dornfeld, K.J., Sanderson, R.J., Savage, M.K., and Mosbaugh, D.W. (1998) Uracil-DNA glycosylase deficiency is phenocopied in human cells by expressing the Ugi protein.

220. Reichenberger, S., and Pfeiffer, P. (1998) Cloning, purification and characterization of DNA polymerase beta from *Xenopus laevis* - studies on its potential role in DNA-end joining. *Eur. J. Biochem.* 251, 81-90.

221. Reisner, A.H. (1984) Gel Protein Stains: A Rapid Procedure. *Meth. Enzymol.* 104, 439-441.

222. Roberts, J.D., and Kunkel, T.A. (1988) Fidelity of a human cell DNA replication complex. *Proc. Natl. Acad. Sci. U.S.A.* 85, 7064-7068.

223. Roberts, J.D., and Kunkel, T.A. (1996) "Fidelity of DNA Replication". *DNA Replication in Eukaryotic Cells* (M. L. DePamphilis) 217-247, Cold Spring Harbor Laboratory Press, Cold Spring Harbor, NY.

224. Robins, P., and Lindahl, T. (1996) DNA ligase IV from HeLa cell nuclei. *J. Biol. Chem.* 271, 24257-24261.

225. Robins, P., Pappin, D.J.C., Wood, R.D., and Lindahl, T. (1994) Structural and functional homology between mammalian DNase IV and the 5'-nuclease domain of *Escherichia coli* DNA polymerase I. *J. Biol. Chem.* 269, 28535-28538.

226. Ropp, P.A., and Copeland, W.C. (1996) Cloning and characterization of the human mitochondrial DNA polymerase, DNA polymerase gamma. *Genomics* 36, 449-458.

227. Ruiz-Rubio, M., and Bockrath, R. (1989) On the possible role of cytosine deamination in delayed photoreversal mutagenesis targeted at thymine-cytosine dimers in *E. coli. Mutat. Res.* 210, 93-102.

228. Sambrook, J., Fritsch, E.F., and Maniatis, T. (1989) *Molecular Cloning: A Laboratory Manual,* Cold Spring Harbor Laboratory, Cold Spring Harbor, NY.

229. Sancar, A. (1995) Excision repair in mammalian cells. *J. Biol. Chem.* 270, 15915-15918.

230. Sancar, A. (1996) DNA excision repair. *Annu. Rev. Biochem.* 65, 43-81.

231. Sanderson, R.J., and Mosbaugh, D.W. (1996) Identification of specific carboxyl groups on uracil-DNA glycosylase inhibitor protein that are required for activity. *J. Biol. Chem.* 271, 29170-29181.

232. Sanderson, R.J., and Mosbaugh, D.W. (1998) Fidelity and mutational specificity of uracil-initiated base excision DNA repair synthesis in human glioblastoma cell extracts. *J. Biol. Chem.* 273, 24822-24831.

233. Santi, D.V., and Danenberg, P.V. (1984) Folates in pyrimidine nucleotide biosynthesis. *Folates and Pterins* (R. L. Blakely and S. J. Benkovic) 345-398, Wiley, New York, N.Y.

234. Saparbaev, M., and Laval, J. (1998) 3,N^4-ethenocytosine, a highly mutagenic adduct, is a primary substrate for *Escherichia coli* double-stranded uracil-DNA glycosylase and human mismatch-specific thymine-DNA glycosylase. *Proc. Natl. Acad. Sci. U.S.A.* 95, 8508-8513.

235. Savva, R., McAuley-Hecht, K., Brown, T., and Pearl, L. (1995) The structural basis of specific base-excision repair by uracil-DNA glycosylase. *Nature* 373, 487-493.

236. Savva, R., and Pearl, L.H. (1995) Cloning and expression of the uracil-DNA glycosylase inhibitor (Ugi) from bacteriophage PBS-1 and crystallization of a uracil-DNA glycosylase-Ugi complex. *Proteins* 22, 287-289.

237. Savva, R., and Pearl, L.H. (1995) Nucleotide mimicry in the crystal structure of the uracil-DNA glycosylase-uracil glycosylase inhibitor protein complex. *Nat. Struct. Biol.* 2, 752-757.

238. Scharer, O.D., Kawate, T., Gallinari, P., Jiricny, J., and Verdine, G.L. (1997) Investigation of the mechanisms of DNA binding of the human G/T glycosylase using designed inhibitors. *Proc. Natl. Acad. Sci. U.S.A.* 94, 4878-4883.

239. Schuster, H. (1960) The reaction of nitrous acid with deoxyribonucleic acid. *Biochem. Biophys. Res. Commun.* 2, 320-323.

240. Setlow, R.B., Carrier, W.L., and Bollum, F.J. (1965) Pyrimidine dimers in UV-irradiated poly dI:dC. *Proc. Natl. Acad. Sci. U.S.A.* 53, 1111-1118.

241. Shapiro, R. (1980) Damage to DNA caused by hydrolysis. *Chromosome damage and repair.* (E. Seeberg and K. Kleppe) 3-18, Plenum Press, New York, N.Y.

242. Shapiro, R., and Klien, R.S. (1966) The deamination of cytidine and cytosine by acidic buffer solution. Mutagenic implications. *Biochemistry* 5, 2358-2362.

243. Shen, C.C., Wertelecki, W., Driggers, W.J., LeDoux, S.P., and Wilson, G.L. (1995) Repair of mitochondrial DNA damage induced by bleomycin in human cells. *Mutat. Res.* 337, 19-23.

244. Shimizu, K., Santocanale, C., Ropp, P.A., Longhese, M.P., Plevani, P., Lucchini, G., and Sugino, A. (1993) Purification and characterization of a new DNA polymerase from budding yeast *Saccharomyces cerevisiae*. A probable homolog of mammalian DNA polymerase beta. *J. Biol. Chem.* 268, 27148-27153.

245. Shlomai, J., and Kornberg, A. (1978) Deoxyuridine triphosphatase of *Escherichia coli*. Purification, properties, and use as a reagent to reduce uracil incorporation into DNA. *J. Biol. Chem.* 253, 3305-3312.

246. Sibghat-Ullah, Gallinari, P., Xu, Y.-Z., Goodman, M.F., Bloom, L.B., Jiricny, J., and Day, R.S., III (1996) Base analog and neighboring base effects on substrate specificity of recombinant human G:T mismatch-specific thymine DNA-glycosylase. *Biochemistry* 35, 12926-12932.

247. Singhal, R.K., Prasad, R., and Wilson, S.W. (1995) DNA polymerase beta conducts the gap-filling step in uracil-initiated base excision repair in a bovine testis nuclear extract. *J. Biol. Chem.* 270, 949-957.

248. Singhal, R.K., and Wilson, S.H. (1993) Short gap-filling synthesis by DNA polymerase beta is processive. *J. Biol. Chem.* 268, 15906-15911.

249. Slupphaug, G., Eftedal, I., Kavli, B., Bharati, S., Helle, N.M., Haug, T., Levine, D.W., and Krokan, H.E. (1995) Properties of a recombinant human uracil-DNA glycosylase from the *UNG* gene and evidence that *UNG* encodes the major uracil-DNA glycosylase. *Biochemistry* 34, 128-138.

250. Slupphaug, G., Markussen, F.-H., Olsen, L.C., Aasland, R., Aarsaether, N., Bakke, O., Krokan, H.E., and Helland, D.E. (1993) Nuclear and mitochondrial forms of human uracil-DNA glycosylase are encoded by the same gene. *Nucleic Acids Res.* 21, 2579-2584.

251. Slupphaug, G., Mol, C.D., Kavli, B., Arvai, A.S., Krokan, H.E., and Tainer, J.A. (1996) A nucleotide-flipping mechanism from the structure of human uracil-DNA glycosylase bound to DNA. *Nature* 384, 87-92.

252. Slupphaug, G., Olsen, L.C., Helland, D., Aasland, R., and Krokan, H.E. (1991) Cell cycle regulation and *in vitro* hybrid arrest analysis of the major human uracil-DNA glycosylase. *Nucleic Acids Res.* 19, 5131-5137.

253. Sobol, R.W., Horton, J.K., Kuhn, R., Gu, H., Singhal, R.K., Prasad, R., Rajewsky, K., and Wilson, S.H. (1996) Requirement of mammalian DNA polymerase-beta in base excsion repair. *Nature* 379, 183-186.

254. Sowers, L.C., Sedwick, W.D., and Shaw, B.R. (1989) Hydrolysis of N^3-methyl-2'-deoxycytidine: model compound for reactivity of protonated cytosine residues in DNA. *Mutation Res.* 215, 131-138.

255. Sowers, L.C., Shaw, B.R., Veigl, M.L., and Sedwick, W.D. (1987) DNA base modification: ionizing base pairs and mutagenesis. *Mutat. Res.* 177, 201-218.

256. Srivastava, D.K., Berg, B.J.V., Prasad, R., Molina, J.T., Beard, W.A., Tomkinson, A.E., and Wilson, S.H. (1998) Mammalian abasic site base excision repair. Identification of the reaction sequence and rate-determining steps. *J. Biol. Chem.* 273, 21203-21209.

257. Stalker, D.M., Mosbaugh, D.W., and Meyer, R.R. (1976) Novikoff hepatoma deoxyribonucleic acid polymerase. Purification and properties of a homogeneous beta polymerase. *Biochemistry* 15, 3114-3121.

258. Syvaoja, J., and Linn, S. (1989) Characterization of a large form of DNA polymerase delta from HeLa cells that is insensitive to proliferating cell nuclear antigen. *J. Biol. Chem.* 264, 2489-2497.

259. Takahashi, I., and Marmur, J. (1963) Replacement of thymidylic acid by deoxyuridylic acid in the deoxyribonucleic acid of a transducing phage for *Bacillus subtilis*. *Nature* 197, 794-795.

260. Talpaert-Borle, M., Campagnari, F., and Creissen, D.M. (1982) Properties of purified uracil-DNA glycosylase from calf thymus. An *in vitro* study using synthetic DNA-like substrates. *J. Biol. Chem.* 257, 1208-1214.

261. Talpaert-Borle, M., Clerici, L., and Campagnari, F. (1979) Isolation and characterization of a uracil-DNA glycosylase from calf thymus. *J. Biol. Chem.* 254, 6387-6391.

262. Tamanoi, F., and Okazaki, T. (1978) Uracil incorporation into nascent DNA of thymine-requiring mutant of *Bacillus subtilis* 168. *Proc. Natl. Acad. Sci. U.S.A.* 75, 2195-2199.

263. Tan, C.K., Castillo, C., So, A.G., and Downey, K.M. (1986) An auxillary protein for DNA polymerase-delta from fetal calf thymus. *J. Biol. Chem.* 261, 12310-12316.

264. Tanabe, K., Bohn, E.W., and Wilson, S.H. (1979) Steady-state kinetics of mouse DNA polymerase beta. *Biochemistry* 18, 3401-3406.

265. Taylor, A.F., and Weiss, B. (1982) Role of exonuclease III in the base excision repair of uracil-containing DNA. *J. Bacteriol.* 151, 351-357.

266. Terry, B.J., Jack, W.E., and Modrich, P. (1985) Facilitated diffusion during catalysis by *Eco*RI endonuclease. Nonspecific interaction in *Eco*RI catalysis. *J. Biol. Chem.* 260, 13130-13137.

267. Tessman, I., and Kennedy, M.A. (1991) The two-step model of UV mutagenesis reassessed: deamination of cytosine in cyclobutane dimers as the likely source of the mutations associated with photoreactivation. *Mol. Gen. Genet.* 227, 144-148.

268. Tessman, I., Kennedy, M.A., and Liu, S.-K. (1994) Unusual kinetics of uracil formation in single and double-stranded DNA by deamination of cytosine in cyclobutane pyrimidine dimers. *J. Mol. Biol.* 235, 807-812.

269. Thomas, D.C., Roberts, J.D., and Kunkel, T.A. (1991) Heteroduplex repair in extracts of human HeLa cells. *J. Biol. Chem.* 266, 3744-3751.

270. Thomas, D.C., Roberts, J.D., Sabatino, R.D., Myers, T.W., Tan, C.-K., Downey, K.M., So, A.G., Bambara, R.A., and Kunkel, T.A. (1991) Fidelity of mammalian DNA replication and replicative DNA polymerases. *Biochemistry* 30, 11751-11759.

271. Thompson, L.H., Brookman, K.W., Jones, N.J., Allen, S.A., and Carrano, A.V. (1990) Molecular cloning of the human XRCC1 gene, which corrects defective DNA strand break repair and sister chromatid exchange. *Mol. Cell. Biol.* 10, 6160-6171.

272. Timkovich, R. (1977) Detection of the stable addition of carbodiimide to proteins. *Anal. Biochem.* 79, 135-143.

273. Tomita, F., and Takahashi, I. (1969) A novel enzyme, dCTP deaminase, found in *Bacillus subtilis* infected with phage PBS1. *Biochim. Biophys. Acta* 179, 18-27.

274. Tomkinson, A.E., Lasko, D.D., Daly, G., and Lindahl, T. (1990) Mammalian DNA ligases. Catalytic domain and size of DNA ligase I. *J. Biol. Chem.* 265, 12611-12617.

275. Tomkinson, A.E., Roberts, E., Daly, G., Totty, N.F., and Lindahl, T. (1991) Three distinct DNA ligases in mammalian cells. *J. Biol. Chem.* 266, 21728-21735.

276. Torpey, L.E., Gibbs, P.E., Nelson, J., and Lawrence, C.W. (1994) Cloning and sequencing of *REV7*, a gene whose function is required for DNA damage-induced mutagenesis in *Saccharomyces cerevisiae*. *Yeast* 10, 1503-1509.

277. Tseng, B.Y., Grafstrom, R.H., Revie, D., Oertel, W., and Goulian, M. (1979) Studies on early intermediates in the synthesis of DNA in animal cells. *Cold Spring Harb. Symp. Quant. Biol.* 43 Pt 1, 263-270.

278. Tsurimoto, T., Melendy, T., and Stillman, B. (1990) Sequential initiation of lagging and leading strand DNA synthesis by two different polymerase complexes at the SV40 DNA replication origin. *Nature* 346, 534-539.

279. Tye, B.-K., Chien, J., Lehman, I.R., Duncan, B.K., and Warner, H.R. (1978) Uracil incorporation: a source of pulse-labeled DNA fragments in the replication of the *Escherichia coli* chromosome. *Proc. Natl. Acad. Sci. U.S.A.* 75, 233-237.

280. Tye, B.-K., and Lehman, I.R. (1977) Excision repair of uracil incorporated in DNA as a result of a defect in dUTPase. *J. Mol. Biol.* 117, 293-306.

281. Tye, B.-K., Nyman, P.-O., Lehman, I.R., Hochhauser, S., and Weiss, B. (1977) Transient accumulation of Okazaki fragments as a result of uracil incorporation into nascent DNA . *Proc. Natl. Acad. Sci. U.S.A.* 74, 154-157.

282. Umar, A., Boyer, J.C., Thomas, D.C., Nguyen, D.C., Risinger, J.I., Boyd, J., Ionov, Y., Perucho, M., and Kunkel, T.A. (1994) Defective mismatch repair in extracts of colorectal and endodermal cancer cell lines exhibiting microsatellite instability. *J. Biol. Chem.* 269, 14367-14370.

283. Upton, C., Stuart, D.T., and McFadden, G. (1993) Identification of a poxvirus gene encoding a uracil DNA glycosylase. *Proc. Natl. Acad. Sci. U.S.A.* 90, 4518-4522.

284. Varshney, U., Hutcheon, T., and van de Sande, J.H. (1988) Sequence analysis, expression, and conservation of Escherichia coli uracil-DNA glycosylase and its gene (ung). *J. Biol. Chem.* 263, 7776-7784.

285. Varshney, U., and van de Sande, J.H. (1991) Specificities and kinetics of uracil excision from uracil-containing DNA oligomers by *Escherichia coli* uracil DNA glycosylase. *Biochemistry* 30, 4055-4061.

286. Verri, A., Mazzarello, P., Spadari, S., and Focher, F. (1992) Uracil-DNA glycosylases preferentially excise mispaired uracil. *Biochem. J.* 287, 1007-1010.

287. Waga, S., Bauer, G., and Stillman, B. (1994) Reconstitution of complete SV40 DNA replication with purified replication factors. *J. Biol. Chem.* 269, 10923-10934.

288. Waga, S., and Stillman, B. (1994) Anatomy of a DNA replication fork revealed by reconstitution of SV40 DNA replication *in vitro*. *Nature* 369, 207-212.

289. Wang, T.S.-F. (1996) Cellular DNA polymerases. *DNA Replication in Eukaryotic Cells*. (M. L. DePamphilis) 461-493, Cold Spring Harbor Laboratory Press, Cold Spring Harbor, N.Y.

290. Wang, T. S.-F., Sedwick, W.D., and Korn, D. (1974) Nuclear deoxyribonucleic acid polymerase. Purification and properties of the homogeneous enzyme from human KB cells. *J. Biol. Chem.* 249, 841-850.

291. Wang, Z., and Mosbaugh, D.W. (1988) Uracil-DNA glycosylase inhibitor of bacteriophage PBS2: cloning and effects of expression of the inhibitor gene in *Escherichia coli*. *J. Bacteriol.* 170, 1082-1091.

292. Wang, Z., and Mosbaugh, D.W. (1989) Uracil-DNA glycosylase inhibitor gene of bacteriophage PBS2 encodes a binding protein specific for uracil-DNA glycosylase. *J. Biol. Chem.* 264, 1163-1171.

293. Wang, Z., Smith, D.G., and Mosbaugh, D.W. (1991) Overproduction and characterization of the uracil-DNA glycosylase inhibitor of bacteriophage PBS2. *Gene* 99, 31-37.

294. Wang, Z., Wu, X., and Friedberg, E.C. (1993) DNA repair synthesis during base excision repair *in vitro* is catalyzed by DNA polymerase epsilon and is influenced by DNA polymerases alpha and delta in *Saccharomyces cerevisiae*. *Mol. Cell. Biol.* 13, 1051-1058.

295. Wang, Z., Wu, X., and Friedberg, E.C. (1997) Molecular mechanism of base excision repair of uracil-containing DNA in yeast cell-free extracts. *J. Biol. Chem.* 272, 24064-24071.

296. Warner, H.R., Demple, B.F., Deutsch, W.A., Kane, C.M., and Linn, S. (1980) Apurinic/apyrimidinic endonucleases in repair of pyrimidine dimers and other lesions in DNA. *Proc. Natl. Acad. Sci. U.S.A.* 77, 4602-4606.

297. Warner, H.R., Duncan, B.K., Garrett, C., and Neuhard, J. (1981) Synthesis and metabolism of uracil-containing deoxyribonucleic acid in *Escherichia coli*. *J. Bacteriol.* 145, 687-695.

298. Waters, T.R., and Swann, P.F. (1998) Kinetics of the action of thymine DNA glycosylase. *J. Biol. Chem.* 273, 20007-20014.

299. Wei, Y.-F., Robins, P., Carter, K., Caldecott, K., Pappin, D.J.C., Yu, G.-L., Wang, R.-P., Shell, B.K., Nash, R.A., Schar, P., Barnes, D.E., Haseltine, W.A., and Lindahl, T. (1995) Molecular cloning and expression of human cDNAs encoding a novel DNA ligase IV and DNA ligase III, an enzyme active in DNA repair and recombination. *Mol. Cell. Biol.* 15, 3206-3216.

300. Weiss, B. (1981) Exodeoxyribonucleases of *Escherichia coli*. *The Enzymes* (P. B. Boyer) 203-231, Academic Press, Inc., New York, N.Y.

301. Wiebauer, K., and Jiricny, J. (1989) *In vitro* correction of G:T mispairs to G:C pairs in nuclear extracts from human cells. *Nature* 339, 234-236.

302. Wiebauer, K., and Jiricny, J. (1990) Mismatch-specific thymine DNA glycosylase and DNA polymerase beta mediate the correction of G:T mispairs in nuclear extracts from human cells. *Proc. Natl. Acad. Sci. U.S.A.* 87, 5842-5845.

303. Wilson, D.M. III, Takeshita, M., and Demple, B. (1997) Abasic site binding by the human apurinic endonuclease, Ape, and determination of the DNA contact sites. *Nucleic Acids Res.* 25, 933-939.

304. Winters, T.A., and Williams, M.V. (1990) Use of the PBS2 uracil-DNA glycosylase inhibitor to differentiate the uracil-DNA glycosylase activities encoded by herpes simplex virus types 1 and 2. *J. Virol. Methods* 29, 233-242.

305. Wittwer, C.U., and Krokan, H. (1985) Uracil-DNA glycosylase in HeLa S3 cells: interconvertibility of 50 and 20 kDa forms and similarity of the nuclear and mitochondrial form of the enzyme. *Biochim. Biophys. Acta* 832, 308-318.

306. Wood, R.D. (1996) DNA repair in eukaryotes. *Annu. Rev. Biochem.* 65, 135-167.

307. Wovcha, M.G., and Warner, H.R. (1973) Synthesis and nucleolytic degredation of uracil-containing deoxyribonucleic acid by *Escherichia coli* deoxyribonucleic acid polymerase I. *J. Biol. Chem.* 248, 1746-1750.

308. Wu, S.M., Zhang, P., Zeng, X.R., Zhang, S.J., Mo, J., Li, B.Q., and Lee, M.Y. (1998) Characterization of the p125 subunit of human DNA polymerase delta and its deletion mutants. Interaction with cyclin-dependent kinase-cyclins. *J. Biol. Chem.* 273, 9561-9569.

309. Wu, X., Li, J., Li, X., Hsieh, C.L., Burgers, P.M., and Lieber, M.R. (1996) Processing of branched DNA intermediates by a complex of human FEN-1 and PCNA. *Nucleic Acids Res.* 24, 2036-2043.

310. Yamaguchi, M., Tanabe, K., Taguchi, Y.N., Nishizawa, M., Takahashi, T., and Matsukage, A. (1980) Chick embryo DNA polymerase beta. Purified enzyme consists of a single Mr=40,000 polypeptide. *J. Biol. Chem.* 255, 9942-9948.

311. Yamamoto, Y., and Fujiwara, Y. (1987) Culture-age effect on uracil-DNA glycosylase activity in normal human skin fibroblasts. *J. Gerontol.* 42, 470-475.

312. Yang, C.L., Chang, L.S., Zhang, P., Hao, H., Zhu, L., Toomey, N.L., and Lee, M.Y. (1992) Molecular cloning of the cDNA for the catalytic subunit of human DNA polymerase delta. *Nucleic Acids Res.* 20, 735-745.

313. Yanisch-Perron, C., Vieira, J., and Messing, J. (1985) Improved M13 phage cloning vectors and host strains: nucleotide sequence of the M13mp18 and pUC19 vectors. *Gene* 33, 103-119.

314. Ye, F., Carrodeguas, J.A., and Bogenhagen, D.F. (1996) The gamma subfamily of DNA polymerases: cloning of a developmentally regulated cDNA encoding *Xenopus laevis* mitochondrial DNA polymerase gamma. *Nucleic Acids Res.* 24, 1481-1488.

315. Yenofsky, R.L., Fine, M., and Pellow, J.W. (1990) A mutant neomycin phosphotransferase II gene reduces the resistance of transformants to antibiotic selection pressure. *Proc. Natl. Acad. Sci. U.S.A.* 87, 3435-3439.

316. Yoshida, S., and Masaki, S. (1979) Utilization *in vitro* of deoxyuridine triphosphate in DNA synthesis by DNA polymerases alpha and beta from calf thymus. *Biochim. Biophys. Acta* 561, 396-402.

317. Zastawny, T.H., Doetsch, P.W., and Dizdaroglu, M. (1995) A novel activity of *E. coli* DNA *N*-glycosylase. Excision of isodialuric acid (5,6-dihydroxyuracil), a major product of oxidative DNA damage, from DNA. *FEBS Lett.* 364, 255-258.

318. Zhang, J., Tan, C.K., McMullen, B., Downey, K.M., and So, A.G. (1995) Cloning of the cDNAs for the small subunits of bovine and human DNA polymerase delta and chromosomal location of the human gene (POLD2). *Genomics* 29, 179-186.

319. Zhou, J.Q., Tan, C.K., So, A.G., and Downey, K.M. (1996) Purification and characterization of the catalytic subunit of human DNA polymerase delta expressed in baculovirus-infected insect cells. *J. Biol. Chem.* 271, 29740-29745.

APPENDIX

APPENDIX

Inhibition of Human UDG by PBS2 Ugi

The crystal structure of Ugi complexed with human uracil-DNA glycosylase (UDG) was recently determined to understand how Ugi might act as a DNA mimic. In order to biochemically characterize this interaction, Ugi inhibition studies of human UDG and *E. coli* uracil-DNA glycosylase (Ung) were conducted to compare and contrast the efficiency of the enzyme•inhibitor interaction between these enzymes in the presence of a uracil-containing DNA substrate. The effect of Ugi on human UDG and *E. coli* Ung activity was determined by measuring the amount of uracil released from calf thymus [uracil-^{3}H]DNA with various amounts of inhibitor protein present in the reaction mixture. The substrate contained primarily U•A base pairs since [^{3}H]-uracil residues were introduced into the DNA by incorporation of [^{3}H]dUMP by *E. coli* DNA polymerase I. Ugi was observed to effectively inactivate UDG activity toward uracil-containing double-stranded DNA (Figure 72A). The human enzyme was inactivated ~3 times more efficiently than an equimolar amount of *E. coli* uracil-DNA glycosylase (Ung), since 50 % inhibition was achieved at Ugi concentrations of 1.2×10^{-11} M and 3.6×10^{-11} M, respectively.

This difference suggested that the human UDG preferentially recognized Ugi. Alternatively, these results could be explained if a subpopulation of enzyme was incapable of forming a stable enzyme•inhibitor complex or if the concentration of the enzyme preparations were miscalculated. To investigate these potential explanations, a defined quantity of [^{35}S]Ugi (300 pmol) was incubated with increasing molar amounts of *E. coli* Ung or human UDG (75 to 3,000 pmol) in order to promote Ung•[^{35}S]Ugi and

Figure 72. Inhibition of *E. coli* and human UDG by uracil-DNA glycosylase inhibitor protein. (A) Two standard uracil-DNA glycosylase inhibitor reaction mixtures (900 µl) were prepared each containing 9 fmol of *E. coli* (*closed circles*) or human (*open circles*) uracil-DNA glycosylase. Aliquots (75 µl) of each reaction mixture were added to 25 µl samples of [^{35}S]Ugi containing the amounts indicated. Each assay mixture, containing 0.07 units of *E. coli* or 0.11 units of human uracil-DNA glycosylase, was incubated for 30 min at 37°C and the amount of [^{3}H]uracil released from calf thymus [uracil-^{3}H]DNA (195 cpm/pmol) was determined as described under "Experimental Procedures". The amount of enzyme activity detected was expressed as the percentage of activity relative to the control lacking Ugi. *E. coli* and human uracil-DNA glycosylase concentrations were determined using the molar extinction coefficients $\varepsilon_{280\ nm} = 4.22 \times 10^{-4}$ and 5.04×10^{-4}, respectively. (B) Complex formation between *E. coli* Ung and Ugi was examined in reaction mixtures (130 µl) containing 300 pmol of [^{35}S]Ugi and 0, 75, 150, 225, 300, 375, 450, 600, 1,500, or 3,000 pmol of *E. coli* Ung (lanes C, 1-9, respectively). Samples were incubated at 25°C for 10 min and 4°C for 20 min, loaded onto 12.5% nondenaturing polyacrylamide gels, and electrophoresis and autoradiography was performed. *Arrows* denote the location of [^{35}S]Ugi and Ung•[^{35}S]Ugi. (C) Following autoradiography, radioactive bands containing [^{35}S]Ugi and Ung•[^{35}S]Ugi were excised from the gel and the ^{35}S radioactivity was measured. The amount of unbound [^{35}S]Ugi (*striped bars*) and Ung•[^{35}S]Ugi complex (*black bars*) was measured as the percentage of the total amount of ^{35}S radioactivity detected as free or complexed Ugi, respectively. (D) Complex formation between human uracil-DNA glycosylase and Ugi was similarly examined in identical reactions containing 300 pmol of [^{35}S]Ugi (lanes C, 1-9). (E) The amount of unbound [^{35}S]Ugi and Ung•[^{35}S]Ugi complex was determined as described above.

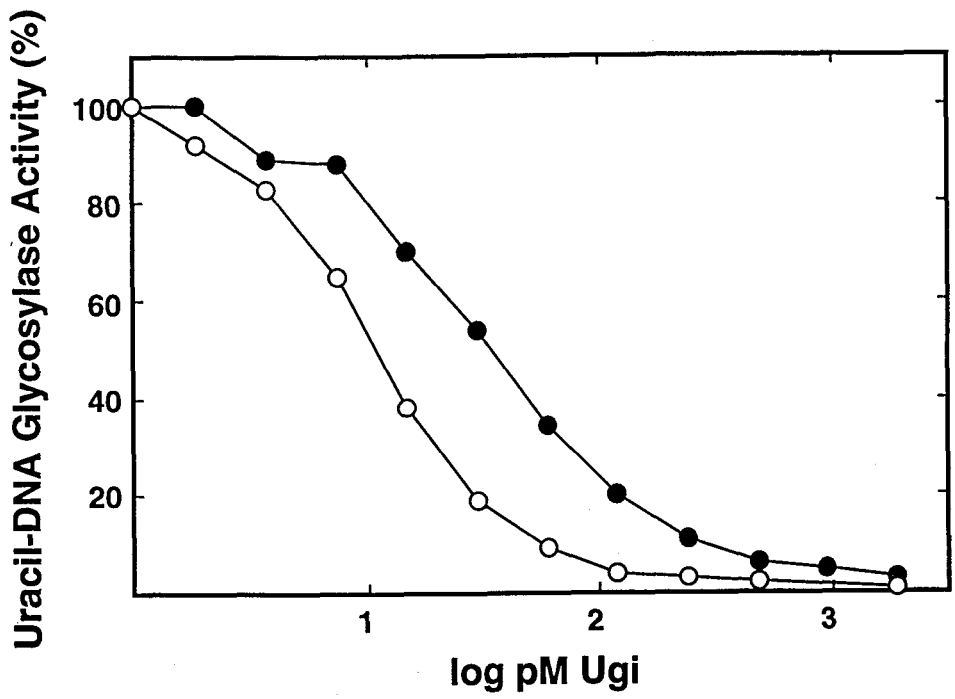
Uracil-DNA Glycosylase Activity (%)
100
80
60
40
20
1
2
3
log pM Ugi

Figure 72

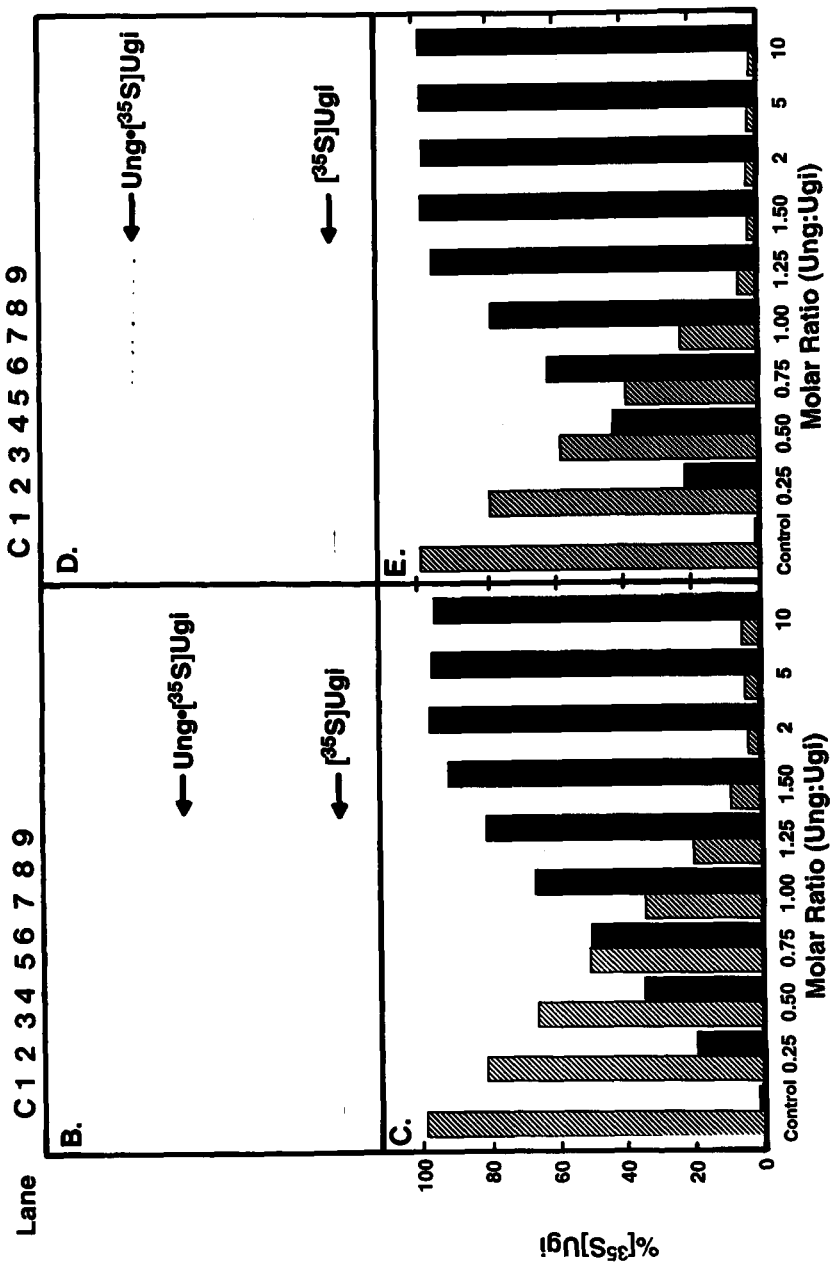

Figure 72 (continued)

UDG•[^{35}S]Ugi complex formation (Figure 72B and D, lanes 1-9) . [^{35}S]Ugi was included as a control to indicate the position of uncomplexed [^{35}S]Ugi (Figure 72B and D, lane C). The complexes were then resolved from their individual components by nondenaturing polyacrylamide gel electrophoresis and subjected to autoradiography. As both human UDG and *E. coli* Ung have been shown to exhibit a 1:1 complex stoichiometry with Ugi (15, 167), [^{35}S]Ugi was expected to form a complex with both enzyme preparations in a manner that was directly proportional to the enzyme•inhibitor molar ratio. Quantitation of the amount of [^{35}S]Ugi in complex with Ung and UDG at an Ung:Ugi molar ratio of 1:1 indicated that ~66 % and ~78 % of the [^{35}S]Ugi was in complex with the *E. coli* and human enzymes, respectively (Figure 72C and E). Based on the complex stoichiometry, it was anticipated that 100 % of the [^{35}S]Ugi would be detected in complex for each enzyme at this ratio. Assuming that both enzyme preparations were fully capable of forming a stable enzyme•inhibitor complex, it appeared that the concentration of human UDG was slightly overestimated relative to that of the *E. coli* enzyme and that both enzyme concentrations were underestimated relative to that of [^{35}S]Ugi. Inherent errors in protein concentration determination by absorbance spectroscopy could have contributed to these differences. To determine if a subpopulation of enzyme was incapable of forming complex, the amount of [^{35}S]Ugi detected in complex with human UDG was divided by the amount detected in complex with *E. coli* Ung for Ung:Ugi molar ratios of 0.25:1, 0.50:1, 0.75:1, and 1:1 and values were calculated. It was estimated that ~1.10-, ~1.23-, ~1.24-, and ~1.18-fold more [^{35}S]Ugi was detected in complex with human UDG than with *E. coli* Ung at each respective ratio. Under circumstances where a subpopulation of human UDG was incapable of forming a stable complex, these values would be expected to decrease as the molar ratio of Ung:Ugi increased. Conversely, these values would be expected to increase proportionally to the Ung:Ugi molar ratio if a subpopulation of *E. coli* Ung was incapable of forming a stable complex. Thus,

the similar excess amount of [^{35}S]Ugi detected for each Ung:Ugi ratio suggested that both enzyme preparations were equally capable of forming complex with [^{35}S]Ugi. Although the amount of human UDG relative to *E. coli* Ung was overestimated by a factor of 1.1- to 1.2-fold in these experiments, this does not account for the observed ~3-fold higher ability of [^{35}S]Ugi to inhibit human UDG. This suggests that Ugi more readily binds human UDG in the presence of a DNA substrate than it binds *E. coli* Ung and more effectively competes DNA out of a human UDG•DNA complex than out of an *E. coli* Ung•DNA complex. Thus, the kinetics for the interaction of Ugi with human UDG are more favorable than that observed for complex formation with *E. coli* Ung. Defined kinetic measurements for the association of Ugi with human UDG have yet to be determined.

In order to determine the structural basis for the interaction of Ugi with human UDG, human placental recombinant UDG was obtained from the laboratory of Dr. H.E. Krokan (University of Trondheim, Norway) and UDG•Ugi complex was purified from its constitutive components and concentrated in preparation for X-ray crystallography. The recombinant human UDG enzyme used for this study lacked the N-terminal 84 amino acids encoded by the *UNG* gene and contained three N-terminal residues encoded by the vector. Specific amino acid contacts between UDG and Ugi were determined by X-ray crystallography in the laboratory of Dr. J.A. Tainer (Scripps Research Institute, La Jolla, CA) in order to provide details of the human UDG•Ugi association and to understand how Ugi might mimic the natural DNA substrate. The crystal structure of the UDG•Ugi complex solved by Mol *et al.* (167) is illustrated in Figure 73. The 1.9 Å crystal structure of PBS2 Ugi complexed with human UDG revealed that the tight association achieved between UDG and Ugi was provided by complementarity shape and electrostatic interactions, specific charged hydrogen bonds, and hydrophobic packing of Leu-272 from the protruding UDG loop. Inhibition of UDG is

Figure 73. Crystal structure of human uracil-DNA glycosylase•inhibitor complex. The crystal structure of the human uracil-DNA glycosylase•inhibitor complex was determined by using a combination of molecular replacement and multiple isomorphous replacement (MIR) methods (167). Uracil-DNA glycosylase (*bottom*) binds to Ugi (*top*) in a 1:1 stoichiometric fashion. In the tertiary structure of complexed enzyme, the β-strands are *yellow*, the α-helices are *purple*, and the random coil/loops are *green*. In the tertiary structure of complexed Ugi, the β-strands are *orange*, the α-helices are *blue*, and the random coil/loops are *red*. β1-strand (*orange arrow, bottom*) of the five-stranded anti-parallel Ugi β sheet inserts into the uracil-DNA glycosylase active site groove roughly perpendicular to the four-stranded parallel uracil-DNA glycosylase β sheet. The sequence-conserved (His-268, Pro-269, Ser-270, Pro-271, Leu-272, and Ser-273) uracil-DNA glycosylase active site loop (*green tube, right*) protrudes upwards into a hydrophobic pocket formed by α2-helix (*blue coil, right*) and the curved β sheet of Ugi.

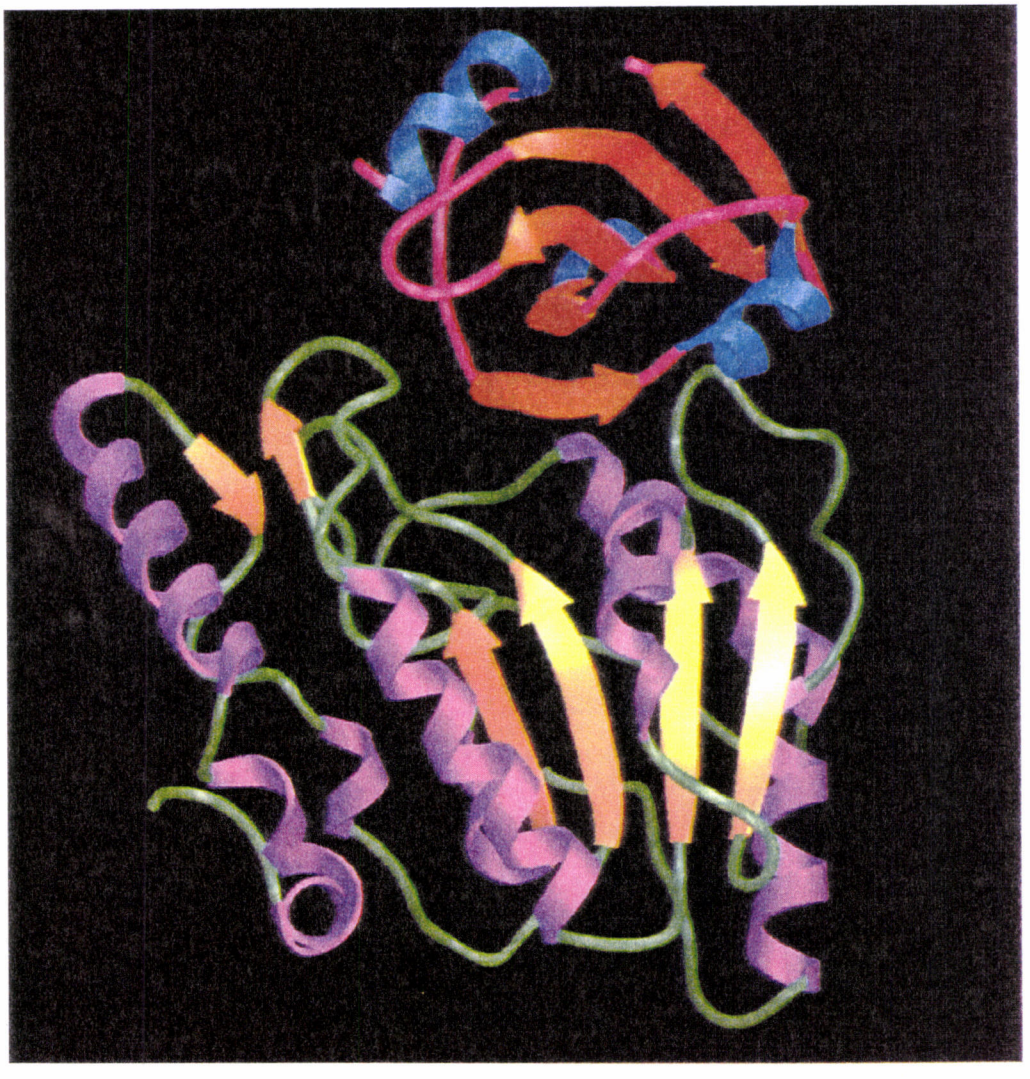

Figure 73

achieved by insertion of the Ugi β1-strand into the conserved DNA binding groove of the enzyme to occlude the active-site uracil-binding pocket. This interaction effectively prevents DNA binding and catalysis.

The UDG•Ugi interface buries ~1200 $Å^2$ of Ugi and contains 18 hydrogen bonds, involving 12 enzyme and 14 inhibitor side chains. Ugi residues involved in the UDG•Ugi interface include the following: Asn-3 from the N-terminus; two residues from the loop connecting the α1-helix and β1-strand (Ile-18 and Gln-19); the entire β1-strand (Glu-20, Ser-21, Ile-22, Leu-23, and Met-24); three residues in the α2-helix (Glu-28, Glu-31, and Val-32); Thr-45 from the β2-strand; two residues from the β3-strand (Asn-54 and Met-56); three residues from the loop connecting the β3- and β4-strands (Asp-61, Ala-62, and Tyr-65); and three residues from the loop between the β3- and β4-strands (Gln-73, Gly-77, and Glu-78). Recently, human UDG has been co-crystallized with a uracil-containing duplex DNA substrate (251). A comparison of important protein-protein contacts between UDG and Ugi and protein-DNA contacts between UDG and its DNA substrate is represented in Table 14. Out of the 14 Ugi amino acid residues that interact with human UDG, 8 of these interact with UDG amino acid residues that are implicated in DNA binding. These interactions are specific for the DNA binding region but not the active-site uracil-binding pocket of UDG. These contacts include the following hydrogen bond interactions: Gln-144 (UDG) and Leu-23 (Ugi); His-148 (UDG) and Ser-21 (Ugi); Ser-169 (UDG) and Glu-20 (Ugi); Ser-247 (UDG) and Glu-28 (Ugi); His-268 (UDG) and Ile-22 (Ugi); and Leu-272 and Tyr-275 (UDG) with Asn-54, Gln-73, and Glu-78 (Ugi). An additional interaction includes a salt bridge between Arg-276 (UDG) and Glu-31 (Ugi). With regards to the EDC/GEE modification study presented in this dissertation, three acidic amino acid residues of the inhibitor protein are involved in hydrogen bonding with conserved UDG residues (Glu-20, Glu-28, and Glu-78). An

Table 14

Amino Acid Contacts of Uracil-DNA Glycosylase with Uracil-DNA and Ugi

Uracil-DNA Glycosylase		Contacts		Sites of DNA Interactions	
Human	*E. coli*	Ugi	DNA	Site	Interaction
Gln-144	Gln-63	+	+	Uracil (O_2)	H-bond (MC)[a]
Asp-145	Asp-64		+	Uracil (O_2)	H-bond (SC)
			+	AP-sugar (C_1)	H-bond (SC)
His-148	His-67	+	+	3' PO_4	H-bond (SC)
			+	AP-sugar (O_4)	H-bond (SC)
Gln-152	Gln-71	+			
Phe-158	Phe-77		+	Uracil	Stacking
			+	Uracil (O_4)	H-bond (SC)
Pro-165	Ala-84	+			
Ser-169	Ser-88	+	+	5' PO_4	H-bond (SC)
			+	5' PO_4	H-bond (MC)
Asn-204	Asn-123		+	Uracil (O_4)	H-bond (SC)
			+	Uracil (N_3)	H-bond (SC)
His-212	Gly-131	+			
Ala-214	Ala-133	+			
Asn-215	His-134	+			
Ser-247	Ser-166	+	+	+2 (3' PO_4)	H-bond (SC)
			+	+2 (3' PO_4)	H-bond (MC)
Val-248	His-167	+			
His-268	His-187	+	+	Uracil (O_2)	H-bond (SC)
			+	+2 (3' PO_4)	H-bond (MC)
Ser-270	Ser-189		+	3' PO_4	H-bond (SC)
Leu-272	Leu-191	+	+	AP-site insert	H-bonds
Ser-273	Ser-192		+	3' sugar (O_4)	H-bond (SC)
Tyr-275	His-194	+	+	+2 (3' sugar O_4)	H-bond (SC)
Arg-276	Arg-195	+	+	+3 (3' PO_4)	H-bond (SC)

[a] The abbreviations, MC and SC, are indicative of main chain and side chain interactions between interacting amino acids of UDG with DNA.

additional interaction with a nonconserved UDG residue involved a salt bridge formed by Glu-31. Out of the 13 amino acid residues of human UDG that interact with DNA, 8 (~62 %) are involved in strong interactions with Ugi. Taken together, these results indicate that Ugi appears to mimic duplex DNA interactions with UDG by interacting with specific residues involved in DNA binding.